Progressive Failure and Post-buckling Response of Tapered Composite Plates

Dai Ying Liu

A Thesis

in

The Department

Mechanical and Industrial Engineering

Presented in Partial Fulfillment of the Requirements

for the Degree of Doctor of Philosophy at

Concordia University,

Montreal, Quebec, Canada

September 2006

Your file Votre référence
ISBN: 978-0-494-30143-2
Our file Notre référence
ISBN: 978-0-494-30143-2

ABSTRACT

Progressive Failure and Post-buckling Response of Tapered Composite Plates

Dai Ying Liu

Concordia University, 2006

Design and manufacture of a variable-thickness composite laminate such as a helicopter yoke or a robot arm involves tapering the laminate by dropping certain individual plies at discrete internal locations, in order to tailor the stiffness of the laminate to the design and performance requirements. The ply drop in the laminate creates geometric and material discontinuities and results in large stress concentration. These in turn cause changes in the response and failure strengths of the laminate. For achieving economical, safe and reliable design, the progressive failure and post-buckling response of tapered laminated plates are important design considerations. Therefore, there is a necessity to investigate the progressive failure of tapered laminates and its effect on the post-buckling response. The present thesis concerns with these aspects.

In the present thesis, a nonlinear finite element formulation is developed based on the first-order shear deformation theory and the geometric nonlinearity in the von Karman sense for the analysis of tapered laminated plates. The tensor polynomial form of failure criterion is used in conjunction with a progressive failure simulation methodology to

study the progressive failure. The developed formulation and progressive failure simulation methodology are validated. A detailed parametric study of the deterministic progressive failure of tapered laminates under the action of uni-axial and bi-axial compression, in-plane positive shear, and in-plane negative shear loadings is conducted. A detailed parametric study on the deterministic progressive failure of tapered laminates under the action of bi-axial compression combined with in-plane shear loading is also conducted. The first-ply failure load, the ultimate failure load, the buckling load, the associated maximum transverse displacements, and the locations and modes of failure of tapered laminated plates are determined for each case. The effects of different taper and laminate configurations, fiber orientations, boundary conditions, addition of uniform-thickness sections are determined. Stochastic progressive failure of tapered laminated plate under the action of bi-axial compression combined with in-plane positive shear loading is investigated. The mean and standard deviation values of failure strengths are calculated considering the material properties as stochastic processes in space.

ACKNOWLEDGEMENTS

I wish to express my gratitude and indebtedness to my supervisor, Dr. Rajamohan Ganesan for his invaluable guidance, financial support and encouragement throughout the development of my thesis. He was devoting his valuable time for me always in spite of his busy schedule.

I would like to acknowledge the support provided for the present work by the Natural Sciences and Engineering Research Council of Canada (NSERC).

Finally, to my parents, parents-in-law, wife and son, I thank all of you for your patience throughout this endeavor. The inspiration and morale support you bring to me makes accomplishments like this possible.

TABLE OF CONTENTS

LIST OF FIGURES

LIST OF TABLES

Chapter 1

Literature Review and Thesis Objectives

1.1 Introduction

Laminated composite structures are increasingly being used in spacecraft, high speed aircraft, naval vessels and other transportation vehicles due to their high specific stiffness and strength, low weight, and elastic tailoring design capability. These allow the development of lighter, more efficient aircraft structures and machine components.

It is well known that the total failure of a laminated composite plate does not always occur at the load corresponding to the first–ply failure. The plate failure in a broad sense can be considered to have occurred when a structural element ceased to function satisfactorily; thus the definition of failure varies from one case to another. The failure characteristics of heterogeneous and anisotropic composite laminates are completely different from that of the isotropic plates. The appearance of detectable cracks in metals is generally considered to be unsafe since a slight amount of damage can rapidly progress into a catastrophic fracture. However, this is not true in the case of composite materials. Although internal damage might appear very early, its propagation is arrested by the internal configuration of the structure. Therefore, composite laminates can still sustain a much higher load after the occurrence of localized damage such as matrix cracking and fiber breaks. Hence the knowledge of the first–ply failure load and the ultimate load of such structures is essential so that these plates can be designed efficiently and economically by fully utilizing their post-initial-failure strength with appropriate reliability and safety. Thus, to accurately predict the failure loads of such structures, the

progressive failure of such structures is an important design consideration for achieving economical, safe and reliable design, and hence it has become an important subject of research. Literature survey has indicated that the existing studies on progressive failure of laminates have concentrated on uniform-thickness laminates.

When composite materials are used in aerospace structural components and machine elements, in some specific applications the composite structures need to be stiff at one end and flexible at the other end. It is usually desirable to tailor the material to match the localized strength and stiffness requirements. For a fibrous composite laminate composed of unidirectional layers, this is often realized by changing the number of plies. Example applications include wing structures of aircrafts, robot arms, helicopter yokes and blades, flywheels, and turbine blades. In many such applications, compressive and shear loadings are encountered. This abrupt change in thickness, which is referred to as a ply-drop-off, introduces a stress concentration that promotes premature delamination failure of a laminate. Tapered laminated structures have received much attention from researchers because of their structure tailoring capability, damage tolerance, and their potential for creating significant weight savings in engineering applications. Figure 1.1 shows five typical taper configurations. A review of existing works on the study of tapered laminated composite structures has been presented by He *et al* [1].

From earlier research works concerning this type of structures, two major categories of work on tapered composites can be identified. The first is to understand failure mechanisms induced by drop-off plies in tapered construction. The second category has been to seek more rational or optimal designs of damage resistant tapered composite

structures by investigating the parameters that have substantial influences on the structural integrity. Literature survey indicated that progressive failure of tapered laminates has not so far been investigated.

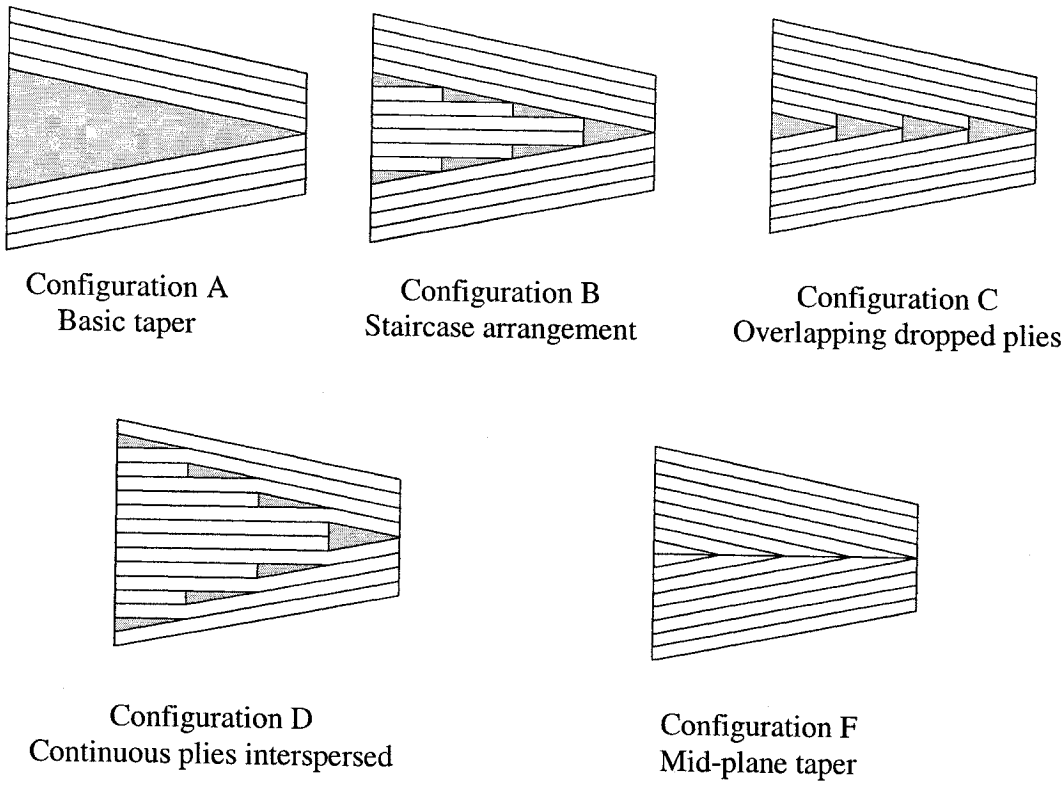

Figure 1.1 Five typical taper configurations

The parameters of any mechanical or structural system possess a random variation as a function of space and / or time. The randomness in failure parameters encompasses the uncertainties involved at the design and manufacturing stages, as well as the uncertain nature of the operating conditions. At the design stage, randomness is present in the test data regarding material strength values, elastic constants, engineering constants, and the material properties pertinent to the service life. The randomness in material properties significantly affects the functioning of the mechanical component and is unavoidable even with the best quality control measures. Literature survey indicates that the existing

works have concentrated on the influence of the randomness in material properties on the response of uniform-thickness composite laminates. Tapered laminates have not so far been considered.

Literature survey indicates that the progressive failure of tapered laminates and their post-buckling response, and the influence of the randomness in material properties on the progressive failure and post-buckling response have not so far been investigated. The present thesis considers these aspects. In the following, a review of existing works on the 1) progressive failure analysis of composite laminates, 2) analysis of tapered composite laminates, and 3) stochastic analysis of composite laminates, is given.

1.2 Progressive Failure Analysis of Composite Laminates

Composite laminates can sustain considerable loading after the first-ply failure. The first-ply failure of laminates has been considered in many research works. In the work of Turvey [2-8] the analytical and numerical solutions for the first-ply failure loads of symmetric and un-symmetric uniform-thickness laminates with simply supported boundary conditions under the transverse loads have been developed. In the work of Reddy and Pandey [9], a finite-element procedure for the prediction of linear first-ply failure loads of uniform-thickness composite laminates that are subjected to transverse loadings and in-plane tensile loadings has been developed. Reddy and Reddy [10] used the finite element formulation based on the first-order shear deformation theory to determine the first-ply failure loads of laminate under transverse loading using linear and non-linear failure analyses.

Considerable interest has been placed on the modeling and analysis of progressive failure of composite laminates. The finite element method has been used in the analysis. Two major approaches have been developed and followed. They are: 1. The stiffness modification approach in which the reduced stiffness matrix of the composite material ply is modified [11-14], 2. The material degradation approach in which internal state variables, which are also called as stiffness degradation factors, that represent the damaged state of the lamina, are introduced [15-27].

Using the stiffness modification approach, Lee [11] analyzed the damage accumulation in uniform-thickness composite laminates containing circular holes and subjected to in-plane bi-axial loading. Ochoa and Engblom [12] used a higher-order plate element and computed transverse stresses from equilibrium equations. The failure analysis procedure presented in this work is similar to that used by Lee [11], but the stresses considered for failure prediction were computed at the Gauss points, and further, the reduced stiffness coefficients were modified in a different manner for the fiber breakage failure mode. Hwang and Sun [13] developed an iterative three-dimensional finite element failure analysis using modified Newton-Raphson scheme for the prediction of laminate failures. Tolson and Zabaras [14] followed a procedure similar to that used by Ochoa and Engblom [12], using a higher order plate element.

A progressive damage model for laminated composites that is based on material degradation approach has been developed by Nuismer and Tan [15] and Tan and Nuismer [16], in which stiffness degradation factors have been introduced to quantify the damage development. Using the above mentioned progressive damage model, Tan [18] investigated the progressive failure of uniform-thickness laminates with cut-out holes

under in-plane tensile loading. The case of symmetric laminate has been considered in order to neglect bending-extension coupling effects, and the damage in a lamina was accounted for by using stiffness degradation factors. The failures such as the fiber breakage and matrix failure are represented by the corresponding stiffness degradation factors. The effective Young's moduli corresponding to the fiber direction and the transverse direction (in the 1-2 plane) and the shear modulus (corresponding to the 1-2 plane) of a damaged ply are expressed in terms of the corresponding undamaged modulus values and the corresponding stiffness degradation factors. Hence different degradation factors were used for calculating the effective longitudinal modulus due to fiber breakage, and for calculating the effective transverse and shear moduli due to matrix failure. The degradation factors of a material system were adjusted through a parametric study and were assumed to be independent of lamination sequence. The same approach was extended to the case of compressive loading by Tan and Perez [19]. Chou *et al* [20] predicted the load-strain relation by combining a failure model developed from tests of un-notched uniform-thickness laminates with a tangent-modulus finite element analysis of the notched laminate.

Chang and Chang [22] developed a progressive damage model for laminated composites and analyzed bolted joints which may fail in either tension mode or shear-out mode using this model. The model consists of the stress analysis and the failure analysis. Stresses and strains in uniform-thickness laminates were analyzed on the basis of the theory of finite elasticity with the consideration of material and geometric nonlinearities. Damage accumulation in the laminate was evaluated using the proposed failure criteria in combination with the proposed property degradation model. The same authors [23]

conducted the failure analysis of notched composite uniform-thickness laminates that are subjected to tensile loading using the progressive damage model presented in reference [22]. Stresses and strains in the laminate were determined based on the classical laminated plate theory with the consideration of material nonlinearity. Chang and Lessard [24] also calculated the stresses and strains inside the uniform-thickness laminates using a nonlinear finite element analysis which was based on the finite deformation theory of elasticity with the consideration of material and geometric nonlinearities. Numerical results were compared with the test data which were obtained during the investigation and presented in reference [25]. Lessard and Shokrieh [26] and Shokrieh and Lessard [27] conducted the failure analysis of pin-loaded composite uniform-thickness laminates using two-dimensional and three dimensional finite element modeling and analyses. In reference [26], a simple two-dimensional linear model and a two-dimensional model that has been enhanced with the consideration of non-linear material behavior and large deformation were used. In reference [27], a three-dimensional nonlinear finite element code was developed to analyze the effects of material nonlinearity on the state of stress and the failure due to stress concentration of a pin-loaded laminated composite plate. A nonlinear material model for in-plane behavior, that had been modified so as to be applicable for three-dimensional cases, was used in this work. In addition, nonlinear shear stress – shear strain relations of a unidirectional ply, in the x-y and z-x planes, have been considered. A failure analysis, using stress based failure criteria, is performed to predict failure initiation load of different configurations.

Chang and Lessard [24] studied the damage development in laminated composites containing an open hole and subjected to compressive loading. A progressive damage

model was developed during the investigation to predict the extent of damage, to quantify the internal damage in the uniform-thickness laminates as a function of the applied load, and to simulate the in-plane response of the uniform-thickness laminates from initial loading to final collapse. In this model, stresses and stains inside the uniform-thickness laminates were calculated using a nonlinear finite element analysis which was based on the finite deformation theory and with the consideration of material and geometric nonlinearities. Numerical results obtained from the model were in good agreement with the test results [25]. The tests reported in reference [25] were performed on T300/976 Graphite/Epoxy composites with five different ply orientations. For each ply orientation, samples with different geometric properties were chosen. A total of over 30 different configurations were tested. The samples were tested for their compressive response through initial detection of failure until ultimate failure.

The buckling of composite plates subjected to bi-axial loading was investigated in reference [28] using experimental study and numerical analysis. It was observed that the loading grips interfere with each other's motion at each corner during the continuous bi-axial compression process. In order to overcome this problem, modified rectangular specimens were introduced. The effects of the modifications of the plate specimen were studied using a finite element analysis in which the large deflection but small strain conditions were considered. The buckling load, as well as the strains and deflections observed from the test, were compared with the results obtained using the finite element analysis and using the analytical solutions [29]. Reasonably good agreement between the test results, finite element solutions and analytical solutions, was reported for the un-stiffened plates. Reasonably good agreement between the buckling stresses determined

using the finite element analysis and that determined from the test results was reported for the so-called "hat-stiffened plate".

The mechanics and mechanisms of delamination, buckling and post-buckling of uniform-thickness composite plates have been studied in reference [30]. In this work, compression tests were carried out on HYE-3574 OH graphite/epoxy composite plates with built-in delaminations in order to evaluate the critical loads, post-buckling behavior and load-carrying capacity of the plates. The delamination buckling mode was found to be closely related to the location and the length of the delamination. Excellent agreement was reported between the experimental values of critical loads and those predicted using the higher-order plate theory. Bansal and Kumosa [31] studied an extension of traditional Iosipescu shear test specimen for applications to the in-plane bi-axial load test. A bi-axial stress test fixture, which was developed based on the original Iosipescu shear test and the Arcan in-plane stress method, was used to characterize mixed-mode failure in both isotropic (PMMA) and orthotropic (teak) Iosipescu specimens under externally applied bi-axial loads. Finite element method was used to evaluate the stress states at the notch tips as a function of the notch-tip radius of bi-axially loaded Iosipescu specimens. Results from the finite element analysis showed that an absolute numerical evaluation of the stress distribution at the notch-tips could be misleading if a linear-elastic material behavior was assumed. However, the analytical approach, which assumed a uniform stress state along the notch-root axis, was found to more accurately represent the notch-tip stresses.

Reddy and Reddy [17] studied the failure of uniform-thickness laminates under axial extension using a finite element formulation based on the layer-wise plate theory. They

applied a prescribed displacement, for which the load was found by integrating stresses through the thickness. Two different types of stiffness reduction methods were tried: (i) Degradation of the elastic modulus and the Poisson's ratios only; (ii) Simultaneous degradation of the elastic and shear moduli and the Poisson's ratios. However, material properties were degraded by the same factor regardless of the failure modes. They concluded that further investigation was required to apply their approach to uniform-thickness laminates under compressive or bending load. Using the Classical Laminated Plate Theory (CLPT) and the total-ply-discount failure analysis, Greif and Chapon [32] conducted three-point bending tests of laminated composite beams and attempted to predict successive failures. After the failure of a ply, the analysis was repeated for a new laminate in which the stiffness of a failed ply was set to be equal to zero. The analysis was continued up to five ply failures. However, their analytical predictions did not match the experimental results.

The post-buckling response of composite uniform-thickness laminates subjected to compressive and shear loadings has been the subject of investigation in many recent research works. Starnes and Rouse [33] conducted experimental investigations on the post-buckling response and failure characteristics of graphite-epoxy panels with and without circular hole, under uni-axial compression. Engelstad *et al* [34] investigated the post-buckling response and failure characteristics of graphite-epoxy panels with and without a circular hole, under uni-axial compression, using a progressive damage model in conjunction with a three-dimensional degenerated shell element. In this study comparisons between the post-buckling responses of composite panels that is determined using the finite element analysis and the post-buckling response that has been observed

from the experimental investigations presented by Starnes and Rouse [33] have also been made. Lee and Hyer [35] studied the post-buckling behavior of a square symmetrically laminated plate with a circular hole under uni-axial compression loading using the maximum stress failure criterion. Kam and Sher [36] studied the non-linear behavior and the first-ply failure strength of transversely loaded laminated composite plates with semi-clamped edges using a method developed based on the von-Karman/Mindlin plate theory in conjunction with the Ritz method.

One of the early studies related to the post-buckling response of laminated plates subjected to shear loading is the work of Kaminski and Ashton [37], who presented an experimental study on rectangular boron/epoxy plates clamped on each edge. Kobayashi *et al* [38] also presented an experimental study on graphite/epoxy laminated plates in which the ultimate failure load was found to be considerably greater than the buckling load. Agrawal [39] examined the post-buckling behavior of multi-bay composite shear webs and studied the failure modes that are typical of composite panels using the NASTRAN finite element code. The investigation of Zhang and Matthews [40] on post-buckling behavior of anisotropic plates under combined compression and shear loads revealed the importance of the direction of applied shear force on the post-buckling behavior of anisotropic uniform-thickness laminates. Stein [41] analyzed long orthotropic plates in combined shear and compression using the method developed in his earlier investigation that dealt with longitudinally compressed plates. Prabhakar and Kennedy [42] conducted a theoretical investigation of the post-buckling behavior of un-symmetric angle-ply uniform-thickness laminates. Kumar and Sindhi [43] used the finite element method to investigate the behavior of isotropic and orthotropic simply supported

rectangular plates under pure shear with in-plane boundary conditions similar to those in the NASTRAN finite element model presented by Agrawal [39]. Using the stress function approach, Kosteletos [44] investigated the post-buckling response of thin flat rectangular generally-layered uniform-thickness laminates with clamped edges under shear and combined in-plane loads. Singh *et al* [45, 46] and Ganesan and Zhang [47] have conducted a detailed investigation of the progressive failure of square symmetric uniform-thickness laminates using a non-linear finite element formulation based on the von Karman theory for the geometric non-linear analysis and the First-order Shear Deformation Theory (FSDT) for composite uniform-thickness laminates. The progressive failure of uniform-thickness laminates subjected to uni-axial compression has been considered in Reference [45], the failure due to in-plane positive and negative shear loads was also considered in Reference [46], and the failure due to in-plane compressive and shear loadings has been studied in Reference [47].

1.3 Analysis of Tapered Laminates

Few researchers have conducted dynamic analysis of tapered composite structures. Farghaly and Gadelrab [48] studied the natural frequency of a one-span composite beam with a stepwise variable cross-section. They concluded that in addition to the results obtained for the conventional beams, the stiffness to mass ratio for the composite stepped cantilever beam may give higher natural frequencies than those made of conventional materials. Rao and Ganesan [49] investigated the harmonic response of tapered composite beams using finite element method based on a higher order shear deformation theory, considering uni-axial bending and ignoring the interlaminar shear stresses. Nabi and Ganesan [50] developed a general finite element based on a first-order deformation

theory to study the free vibration characteristics of laminated composite beams. They also conducted a parametric study on the influence of beam geometry and boundary conditions on natural frequencies. Karabalis and Beskos [51] used finite element method based on an exact flexural and axial stiffness matrix and approximate consistent mass and geometric stiffness matrices to study a linearly tapered beam with constant width. Tong *et al* [52] obtained an analytic solution for free and forced vibrations of stepped Timoshenko beams. Recently, Ganesan and Abd El-Maksoud [53] studied the dynamic analysis of uniform and mid-plane tapered composite beams by using conventional and higher order finite element formulations. Ganesan and Zabihollah [54, 55] presented the vibration and buckling analysis of uniform and tapered composite beams using conventional and advanced finite element methods based on the classical laminate theory and the first-order shear deformation theory. Ganesan and Chen [56] studied the free vibration response of tapered composite beams using hierarchical finite element method. Liu [57] conducted dynamic instability analysis of tapered composite plates using finite element and Ritz methods.

How to accurately describe the intralaminar and interlaminar stress state is the main task for researchers who studied the failure of tapered laminates. Finite element method is the most prevalent and powerful tool in dealing with geometrically complex problems such as tapered composites as applied by a large number of authors. As for other composite structures, the majority of approaches for failure analysis of tapered composites are based on finite element methods.

The full three-dimensional displacement based finite element approach was employed in some of the studies. Adams *et al* [58] investigated nonlinear material response and

thermal residual stresses of porous laminates with ply-drop-offs. Free-edge effects, however, were not included due to the generalized plane strain assumption imposed. Finite element meshing adopted in this model was very coarse in that at the ply-drop region no longitudinal mesh refinement was made. By using three-dimensional finite element models, Hoa *et al* [59] studied the interlaminar stresses in tapered laminates, in which the three-dimensional mesh at the ply-drop region was refined by a sub-modeling technique. This approach involved successive reduction and refinement of the mesh in the region of interest while retaining the results of the previous iteration as boundary conditions for the refined mesh. The purpose of this method was to have a refined mesh in the region of large stress gradients, while keeping the number of degrees of freedom of the solution required for each pass of the finite element solver within the capability of the computer that was available. As an extension of this work, Daoust and Hoa [60] employed three-dimensional finite elements with development of a more efficient computer program for parametric analysis.

Some of the studies employed Quasi-3D (Q3D) displacement based finite element approaches by reducing the domain into two-dimensional boundary problem based on the assumptions of either generalized plane deformation, or generalized plane strain. In both the theories all the cross sections would remain plane, and the stresses, geometric and material properties, and strains would be independent of the coordinate normal to the plane of analysis. The difference between these two theories lies in the fact that the former allows bending about the coordinates comprised of the analyzed plane and twisting about the remaining coordinate, of which the variables are independent. This theory is applicable to non-symmetric laminates under extension loading conditions

prescribed so as to accommodate deflections and rotations caused by the eccentricity of the load path. The latter is ideal for the analysis of long symmetric structures under tensile loading condition. Typical applications of Q3D approaches based on the above theories for transverse-ply-drop-off tapers include the work of Curry *et al* [61] and Kemp and Johnson [62]. In each of these models, the displacements normal to the plane of the model were still included and therefore these models had five or six nonzero components of strain. In Reference [62], four elements through the thickness in the plies in the vicinity of the drop-off were set up to perform the analysis as required to reasonably satisfy the continuity of intralaminar stresses and strains. The analyzed results show that the interlaminar stresses reach the maximum at the ply-drop location. Curry *et al* [61] applied global/local approach for the analysis of tapered composite plates. The global analysis was performed using the general-purpose computer program STAGS, while the local analysis for determining the three-dimensional state of stress in the vicinity of the dropped plies was based on the generalized plane deformation. Their study shows that interlaminar normal stress in the interface or resin layer reaches a maximum at the end of the dropped plies, and at the same location where the interlaminar shear stress is close to its maximum value. Variughese and Mukherjeel [63] also applied the global-local approach for the analysis of tapered composites. Considering that the drop-off needs not pass through a nodal line in global analysis, they developed drop-off elements that can be independent of the location of the drop-offs. The elements were used in global analysis to reduce the size of global structural matrix and showed more flexibility in meshing division. An accurate stress distribution around the ply-drop-offs was determined by local analysis with refined finite elements over the critical region and the input from the global

analysis as the boundary conditions. Good correlation was found by comparing the results obtained using this approach with published results obtained based on three-dimensional modeling.

Some of the authors, however, were more interested in performing plane stress and plane strain finite element analysis by reasonably reducing the domain of the problem into two dimensions in order to avoid the computationally intensive nature of three-dimensional finite element model. Salpekar *et al* [64] and Murri *et al* [65, 66 and 67] are among those authors who performed interlaminar analysis and furthermore determined strain energy release rate associated with the delamination growth.

Assumed stress hybrid finite element approaches were employed in some of the studies. Fish and Lee [68] first introduced hybrid elements in the analysis of tapered composites. They used 3D assumed hybrid elements to develop a methodology for the prediction of delamination onset in tapered composite laminates containing multiple ply-drop steps, and the study has shown that the assumed stress hybrid element used could provide more accurate stresses than linear displacement element.

The research group at University of Maryland employed this approach systematically. the topics that they studied with this method also include delamination failure mechanism analysis [69], delamination prevention techniques [70], effects of realistic taper geometries on the stress state at critical regions [71], shear-lag analysis about an internally-dropped ply [72], delamination of ply-drop configurations and tailoring concepts [73-75]. He [76] developed and applied partial hybrid finite element and physical concept based shear-lag models to examine interlaminar stress distributions in

the vicinity of ply terminations, and to investigate failure mechanisms using linear fracture mechanics methods.

In order to predict delamination onset and growth and hence the performance of the various laminates studied, some kind of failure analysis was applied. Two general approaches exist for this purpose. They are the strength-of-materials approach (stress-strength approach) and the strain-energy-release-rate approach (fracture mechanics approach). In the strength-of-materials approach, the local stress or strain state is compared to the material strength allowable. In the strain-energy-release-rate approach, which is based on fracture mechanics, the laminate is assumed to fail when the available strain energy of a delamination crack in a ply interface exceeds the critical strain energy release rate for the material. The present review is limited to the strength-of-materials approach.

In application of strength-of-material approach to perform delamination analysis, usually more than one failure criterion was used to predict the weakest location over the whole structure. Frequently, different criteria were used for prediction of in-plane and out-of-plane failures of the plies as well as for out-of-plane failure between plies.

Kemp and Johnson [62] used the maximum stress criterion to predict the failure in the resin-rich area surrounding the dropped plies, while applying the Tsai-Wu criterion for intralaminar failure prediction. With these criteria in consideration, they found that majority of the first failure events in either tension or compression were resin failures in a few cases for which failure occurred at the ply-drop. Both interlaminar and intralaminar failure criteria were used by Curry *et al* [61] for their analysis. The interlaminar criterion

they used, which is based on matrix failure mode developed by Hashin, was evaluated at all interfaces between plies with different fiber orientations in the local model, while the intralaminar criterion was a modification of Tsai-Wu criterion, in which only the strength parameters that correspond to the failure mode were included. Fish and Lee [68] used modified Tsai-Wu criterion to predict the out-of-plane failure of the composite laminates in their study. They introduced the average stress concept for the situations where the stress state is dominated by a single stress and applied it to the out-of-plane stress distributions obtained from the numerical analysis, thus the maximum stress failure was considered. On the basis of the assumption that the primary failure in the tapered composites is to be delamination and to occur in the inter-ply resin layer, Vizzini [71, 77] employed the von Mises stress criterion, an isotropic failure criterion, to be a measure of the overall stress state for a given configuration. In Reference [71], it was shown that the maximum von Mises stress in the realistic laminate with an ill-formed pocket modeled as to be four sided rather than triangular as is usually assumed, or with un-symmetric ply-drops, occurred around the last ply-drop-offs. The author found that the results agreed well with his finite element analysis, and further the von Mises stress for the laminate with a fracture void increased by more than 50%, which indicated that the presence of a void greatly affected the stress state around the ply-drop and that the interlaminar stress criterion that excludes voids will overpredict the onset of damage. In Reference [77], the von Mises criterion was used to determine the strength of the resin pocket at the discontinuity. Falling within the scatter of the experimental data for delamination initiation, this resin pocket model predicted very well the initiation of damage for the laminates dominated by the internal edge failure. Harrison and Johnson [78] used the

delamination fraction concept as a measure to investigate the effect of eccentricity and stiffness discontinuity on the tendency of laminates with dropped plies to delaminate. In combination with their mixed variational approach, they found that the highest delamination fraction value is contributed by both the interlaminar normal and shear stresses at ply-drop region and showed that it is the stiffness discontinuity rather than eccentricity of the laminate that has a larger influence on the interlaminar stresses and eventual delamination. Mortensen and Thomsen [79] applied a point stress criterion for prediction of delamination failure in composite laminates with external ply-drop-offs. The stress at a certain characteristic length away from the drop step was evaluated with a simplified analytical model. Delamination failure was considered to have occured if the calculated stress exceeded the strength of the inter-ply resin layers. An empirical formula for the characteristic length calculation and the respective characteristic length stress criterion were suggested. It was concluded that the proposed approach would work well due to the good match between experimental and analytical results.

1.4 Stochastic Analysis of Composite Laminate

Stock *et al* [80] and Fukuda [81] carried out the probabilistic analysis of composite strength and effective properties using the Monte Carlo simulation technique. The simulation procedure required extensive computational resources for any new set of structural parameters and properties of the constituents.

Composites have inherent scatter in their elastic and strength properties. A probabilistic model utilizing random material characteristic to predict damage evolution in orthotropic laminated composites is presented by Dzenis *et al* [82], Joshi and Frantziskonis [83] and

Larder [84]. Cassenti [85] investigated the probabilistic static failure of composite materials. Probabilistic failure strength analysis of graphite/epoxy cross-ply composite laminates has been performed by Fukunaga and Chou [86]. This paper treated the failure characteristics of (0/90/0) and (90/0/90) cross-ply laminates based upon the statistical strength analysis. The stress redistributions at the failure of the 90° ply were analyzed using a shear-lag model.

The well-known probabilistic theories for the tensile strength of unidirectional composites have been proposed by Rosen [87] and Zweben [88] and further developments have been reported in detail in References [89, 90]. These models give satisfactory strength estimation when the failure of the composite material is predominantly affected by the stochastic strength distribution of reinforcement fibers.

The analysis of structures, whether subjected to random or deterministic external loads, has been developed mainly under the assumption that the structure's parameters are deterministic quantities. In a significant number of circumstances, this assumption is not valid, and the probabilistic aspects of the structure need to be taken into account. The necessity to account for random effects in determining the response of a mechanical system is due, in general, to three different sources: random external loadings, random boundary conditions, and random material parameters. In the last twenty years the powerful finite element method has undergone various new developments to incorporate the randomness, and is now termed as Stochastic Finite Element Method (SFEM). The developments in this field are reviewed by Contreras [91], Vanmarcke *et al* [92], Benaroya and Rehak [93], Yamazaki *et al* [94], Ostoja-Starzewshi [95], and Vanmarcke

[94]. The stochastic finite element method is capable of dealing with random structural properties described by random fields very efficiently. Relatively recent developments, such as the weighted integral technique [97, 98], provide an accurate and consistent transition from continuous type random fields to discrete type stochastic finite elements.

Ramu and Ganesan [99] developed a new finite element method to analyze the structures with more than one parameter behaving in a stochastic manner using the Galerkin weighted residual method. The stochastic finite element analysis based on the local averages of random vector fields is formulated by Zhu *et al* [100] for eigenvalue problems. Jensen and Iwan [101] presented a method for the dynamic analysis of linear systems with uncertain parameters to stochastic excitation. Liu *et al* [102] studied the application of the SFEM in elastic/plastic dynamics with random material properties. Ghanem and Spanos [103] proposed a new method for the solution of problems involving material variability. The material property was modeled as a stochastic process. The method made use of a convergent orthogonal expansion of the process. Ganesan *et al* [104] developed a stochastic finite element method to solve the more general non-self-adjoint eigenvalue problems. Shinozuka *et al* [105] developed a method for the estimation of the structural reliability when a structure is subjected to loads that can be idealized in terms of a Gaussian random vector process. Ramu and Ganesan [106] analyzed the free vibrational characteristics of a beam-column, which had randomly varying Young's modulus and mass density and subjected to randomly distributed axial loading. In their study, the Hamilton's principle was used to formulate the problem using stochastic FEM. Ren *et al* [107] proposed a new version of finite element method for the mean and covariance functions of the displacement for bending of beams with spatially

random stiffness based on the variational principles. Sankar, Ramu and Ganesan [108] derived the sensitivities of SIF and COD of cracked structural systems to fluctuations in material property values and external loadings. In their study, a Taylor series expansion was used to express the SIF and COD in terms of averaged values. Sankar, Ramu and Ganesan [109] described an effective method for integrating the concepts of probabilistic structural mechanics with the finite element analysis for dynamic systems.

The successful application of the mechanics of composites for achieving safer and reliable designs is hindered by the inherent uncertain distributions of material and geometric properties. In recent years, composite structures involving random material properties have been studied by many researchers. Among them Liaw and Yang [110] developed a 16-dof quadrilateral stochastic laminated thin-plate element. Ganesan and Hoa [111] presented the stress analysis of composite structures with stochastic parameters. Nakagiri, Takabatake and Tani [112] presented a methodology of stochastic finite element method applied to the uncertain eigenvalue problem of linear vibration which arises from the fluctuation of the overall stiffness due to uncertain variation of the stacking sequence of composite laminates. Engelstad and Reddy [113] developed a probabilistic finite element analysis procedure for laminated composite shells. In their study, a total Lagrangian finite element formulation, employing a degenerated three-dimensional laminated composite shell element with the full Green-Lagrange strains and first-order shear deformable kinematics, was used. Chang and Yang [114] formulated a geometrically non-linear stochastic thin-plate finite element to study the reliability of fiber-reinforced laminates made of advanced composite materials. The modeling

involved two steps: a micro-mechanical simulation of the degradation of a small cell of the composite, and a random-damage finite element simulation of material failure.

Studies on the reliability of the static strength of fibrous composites can be classified into three groups: 1) studies that investigate experimentally the factors that effect the variation or the scatter of the strength using a number of specimens, 2) studies that analyze the variation of the strength theoretically using micro-mechanical models, 3) studies that analyze the reliability of the strength of unidirectional and laminated composites using a macroscopic failure criterion and fundamental data on the variations of the strengths along the principal directions. The strength and stiffness of composite materials change remarkably by changing the kinds, volume contents and orientations of the reinforcing fibers and stacking sequences, therefore, the optimum material design can be performed under a given loading condition. Mitsunori *et al* [115] have presented a method to evaluate the reliability of unidirectional fibrous composites under any plane stress condition, and the effects of various factors on the reliability were investigated. It has been found that the orientation angle that results in the maximum reliability and the optimum angle that corresponds to the design criterion vary with the variation in the applied stress in some cases. It has been found that the optimum fiber orientations of unidirectional composite materials under probabilistic loading conditions are found to be different from those under deterministic loading conditions. Miki *et al* [116] also proposed a simple and intuitive method called the interior tangent ellipsoid (ITE) method for the optimum design of composites under the action of loads with variations. Shaowen *et al* [117] presented a discussion on the optimum design of multiaxially laminated fibrous composites under probabilistic conditions of loads and material conditions. The

first-ply failure criterion is adopted for conducting the reliability analysis. Mitsunori *et al* [118] have presented a discussion on the optimum fiber orientation angles of multiaxial laminates based on reliability analysis. The probabilistic properties of the applied loads and the elastic constants of the ply material were discussed from the viewpoint of reliability and optimum design. The effects of the correlation between various random variables on the reliability and reliability-based design of composite plates subjected to buckling have been discussed by Kogiso *et al* [119], and the reliability was maximized in terms of the mean ply orientation angles. The study showed that reliability-based design ignoring correlation was sometimes less safe than even a deterministic buckling load maximization design when random variables are correlated. By viewing the composite lamina as a homogeneous solid whose directional strengths are random variables, Thomas and Wetherhold [120] proposed some physically plausible phenomenological rules for the redistribution of load after a lamina has failed within the confines of a laminate. Using a non-interactive criterion for demonstration purposes, laminate reliabilities are calculated assuming previously established load sharing rules for the redistribution of the load as the failure of the lamina occurs. Cohen [121] presented a composite vessel design approach that was based on the reliability and the probabilistic failure strength distribution concepts. This method was based on fiber strain-strength interference reliability theory. The fiber statistical strength distribution was analyzed using the Weibull distribution function.

1.5 Objectives of the thesis

The objectives of the present thesis are: (1) to develop a nonlinear finite element formulation that is based on the first-order shear deformation theory and the geometric

nonlinearity in the von Karman sense for the analysis of tapered composite plates; (2) to present a progressive failure simulation methodology for tapered laminates; (3) to predict the first-ply failure load, the ultimate failure load, the buckling load, the associated maximum transverse displacements, and locations and modes of failure of tapered laminated plates under the action of different kinds of loading, including uni-axial compression, bi-axial compression, in-plane positive shear, in plane negative shear, bi-axial compression combined with in-plane positive shear, and bi-axial compression combined with in-plane negative shear; (4) to investigate the influences of different taper configurations and laminate configurations on the progressive failure; (5) to study the stochastic progressive failure of tapered laminated plate under the action of biaxial compression combined with in-plane positive shear. Considering the excessive computational time involved, only one set of loading case, laminate configuration and taper configuration is considered. In all cases, the load-deflection curve is determined. The progressive failure analysis is conducted until the occurrence of ultimate failure and thus encompasses the post-buckling behavior of the tapered laminate.

1.6 Layout of the Thesis

In the present chapter, a brief introduction and literature review on progressive failure of composite laminates, stress analysis of tapered laminates and stochastic analysis of composite laminates, is given.

In Chapter 2, a nonlinear finite element formulation based on the first-order shear deformation theory and the geometric nonlinearity in the von Karman sense for the analysis of tapered composite plates is developed, and a progressive failure simulation methodology for tapered laminates is presented.

In Chapter 3, the progressive failure of tapered plates under the action of uni-axial and bi-axial compression is studied. The first-ply failure load, the ultimate failure load, the buckling load, the associated maximum transverse displacements, and the locations and modes of failure of tapered laminated plates under the action of compression are given.

In Chapter 4, the progressive failure of tapered plates under the action of in-plane positive shear and in-plane negative shear is studied. The first-ply failure load, the ultimate failure load, the buckling load, the associated maximum transverse displacements, and the locations and modes of failure of tapered laminated plates under the action of in-plane shear are given.

In Chapter 5, the progressive failure of tapered plates under the action of bi-axial compression combined with in-plane positive shear and bi-axial compression combined with in-plane negative shear is studied. The first-ply failure load, the ultimate failure load, the buckling load, the associated maximum transverse displacements, and the locations and modes of failure of tapered laminated plates under the action of bi-axial compression combined with in-plane shear are given.

In Chapter 6, the stochastic progressive failure of tapered laminated plate under the action of biaxial compression combined with in-plane positive shear is studied. The mean values and standard deviation values of the first-ply failure load, the ultimate failure load, and the corresponding maximum deflection are determined and given.

In Chapter 7, the conclusions of the present work and suggestions for future work are given.

Chapter 2

Formulations for Progressive Failure Analysis

2.1 Introduction

In this chapter, the stiffness and compliance matrices for a ply in a tapered composite plate are determined first, and then, the development of nonlinear finite element formulation for tapered composite plate is presented. The nonlinear finite element formulation is developed based on the first-order shear deformation theory and the geometric nonlinearity in the von Karman sense. The tensor polynomial form of failure criterion, a progressive failure simulation methodology, and the validation of the analysis are also given.

2.2 Stiffness and Compliance of a Ply in a Tapered Composite Plate

To determine the stiffness and compliance matrices of a single ply in a tapered laminate, three coordinate systems have been defined: the principal material coordinate system (x_1, x_2, x_3), the global coordinate system (x, y, z), and the local coordinate system (x', y', z'). These systems are shown in Figures 2.1 and 2.2. As can be seen in these figures, (i) the x_1 axis makes an angle θ with axis x', and axes x_3 and z' coincide with each other; (ii) the axis x' makes an angle α with x, and axes y' and y coincide with each other; (iii) the fiber orientation angle θ corresponds to rotation about x_3 (or z') axis; and (iv) taper angle α corresponds to rotation about y (or y'). To obtain the stiffness constants C_{ij} or the compliance constants S_{ij} in the global coordinate system, two

coordinate transformations have to be done. The first transformation is from the principal material coordinate system to the local coordinate system, and the second transformation is from the local coordinate system to the global coordinate system.

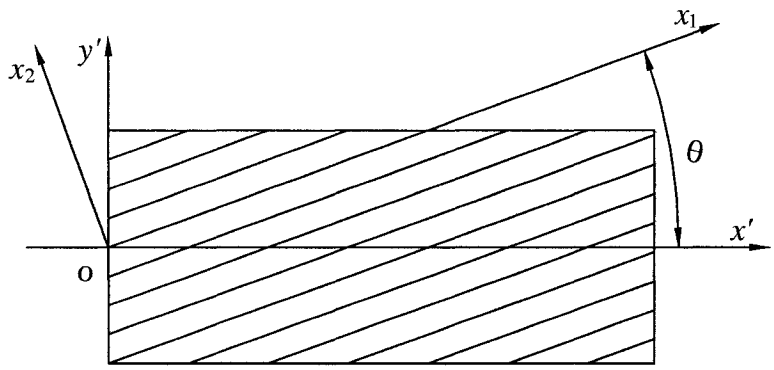

Figure 2.1 The principal material coordinate system (x_1, x_2, x_3) and the local coordinate system (x', y', z')

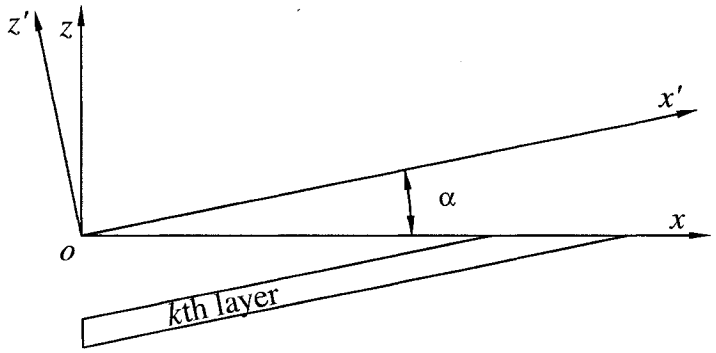

Figure 2.2 The global coordinate system (x, y, z) and the local coordinate system(x', y', z')

In the principal material coordinate system (x_1, x_2, x_3), strain-stress relation is defined as,

$$\begin{Bmatrix} \varepsilon_{11} \\ \varepsilon_{22} \\ \varepsilon_{33} \\ \gamma_{23} \\ \gamma_{13} \\ \gamma_{12} \end{Bmatrix} = \begin{bmatrix} S_{11} & S_{12} & S_{13} & 0 & 0 & 0 \\ S_{12} & S_{22} & S_{23} & 0 & 0 & 0 \\ S_{13} & S_{23} & S_{33} & 0 & 0 & 0 \\ 0 & 0 & 0 & S_{44} & 0 & 0 \\ 0 & 0 & 0 & 0 & S_{55} & 0 \\ 0 & 0 & 0 & 0 & 0 & S_{66} \end{bmatrix} \begin{Bmatrix} \sigma_{11} \\ \sigma_{22} \\ \sigma_{33} \\ \tau_{23} \\ \tau_{13} \\ \tau_{12} \end{Bmatrix} \tag{2.1a}$$

$$\begin{Bmatrix} \sigma_{11} \\ \sigma_{22} \\ \sigma_{33} \\ \tau_{23} \\ \tau_{13} \\ \tau_{12} \end{Bmatrix} = \begin{bmatrix} C_{11} & C_{12} & C_{13} & 0 & 0 & 0 \\ C_{12} & C_{22} & C_{23} & 0 & 0 & 0 \\ C_{13} & C_{23} & C_{33} & 0 & 0 & 0 \\ 0 & 0 & 0 & C_{44} & 0 & 0 \\ 0 & 0 & 0 & 0 & C_{55} & 0 \\ 0 & 0 & 0 & 0 & 0 & C_{66} \end{bmatrix} \begin{Bmatrix} \varepsilon_{11} \\ \varepsilon_{22} \\ \varepsilon_{33} \\ \gamma_{23} \\ \gamma_{13} \\ \gamma_{12} \end{Bmatrix} \tag{2.1b}$$

where, ε_{ij} and σ_{ij} are the strains and stresses in the principal material coordinate system (x_1, x_2, x_3), and S_{ij} and C_{ij} are the corresponding compliance and stiffness coefficients. Equations (2.1) can be expressed as:

$$\{\varepsilon\}_{123} = [S]_{123}\{\sigma\}_{123} \tag{2.2a}$$

$$\{\sigma\}_{123} = [C]_{123}\{\varepsilon\}_{123} \tag{2.2b}$$

where, $\{\varepsilon\}_{123}$ and $\{\sigma\}_{123}$ are strain and stress vectors in the principal material coordinate system (x_1, x_2, x_3); $[C]_{123}$ and $[S]_{123}$ are the stiffness and compliance matrices of the ply in the principal material coordinate system.

As can seen from Figure 2.1, there is an anticlockwise rotation of angle θ about x_3 (or z') from the local coordinate system (x', y', z') to the principal coordinate system (x_1, x_2, x_3) in the plane $x_1 o x_2$. The direction cosines of the local coordinate system (x', y', z') and the principal coordinate system (x_1, x_2, x_3) are shown in Table 2.1.

Table 2.1 Direction Cosines of $x'y'z'$ and $x_1x_2x_3$

	x_1	x_2	x_3
x'	$\cos\theta$	$-\sin\theta$	0
y'	$\sin\theta$	$\cos\theta$	0
z'	0	0	1

The stresses in the local coordinate system (x', y', z') can be expressed with respect to stresses in the principal coordinate system (x_1, x_2, x_3) as:

$$\begin{Bmatrix} \sigma_{x'} \\ \sigma_{y'} \\ \sigma_{z'} \\ \tau_{y'z'} \\ \tau_{x'z'} \\ \tau_{x'y'} \end{Bmatrix} = \begin{bmatrix} \cos^2\theta & \sin^2\theta & 0 & 0 & 0 & -2\cos\theta\sin\theta \\ \sin^2\theta & \cos^2\theta & 0 & 0 & 0 & 2\cos\theta\sin\theta \\ 0 & 0 & 1 & 0 & 0 & 0 \\ 0 & 0 & 0 & \cos\theta & \sin\theta & 0 \\ 0 & 0 & 0 & -\sin\theta & \cos\theta & 0 \\ \cos\theta\sin\theta & -\cos\theta\sin\theta & 0 & 0 & 0 & \cos^2\theta-\sin^2\theta \end{bmatrix} \begin{Bmatrix} \sigma_{11} \\ \sigma_{22} \\ \sigma_{33} \\ \tau_{23} \\ \tau_{13} \\ \tau_{12} \end{Bmatrix} \quad (2.3)$$

Or written in short form,

$$\{\sigma\}_{x'y'z'} = [T_{\sigma\theta}]\{\sigma\}_{123} \quad (2.4)$$

where θ is defined in Figure 2.1. $\{\sigma\}_{x'y'z'}$ is the stress vector in the local coordinate system (x', y', z'). $[T_{\sigma\theta}]$ is the stress transformation matrix that is due to the fiber orientation angle θ.

Similarly, the strains in the local coordinate system (x', y', z') can be defined as:

$$\begin{Bmatrix} \varepsilon_{x'} \\ \varepsilon_{y'} \\ \varepsilon_{z'} \\ \gamma_{y'z'} \\ \gamma_{x'z'} \\ \gamma_{x'y'} \end{Bmatrix} = \begin{bmatrix} \cos^2\theta & \sin^2\theta & 0 & 0 & 0 & -\cos\theta\sin\theta \\ \sin^2\theta & \cos^2\theta & 0 & 0 & 0 & \cos\theta\sin\theta \\ 0 & 0 & 1 & 0 & 0 & 0 \\ 0 & 0 & 0 & \cos\theta & \sin\theta & 0 \\ 0 & 0 & 0 & -\sin\theta & \cos\theta & 0 \\ 2\cos\theta\sin\theta & -2\cos\theta\sin\theta & 0 & 0 & 0 & \cos^2\theta-\sin^2\theta \end{bmatrix} \begin{Bmatrix} \varepsilon_1 \\ \varepsilon_2 \\ \varepsilon_3 \\ \gamma_{23} \\ \gamma_{13} \\ \gamma_{12} \end{Bmatrix} \quad (2.5)$$

Or written in short form:

$$\{\varepsilon\}_{x'y'z'} = [T_{\sigma\theta}]\{\varepsilon\}_{123} \tag{2.6}$$

Likewise, $[T_{\varepsilon\theta}]$ is the strain transformation matrix that is due to the fiber orientation angle θ. The relationship between the strain transformation matrix and the stress transformation matrix is defined as:

$$[T_{\sigma\theta}]^{-1} = [T_{\varepsilon\theta}]^{T} \tag{2.7}$$

$$[T_{\varepsilon\theta}]^{-1} = [T_{\sigma\theta}]^{T} \tag{2.8}$$

Substituting Equations (2.2a) and (2.4) into Equation (2.6), it can be show that:

$$\{\varepsilon\}_{x'y'z'} = [T_{\varepsilon\theta}]\,[S]_{123}\,[T_{\sigma\theta}]^{-1}\{\sigma\}_{x'y'z'} = [S]_{x'y'z}\{\sigma\}_{x'y'z'} \tag{2.9}$$

Thus the compliance matrix in the local coordinate system (x', y', z') can be defined as:

$$[S]_{x'y'z'} = [T_{\varepsilon\theta}]\,[S]_{123}\,[T_{\sigma\theta}]^{-1} \tag{2.10}$$

Similarly, the stiffness matrix in the local coordinate system (x', y', z') can be defined as:

$$[C']_{x'y'z'} = [T_{\sigma\theta}]\,[C]_{123}\,[T_{\varepsilon\theta}]^{-1} \tag{2.11}$$

The second transformation is from local coordinate system to the global coordinate system. As shown in Figure 2.2, there is an anticlockwise rotation of angle α about y' (or y) from the global coordinate system (x, y, z) to the local coordinate system (x', y', z'). Note that all the layers below the mid-plane have a positive oblique angle α and the others above the mid-plane have a negative oblique angle $-\alpha$. The direction cosines of the local coordinate system (x', y', z') and the principal coordinate system (x_1, x_2, x_3) are shown in Table 2.2.

Table 2.2 Direction Cosines of $x'y'z'$ and xyz

	x'	y'	z'
x	$\cos\alpha$	0	$-\sin\alpha$
y	0	1	0
z	$\sin\alpha$	0	$\cos\alpha$

The stresses in the global coordinate system (x, y, z) can be expressed with respect to stresses in the local coordinate system (x', y', z') as:

$$\begin{Bmatrix}\sigma_x\\ \sigma_y\\ \sigma_z\\ \tau_{yz}\\ \tau_{xz}\\ \tau_{xy}\end{Bmatrix}=\begin{bmatrix}\cos^2\alpha & 0 & \sin^2\alpha & 0 & -2\cos\alpha\sin\alpha & 0\\ 0 & 1 & 0 & 0 & 0 & 0\\ \sin^2\alpha & 0 & \cos^2\alpha & 0 & 2\cos\alpha\sin\alpha & 0\\ 0 & 0 & 0 & \cos\alpha & 0 & \sin\alpha\\ \cos\alpha\sin\alpha & 0 & -\cos\alpha\sin\alpha & 0 & \cos^2\alpha-\sin^2\alpha & 0\\ 0 & 0 & 0 & -\sin\alpha & 0 & \cos\alpha\end{bmatrix}\begin{Bmatrix}\sigma_{x'}\\ \sigma_{y'}\\ \sigma_{z'}\\ \tau_{y'z'}\\ \tau_{x'z'}\\ \tau_{x'y'}\end{Bmatrix} \tag{2.12}$$

Written in short form:

$$\{\sigma\}_{xyz}=[T_{\sigma\alpha}]\{\sigma\}_{x'y'z'} \tag{2.13}$$

where $\{\sigma\}_{xyz}$ is the stress vector in the global coordinate system (x, y, z). $[T_{\sigma\alpha}]$ is the stress transformation matrix that is due to the taper angle α.

Similarly, the strains in the global coordinate system (x, y, z) can be defined as:

$$\begin{Bmatrix}\varepsilon_x\\ \varepsilon_y\\ \varepsilon_z\\ \gamma_{yz}\\ \gamma_{xz}\\ \gamma_{xy}\end{Bmatrix}=\begin{bmatrix}\cos^2\alpha & 0 & \sin^2\alpha & 0 & -\cos\alpha\sin\alpha & 0\\ 0 & 1 & 0 & 0 & 0 & 0\\ \sin^2\alpha & 0 & \cos^2\alpha & 0 & \cos\alpha\sin\alpha & 0\\ 0 & 0 & 0 & \cos\alpha & 0 & \sin\alpha\\ 2\cos\alpha\sin\alpha & 0 & -2\cos\alpha\sin\alpha & 0 & \cos^2\alpha-\sin^2\alpha & 0\\ 0 & 0 & 0 & -\sin\alpha & 0 & \cos\alpha\end{bmatrix}\begin{Bmatrix}\varepsilon_{x'}\\ \varepsilon_{y'}\\ \varepsilon_{z'}\\ \gamma_{y'z'}\\ \gamma_{x'z'}\\ \gamma_{x'y'}\end{Bmatrix} \tag{2.14}$$

Written in short form:

$$\{\varepsilon\}_{xyz}=[T_{\varepsilon\alpha}]\{\varepsilon\}_{x'y'z'} \tag{2.15}$$

Likewise, $\{\varepsilon\}$ is the strain vector in the global coordinate system (x, y, z). $[T_{\varepsilon\alpha}]$ is the strain transformation matrix that is due to the taper angle α. The relationship between $[T_{\varepsilon\alpha}]$ and $[T_{\sigma\alpha}]$ is defined as:

$$[T_{\sigma\alpha}]^{-1} = [T_{\varepsilon\alpha}]^T \tag{2.16}$$

$$[T_{\varepsilon\alpha}]^{-1} = [T_{\sigma\alpha}]^T \tag{2.17}$$

Substituting Equations (2.9) and (2.13) into Equation (2.15), it can be shown that:

$$\begin{aligned}\{\varepsilon\}_{xyz} &= [S]_{xyz}\{\sigma\}_{xyz} = [T_{\varepsilon\alpha}]\,[S]_{x'y'z'}\,[T_{\sigma\alpha}]^{-1}\{\sigma\}_{xyz} \\ &= [T]_{\varepsilon\alpha}\cdot[T]_{\varepsilon\theta}\cdot[S]_{123}\cdot[T]_{\sigma\theta}^{-1}\cdot[T]_{\sigma\alpha}^{-1}\{\sigma\}_{xyz}\end{aligned} \tag{2.18}$$

Then, the compliance matrix in the global coordinate system can be defined as:

$$[S]_{xyz} = [T_{\varepsilon\alpha}]\,[S]_{x'y'z'}\,[T_{\sigma\alpha}]^{-1} = [T]_{\varepsilon\alpha}\cdot[T]_{\varepsilon\theta}\cdot[S]_{123}\cdot[T]_{\sigma\theta}^{-1}\cdot[T]_{\sigma\alpha}^{-1} \tag{2.19}$$

Similarly, the stiffness matrix in the global coordinate system can be defined as:

$$[C]_{xyz} = [T]_{\sigma\alpha}\cdot[T]_{\sigma\theta}\cdot[C]_{123}\cdot[T]_{\varepsilon\theta}^{-1}\cdot[T]_{\varepsilon\alpha}^{-1}\,[\overline{C}] = [T_{\sigma\alpha}]\,[C']\,[T_{\varepsilon\alpha}]^{-1} \tag{2.20}$$

Hence, in the global coordinate system, the stress-strain relationship for a ply in a tapered laminate can be defined as:

$$\begin{Bmatrix}\sigma_x\\ \sigma_y\\ \sigma_z\\ \tau_{yz}\\ \tau_{xz}\\ \tau_{xy}\end{Bmatrix} = \begin{bmatrix}\overline{C}_{11} & \overline{C}_{12} & \overline{C}_{13} & \overline{C}_{14} & \overline{C}_{15} & \overline{C}_{16}\\ & \overline{C}_{22} & \overline{C}_{23} & \overline{C}_{24} & \overline{C}_{25} & \overline{C}_{26}\\ & & \overline{C}_{33} & \overline{C}_{34} & \overline{C}_{35} & \overline{C}_{36}\\ & & & \overline{C}_{44} & \overline{C}_{45} & \overline{C}_{46}\\ & & & & \overline{C}_{55} & \overline{C}_{56}\\ sym & & & & & \overline{C}_{66}\end{bmatrix}\begin{Bmatrix}\varepsilon_x\\ \varepsilon_y\\ \varepsilon_z\\ \gamma_{yz}\\ \gamma_{xz}\\ \gamma_{xy}\end{Bmatrix} \tag{2.21}$$

Written in short form:

$$\{\sigma\}_{xyz} = [C]_{xyz}\{\varepsilon\}_{xyz} \tag{2.22}$$

2.3 The First-order Shear Deformation Theory

Composite laminates are formed by stacking layers of composite materials with different orientations. By construction, composite laminates have their planar dimensions one to two orders of magnitude larger than their thickness. Often laminates are used in applications that require membrane and bending strengths. Composite laminates are most often analyzed using Equivalent Single-Layer theories (ESL).

The simplest ESL laminated plate theory is Classical Laminated Plate Theory (CLPT) which is an extension of the Kirchhoff (classical) plate theory to laminated composite plates. It is based on the displacement field:

$$u(x,y,z) = u_0(x,y) - z\frac{\partial w_0}{\partial x} \tag{2.23}$$

$$v(x,y,z) = v_0(x,y) - z\frac{\partial w_0}{\partial y} \tag{2.24}$$

$$w(x,y,z) = w_0(x,y) \tag{2.25}$$

The CLPT assumes that the following Kirchhoff hypotheses hold:

(1) Straight lines perpendicular to the midsurface (i.e., transverse normals) before deformation remain straight after the deformation.

(2) The transverse normals do not experience elongation (i.e., there are inextensible).

(3) The transverse normals rotate such that they remain perpendicular to the midsurface after deformation.

In the First-order Shear Deformation laminated plate Theory (FSDT), the Kirchhoff hypothesis is relaxed by removing the third hypothesis; i.e., the transverse normals do not remain perpendicular to the midsurface after deformation. This amounts to including transverse shear strains in the theory. The resulting displacement field is given by:

$$u(x,y,z)=u_0(x,y)+z\phi_x \tag{2.26}$$

$$v(x,y,z)=v_0(x,y)+z\phi_y \tag{2.27}$$

$$w(x,y,z)=w_0(x,y) \tag{2.28}$$

where (u_0,v_0,w_0) denote the displacements of a point on the plane $z=0$. Note that

$$\frac{\partial u}{\partial z}=\phi_x,\frac{\partial v}{\partial z}=\phi_y \tag{2.29}$$

which indicate that ϕ_x and ϕ_y are the rotations of a transverse normal about y- and x-axes, respectively.

2.4 The Nonlinear Strain-displacement Relations

The von Karman assumption: the displacements u and v are small and the displacement w is large. Correspondingly, the products and square of the in-plane displacement gradients are neglected in the nonlinear strain-displacement relations.

$$\varepsilon_x=\frac{\partial u}{\partial x}+\frac{1}{2}\left[\left(\frac{\partial u}{\partial x}\right)^2+\left(\frac{\partial v}{\partial x}\right)^2+\left(\frac{\partial w}{\partial x}\right)^2\right]=\frac{\partial u}{\partial x}+\frac{1}{2}\left(\frac{\partial w}{\partial x}\right)^2 \tag{2.30}$$

$$\varepsilon_y=\frac{\partial v}{\partial y}+\frac{1}{2}\left[\left(\frac{\partial u}{\partial y}\right)^2+\left(\frac{\partial v}{\partial y}\right)^2+\left(\frac{\partial w}{\partial y}\right)^2\right]=\frac{\partial v}{\partial y}+\frac{1}{2}\left(\frac{\partial w}{\partial y}\right)^2 \tag{2.31}$$

$$\varepsilon_z=\frac{\partial w}{\partial z}+\frac{1}{2}\left[\left(\frac{\partial u}{\partial z}\right)^2+\left(\frac{\partial v}{\partial z}\right)^2+\left(\frac{\partial w}{\partial z}\right)^2\right]=\frac{\partial w}{\partial z}+\frac{1}{2}\left(\frac{\partial w}{\partial z}\right)^2=0 \tag{2.32}$$

$$\gamma_{xy}=\frac{\partial v}{\partial x}+\frac{\partial u}{\partial y}+\frac{\partial u}{\partial x}\frac{\partial u}{\partial y}+\frac{\partial v}{\partial x}\frac{\partial v}{\partial y}+\frac{\partial w}{\partial x}\frac{\partial w}{\partial y}=\frac{\partial v}{\partial x}+\frac{\partial u}{\partial y}+\frac{\partial w}{\partial x}\frac{\partial w}{\partial y} \tag{2.33}$$

$$\gamma_{yz}=\frac{\partial v}{\partial z}+\frac{\partial w}{\partial y}+\frac{\partial u}{\partial y}\frac{\partial u}{\partial z}+\frac{\partial v}{\partial y}\frac{\partial v}{\partial z}+\frac{\partial w}{\partial y}\frac{\partial w}{\partial z}=\frac{\partial v}{\partial z}+\frac{\partial w}{\partial y}+\frac{\partial w}{\partial y}\frac{\partial w}{\partial z} \tag{2.34}$$

$$\gamma_{xz} = \frac{\partial u}{\partial z} + \frac{\partial w}{\partial x} + \frac{\partial u}{\partial x}\frac{\partial u}{\partial z} + \frac{\partial v}{\partial x}\frac{\partial v}{\partial z} + \frac{\partial w}{\partial x}\frac{\partial w}{\partial z} = \frac{\partial u}{\partial z} + \frac{\partial w}{\partial x} + \frac{\partial w}{\partial x}\frac{\partial w}{\partial z} \tag{2.35}$$

Substituting equations (2.26-2.28) into the nonlinear strain-displacement relations (2.30-2.35), it can be shown that:

$$\varepsilon_x = \frac{\partial u}{\partial x} + \frac{1}{2}\left(\frac{\partial w}{\partial x}\right)^2 = \frac{\partial u_0}{\partial x} + z\frac{\partial \phi_x}{\partial x} + \frac{1}{2}\left(\frac{\partial w_0}{\partial x}\right)^2 = \varepsilon_x^0 + zk_x \tag{2.36}$$

$$\varepsilon_y = \frac{\partial v}{\partial y} + \frac{1}{2}\left(\frac{\partial w}{\partial y}\right)^2 = \frac{\partial v_0}{\partial y} + z\frac{\partial \phi_y}{\partial y} + \frac{1}{2}\left(\frac{\partial w_0}{\partial y}\right)^2 = \varepsilon_y^0 + zk_y \tag{2.37}$$

$$\varepsilon_z = \frac{\partial w}{\partial z} + \frac{1}{2}\left(\frac{\partial w}{\partial z}\right)^2 = 0 \tag{2.38}$$

$$\gamma_{xy} = \frac{\partial v}{\partial x} + \frac{\partial u}{\partial y} + \frac{\partial w}{\partial x}\frac{\partial w}{\partial y} = \frac{\partial v_0}{\partial x} + \frac{\partial u_0}{\partial y} + \frac{\partial w_0}{\partial x}\frac{\partial w_0}{\partial y} + z\left(\frac{\partial \phi_x}{\partial y} + \frac{\partial \phi_y}{\partial x}\right) = \gamma_{xy}^0 + zk_{xy} \tag{2.39}$$

$$\gamma_{yz} = \frac{\partial v}{\partial z} + \frac{\partial w}{\partial y} + \frac{\partial w}{\partial y}\frac{\partial w}{\partial z} = \frac{\partial w_0}{\partial y} + \phi_y = \gamma_{yz}^0 \tag{2.40}$$

$$\gamma_{xz} = \frac{\partial u}{\partial z} + \frac{\partial w}{\partial x} + \frac{\partial w}{\partial x}\frac{\partial w}{\partial z} = \frac{\partial w_0}{\partial x} + \phi_x = \gamma_{xz}^0 \quad (\frac{\partial w}{\partial z} = 0) \tag{2.41}$$

where

$$\varepsilon_x^0 = \frac{\partial u_0}{\partial x} + \frac{1}{2}\left(\frac{\partial w_0}{\partial x}\right)^2 \tag{2.42}$$

$$k_x = \frac{\partial \phi_x}{\partial x} \tag{2.43}$$

$$\varepsilon_y^0 = \frac{\partial v_0}{\partial y} + \frac{1}{2}\left(\frac{\partial w_0}{\partial y}\right)^2 \tag{2.44}$$

$$k_y = \frac{\partial \phi_y}{\partial y} \tag{2.45}$$

$$\gamma_{xy}^0 = \frac{\partial v_0}{\partial x} + \frac{\partial u_0}{\partial y} + \frac{\partial w_0}{\partial x}\frac{\partial w_0}{\partial y} \tag{2.46}$$

$$k_{xy} = \frac{\partial \phi_x}{\partial y} + \frac{\partial \phi_y}{\partial x} \tag{2.47}$$

$$\gamma_{yz}^0 = \frac{\partial w_0}{\partial y} + \phi_y \tag{2.48}$$

$$\gamma_{xz}^0 = \frac{\partial w_0}{\partial x} + \phi_x \tag{2.49}$$

2.5 Nonlinear Response of Tapered Composite Plate

The force and moment resultants N_i and M_i are defined as:

$$\begin{Bmatrix} N_x \\ N_y \\ N_{xy} \end{Bmatrix} = \int_{-\frac{h}{2}}^{\frac{h}{2}} \begin{Bmatrix} \sigma_x \\ \sigma_y \\ \tau_{xy} \end{Bmatrix} dz = \sum_{k=1}^{n} \int_{z_{k-1}}^{z_k} \begin{Bmatrix} \sigma_x \\ \sigma_y \\ \tau_{xy} \end{Bmatrix} dz \tag{2.50}$$

$$\begin{Bmatrix} M_x \\ M_y \\ M_{xy} \end{Bmatrix} = \int_{-\frac{h}{2}}^{\frac{h}{2}} \begin{Bmatrix} \sigma_x \\ \sigma_y \\ \tau_{xy} \end{Bmatrix} z dz = \sum_{k=1}^{n} \int_{z_{k-1}}^{z_k} \begin{Bmatrix} \sigma_x \\ \sigma_y \\ \tau_{xy} \end{Bmatrix} z dz \tag{2.51}$$

$$\begin{Bmatrix} Q_{yz} \\ Q_{xz} \end{Bmatrix} = \int_{-\frac{h}{2}}^{\frac{h}{2}} \begin{Bmatrix} \tau_{yz} \\ \tau_{xz} \end{Bmatrix} dz = \sum_{k=1}^{n} \int_{z_{k-1}}^{z_k} \begin{Bmatrix} \tau_{yz} \\ \tau_{xz} \end{Bmatrix} dz \tag{2.52}$$

From Equation (2.21), the equation for σ_x is defined as:

$$\sigma_x = \overline{C}_{11}\varepsilon_x + \overline{C}_{12}\varepsilon_y + \overline{C}_{13}\varepsilon_z + \overline{C}_{14}\gamma_{yz} + \overline{C}_{15}\gamma_{xz} + \overline{C}_{16}\gamma_{xy} \tag{2.53}$$

Substituting Equations (2.36-2.41) into the Equation (2.53), it can be shown that:

$$\begin{aligned} \sigma_x &= \overline{C}_{11}\left(\varepsilon_x^0 + zk_x\right) + \overline{C}_{12}\left(\varepsilon_y^0 + zk_y\right) + \overline{C}_{14}\gamma_{yz}^0 + \overline{C}_{15}\gamma_{xz}^0 + \overline{C}_{16}(\gamma_{xy}^0 + zk_{xy}) \\ &= \overline{C}_{11}\varepsilon_x^0 + \overline{C}_{12}\varepsilon_y^0 + \overline{C}_{16}\gamma_{xy}^0 + \overline{C}_{11}zk_x + \overline{C}_{12}zk_y + \overline{C}_{16}zk_{xy} + \overline{C}_{14}\gamma_{yz}^0 + \overline{C}_{15}\gamma_{xz}^0 \end{aligned} \tag{2.54}$$

Substituting Equation (2.54) into the equation for N_x in the Equation (2.50), it can be

shown that:

$$N_x = \int_{-\frac{h}{2}}^{\frac{h}{2}} \sigma_x dz = \int_{-\frac{h}{2}}^{\frac{h}{2}} (\overline{C}_{11}\varepsilon_x^0 + \overline{C}_{12}\varepsilon_y^0 + \overline{C}_{16}\gamma_{xy}^0 + \overline{C}_{11}zk_x + \overline{C}_{12}zk_y + \overline{C}_{16}zk_{xy} + \overline{C}_{14}\gamma_{yz}^0 + \overline{C}_{15}\gamma_{xz}^0)dz$$
$$= A_{11}\varepsilon_x^0 + A_{12}\varepsilon_y^0 + A_{16}\gamma_{xy}^0 + B_{11}k_x + B_{12}k_y + B_{16}k_{xy} + A_{14}\gamma_{yz}^0 + A_{15}\gamma_{xz}^0 . \quad (2.55)$$

Similarly the equations for other stress resultants can be obtained. They are written in the following form.

$$\begin{Bmatrix} N_x \\ N_y \\ N_{xy} \\ M_x \\ M_y \\ M_{xy} \\ Q_{yz} \\ Q_{xz} \end{Bmatrix} = \begin{bmatrix} A_{11} & A_{12} & A_{16} & B_{11} & B_{12} & B_{16} & kA_{14} & kA_{15} \\ A_{21} & A_{22} & A_{26} & B_{21} & B_{22} & B_{26} & kA_{24} & kA_{25} \\ A_{61} & A_{62} & A_{66} & B_{61} & B_{62} & B_{66} & kA_{64} & kA_{65} \\ B_{11} & B_{12} & B_{16} & D_{11} & D_{12} & D_{16} & kB_{14} & kB_{15} \\ B_{21} & B_{22} & B_{26} & D_{21} & D_{22} & D_{26} & kB_{24} & kB_{25} \\ B_{61} & B_{62} & B_{66} & D_{61} & D_{62} & D_{66} & kB_{64} & kB_{65} \\ kA_{41} & kA_{42} & kA_{64} & kB_{41} & kB_{42} & kB_{46} & kA_{44} & kA_{45} \\ kA_{51} & kA_{52} & kA_{56} & kB_{51} & kB_{52} & kB_{56} & kA_{54} & kA_{55} \end{bmatrix} \begin{Bmatrix} \varepsilon_x^0 \\ \varepsilon_y^0 \\ \gamma_{xy}^0 \\ k_x \\ k_y \\ k_{xy} \\ \gamma_{yz}^0 \\ \gamma_{xz}^0 \end{Bmatrix} \quad (2.56)$$

Written in short form,

$$\{N\} = [F]\{\varepsilon\} \quad (2.57)$$

where, $A_{ij} = \int_{-\frac{h}{2}}^{\frac{h}{2}} \overline{C}_{ij} dz$ i, j = 1, 2, 4, 5, 6 (2.58)

$$B_{ij} = \int_{-\frac{h}{2}}^{\frac{h}{2}} \overline{C}_{ij} z dz \quad \text{i, j = 1, 2, 4, 5, 6} \quad (2.59)$$

$$D_{ij} = \int_{-\frac{h}{2}}^{\frac{h}{2}} \overline{C}_{ij} z^2 dz \quad \text{i, j = 1, 2, 6} \quad (2.60)$$

where A_{ij} is the extensional stiffness; D_{ij} is bending stiffness; and B_{ij} is bending-extensional coupling stiffness; $[F]^T = [F]$. In Equation (2.56), k is the shear correction

factor, and $k = 5/6$.

The strain matrix can be decomposed into two parts:

$$\{\varepsilon\} = \{\varepsilon_L\} + \{\varepsilon_N\} = \begin{Bmatrix} \dfrac{\partial u_0}{\partial x} \\ \dfrac{\partial v_0}{\partial y} \\ \dfrac{\partial u_0}{\partial y} + \dfrac{\partial v_0}{\partial x} \\ \dfrac{\partial \phi_x}{\partial x} \\ \dfrac{\partial \phi_y}{\partial y} \\ \dfrac{\partial \phi_x}{\partial y} + \dfrac{\partial \phi_y}{\partial x} \\ \phi_y + \dfrac{\partial w_0}{\partial y} \\ \phi_x + \dfrac{\partial w_0}{\partial x} \end{Bmatrix} + \begin{Bmatrix} \dfrac{1}{2}\left(\dfrac{\partial w_0}{\partial x}\right)^2 \\ \dfrac{1}{2}\left(\dfrac{\partial w_0}{\partial y}\right)^2 \\ \dfrac{\partial w_0}{\partial y}\dfrac{\partial w_0}{\partial x} \\ 0 \\ 0 \\ 0 \\ 0 \\ 0 \end{Bmatrix} \tag{2.61}$$

where

$$\{\varepsilon_L\} = \left[\frac{\partial u_0}{\partial x} \quad \frac{\partial v_0}{\partial y} \quad \frac{\partial u_0}{\partial y} + \frac{\partial v_0}{\partial x} \quad \frac{\partial \phi_x}{\partial x} \quad \frac{\partial \phi_y}{\partial y} \quad \frac{\partial \phi_x}{\partial y} + \frac{\partial \phi_y}{\partial x} \quad \phi_y + \frac{\partial w_0}{\partial y} \quad \phi_x + \frac{\partial w_0}{\partial x} \right]^T \tag{2.62}$$

$$\{\varepsilon_N\} = \begin{Bmatrix} \dfrac{1}{2}\left(\dfrac{\partial w_0}{\partial x}\right)^2 \\ \dfrac{1}{2}\left(\dfrac{\partial w_0}{\partial y}\right)^2 \\ \dfrac{\partial w_0}{\partial y}\dfrac{\partial w_0}{\partial x} \\ 0 \\ 0 \\ 0 \\ 0 \\ 0 \end{Bmatrix} \tag{2.63}$$

It is known that for the uniform-thickness laminate, A_{ij}, B_{ij}, and D_{ij} are all constants throughout the entire plate before the onset of first-ply failure. If the lay-up is symmetric, B_{ij} are equal to zero. But for the tapered laminate, because some plies are dropped off, none of the coefficients A_{ij}, B_{ij} and D_{ij} are constant within the plate. In addition, for taper configurations B (Staircase arrangement), C (Overlapping dropped plies) and D (Continuous plies interspersed), they are also discontinuous at the ply drop-off locations. For thickness-tapered laminate, before the onset of first-ply failure, A_{ij}, B_{ij} and D_{ij} are all functions of x for all taper configurations and are continuous or discontinuous depending on the taper configuration. Even if the lay-up is symmetric, B_{ij} are not necessarily equal to zero, because all the layers below the mid-plane have a positive oblique angle α and the others above the mid-plane have a negative oblique angle $-\alpha$.

2.6 Energy Formulation, Displacement Field and Finite Element Equations

The minimum potential energy principle is considered in the analysis of tapered composite plate. The total potential energy Π is expressed as the sum of strain energy U and the potential energy of external loads W. For the plate subjected to uni-axial compression at the right end, U, W and Π are defined as:

$$\Pi = U + W \tag{2.64}$$

$$U = \frac{1}{2}\int_{\Omega}\{N\}^{T}\{\varepsilon\}d\Omega = \frac{1}{2}\int_{\Omega}\{\varepsilon\}^{T}[F]^{T}\{\varepsilon\}d\Omega = \frac{1}{2}\int_{\Omega}\{\varepsilon\}^{T}[F]\{\varepsilon\}d\Omega \tag{2.65}$$

$$W = -\int_{0}^{b} N_x u_0\Big|_{x=a} dy \tag{2.66}$$

Substituting Equation (2.61) into Equation (2.65), it can be shown that:

$$
\begin{aligned}
U &= \frac{1}{2}\int_{\Omega}\{\varepsilon\}^T[F]\{\varepsilon\}d\Omega \\
&= \frac{1}{2}\int_{\Omega}(\{\varepsilon_L\}+\{\varepsilon_N\})^T[F](\{\varepsilon_L\}+\{\varepsilon_N\})d\Omega \\
&= \frac{1}{2}\int_{\Omega}\{\varepsilon_L\}^T[F]\{\varepsilon_L\}d\Omega+\frac{1}{2}\int_{\Omega}\{\varepsilon_L\}^T[F]\{\varepsilon_N\}d\Omega+ \\
&\qquad \frac{1}{2}\int_{\Omega}\{\varepsilon_N\}^T[F]\{\varepsilon_L\}d\Omega+\frac{1}{2}\int_{\Omega}\{\varepsilon_N\}^T[F]\{\varepsilon_N\}d\Omega \\
&= \frac{1}{2}\int_{\Omega}\{\varepsilon_L\}^T[F]\{\varepsilon_L\}d\Omega+\int_{\Omega}\{\varepsilon_L\}^T[F]\{\varepsilon_N\}d\Omega+\frac{1}{2}\int_{\Omega}\{\varepsilon_N\}^T[F]\{\varepsilon_N\}d\Omega \\
&= U_L+U_{N1}+U_{N2}
\end{aligned}
\tag{2.67}
$$

where the linear part is defined as:

$$U_L = \frac{1}{2}\int_{\Omega}\{\varepsilon_L\}^T[F]\{\varepsilon_L\}d\Omega \tag{2.68}$$

Next nonlinear part 1 is defined as:

$$U_{N1} = \int_{\Omega}\{\varepsilon_L\}^T[F]\{\varepsilon_N\}d\Omega \tag{2.69}$$

Nonlinear part 2 is defined as:

$$U_{N2} = \frac{1}{2}\int_{\Omega}\{\varepsilon_N\}^T[F]\{\varepsilon_N\}d\Omega \tag{2.70}$$

In equation (2.70), the following assumption is considered:

$$\frac{1}{2}\int_{\Omega}\{\varepsilon_L\}^T[F]\{\varepsilon_N\}d\Omega = \frac{1}{2}\int_{\Omega}\{\varepsilon_N\}^T[F]\{\varepsilon_L\}d\Omega \tag{2.71}$$

The nine-node Lagrange element that has five degrees of freedom per node is used in the analysis. The element is shown in Figure 2.3. The five degrees of freedom are: the translation displacement in the x, y, and z directions that are u, v, and w respectively, and rotations ϕ_x and ϕ_y due to shear deformation. The displacement field is defined as:

$$u = \sum_{i=1}^{9} \overline{N}_i u_i \quad , \quad v = \sum_{i=1}^{9} \overline{N}_i v_i \quad , \quad w = \sum_{i=1}^{9} \overline{N}_i w_i \quad , \quad \phi_x = \sum_{i=1}^{9} \overline{N}_i \phi_{xi} \quad , \quad \phi_y = \sum_{i=1}^{9} \overline{N}_i \phi_{yi} \tag{2.72}$$

where $\overline{N}_i(x, y)$ are the Lagrange shape functions that are given below.

$$\overline{N}_1 = \frac{(x - x_2)(x - x_3)(y - y_4)(y - y_7)}{(x_1 - x_2)(x_1 - x_3)(y_1 - y_4)(y_1 - y_7)} \tag{2.73}$$

$$\overline{N}_2 = \frac{(x - x_1)(x - x_3)(y - y_4)(y - y_7)}{(x_2 - x_1)(x_2 - x_3)(y_2 - y_4)(y_2 - y_7)} \tag{2.74}$$

$$\overline{N}_3 = \frac{(x - x_1)(x - x_2)(y - y_4)(y - y_7)}{(x_3 - x_2)(x_3 - x_2)(y_3 - y_4)(y_3 - y_7)} \tag{2.75}$$

$$\overline{N}_4 = \frac{(x - x_2)(x - x_3)(y - y_1)(y - y_7)}{(x_4 - x_2)(x_4 - x_3)(y_4 - y_1)(y_4 - y_7)} \tag{2.76}$$

$$\overline{N}_5 = \frac{(x - x_1)(x - x_3)(y - y_1)(y - y_7)}{(x_5 - x_1)(x_5 - x_3)(y_5 - y_1)(y_5 - y_7)} \tag{2.77}$$

$$\overline{N}_6 = \frac{(x - x_1)(x - x_2)(y - y_1)(y - y_7)}{(x_6 - x_1)(x_6 - x_2)(y_6 - y_1)(y_6 - y_7)} \tag{2.78}$$

$$\overline{N}_7 = \frac{(x - x_2)(x - x_3)(y - y_1)(y - y_4)}{(x_7 - x_2)(x_7 - x_3)(y_7 - y_1)(y_7 - y_4)} \tag{2.79}$$

$$\overline{N}_8 = \frac{(x - x_1)(x - x_3)(y - y_1)(y - y_4)}{(x_8 - x_1)(x_8 - x_3)(y_8 - y_1)(y_8 - y_4)} \tag{2.80}$$

$$\overline{N}_9 = \frac{(x - x_1)(x - x_2)(y - y_1)(y - y_4)}{(x_9 - x_1)(x_9 - x_2)(y_9 - y_1)(y_9 - y_4)} \tag{2.81}$$

where, x_i and y_i denote the i-th nodal coordinates in the element coordinate system (X_e, Y_e) as shown in Figure 2.3.

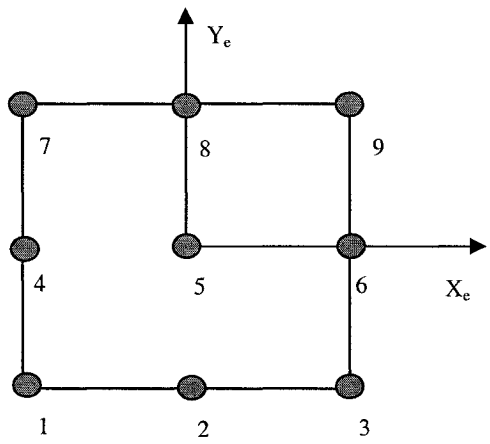

Figure 2.3 The 9-node element

Substituting Equations (2.72-2.81) into Equation (2.62), it can be shown that:

$$\{\varepsilon_L\} = [\overline{B}_L]\{\overline{u}\} \tag{2.82}$$

where the element nodal displacement vector $\{\overline{u}\}$ and matrix $[\overline{B}_L]$ are given by

$$\{\overline{u}\} = [u_1, v_1, w_1, \phi_{1x}, \phi_{1y}, \cdots \quad \cdots \quad , u_9, v_9, w_9, \phi_{9x}, \phi_{9y}]^T \tag{2.83}$$

$$[\overline{B}_L] = [[\overline{B}_L^1] \quad [\overline{B}_L^2] \quad \cdots \quad \cdots \quad [\overline{B}_L^9]] \tag{2.84}$$

$$[\overline{B}_L{}^i] = \begin{bmatrix} \frac{\partial \overline{N}_i}{\partial x} & 0 & 0 & 0 & 0 \\ 0 & \frac{\partial \overline{N}_i}{\partial y} & 0 & 0 & 0 \\ \frac{\partial \overline{N}_i}{\partial y} & \frac{\partial \overline{N}_i}{\partial x} & 0 & 0 & 0 \\ 0 & 0 & 0 & \frac{\partial \overline{N}_i}{\partial x} & 0 \\ 0 & 0 & 0 & 0 & \frac{\partial \overline{N}_i}{\partial y} \\ 0 & 0 & 0 & \frac{\partial \overline{N}_i}{\partial y} & \frac{\partial \overline{N}_i}{\partial x} \\ 0 & 0 & \frac{\partial \overline{N}_i}{\partial y} & 0 & \overline{N}_i \\ 0 & 0 & \frac{\partial \overline{N}_i}{\partial x} & \overline{N}_i & 0 \end{bmatrix} \tag{2.85}$$

Linear part of the strain energy, its first order variation and the second order variation are defined as:

$$U_L = \frac{1}{2}\int_{\Omega}\{\varepsilon_L\}^T[F]\{\varepsilon_L\}d\Omega = \frac{1}{2}\{\bar{u}\}^T\left(\int_{\Omega}[\bar{B}_L]^T[F][\bar{B}_L]d\Omega\right)\{\bar{u}\} \tag{2.86}$$

$$\delta U_L = \delta\{\bar{u}\}^T\left(\int_{\Omega}[\bar{B}_L]^T[F][\bar{B}_L]d\Omega\right)\{\bar{u}\} \tag{2.87}$$

$$\delta^2 U_L = \delta\{\bar{u}\}^T\left(\int_{\Omega}[\bar{B}_L]^T[F][\bar{B}_L]d\Omega\right)\delta\{\bar{u}\} \tag{2.88}$$

Equations for $\{\varepsilon_N\}, \delta\{\varepsilon_N\}$ and $\delta^2\{\varepsilon_N\}$ are derived as follows:

$$\{\varepsilon_N\} = \begin{Bmatrix} \frac{1}{2}\left(\frac{\partial w_0}{\partial x}\right)^2 \\ \frac{1}{2}\left(\frac{\partial w_0}{\partial y}\right)^2 \\ \frac{\partial w_0}{\partial x}\frac{\partial w_0}{\partial y} \\ 0 \\ 0 \\ 0 \\ 0 \\ 0 \end{Bmatrix} = \frac{1}{2}\begin{bmatrix} \frac{\partial w_0}{\partial x} & 0 \\ 0 & \frac{\partial w_0}{\partial y} \\ \frac{\partial w_0}{\partial y} & \frac{\partial w_0}{\partial x} \\ 0 & 0 \\ 0 & 0 \\ 0 & 0 \\ 0 & 0 \\ 0 & 0 \end{bmatrix}\begin{Bmatrix} \frac{\partial w_0}{\partial x} \\ \frac{\partial w_0}{\partial y} \end{Bmatrix} = \frac{1}{2}[H]\begin{Bmatrix} \frac{\partial w_0}{\partial x} \\ \frac{\partial w_0}{\partial y} \end{Bmatrix} \tag{2.89}$$

where

$$[H] = \begin{bmatrix} \frac{\partial w_0}{\partial x} & 0 & \frac{\partial w_0}{\partial y} & 0 & 0 & 0 & 0 & 0 \\ 0 & \frac{\partial w_0}{\partial y} & \frac{\partial w_0}{\partial y} & 0 & 0 & 0 & 0 & 0 \end{bmatrix}^T \tag{2.90}$$

$$\delta\{\varepsilon_N\}=\begin{Bmatrix} \dfrac{\partial w_0}{\partial x}\delta\left(\dfrac{\partial w_0}{\partial x}\right) \\ \dfrac{\partial w_0}{\partial y}\delta\left(\dfrac{\partial w_0}{\partial y}\right) \\ \delta\left(\dfrac{\partial w_0}{\partial x}\right)\left(\dfrac{\partial w_0}{\partial y}\right)+\left(\dfrac{\partial w_0}{\partial x}\right)\delta\left(\dfrac{\partial w_0}{\partial y}\right) \\ 0 \\ 0 \\ 0 \\ 0 \\ 0 \end{Bmatrix}=[H]\begin{Bmatrix} \delta\left(\dfrac{\partial w_0}{\partial x}\right) \\ \delta\left(\dfrac{\partial w_0}{\partial y}\right) \end{Bmatrix} \tag{2.91}$$

$$\begin{Bmatrix} \delta\left(\dfrac{\partial w_0}{\partial x}\right) \\ \delta\left(\dfrac{\partial w_0}{\partial y}\right) \end{Bmatrix}=\begin{bmatrix} 0 & 0 & \dfrac{\partial \overline{N}_1}{\partial x} & 0 & 0 & \cdots & \cdots & 0 & 0 & \dfrac{\partial \overline{N}_9}{\partial x} & 0 & 0 \\ 0 & 0 & \dfrac{\partial \overline{N}_1}{\partial y} & 0 & 0 & \cdots & \cdots & 0 & 0 & \dfrac{\partial \overline{N}_9}{\partial y} & 0 & 0 \end{bmatrix}_{2*45} \delta\{\overline{u}\}=[S]\delta\{\overline{u}\} \tag{2.92}$$

where

$$[S]=\begin{bmatrix} 0 & 0 & \dfrac{\partial \overline{N}_1}{\partial x} & 0 & 0 & \cdots & \cdots & 0 & 0 & \dfrac{\partial \overline{N}_9}{\partial x} & 0 & 0 \\ 0 & 0 & \dfrac{\partial \overline{N}_1}{\partial y} & 0 & 0 & \cdots & \cdots & 0 & 0 & \dfrac{\partial \overline{N}_9}{\partial y} & 0 & 0 \end{bmatrix}_{2*45} \tag{2.93}$$

$$\delta^2\{\varepsilon_N\}=\begin{bmatrix} \delta\left(\dfrac{\partial w_0}{\partial x}\right) & 0 \\ 0 & \delta\left(\dfrac{\partial w_0}{\partial y}\right) \\ \delta\left(\dfrac{\partial w_0}{\partial y}\right) & \delta\left(\dfrac{\partial w_0}{\partial x}\right) \\ 0 & 0 \\ 0 & 0 \\ 0 & 0 \\ 0 & 0 \\ 0 & 0 \end{bmatrix}_{8*2} \begin{Bmatrix} \delta\left(\dfrac{\partial w_0}{\partial x}\right) \\ \delta\left(\dfrac{\partial w_0}{\partial y}\right) \end{Bmatrix}_{2*1} \tag{2.94}$$

Nonlinear part 1 of the strain energy, its first order variation and the second order variation are defined as:

$$U_{N1} = \int_{\Omega} \{\varepsilon_L\}^T [F] \{\varepsilon_N\} d\Omega \tag{2.95}$$

$$\delta U_{N1} = \int_{\Omega} \delta\{\varepsilon_L\}^T [F] \{\varepsilon_N\} d\Omega + \int_{\Omega} \delta\{\varepsilon_N\}^T [F] \{\varepsilon_L\} d\Omega \tag{2.96}$$

$$\delta^2 U_{N1} = \int_{\Omega} \delta\{\varepsilon_L\}^T [F] \delta\{\varepsilon_N\} d\Omega + \int_{\Omega} \delta\{\varepsilon_N\}^T [F] \delta\{\varepsilon_L\} d\Omega + \int_{\Omega} \delta^2\{\varepsilon_N\}^T [F] \{\varepsilon_L\} d\Omega \tag{2.97}$$

Let

$$\{N_L\}_{8*1} = [F]_{8*8} \{\varepsilon_L\}_{8*1}$$

With equations (2.89), (2.91) and (2.94), parts of δU_{N1} and $\delta^2 U_{N1}$ are obtained as:

$$\int_{\Omega} \delta^2\{\varepsilon_N\}^T [F] \{\varepsilon_L\} d\Omega = \int_{\Omega} \delta^2\{\varepsilon_N\}^T \{N_L\} d\Omega =$$

$$= \int_{\Omega} \left[\delta\left(\frac{\partial w}{\partial x}\right) \quad \delta\left(\frac{\partial w}{\partial y}\right) \right] \begin{Bmatrix} N_{L1} \delta\left(\frac{\partial w}{\partial x}\right) + N_{L3} \delta\left(\frac{\partial w}{\partial y}\right) \\ N_{L3} \delta\left(\frac{\partial w}{\partial x}\right) + N_{L2} \delta\left(\frac{\partial w}{\partial y}\right) \end{Bmatrix} d\Omega$$

$$= \int_{\Omega} \left[\delta\left(\frac{\partial w}{\partial x}\right) \quad \delta\left(\frac{\partial w}{\partial y}\right) \right] \begin{bmatrix} N_{L1} & N_{L3} \\ N_{L3} & N_{L2} \end{bmatrix} \begin{Bmatrix} \delta\left(\frac{\partial w}{\partial x}\right) \\ \delta\left(\frac{\partial w}{\partial y}\right) \end{Bmatrix} d\Omega$$

$$= \int_{\Omega} \delta\{\bar{u}\}^T [S]^T \begin{bmatrix} N_{L1} & N_{L3} \\ N_{L3} & N_{L2} \end{bmatrix} [S] \delta\{\bar{u}\} d\Omega$$

$$= \delta\{\bar{u}\}^T \left(\int_{\Omega} [S]^T \begin{bmatrix} N_{L1} & N_{L3} \\ N_{L3} & N_{L2} \end{bmatrix} [S] d\Omega \right) \delta\{\bar{u}\} \tag{2.98}$$

$$\int_{\Omega} \delta\{\varepsilon_N\}^T [F] \delta\{\varepsilon_L\} d\Omega$$

$$= \int_{\Omega} (([H][S]\delta\{\bar{u}\})^T [F] [\bar{B}_L] \delta\{\bar{u}\} d\Omega = \delta\{\bar{u}\}^T \left(\int_{\Omega} [S]^T [H]^T [F] [\bar{B}_L] d\Omega \right) \delta\{\bar{u}\} \tag{2.99}$$

$$\int_{\Omega} \delta\{\varepsilon_L\}^T [F] \delta\{\varepsilon_N\} d\Omega$$
$$= \int_{\Omega} \left([\overline{B}_L]\delta\{\overline{u}\}\right)^T [F][H][S]\delta\{\overline{u}\} d\Omega = \delta\{\overline{u}\}^T \left(\int_{\Omega} [\overline{B}_L]^T [F][H][S] d\Omega \right) \delta\{\overline{u}\} \tag{2.100}$$

$$\int_{\Omega} \delta\{\varepsilon_N\}^T [F]\{\varepsilon_L\} d\Omega$$
$$= \int_{\Omega} \left([H][S]\delta\{\overline{u}\}\right)^T [F][\overline{B}_L]\{\overline{u}\} d\Omega = \delta\{\overline{u}\}^T \left(\int_{\Omega} [S]^T [H]^T [F][\overline{B}_L] d\Omega \right) \{\overline{u}\} \tag{2.101}$$

$$\int_{\Omega} \delta\{\varepsilon_L\}^T [F]\{\varepsilon_N\} d\Omega$$
$$= \int_{\Omega} \left([\overline{B}_L]\delta\{\overline{u}\}\right)^T [F]\left(\frac{1}{2}[H][S]\{\overline{u}\}\right) d\Omega = \delta\{\overline{u}\}^T \left(\frac{1}{2}\int_{\Omega} [\overline{B}_L]^T [F][H][S] d\Omega \right) \{\overline{u}\} \tag{2.102}$$

Combining the above equations, δU_{N1} and $\delta^2 U_{N1}$ can be defined as:

$$\delta U_{N1} = \delta\{\overline{u}\}^T \left[\left(\frac{1}{2}\int_{\Omega} [\overline{B}_L]^T [F][H][S] d\Omega \right) + \left(\int_{\Omega} [S]^T [H]^T [F][\overline{B}_L] d\Omega \right) \right] \{\overline{u}\} \tag{2.103}$$

$$\delta^2 U_{N1} = \delta\{\overline{u}\}^T \left[\begin{array}{l} \left(\int_{\Omega} [\overline{B}_L]^T [F][H][S] d\Omega \right) + \left(\int_{\Omega} [S]^T [H]^T [F][\overline{B}_L] d\Omega \right) \\ + \left(\int_{\Omega} [S]^T \begin{bmatrix} N_{L1} & N_{L3} \\ N_{L3} & N_{L2} \end{bmatrix} [S] d\Omega \right) \end{array} \right] \delta\{\overline{u}\} \tag{2.104}$$

Nonlinear part 2 of the strain energy, its first order variation and its second order variation are defined as:

$$U_{N2} = \frac{1}{2}\int_{\Omega} \{\varepsilon_N\}^T [F]\{\varepsilon_N\} d\Omega \tag{2.105}$$

$$\delta U_{N2} = \int_{\Omega} \delta\{\varepsilon_N\}^T [F]\{\varepsilon_N\} d\Omega$$
$$= \int_{\Omega} \left([H][S]\delta\{\overline{u}\}\right)^T [F]\left(\frac{1}{2}[H][S]\{\overline{u}\}\right) d\Omega = \delta\{\overline{u}\}^T \left(\frac{1}{2}\int_{\Omega} [S]^T [H]^T [F][H][S] d\Omega \right) \{\overline{u}\} \tag{2.106}$$

$$\delta^2 U_{N2} = \int_\Omega \delta\{\varepsilon_N\}^T [F] \delta\{\varepsilon_N\} d\Omega + \int_\Omega \delta^2\{\varepsilon_N\}^T [F] \{\varepsilon_N\} d\Omega \tag{2.107}$$

where

$$\begin{aligned} \int_\Omega \delta\{\varepsilon_N\}^T [F] \delta\{\varepsilon_N\} d\Omega &= \int_\Omega (([H][S]\delta\{\bar{u}\})^T [F] ([H][S]\delta\{\bar{u}\}) d\Omega \\ &= \delta\{\bar{u}\}^T \left(\int_\Omega [S]^T [H]^T [F][H][S] d\Omega \right) \{\bar{u}\} \end{aligned} \tag{2.108}$$

$$\begin{aligned} \int_\Omega \delta^2\{\varepsilon_N\}^T [F] \{\varepsilon_N\} d\Omega &= \int_\Omega \delta^2\{\varepsilon_N\}^T \{N_N\} d\Omega \\ &= \int_\Omega \left[\delta\left(\frac{\partial w}{\partial x}\right) \quad \delta\left(\frac{\partial w}{\partial y}\right) \right] \begin{Bmatrix} N_{N1}\delta\left(\frac{\partial w}{\partial x}\right) + N_{N3}\delta\left(\frac{\partial w}{\partial y}\right) \\ N_{N3}\delta\left(\frac{\partial w}{\partial x}\right) + N_{N2}\delta\left(\frac{\partial w}{\partial y}\right) \end{Bmatrix} d\Omega \\ &= \int_\Omega \left[\delta\left(\frac{\partial w}{\partial x}\right) \quad \delta\left(\frac{\partial w}{\partial y}\right) \right] \begin{bmatrix} N_{N1} & N_{N3} \\ N_{N3} & N_{N2} \end{bmatrix} \begin{Bmatrix} \delta\left(\frac{\partial w}{\partial x}\right) \\ \delta\left(\frac{\partial w}{\partial y}\right) \end{Bmatrix} d\Omega \\ &= \int_\Omega \delta\{\bar{u}\}^T [S]^T \begin{bmatrix} N_{N1} & N_{N3} \\ N_{N3} & N_{N2} \end{bmatrix} [S] \delta\{\bar{u}\} d\Omega \\ &= \delta\{\bar{u}\}^T \left(\int_\Omega [S]^T \begin{bmatrix} N_{N1} & N_{N3} \\ N_{N3} & N_{N2} \end{bmatrix} [S] d\Omega \right) \delta\{\bar{u}\} \end{aligned} \tag{2.109}$$

Therefore, $\delta^2 U_{N2}$ can be expressed further as:

$$\delta^2 U_{N2} = \delta\{\bar{u}\}^T \left[\left(\int_\Omega [S]^T [H]^T [F][H][S] d\Omega \right) + \left(\int_\Omega [S]^T \begin{bmatrix} N_{N1} & N_{N3} \\ N_{N3} & N_{N2} \end{bmatrix} [S] d\Omega \right) \right] \{\bar{u}\} \tag{2.110}$$

Finally, putting the linear part, the nonlinear part 1 and part 2 together, δU and $\delta^2 U$ are obtained as:

$$\delta U = \delta\{\bar{u}\}^T [K_e] \{\bar{u}\} \tag{2.111}$$

$$\delta^2 U = \delta\{\bar{u}\}^T [K_{eT}] \delta\{\bar{u}\} \tag{2.112}$$

where the stiffness matrix is:

$$[K_e] = \begin{bmatrix} (\int_\Omega [\bar{B}_L]^T [F][\bar{B}_L] d\Omega) + \\ \left(\frac{1}{2}\int_\Omega [\bar{B}_L]^T [F][H][S] d\Omega\right) + \left(\int_\Omega [S]^T [H]^T [F][\bar{B}_L] d\Omega\right) + \\ \left(\frac{1}{2}\int_\Omega [S]^T [H]^T [F][H][S] d\Omega\right) \end{bmatrix}_{45\times 45} \tag{2.113}$$

The tangent stiffness matrix is:

$$[K_{eT}] = \begin{bmatrix} (\int_\Omega [\bar{B}_L]^T [F][\bar{B}_L] d\Omega) + \\ \left(\int_\Omega [\bar{B}_L]^T [F][H][S] d\Omega\right) + \left(\int_\Omega [S]^T [H]^T [F][\bar{B}_L] d\Omega\right) + \left(\int_\Omega [S]^T \begin{bmatrix} N_{L1} & N_{L3} \\ N_{L3} & N_{L2} \end{bmatrix} [S] d\Omega\right) + \\ \left(\int_\Omega [S]^T [H]^T [F][H][S] d\Omega\right) + \left(\int_\Omega [S]^T \begin{bmatrix} N_{N1} & N_{N3} \\ N_{N3} & N_{N2} \end{bmatrix} [S] d\Omega\right) \end{bmatrix}_{45\times 45} \tag{2.114}$$

Once the element stiffness matrix is obtained, equilibrium equations for the element can be expressed as

$$[K_e]\{\bar{u}\} = \{P_e\} \tag{2.115}$$

Here subscript e denotes that the corresponding quantity is relevant to the element. $\{P_e\}$ is the nodal force matrix corresponding to nodal displacement matrix $\{\bar{u}\}$.

$$\{P_e\} = [f_{u1}, f_{v1}, f_{w1}, m_{1x}, m_{1y}, \cdots \quad \cdots \quad , f_{u9}, f_{v9}, f_{w9}, m_{9x}, m_{9y}]^T \tag{2.116}$$

Numerical integration is used to evaluate the stiffness matrix and the tangent stiffness matrix using Gauss quadrature. The nonlinear algebraic equations are solved using the Newton-Raphson method. Buckling loads are determined considering the singularity of the tangent stiffness matrix.

2.7 Failure Criterion and Progressive Failure Analysis

A review of the tensor polynomial failure criterion, with its various degenerate cases, has been presented by Reddy and Reddy [9], and Singh *et al* [44]. Here, because of its simplicity, the tensor polynomial form of the maximum stress failure criterion is used for the cases of uni-axial compression and bi-axial compression.

A detailed review of various failure criteria used for the prediction of failure loads of laminated composite plates for the case of in-plane shear has been made by Singh *et al.* [122] and [123]. It was observed that the difference in failure loads predicted by the various failure criteria is strongly dependent on plate lay-up and boundary conditions. It was also observed that the Hashin criterion and the tensor polynomial form of the maximum strain criterion give the most inconsistent results as compared with other criteria. Moreover, the difference in failure loads predicted by tensor polynomial form of the Tsai-Hill criterion and Tsai-Wu criterion is small for non-linear analysis. Owing to the lack of experimental data, it is not possible to say which criterion is best for the prediction of failure loads. Here, the tensor polynomial form of the 3D Tsai-Hill criterion is used as one of the failure models for a lamina failure and resin failure in the cases of in-plane shear and bi-axial compression combined with in-plane shear, and the terms associated with the normal stress component in the third principal material direction are omitted.

In contrast, the maximum stress criterion is used to predict the onset of delamination because of its simplicity.

The most general polynomial failure criterion is expressed as [124]

$$F_1\sigma_1 + F_2\sigma_2 + F_3\sigma_3 + 2F_{12}\sigma_1\sigma_2 + 2F_{13}\sigma_1\sigma_3 + 2F_{23}\sigma_2\sigma_3 + F_{11}\sigma_1^2 + F_{22}\sigma_2^2 + F_{33}\sigma_3^2 + F_{44}\sigma_4^2 + F_{55}\sigma_5^2 + F_{66}\sigma_6^2 + \cdots \geq 1 \quad (2.117)$$

where, σ_1, σ_2 and σ_3 are the normal stress components, and σ_4, σ_5 and σ_6 are the shear stress components τ_{23}, τ_{13} and τ_{12} respectively in the principal material directions. The subscripts 1 and 2 refer to the fiber direction and in-plane transverse direction, and subscript 3 refers to the ply out-of-plane direction. Particular cases of the above criterion differ from one another by their strength tensors F_{ij}. Hence, various degenerate cases of the tensor polynomial criterion can be obtained by substituting the appropriate tensor strength factors F_{ij} into the Equation (2.117).

In the maximum stress criterion [125], the strength tensors F_{ij} are defined as

$$F_1 = \frac{1}{X_T} - \frac{1}{X_c}; F_2 = \frac{1}{Y_T} - \frac{1}{Y_c}; F_3 = \frac{1}{Z_T} - \frac{1}{Z_c}; F_{11} = \frac{1}{X_T X_c}; F_{22} = \frac{1}{Y_T Y_c}; F_{33} = \frac{1}{Z_T Z_c};$$

$$F_{44} = \frac{1}{R^2}; F_{55} = \frac{1}{S^2}; F_{66} = \frac{1}{T^2}; F_{12} = -\frac{F_1 F_2}{2}; F_{13} = -\frac{F_1 F_3}{2}; F_{23} = -\frac{F_2 F_3}{2}. \quad (2.118)$$

The remaining strength tensor terms are equal to zero. In the above expression, X_t and Y_t are the tensile strengths of the lamina in the fiber direction and in the direction transverse to it, respectively; X_c and Y_c are the corresponding compressive strengths; Z_t and Z_c are the tensile and the compressive strengths, respectively, in the principal direction 3 of the lamina. R and T are the shear strengths of lamina in planes 2-3 and 1-2, respectively. The shear strength in plane 1-3 is designated as S.

In the Tsai-Hill criterion [126], the strength tensors F_{ij} are defined as

$$F_1 = F_2 = F_3 = 0;\ F_{11} = \frac{1}{X^2};F_{22} = \frac{1}{Y^2};F_{22} = \frac{1}{Z^2};F_{44} = \frac{1}{R^2};F_{55} = \frac{1}{S^2};F_{66} = \frac{1}{T^2};$$

$$F_{12} = -\frac{1}{2}\left(\frac{1}{X^2}+\frac{1}{Y^2}-\frac{1}{Z^2}\right);F_{13} = -\frac{1}{2}\left(\frac{1}{X^2}+\frac{1}{Z^2}-\frac{1}{Y^2}\right);F_{23} = -\frac{1}{2}\left(\frac{1}{Y^2}+\frac{1}{Z^2}-\frac{1}{X^2}\right) \quad (2.119)$$

The values of X, Y and Z are taken as either X_t, Y_t and Z_t, or as X_c, Y_c and Z_c, depending upon the sign of σ_1, σ_2 and σ_3 respectively.

In order to determine the failure of resin, the above criterion is simplified considering the isotropic nature of the resin material. For resin failure, σ_1, σ_2 and σ_3 are the normal stress components, and σ_4, σ_5 and σ_6 are the shear stress components τ_{23}, τ_{13}, and τ_{12} respectively in the global coordinate system in Equation (2.117). In Equations (2.118) and (2.119), the compressive strengths are taken to be same in all directions and so are tensile strengths. The shear strengths corresponding to the planes 1-2, 1-3, and 2-3 are taken to be the same. With the objective of following the same computational procedure for both the composite ply and resin, the resin pocket is considered (imagined) to be made up of layers of isotropic resin material.

Lamina failure in the cases of uni-axial compression and bi-axial compression is said to have occurred when the state of stress at any Gauss point within the lamina satisfies the tensor polynomial form of the maximum stress criterion.

Lamina failure in the case of in-plane shear loading and bi-axial compression combined with in-plane shear loading is said to have occurred when the state of stress at any Gauss point within the lamina (at mid-thickness) satisfies the tensor polynomial form of the

Tsai-Hill criterion in which the terms associated with the normal stress component in the third principal material direction are omitted.

A similar consideration is used for determining the failure of resin. The first-ply failure refers to the first instant at which any layer or more than one layer fail at the same load.

Delamination at any interface between two adjacent layers is said to have occurred when any of the three transverse stress components in any of the two layers (adjacent to the interface) becomes equal to or greater than its corresponding allowable strength (the transverse interlaminar normal strength is taken to be the tensile strength of lamina in principal material direction 3). A similar consideration is used for determining the delamination of (imagined) resin layer.

The procedure used for simulating the progressive failure is explained in the following. At each load step, Gauss point stresses in all the elements of each layer, including the composite material ply and the (imagined) resin layer, are calculated and used in the maximum stress criterion in the cases of uni-axial compression and bi-axial compression, and in the Tsai-Hill failure criterion in the case of in-plane shear loading and bi-axial compression combined with in-plane shear loading. When failure occurs at a Gauss point according to the maximum stress criterion in the cases of uni-axial compression and bi-axial compression, and when failure occurs at a Gauss point in a layer in the case of in-plane shear loading and bi-axial compression combined with in-plane shear loading, a reduction in the corresponding lamina modulus is introduced as per the mode of failure everywhere in the lamina, but only in the corresponding element. This causes the changes

in the corresponding element laminate stiffness. Following indices are used to determine the failure modes.

$$H_1 = F_1\sigma_1 + F_{11}\sigma_1^2,\ H_2 = F_2\sigma_2 + F_{22}\sigma_2^2,\ H_4 = F_{44}\sigma_4^2,\ H_5 = F_{55}\sigma_5^2,\ H_6 = F_{66}\sigma_6^2 \quad (2.220)$$

The dominant failure mode is selected to be the one that corresponds to the largest H_i term, and the corresponding modulus is reduced to zero. H_1 corresponds to the modulus E_1 ; H_2 to E_2 ; H_4 to G_{23} ; H_5 to G_{13} ; H_6 to G_{12} ; An outline of the computational procedure is described as follows:

(a) After iterative convergence is achieved at each load step in the nonlinear analysis, the stresses at the middle of each ply and at interfaces with the adjacent layers are calculated at each Gauss point. A similar calculation is performed for resin pocket. All the six stress components are calculated. However in order to predict the failure of a lamina, only five stress components (three in-plane stresses and two transverse shear stresses) are used in the failure criterion.

(b) For composite material ply, the stresses are transformed into the stresses in the principal directions; for resin pocket, such a transformation is not needed, and the stresses in global coordinate system can directly be used in the failure criterion and in Equation (2.117).

(c) The corresponding failure criterion in the tensor polynomial form is used to determine whether failure has occurred or not.

(d) If failure has occurred, the values of indices H_1, H_2, H_4, H_5, H_6 are calculated and the largest one is found out. The appropriate lamina modulus is reduced to zero and the laminate stiffness at each Gauss point is recalculated. The nonlinear analysis at

the same load step is restarted and the above mentioned steps (a) to (c) are repeated.

(e) If no failure occurs, the analysis is continued to the next load step.

(f) Final failure occurs when delamination occurs or when the plate is no longer able to carry any further load because of very large deflection.

2.8 Validation

No results are available in the literature on the first-ply failure load and the ultimate failure load of tapered laminates under the action of uni-axial compression and therefore the comparison with existing works could not be made. In order to validate the formulation and analysis, first, the taper angle is set to be zero, and the resulting uniform thickness laminates have been analyzed and the results have been compared with that available in literature for uniform-thickness laminates [45, 47]. Second, the result for tapered laminate with taper configuration F (Mid-plane taper) that has sixteen layers at the thick section and fourteen layers at the thin section are obtained and compared with the results for a uniform-thickness laminate with 16 layers and that for a uniform-thickness laminate with 14 layers. Third, the nonlinear load-deflection curve was calculated for a tapered laminate with 16 and 8 layers at thick and thin sections respectively, using the present formulation and using the Ritz method, and the results were compared.

2.8.1 Comparison of Results for Uniform-Thickness Laminate

Uniform-thickness laminates with simply-supported boundary condition subjected to uni-axial compression are analyzed using the present work by setting the taper angle to be equal to zero, and the results are compared with the results given in the work of Singh et al [45], and in the work of Ganesan and Zhang [47].

The dimensions of the uniform-thickness plate are: length a = 279 mm, width b = 279 mm and the laminate thickness H = 2.16 mm, ply thickness t = 0.135 mm. The properties of the composite material used are presented in Table 2.3. The boundary conditions are shown in Figure 2.4. A 5 by 5 finite element mesh is used. Here the first number refers to the number of elements in the x direction, and the second number corresponds to that in the y direction. The finite element mesh is shown in Figure 2.5.

Table 2.3 Material properties of T300/5208 graphite-epoxy composite material

Mechanical properties	Values	Strength properties	Values
E_1	132.58 GPa	X_t	1.515 GPa
E_2	10.8 GPa	X_c	1.697 GPa
E_3	10.8GPa	$Y_t = Z_t$	43.8 MPa
$G_{12} = G_{13}$	5.7 GPa	$Y_c = Z_c$	43.8 MPa
$\nu_{12} = \nu_{13}$	0.24	R	67.6 MPa
ν_{23}	0.49	S=T	86.9 MPa

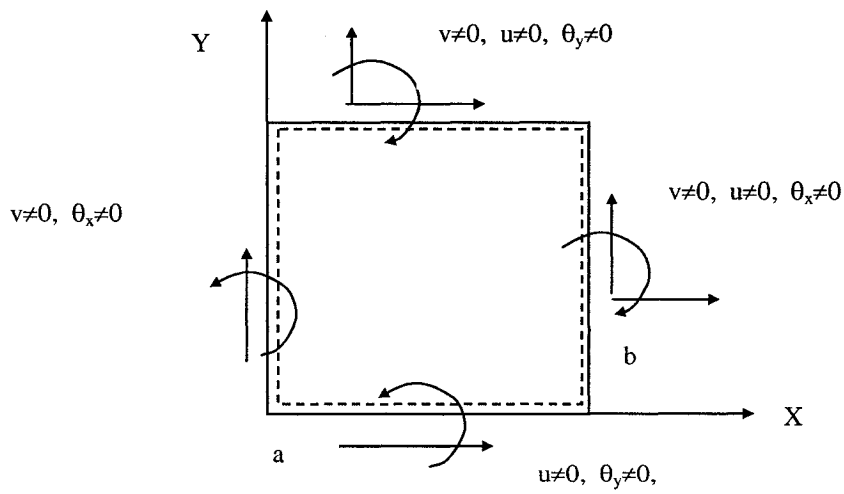

Figure 2.4 Details of boundary conditions for the laminated plate

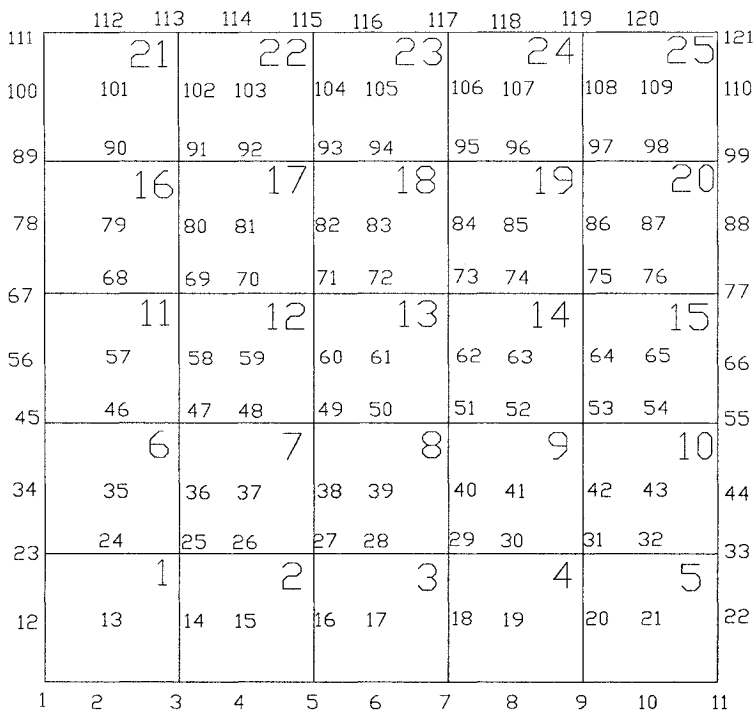

Figure 2.5 5 by 5 finite element mesh for the plate

Two lay-up configurations, (a) $(\pm 45/0/90)_{2s}$ and (b) $(\pm 45)_{4s}$, which are subjected to uni-axial compressive loading have been analyzed. The first-ply and the ultimate failure loads have been calculated, and these values are compared in Tables 2.4 and 2.5 with that given in the works of Singh et al [45] and Ganesan and Zhang [47]. The non-dimensional coefficient: $N_x b^2/E_2 h^3$ has been used to present the failure loads in Tables 2.4 and 2.5. As can be observed from these tables, the present results are in very good agreement with that given in the reference works.

Table 2.4 The first-ply failure load and the ultimate failure load for $(\pm 45/0/90)_{2s}$ laminate subjected to uni-axial compression

	First-ply failure load ($N_x b^2/E_2 h^3$)	Ultimate failure load ($N_x b^2/E_2 h^3$)
Singh *et al* [45]	58.09	77.45
Ganesan and Zhang [47]	55.78	81.53
Present study	54.18	79.92

Table 2.5 The first-ply failure load and the ultimate failure load for $(\pm 45)_{4s}$ laminate subjected to uni-axial compression

	First-ply failure load $(N_x b^2/E_2 h^3)$	Ultimate failure load $(N_x b^2/E_2 h^3)$
Singh *et al* [45]	49.06	65.83
Ganesan and Zhang [47]	47.92	67.94
Present study	48.34	66.98

2.8.2 Comparison of Results for Tapered Plates

A tapered plate with only two dropped plies has been analyzed. The dimensions of the plate are: length a = 279 mm, width b = 279 mm, and ply thickness t = 0.135 mm. The plate has the taper configuration F (Mid-plane taper) and has 16 layers at the left end with $(0/90)_{4s}$ lay-up, and 14 layers at the right end with $((0/90)_3/0)_s$ lay-up. The boundary condition and finite element mesh are the same as shown in Figure 2.4 and Figure 2.5. The properties of the composite material are the same as shown in Table 2.3. The results are compared with that of two uniform-thickness laminated plates with lay-up configurations $(0/90)_{4s}$ and $((0/90)_3/0)_s$ respectively, thus having 16 and 14 layers respectively. The composite material of the uniform-thickness plates is the same as that of tapered plate.

The first-ply failure load, the critical buckling load and the ultimate failure load for these three laminates under the action of uni-axial compression are given in Table 2.6. Figure 2.6 shows the load versus the central deflection response. As can be observed, the results for tapered laminates are between those of the 16-layers uniform-thickness laminate and those of 14-layers uniform-thickness laminate.

Table 2.6 The first-ply failure load, the critical buckling load and the ultimate failure load for uniform-thickness and tapered composite plates subjected to uni-axial compression

	Buckling load (N/m)	Fist-ply failure load (N/m)	Ultimate failure load (N/m)
16-layers uniform plate	19500	83250	110250
14-layers uniform plate	12750	68625	89625
Tapered plate	15750	70500	94500

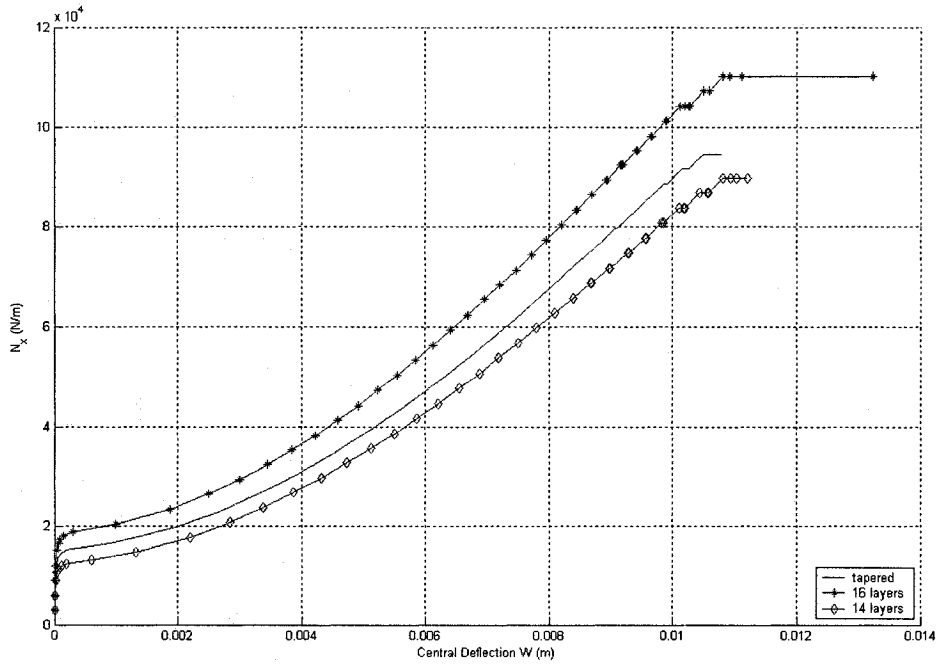

Figure 2.6 Load versus the central deflection response of uniform-thickness and tapered plates subjected to uni-axial compression

2.8.3 Comparison with Ritz Solution

The nonlinear load-deflection curve for a tapered laminate is determined using the present formulation and the Ritz method, and the results are compared.

A tapered composite plate with configuration F (Mid-plane taper) and made up of T300/5208 graphite-epoxy composite material is considered. The properties of the composite material were given in Table 2.1. The geometric properties of the plate are:

length $a = 0.279$ m and width $b = 0.279$ m; individual ply thickness $t = 0.000135$ m. This tapered plate has 16 layers at the left end and 8 layers at the right end as shown in Figure 2.7. The lay-up is $(0/90)_{4s}$ at the left end and $(0/90)_{2s}$ at the right end and the plies are dropped off as shown in Figure 2.7.

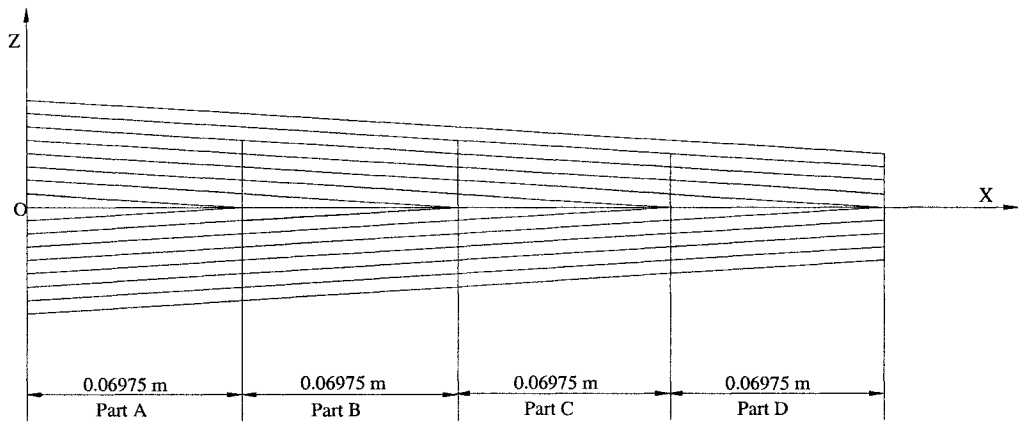

Figure 2.7 Tapered plate with configuration F (Mid-plane taper)

The boundary conditions are defined as following:

$$u_0(x,0)=0,\ u_0(x,b)=0,\quad v_0(0,y)=0,\quad v_0(a,y)=0; \tag{2.221}$$

$$w_0(x,0)=0,\ w_0(x,b)=0,\quad w_0(0,y)=0,\quad w_0(a,y)=0; \tag{2.222}$$

$$\phi_x(x,0)=0,\ \phi_x(x,b)=0,\quad \phi_y(0,y)=0,\quad \phi_x(a,y)=0. \tag{2.223}$$

To obtain the approximate solution using Ritz method, in view of the above boundary conditions, the mid-plane displacements are assumed as

$$u_0=\sum_m\sum_n U_{mn}\cos\left(\frac{m\pi x}{a}\right)\sin\left(\frac{n\pi y}{b}\right) \tag{2.224}$$

$$v_0=\sum_m\sum_n V_{mn}\sin\left(\frac{m\pi x}{a}\right)\cos\left(\frac{n\pi y}{b}\right) \tag{2.225}$$

$$w_0 = \sum_m \sum_n W_{mn} \sin\left(\frac{m\pi x}{a}\right) \sin\left(\frac{n\pi y}{b}\right) \tag{2.226}$$

$$\phi_x = \sum_m \sum_n X_{mn} \cos\left(\frac{m\pi x}{a}\right) \sin\left(\frac{n\pi y}{b}\right) \tag{2.227}$$

$$\phi_y = \sum_m \sum_n Y_{mn} \sin\left(\frac{m\pi x}{a}\right) \cos\left(\frac{n\pi y}{b}\right) \tag{2.228}$$

Equations (2.224-2.228) are substituted into Equation (2.66) and Equation (2.67), and the integrations in Equation (2.66) and Equation (2.67) are numerically evaluated using Gauss quadrature. In total potential energy Π, $U_{mn}, V_{mn}, W_{mn}, X_{mn}, Y_{mn}$ are undetermined coefficients. The unknown coefficients are determined by the following stationary condition.

$$\frac{\partial \Pi}{\partial U_{mn}} = 0 \tag{2.229}$$

$$\frac{\partial \Pi}{\partial V_{mn}} = 0 \tag{2.230}$$

$$\frac{\partial \Pi}{\partial W_{mn}} = 0 \tag{2.231}$$

$$\frac{\partial \Pi}{\partial X_{mn}} = 0 \tag{2.232}$$

$$\frac{\partial \Pi}{\partial Y_{mn}} = 0 \tag{2.233}$$

The resulting non-linear algebraic equations are solved using Newton-Raphson method.

Figure 2.8 shows the nonlinear load-deflection curves for a tapered laminate subjected to uni-axial compression which is based on Ritz method.

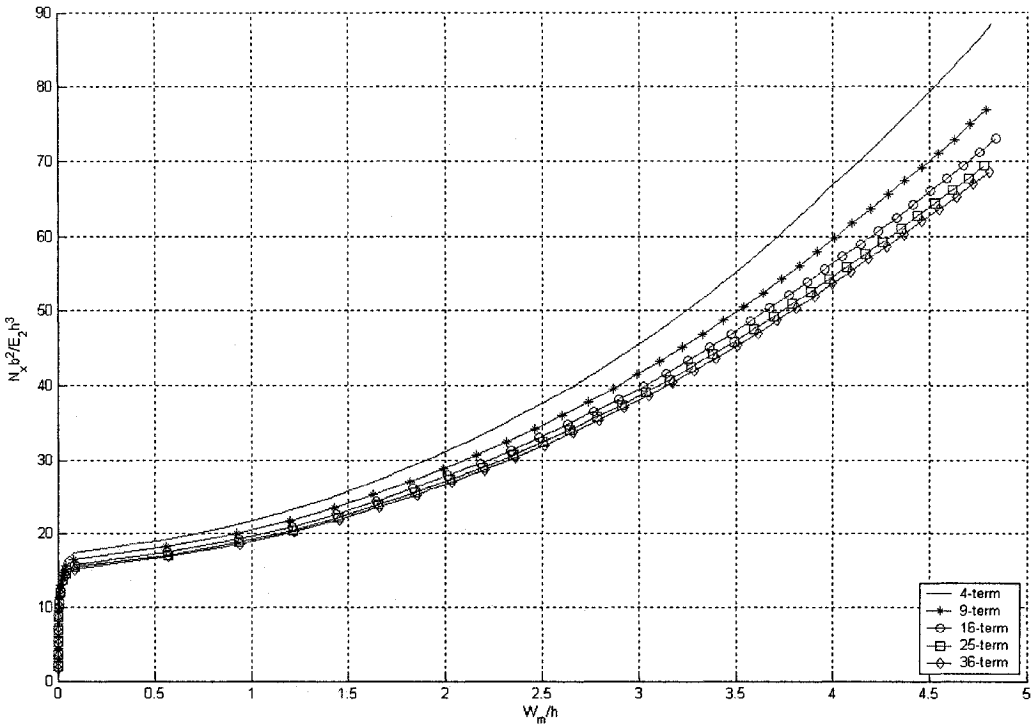

Figure 2.8 Nonlinear load-deflection curves for a tapered laminate subjected to uni-axial compression which is based on Ritz method

Figure 2.9 represents the nonlinear load-deflection curve for a tapered laminate subjected to uni-axial compression which is based on FEM.

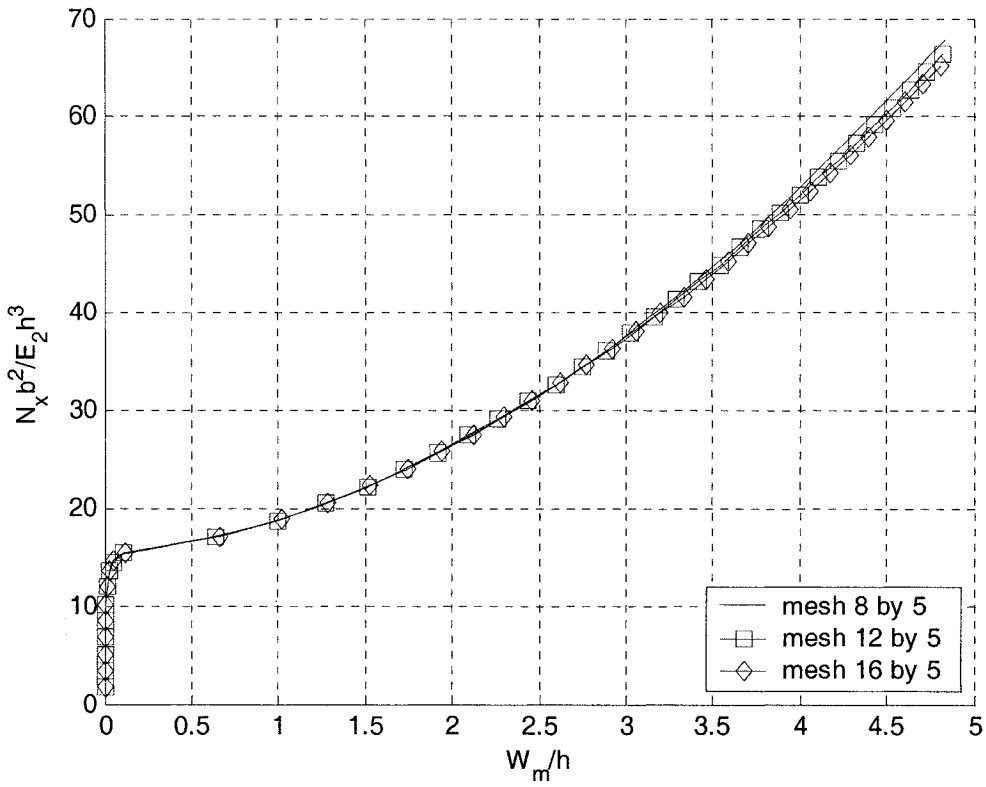

Figure 2.9 Nonlinear load-deflection curves for a tapered laminate subjected to uni-axial compression based on FEM analysis

Figure 2.10 gives a comparison of results based on FEM with those obtained by Ritz method. It is observed that the results obtained using the Ritz method are close to that obtained using the present finite element formulation.

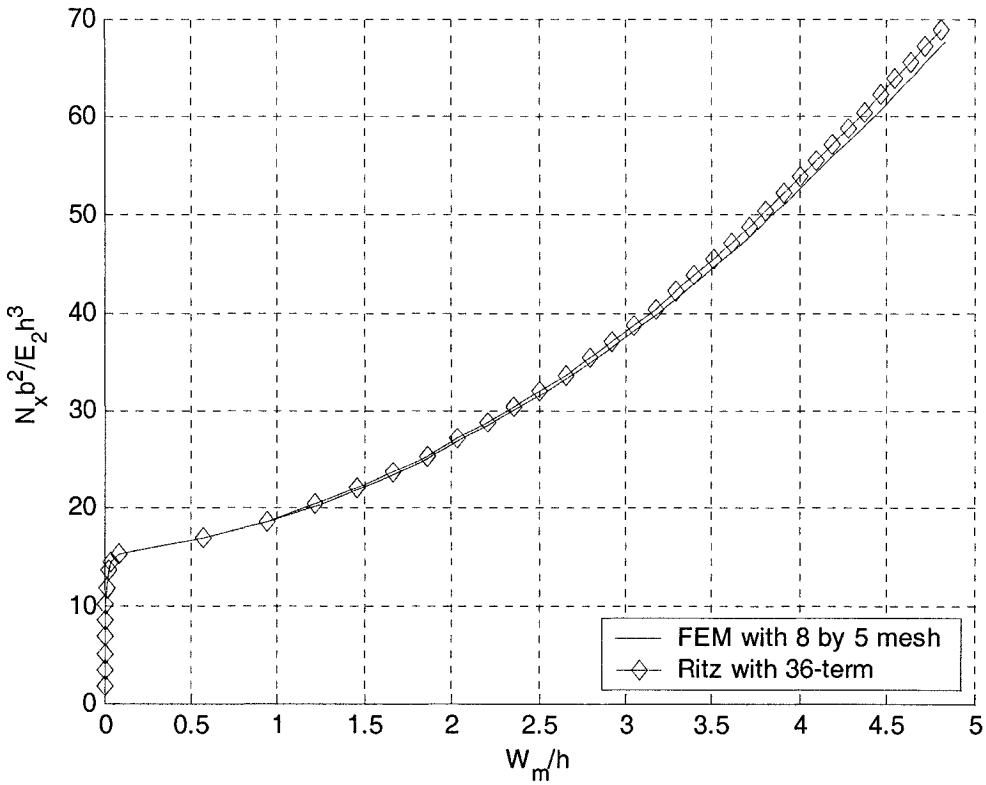

Figure 2.10 Comparison of nonlinear load-deflection curves obtained using FEM and Ritz method for a tapered laminate subjected to uni-axial compression

2.9 Conclusion

In the present chapter, a finite element formulation for the progressive failure analysis of tapered laminated plate has been developed. The failure criterion and the procedure for progressive failure simulation have been presented. Verification of the formulation and associated computer program has been conducted as follows. First, the taper angle has been taken to be zero, and the results obtained for a uniform plate using the present formulation have been compared with the results available in the literature. Second, two uniform-thickness composite plates with 16 layers and 14 layers, respectively, and a tapered laminated plate with 16 layers at the left end and 14 layers at the right end have been analyzed using the present formulation. The corresponding results have been

compared. Third, nonlinear load-deflection curve for a tapered plate with 16 and 8 layers at the left end and the right end respectively is determined using the present formulation and using the Ritz method. The results have been compared. In all the three cases, a very good agreement has been observed.

Chapter 3

Progressive Failure and Post-buckling Response under Compression

3.1 Introduction

Tapered composite plates are increasingly being used in mechanical and aerospace structures. The progressive failure of such tapered plates is an important design consideration for achieving economically safe and reliable design. In this chapter, the progressive failure of tapered plates under uni-axial and bi-axial compression is studied. The objective is to predict the first-ply failure load, the ultimate failure load, the buckling load, the associated maximum transverse displacements, and locations and modes of failure of tapered laminated plate under the action of compression.

3.2 Description

In the parametric study, five taper configurations and for each taper configuration, six lay-up configurations are considered. The taper configurations considered include configurations A (Basic taper), B (Staircase arrangement), C (Overlapping dropped plies), D (Continuous plies interspersed) and F (Mid-plane taper) which are shown in Figures 3.1, 3.2, 3.3, 3.4 and 3.5 respectively. The six lay-up configurations are defined in Table 3.1. As can be seen from Table 3.1, the lay-up configuration at the right (thin) end varies according to the taper configuration, and the lay-up of configuration D is different from that of other four taper configurations. In addition to the above mentioned six lay-up configurations, tapered laminates with $(\pm\theta)4s$ lay-up at the left (thick) end are also

considered to understand the influence of fiber orientation on the failure strength of the laminate. The boundary condition that has been considered in the present study is shown in Figure 3.6. Material properties of the composite material used in the present study are presented in Table 3.2, and the properties of the resin material are given in Table 3.3.

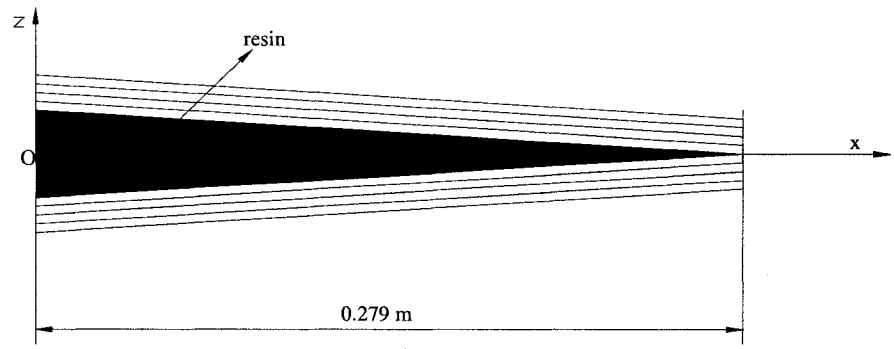

Figure 3.1 Tapered plate with configuration A (Basic taper)

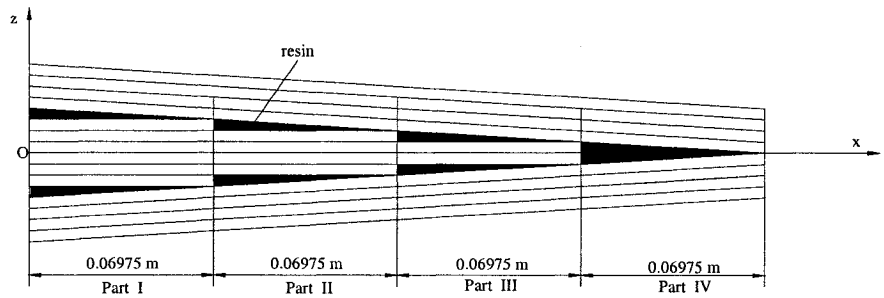

Figure 3.2 Tapered plate with configuration B (Staircase arrangement)

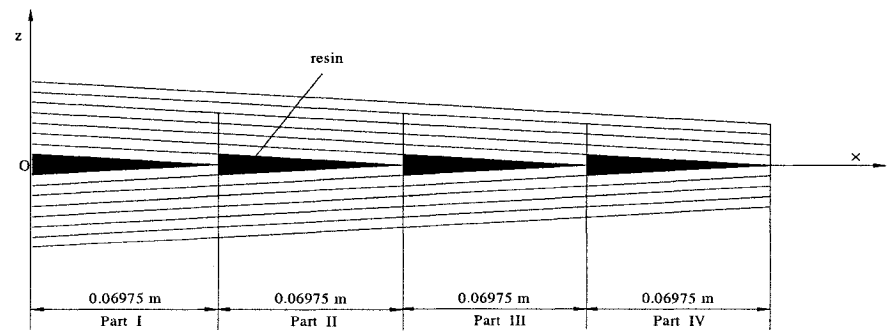

Figure 3.3 Tapered plate with configuration C (Overlapping dropped plies)

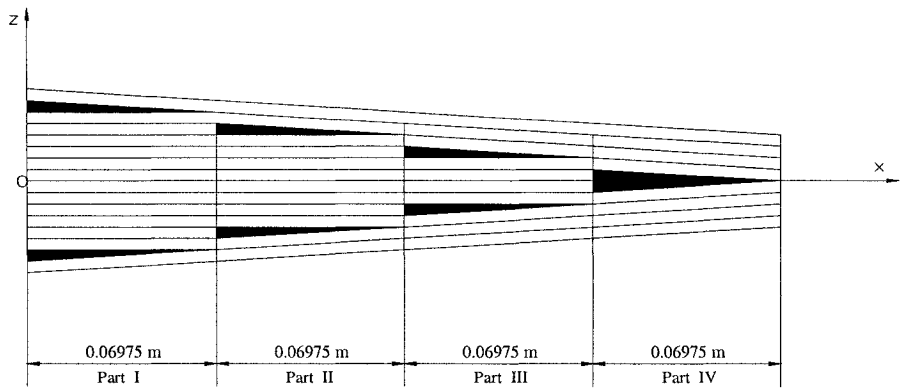

Figure 3.4 Tapered plate with configuration D (Continuous plies interspersed)

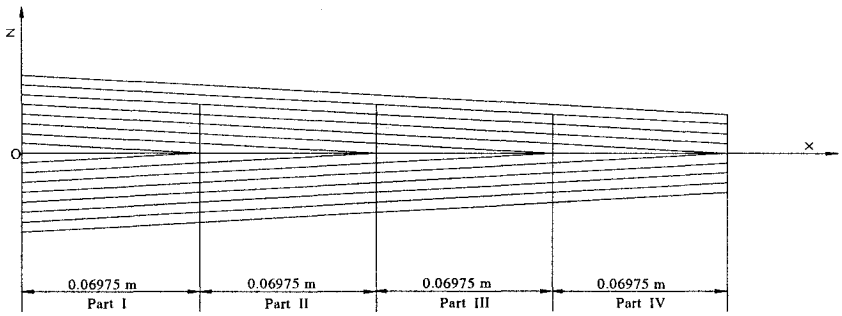

Figure 3.5 Tapered plate with configuration F (Mid-plane taper)

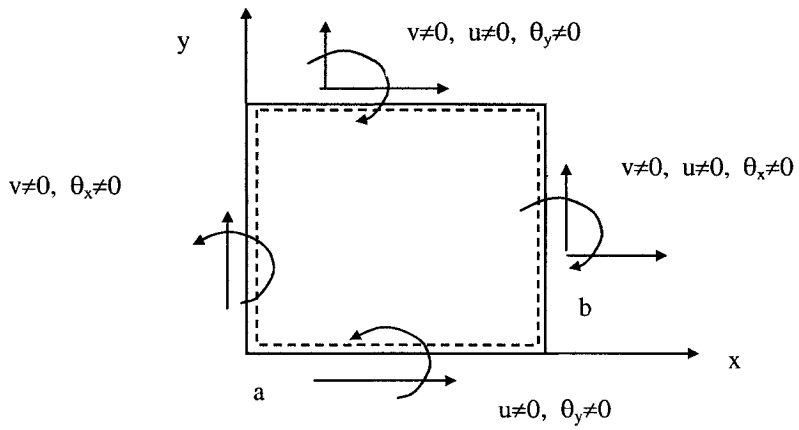

Figure 3.6 Details of boundary condition for the laminated plate

In the Figure 3.6, a and b are dimensions of the full plate in x and y directions. Dimensions of the plate are: a = 279 mm, b = 279 mm, and ply thickness t = 0.135 mm.

Table 3.1 Lay-up Configurations

Lay-up Configuration	Lay-up at the left (thick) end	Lay-up at the right (thin) end	
	Taper configurations A, B, C, D and F	Taper configurations A, B, C and F	Taper configuration D
LC(1)	$(0/90)_{4s}$	$(0/90)_{2s}$	$(0)_8$
LC(2)	$(\pm45/0/90)_{2s}$	$(\pm45/0/90)_s$	$(45/0)_{2s}$
LC(3)	$(\pm45)_{4s}$	$(\pm45)_{2s}$	$(45)_8$
LC(4)	$(0/90)_8$	$(0/90)_4$	$(0_4/90_4)$
LC(5)	$(\pm45/0/90)_4$	$(\pm45/0/90)_2$	$((45/0)_2/(-45/90)_2)$
LC(6)	$(\pm45)_8$	$(\pm45)_4$	$((45)_4/(-45)_4)$

Table 3.2 Material properties of T300/5208 graphite-epoxy composite material

Mechanical property	Value	Strength property	Value
E_1	132.58 GPa	X_t	1.515 GPa
E_2	10.8 GPa	X_c	1.697 GPa
E_3	10.8 GPa	$Y_t = Z_t$	43.8 MPa
$G_{12} = G_{13}$	5.7 GPa	$Y_c = Z_c$	43.8 MPa
$\nu_{12} = \nu_{13}$	0.24	R	67.6 MPa
ν_{23}	0.49	S=T	86.9 MPa

In the Table 3.2, ν_{12}, ν_{13} and ν_{23} are the Poisson's ratios in the planes 1-2, 1-3 and 2-3, respectively. E_1, E_2 and E_3 are the Young's moduli in the fiber direction and in the directions transverse to it, respectively. G_{12}, G_{13} and G_{23} are the shear moduli associated with planes 1-2, 1-3 and 2-3, respectively. X_t is the tensile strength of lamina in fiber direction. X_c is the compressive strength of lamina in fiber direction. Y_t is the tensile strength of lamina in the direction transverse to fiber direction (in plane 1-2). Y_c is the compressive strength of lamina in the same direction. Z_t is the tensile strength of lamina in principal material direction 3. Z_c is the compressive strength of lamina in principal material direction 3. R, S and T are shear strengths of lamina in planes 2-3, 1-3 and 1-2, respectively.

Table 3.3 Material properties of 5208 epoxy material

Mechanical property	Value	Strength property	Value
E	3.8 GPa	σ_T	43.8 MPa
ν	0.38	σ_C	43.8 MPa
G	1.38 GPa	σ_S	67.6 MPa

In Table 3.3, E is the Young's modulus, ν is the Poisson's ratio, and G is the shear modulus. σ_T , σ_C and σ_S denote the tensile strength, compressive strength and shear strength, respectively.

A 8 by 5 finite element mesh is used in the present analysis. Here, the first number refers to the number of elements in the x direction (the dimension of the plate in the x direction is denoted as a) and the second number corresponds to the y direction (the dimension of the plate in the y direction is denoted as b). Figure 3.7 shows the finite element mesh for a square plate.

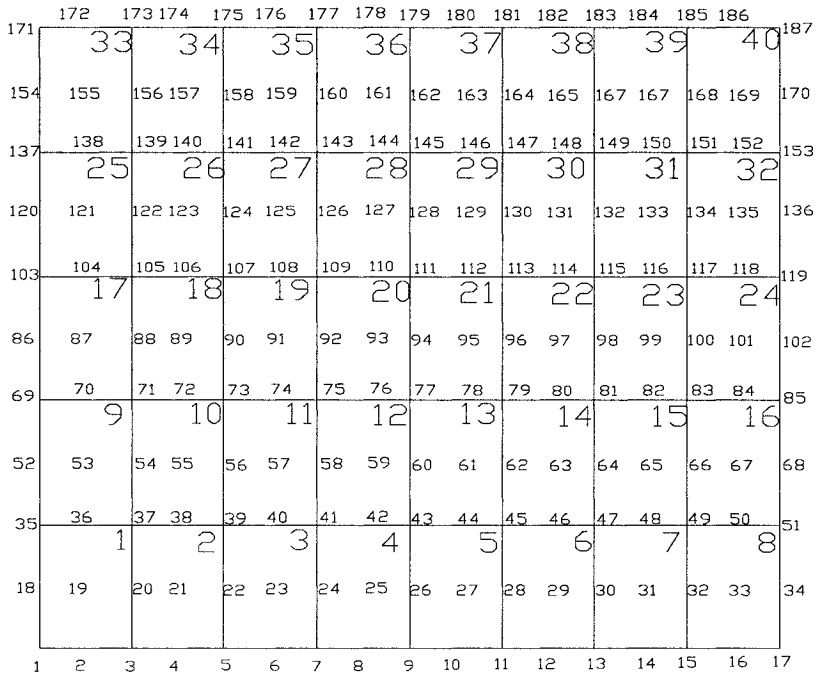

Figure 3.7 Finite element mesh for the plate

3.3 Parametric Study on Uni-axial Compression

3.3.1 Influence of Taper Configuration

Figure 3.8 shows the load versus the maximum deflection curves of the five laminates all with LC(1) lay-up configuration and each with a different taper configuration under the action of uni-axial compression. Table 3.4 gives the buckling load, the first-ply failure load and the ultimate failure load for these laminates. In Figure 3.8 and in all the figures that follow, W_m denotes the maximum deflection of the laminate. In Table 3.4 and in all the tables that follow, the buckling load and the failure loads are presented in the non-dimensional form $P_x hb^2/E_2h^3$. Here, P_x is the applied axial compression per unit area at the right (thin) end of the tapered plate. The corresponding maximum (transverse) deflection is also expressed in non-dimensional form as W_m/h, where h is the average thickness of the tapered laminate.

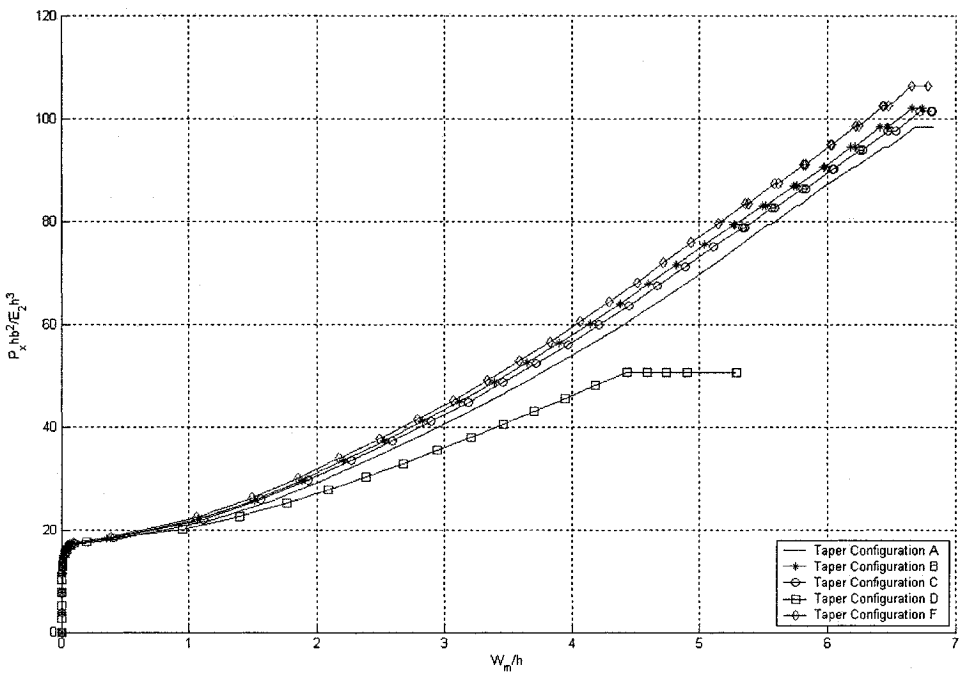

Figure 3.8 Load versus the maximum deflection curves of the laminates with LC(1) lay-up configuration for five taper configurations under uni-axial compression

Table 3.4 Failure data of the laminates with LC(1) lay-up configuration for five taper configurations under uni-axial compression

Taper	Buckling Load ($P_x hb^2/E_2h^3$)	First-ply failure load ($P_x hb^2/E_2h^3$)	Ultimate failure load ($P_x hb^2/E_2h^3$)	$(W_m/h)^*$	Failure location (FL,FE) ♣	First-ply failure mode	Ultimate failure mode
A	17.588	78.200	98.296	5.532	1,8	T♠	D#
B	17.793	79.224	102.110	5.261	1,40	T	D
C	17.686	78.772	101.426	5.332	1,40	T	D
D	16.818	50.604	50.604	4.429	1,24	T	D
F	17.989	83.382	106.270	5.360	1,8	T	D

* Non-dimensionalized maximum deflection at first-ply failure
♣ FL and FE are the failed layer number and failed element number at first-ply failure
♠ Transverse mode of failure refers to the matrix failure
Delamination failure

For lay-up configuration LC(1), both the first-ply failure and the ultimate failure occur at the same value of the loading for taper configuration D. The first-ply failure load is found to be about 4.4 times the buckling load for taper configuration A, 4.5 times for taper configurations B and C, 3.0 times for taper configuration D, and 4.6 times for taper configuration F. The ultimate failure load is about 5.6 times the buckling load for configuration A, 5.7 times for configurations B and C, 3.0 times for configuration D, and 5.9 times for configuration F. The ultimate failure load is about 1.3 times the first-ply failure load for configurations A, B, C and F, and 1 time for configuration D. Hence, it can be observed that considerable residual strength exists in the tapered laminates beyond the onset of buckling. Moreover, except the taper configuration D, all other taper configurations can on an average sustain about 30% more loading after first-ply failure until ultimate failure by delaminiation. Locations corresponding to the first-ply failure lie near the loaded edge of the plate (i.e. the thin end of the plate), and at the outermost bottom layer.

Figure 3.9 shows the load versus the maximum deflection curves of the five laminates all with LC(2) lay-up configuration and each with a different taper configuration under the action of uni-axial compression. Table 3.5 gives the buckling load, the first-ply failure load and the ultimate failure load for these laminates.

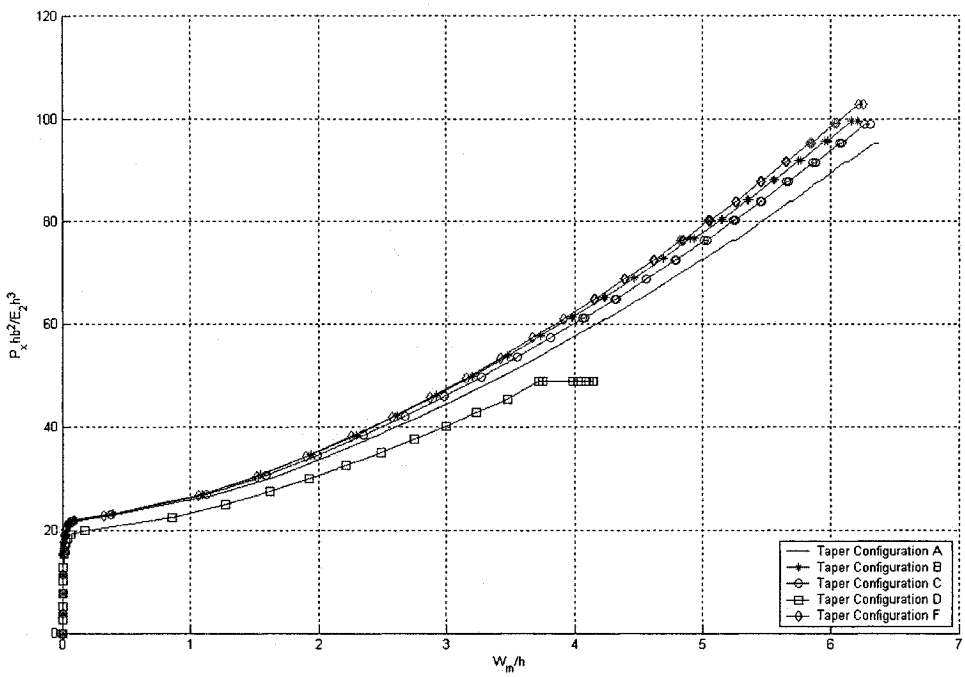

Figure 3.9 Load versus maximum deflection curves of the laminates with LC(2) lay-up configuration for five taper configurations under uni-axial compression

Table 3.5 Failure data of the laminates with LC(2) lay-up configuration for five taper configurations under uni-axial compression

Taper	Buckling Load (P_xhb^2/E_2h^3)	First-ply failure load (P_xhb^2/E_2h^3)	Ultimate failure load (P_xhb^2/E_2h^3)	$(W_m/h)^*$	Failure location (FL,FE) ♣	First-ply failure mode	Ultimate failure mode
A	22.238	60.954	95.283	4.238	1,40	T♠	D#
B	22.581	61.297	99.440	3.978	1,40	T	D
C	22.506	61.028	98.982	4.065	1,40	T	D
D	21.107	48.807	48.807	3.723	1,32	T	D
F	22.798	64.768	102.910	4.155	1,40	T	D

For lay-up configuration LC(2), the values of both the first-ply failure load and the ultimate failure load are the same for taper configuration D. The first-ply failure load is

found to be about 2.7 times the buckling load for configurations A, B and C, 2.3 times for taper configuration D, and 2.8 times for taper configuration F, whereas, the ultimate failure load is about 4.3 times the buckling load for configuration A, 4.4 times for configurations B and C, 2.3 times for configuration D, and 4.5 times for configuration F. The ultimate failure load is about 1.6 times the first-ply failure load for configurations A, B, C and F, and 1 time for configuration D. Locations corresponding to the first-ply failure lie near the loaded edge of the plate (i.e. the thin end of the plate), and at the outermost bottom layer.

In order to illustrate the positive deflection of the plate under uni-axial compression, a typical deformed configuration is given. Figure 3.10 shows the deformed configuration of the laminate with LC(2) lay-up configuration and with taper configuration B. It is observed that the entire laminate undergoes positive (upward) deflection.

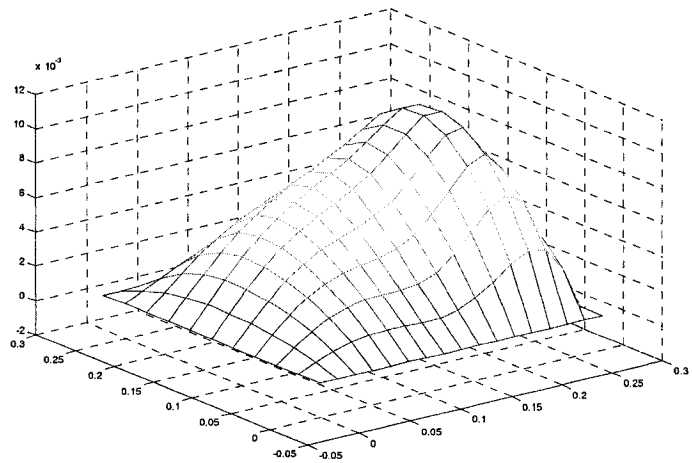

Figure 3.10 The deformed configuration of the laminate with LC(2) lay-up configuration and with taper configuration B under uni-axial compression

Figure 3.11 shows the load versus the maximum deflection curves of the five laminates all with LC(3) lay-up configuration and each with a different taper configuration under

the action of uni-axial compression. Table 3.6 gives the buckling load, the first-ply failure load and the ultimate failure load for these laminates.

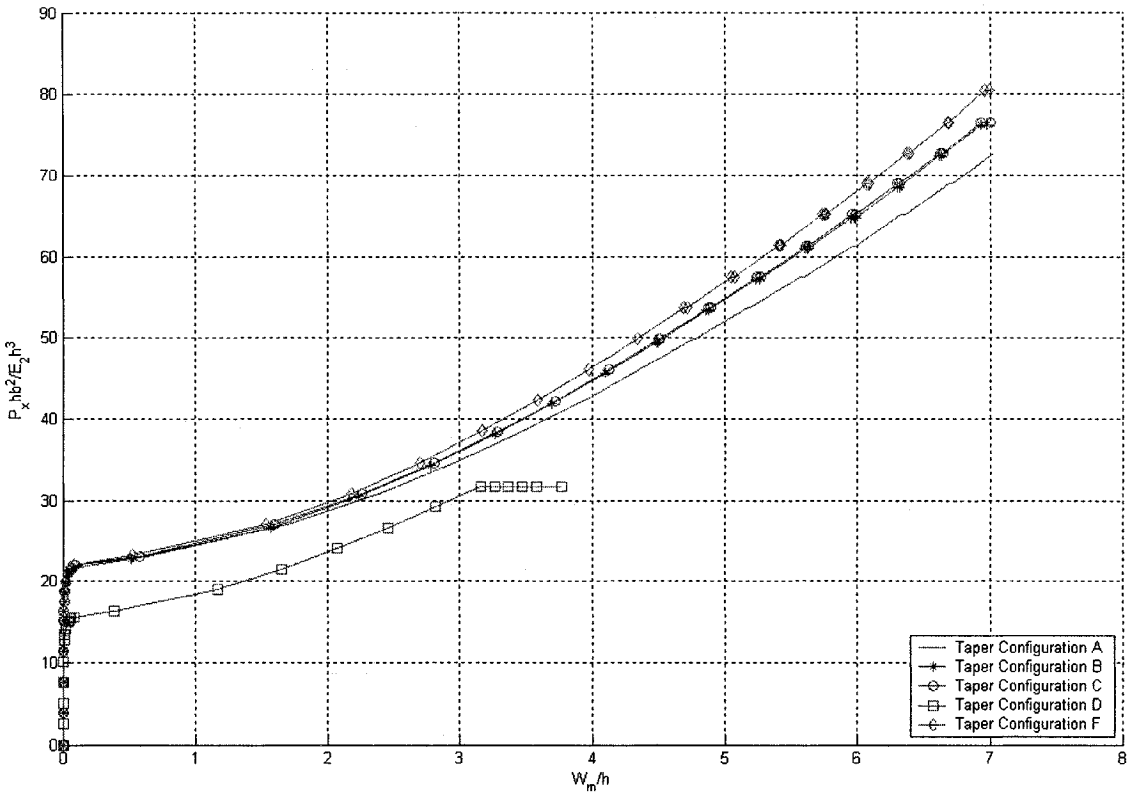

Figure 3.11 Load versus maximum deflection curves of the laminates with LC(3) lay-up configuration for five taper configurations under uni-axial compression

Table 3.6 Failure data of the laminates with LC(3) lay-up configuration for five taper configurations under uni-axial compression

Taper	Buckling Load (P_xhb^2/E_2h^3)	First-ply failure load (P_xhb^2/E_2h^3)	Ultimate failure load (P_xhb^2/E_2h^3)	$(W_m/h)^*$	Failure location (FL,FE) ♣	First-ply failure mode	Ultimate failure mode
A	22.181	49.854	72.740	4.765	1,40	T♠	D#
B	22.238	49.510	76.211	4.485	1,40	T	D
C	22.581	49.854	76.554	4.501	1,40	T	D
D	16.072	31.710	31.710	3.158	1,32	T	D
F	22.619	53.706	80.407	4.692	1,32	T	D

For lay-up configuration LC(3), the values of both the first-ply failure load and the ultimate failure load are the same for taper configuration D. The first-ply failure load is

found to be about 2.2 times the buckling load for configurations A, B and C, 2.0 times for taper configuration D, and 2.4 times for taper configuration F, whereas, the ultimate failure load is about 3.3 times the buckling load for configuration A, 2.4 times for configurations B and C, 2.0 times for configuration D, and 3.6 times for configuration F. The ultimate failure load is about 1.5 times the first-ply failure load for configurations A, B, C and F, and 1 time for configuration D. Locations corresponding to the first-ply failure lie near the loaded edge of the plate (i.e. the thin end of the plate), and at the outermost bottom layer.

Figure 3.12 shows the load versus the maximum deflection curves of the five laminates all with LC(4) lay-up configuration and each with a different taper configuration under the action of uni-axial compression. Table 3.7 gives the buckling load, the first-ply failure load and the ultimate failure load for these laminates.

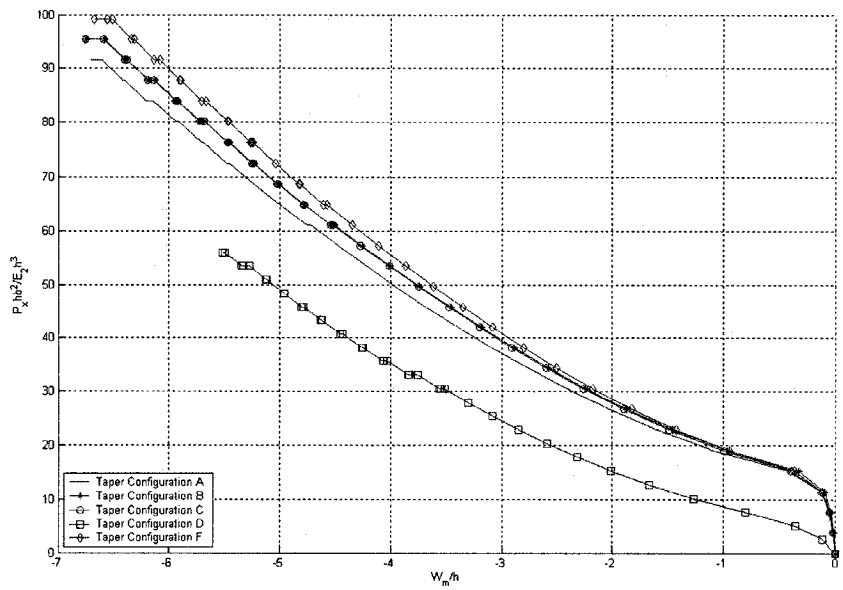

Figure 3.12 Load versus maximum deflection curves of the laminates with LC(4) lay-up configuration for five taper configurations under uni-axial compression

Table 3.7 Failure data of the laminates with LC(4) lay-up configuration for five taper configurations under uni-axial compression

Taper	Buckling Load ($P_x hb^2/E_2h^3$)	First-ply failure load ($P_x hb^2/E_2h^3$)	Ultimate failure load ($P_x hb^2/E_2h^3$)	$(W_m/h)^*$	Failure location (FL,FE) ♣	First-ply failure mode	Ultimate failure mode
A	17.063	61.003	91.545	-4.722	10,8	T♠	D#
B	17.165	61.030	95.359	-4.508	10,16	T	D
C	17.165	61.030	95.359	-4.516	10,16	T	D
D	8.900	30.515	55.944	-3.518	10,16	T	D
F	17.565	64.844	99.173	-4.692	10,32	T	D

For lay-up configuration LC(4), the first-ply and ultimate failures do not occur at the same load value for taper configuration D, unlike LC(1), LC(2) and LC(3) lay-up configurations that are symmetric. As in the case of LC(3), the taper configuration D considerably weakens the laminate with LC(4) lay-up, in terms of buckling, first-ply and ultimate failure strengths. The first-ply failure load is found to be about 3.6 times the buckling load for configurations A, B and C, 3.4 times for taper configuration D, and 3.7 times for taper configuration F, whereas, the ultimate failure load is about 5.4 times the buckling load for configuration A, 5.6 times for configurations B, C and F, 6.3 times for configuration D. The ultimate failure load is about 1.5 times the first-ply failure load for configurations A and F, 1.6 times for configurations B and C, and 1.8 times for configuration D. Locations corresponding to the first-ply failure lie near the loaded edge of the plate (i.e. the thin end of the plate), and at the outermost top layer unlike the symmetric LC(1), LC(2) and LC(3) lay-up configurations. The deflections for lay-up configuration LC(4) are negative, that is, downward.

In order to illustrate the negative deflection of the plate under uni-axial compression, a typical deformed configuration is given. Figure 3.13 shows the deformed configuration of the laminate with LC(4) lay-up configuration and with taper configuration B. It is observed that the entire laminate undergoes negative (downward) deflection.

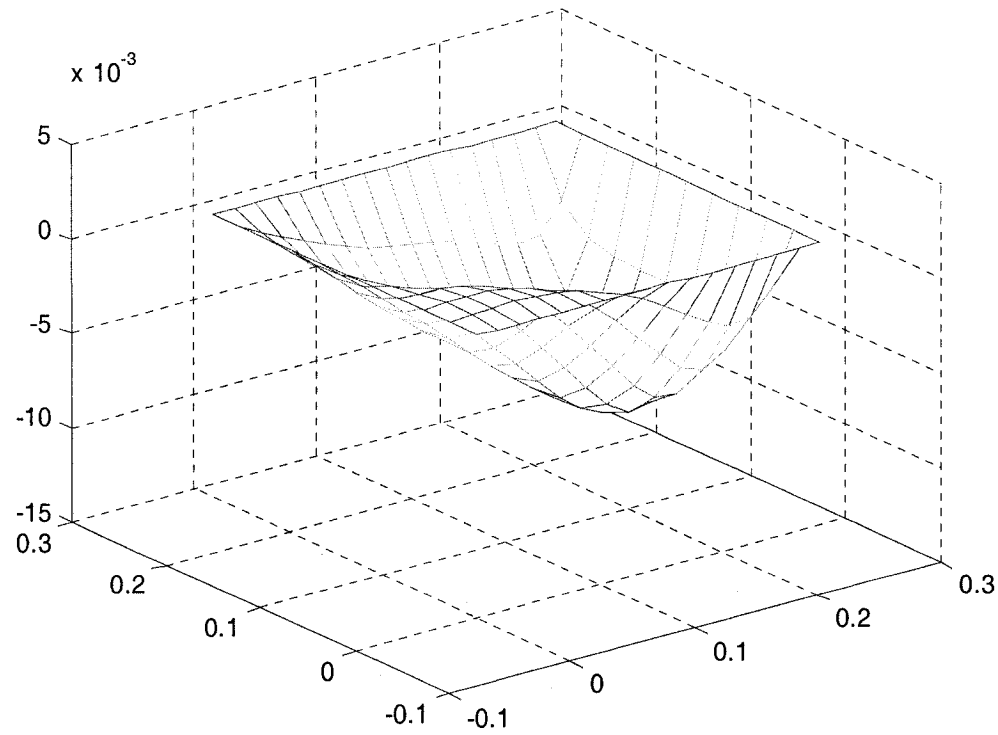

Figure 3.13 The deformed configuration of the laminate with LC(4) lay-up configuration and with taper configuration B under uni-axial compression

Figure 3.14 shows the load versus the maximum deflection curves of the five laminates all with LC(5) lay-up configuration and each with a different taper configuration under the action of uni-axial compression. Table 3.8 gives the buckling load, the first-ply failure load and the ultimate failure load for these laminates.

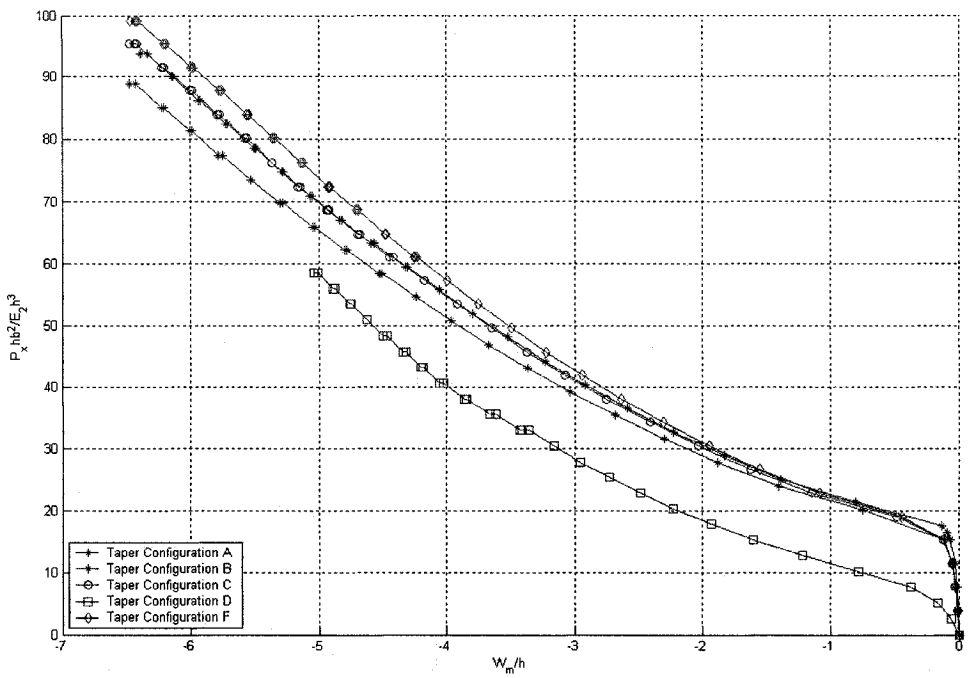

Figure 3.14 Load versus maximum deflection curves of the laminates with LC(5) lay-up configuration for five taper configurations under uni-axial compression

Table 3.8 Failure data of the laminates with LC(5) lay-up configuration for five taper configurations under uni-axial compression

Taper	Buckling Load (P_xhb^2/E_2h^3)	First-ply failure load (P_xhb^2/E_2h^3)	Ultimate failure load (P_xhb^2/E_2h^3)	$(W_m/h)^*$	Failure location (FL,FE) ♣	First-ply failure mode	Ultimate failure mode
A	19.123	58.360	88.875	-4.502	10,16	T♠	D#
B	19.453	59.504	93.833	-4.306	10,16	T	D
C	20.979	61.030	95.357	-4.415	10,8	T	D
D	11.444	33.058	58.487	-3.361	10,16	T	D
F	20.979	61.030	99.171	-4.225	10,8	T	D

For lay-up configuration LC(5), the taper configuration D has weakened the plate as it did in the case of the plate with LC(4) lay-up configuration that is also un-symmetric. The first-ply failure load is found to be about 3.1 times the buckling load for configurations A and B, 2.9 times for taper configurations B, C and D, whereas, the ultimate failure load is about 4.6 times the buckling load for configuration A, 4.8 times

for configuration B, 4.5 times for configuration C, 5.1 times for configuration D, 4.7 times for configuration F. The ultimate failure load is about 1.5 times the first-ply failure load for configurations A, 1.6 times for configurations B C and F, and 1.8 times for configuration D. Locations corresponding to the first-ply failure lie near the loaded edge of the plate (i.e. the thin end of the plate), and at the outermost top layer as in the case of LC(4) laminates. The deflections for lay-up configuration LC(5) are negative, that is, downward.

Figure 3.15 shows the load versus the maximum deflection curves of the five laminates all with LC(6) lay-up configuration and each with a different taper configuration under the action of uni-axial compression. Table 3.9 gives the buckling load, the first-ply failure load and the ultimate failure load for these laminates.

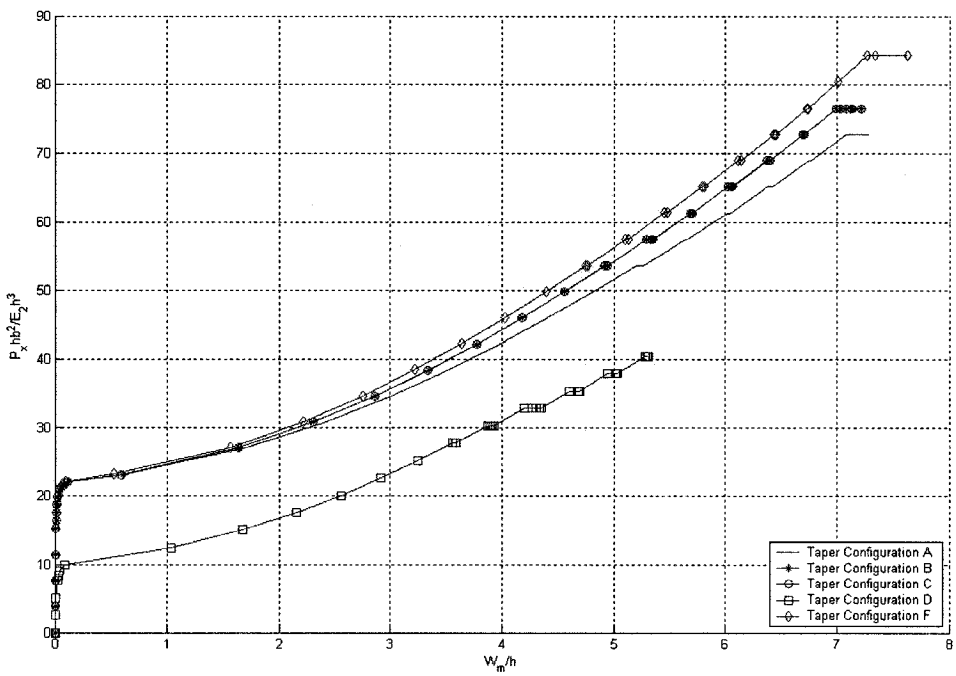

Figure 3.15 Load versus maximum deflection curves of the laminates with LC(6) lay-up configuration for five taper configurations under uni-axial compression

Table 3.9 Failure data of the laminates with LC(6) lay-up configuration for five taper configurations under uni-axial compression

Taper	Buckling Load ($P_x hb^2/E_2h^3$)	First-ply failure load ($P_x hb^2/E_2h^3$)	Ultimate failure load ($P_x hb^2/E_2h^3$)	$(W_m/h)^*$	Failure location (FL,FE) ♣	First-ply failure mode	Ultimate failure mode
A	22.576	53.138	72.740	5.203	1,32	T♠	D#
B	22.581	53.668	76.554	4.921	1,32	T	D
C	22.581	53.668	76.554	4.918	1,40	T	D
D	11.189	27.718	40.432	3.558	1,40	T	D
F	22.679	53.706	84.221	4.742	1,32	T	D

For lay-up configuration LC(6), the taper configuration D has weakened the plate as it did in the cases of the plates with LC(4) and LC(5) lay-up configurations that are also un-symmetric. The first-ply failure load is found to be about 2.4 times the buckling load for configurations A, B, C and F, 2.5 times for taper configuration D, whereas, the ultimate failure load is about 3.2 times the buckling load for configuration A, 3.4 times for configurations B and C, 3.6 times for configuration D, and 3.7 times for configuration F. The ultimate failure load is about 1.4 times the first-ply failure load for configurations A, B and C, 1.5 times for configuration D, and 1.6 times for configuration F. The deflections for all taper configurations are positive, that is, upward. Locations corresponding to the first-ply failure lie near the loaded edge of the plate (i.e. the thin end of the plate), and at the outermost bottom layer as in the case of LC(1), LC(2) and LC(3) laminates that are symmetric.

Summary

From Figures 3.8 – 3.15 and Tables 3.4 – 3.9, the following general observations are also made.

1 For all the six lay-up configurations, the taper configuration F (Mid-plane taper) is the strongest one, and the taper configuration D (Continuous plies interspersed) is the

weakest one among all taper configurations with respect to the first-ply failure load, the ultimate failure load and the buckling load. However, taper configuration F is not easy to manufacture compared to other taper configurations. Considering this, the next strongest taper configuration is identified. For the lay-up configurations LC(1) and LC(2), the taper configuration B (Staircase arrangement) is the best choice among all taper configurations considering the first-ply failure load, the ultimate failure load and the buckling load. For the lay-up configuration LC(5), the taper configuration C (Overlapping dropped plies) is the best choice. For the lay-up configurations LC(4) and LC(6), the taper configuration B and the taper configuration C display nearly the same behavior in terms of the first-ply failure load, the ultimate failure load and the buckling load, so either can be the best choice.

2 For the three symmetric lay-up configurations LC(1), LC(2) and LC(3), the first-ply failure load and the ultimate failure load are the same for the taper configuration D (Continuous plies interspersed). But for the three un-symmetric lay-up configurations LC(4), LC(5) and LC(6), the first-ply failure load and the ultimate failure load are different and considerable residual strength exists in these laminates after first-ply failure until the occurrence of ultimate failure.

3 For the lay-up configurations LC(4) and LC(5), the deflections are negative, that is, downward. But for other lay-up configurations including the un-symmetric lay-up configuration LC(6), the deflections are positive, that is, upward.

3.3.2 Influence of Lay-up Configuration

Figure 3.16 shows the load versus maximum deflection curves of the three symmetric laminates LC(1), LC(2) and LC(3) for taper configuration A under the action of uni-axial

compression. It is observed that the largest stiffness is exhibited by the lay-up configuration LC(2). It is also observed that the least stiffness is exhibited by the lay-up configuration LC(1) within the deflection range $W_m/h \leq 1.90$ and by the lay-up configuration LC(3) for the deflection range $W_m/h > 1.90$.

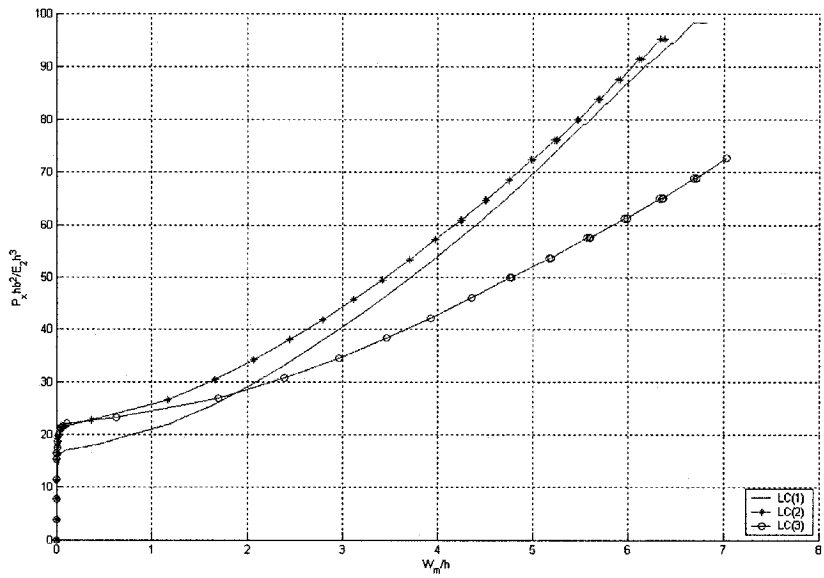

Figure 3.16 Load versus maximum deflection curves of the three symmetric laminates LC(1), LC(2) and LC(3) for taper configuration A under uni-axial compression

Figure 3.17 shows the load versus maximum deflection curves of the six laminates all with taper configuration A and each with a different lay-up configuration under the action of uni-axial compression. Table 3.10 gives the buckling load, the first-ply failure load and the ultimate failure load for these laminates.

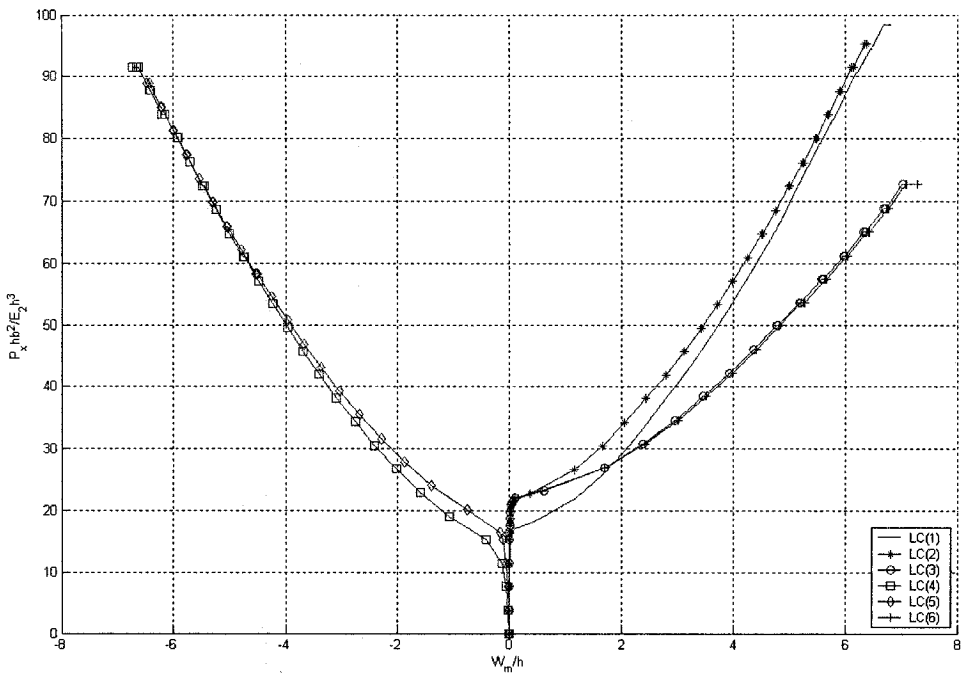

Figure 3.17 Load versus maximum deflection curves of the laminates with taper configuration A for all the six lay-up configurations under uni-axial compression

Table 3.10 Failure data of the laminates with taper configuration A for all the six lay-up configurations under uni-axial compression

Lay-up	Buckling Load (P_xhb^2/E_2h^3)	First-ply failure load (P_xhb^2/E_2h^3)	Ultimate failure load (P_xhb^2/E_2h^3)	$(W_m/h)^*$	Failure location (FL,FE) ♣	First-ply failure mode	Ultimate failure mode
LC(1)	17.588	78.200	98.296	5.532	1,8	T♠	D#
LC(2)	22.238	60.954	95.283	4.238	1,40	T	D
LC(3)	22.181	49.854	72.740	4.765	1,40	T	D
LC(4)	17.063	61.003	91.545	-4.722	10,8	T	D
LC(5)	19.123	58.360	88.875	-4.502	10,16	T	D
LC(6)	22.576	53.138	72.740	5.203	1,32	T	D

For taper configuration A, the lay-up configuration LC(6) is the best choice among all the six lay-up configurations with respect to the buckling load, and lay-up configuration LC(1) is the best choice with respect to both the first-ply failure load and the ultimate failure load.

Figure 3.18 shows the load versus maximum deflection curves of the three symmetric laminates LC(1), LC(2) and LC(3) for taper configuration B under the action of uni-axial compression. It is observed that the largest stiffness is exhibited by the lay-up configuration LC(2). It is also observed that the smallest stiffness is exhibited by the lay-up configuration LC(1) within the deflection range $W_m/h \leq 1.62$ and by the lay-up configuration LC(3) for the deflection range $W_m/h > 1.62$.

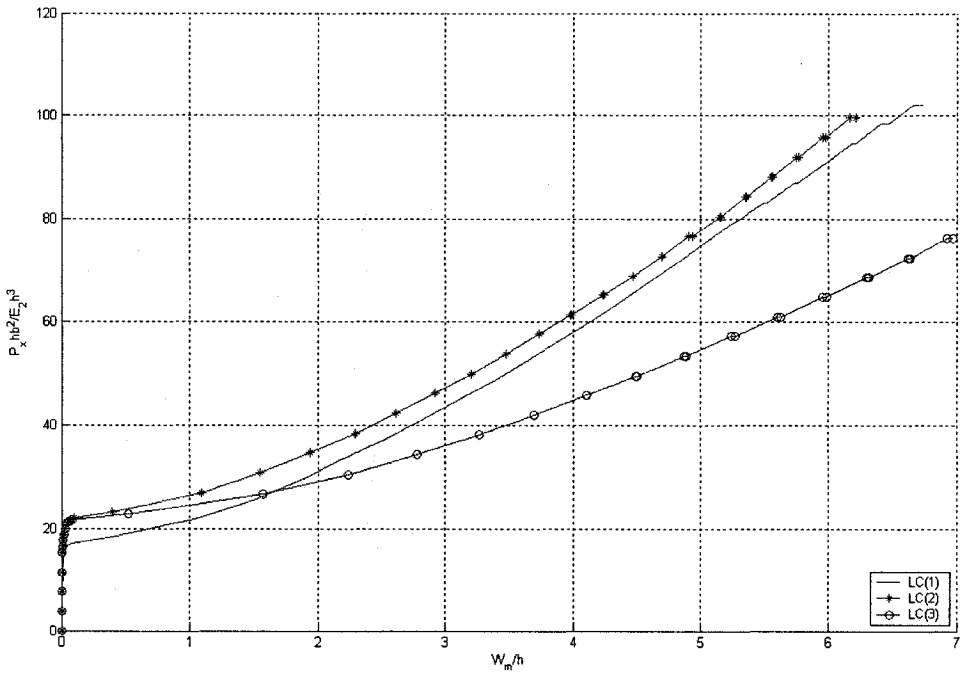

Figure 3.18 Load versus maximum deflection curves of the three symmetric laminates LC(1), LC(2) and LC(3) for taper configuration B under uni-axial compression

Figure 3.19 shows the load versus maximum deflection curves of the six laminates all with taper configuration B and each with a different lay-up configuration under the action of uni-axial compression. Table 3.11 gives the buckling load, the first-ply failure load and the ultimate failure load for these laminates.

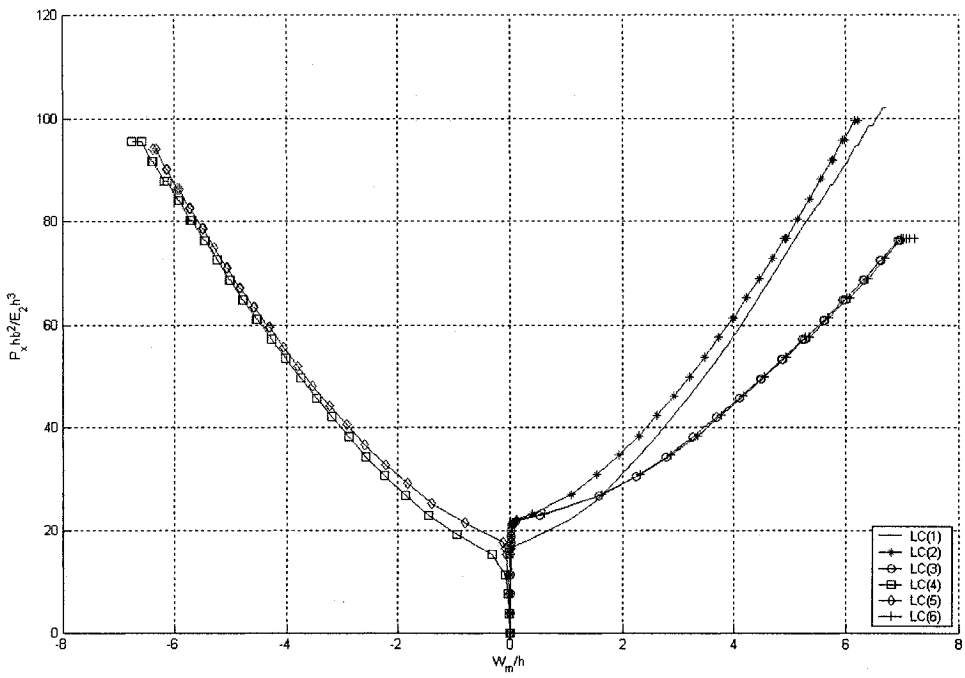

Figure 3.19 Load versus maximum deflection curves of the laminates with taper configuration B for all the six lay-up configurations under uni-axial compression

Table 3.11 Failure data of the laminates with taper configuration B for all the six lay-up configurations under uni-axial compression

Lay-up	Buckling Load ($P_x hb^2/E_2 h^3$)	First-ply failure load ($P_x hb^2/E_2 h^3$)	Ultimate failure load ($P_x hb^2/E_2 h^3$)	$(W_m/h)^*$	Failure location (FL,FE) ♣	First-ply failure mode	Ultimate failure mode
LC(1)	17.793	79.224	102.110	5.261	1,40	T♠	D#
LC(2)	22.581	61.297	99.440	3.978	1,40	T	D
LC(3)	22.238	49.510	76.211	4.485	1,40	T	D
LC(4)	17.165	61.030	95.359	-4.508	10,16	T	D
LC(5)	19.453	59.504	93.833	-4.306	10,16	T	D
LC(6)	22.581	53.668	76.554	4.921	1,32	T	D

For taper configuration B, the lay-up configurations LC(2) and LC(6) are the best choice among all the six lay-up configurations with respect to the buckling load, and the lay-up configuration LC(1) is the best choice with respect to both the first-ply failure load and the ultimate failure load.

Figure 3.20 shows the load versus maximum deflection curves of the three symmetric laminates LC(1), LC(2) and LC(3) for taper configuration C under the action of uni-axial compression. It is observed that the largest stiffness is exhibited by the lay-up configuration LC(2). It is also observed that the smallest stiffness is exhibited by the lay-up configuration LC(1) within the deflection range $W_m/h \leq 1.75$ and by the lay-up configuration LC(3) for the deflection range $W_m/h > 1.75$.

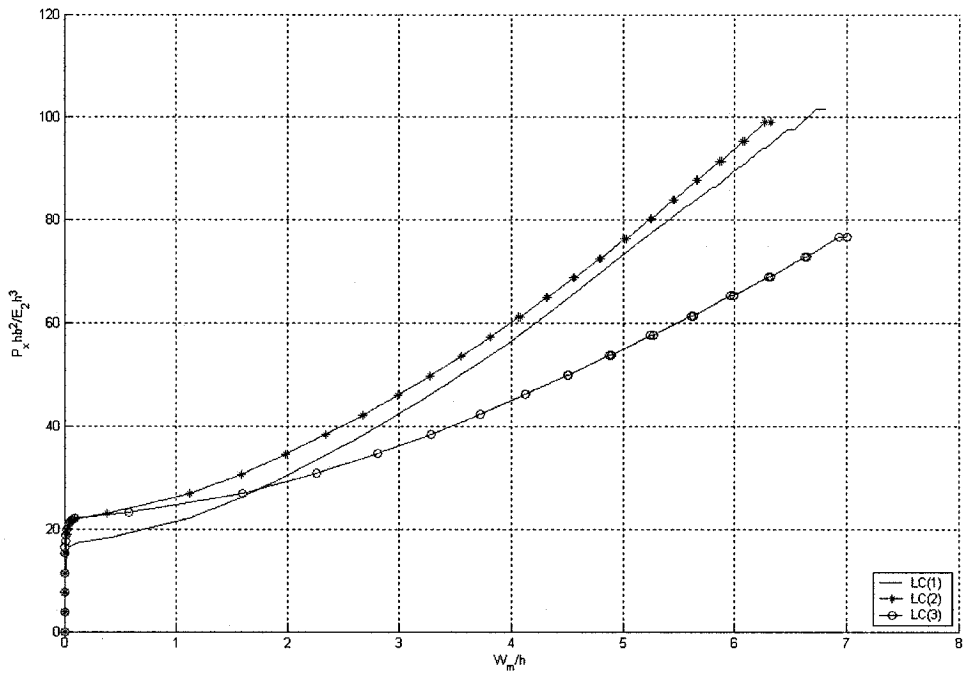

Figure 3.20 Load versus maximum deflection curves of the three symmetric laminates LC(1), LC(2) and LC(3) for taper configuration C under uni-axial compression

Figure 3.21 shows the load versus maximum deflection curves of the six laminates all with taper configuration C and each with a different lay-up configuration under the action of uni-axial compression. Table 3.12 gives the buckling load, the first-ply failure load and the ultimate failure load for these laminates.

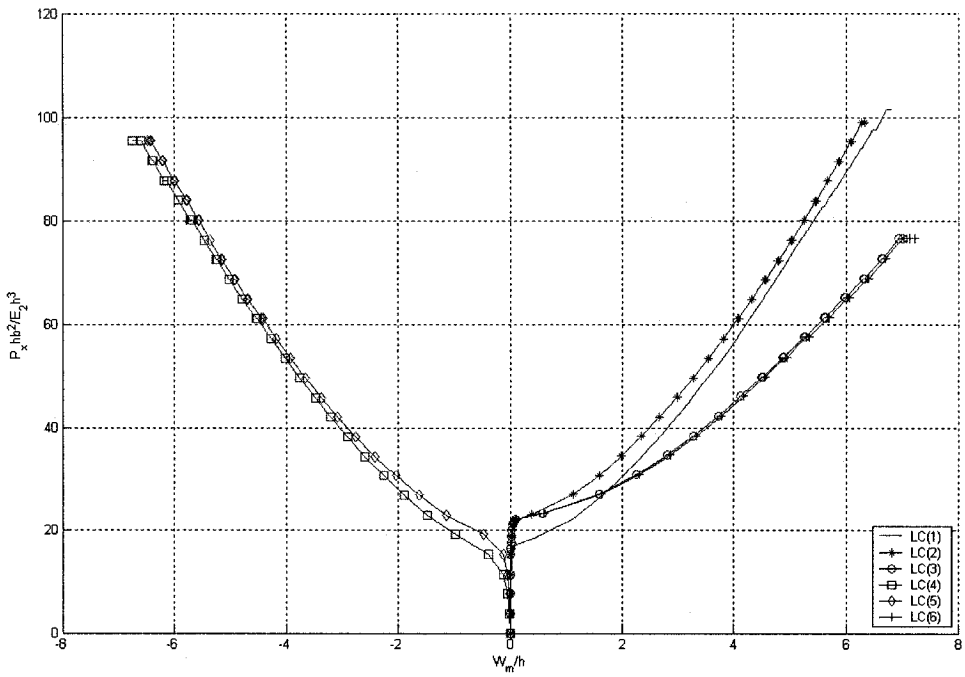

Figure 3.21 Load versus maximum deflection curves of the laminates with taper configuration C for all the six lay-up configurations under uni-axial compression

Table 3.12 Failure data of the laminates with taper configuration C for all the six lay-up configurations under uni-axial compression

Lay-up	Buckling Load (P_xhb^2/E_2h^3)	First-ply failure load (P_xhb^2/E_2h^3)	Ultimate failure load (P_xhb^2/E_2h^3)	$(W_m/h)^*$	Failure location (FL,FE) ♣	First-ply failure mode	Ultimate failure mode
LC(1)	17.686	78.772	101.426	5.332	1,40	T♠	D#
LC(2)	22.506	61.028	98.982	4.065	1,40	T	D
LC(3)	22.581	49.854	76.554	4.501	1,40	T	D
LC(4)	17.165	61.030	95.359	-4.516	10,16	T	D
LC(5)	20.979	61.030	95.357	-4.415	10,8	T	D
LC(6)	22.581	53.668	76.554	4.918	1,40	T	D

For taper configuration C, the lay-up configurations LC(2), LC(3) and LC(6) are the best choice among all the six lay-up configurations with respect to the buckling load, and lay-up configuration LC(1) is the best choice with respect to both the first-ply failure load and the ultimate failure load and.

Figure 3.22 shows the load versus maximum deflection curves of the three symmetric laminates LC(1), LC(2) and LC(3) for taper configuration D under the action of uni-axial compression. It is observed that the largest stiffness is exhibited by the lay-up configuration LC(2). It is also observed that the smallest stiffness is exhibited by the lay-up configuration LC(3).

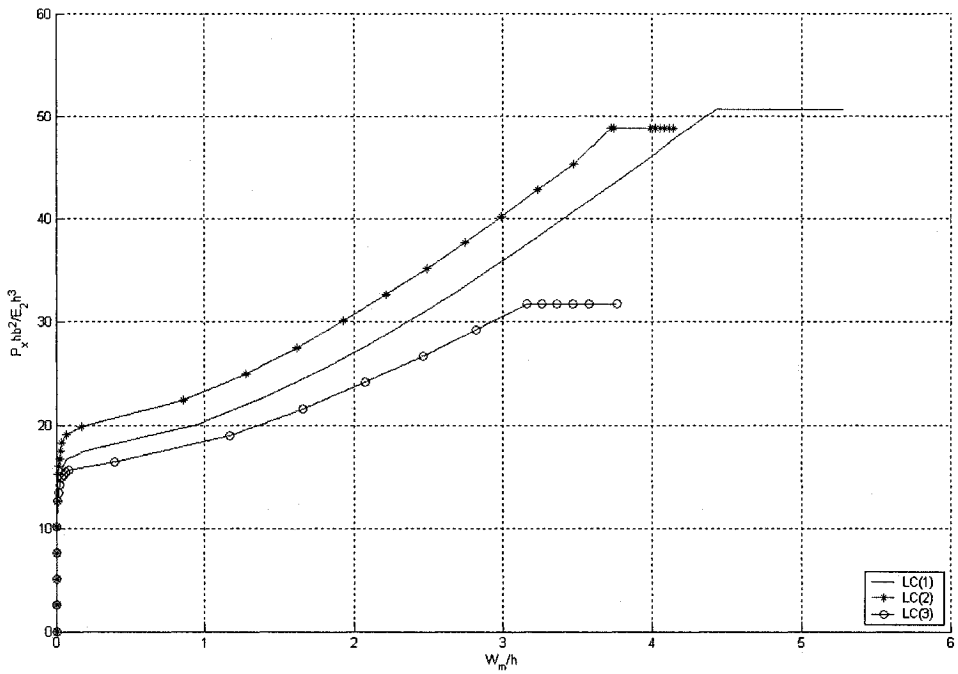

Figure 3.22 Load versus maximum deflection curves of the three symmetric laminates LC(1), LC(2) and LC(3) for taper configuration D under uni-axial compression

Figure 3.23 shows the load versus maximum deflection curves of the six laminates all with taper configuration D and each with a different lay-up configuration under the action of uni-axial compression. Table 13 gives the buckling load, the first-ply failure load and the ultimate failure load for these laminates.

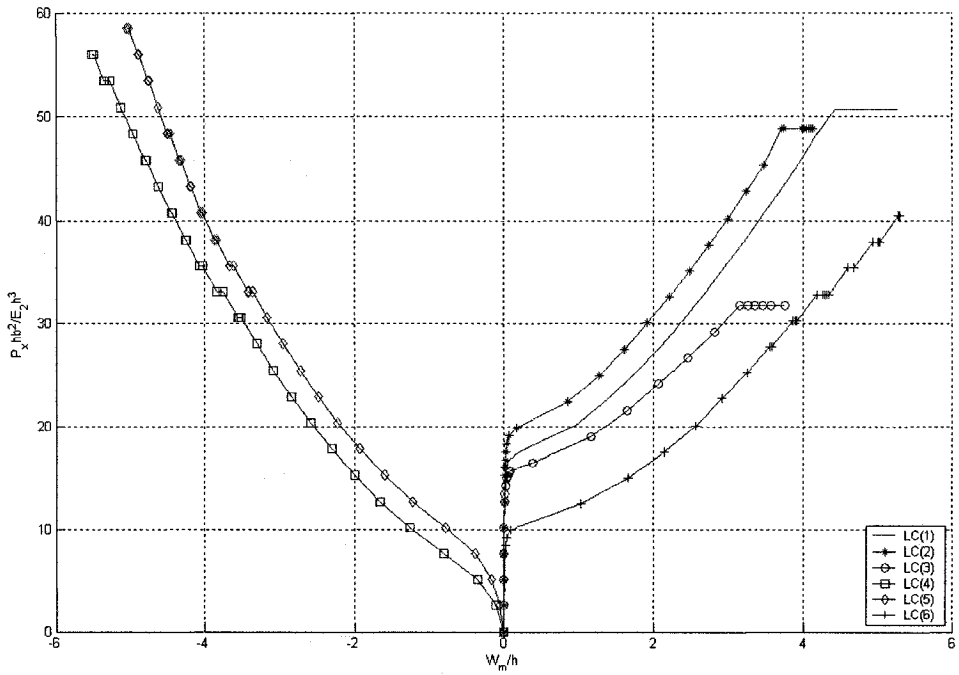

Figure 3.23 Load versus maximum deflection curves of the laminates with taper configuration D for all the six lay-up configurations under uni-axial compression

Table 3.13 Failure data of the laminates with taper configuration D for all the six lay-up configurations under uni-axial compression

Lay-up	Buckling Load (P_xhb^2/E_2h^3)	First-ply failure load (P_xhb^2/E_2h^3)	Ultimate failure load (P_xhb^2/E_2h^3)	$(W_m/h)^*$	Failure location (FL,FE) ♣	First-ply failure mode	Ultimate failure mode
LC(1)	16.818	50.604	50.604	4.429	1,24	T♠	D#
LC(2)	21.107	48.807	48.807	3.723	1,32	T	D
LC(3)	16.072	31.710	31.710	3.158	1,32	T	D
LC(4)	8.900	30.515	55.944	-3.518	10,16	T	D
LC(5)	11.444	33.058	58.487	-3.361	10,16	T	D
LC(6)	11.189	27.718	40.432	3.558	1,40	T	D

For taper configuration D, the lay-up configuration LC(2) is the best choice among all the six lay-up configurations with respect to the buckling load, the lay-up configuration LC(1) is the best choice with respect to the first-ply failure load, and the lay-up configuration LC(4) is the best choice with respect to the ultimate failure load.

Figure 3.24 shows the load versus maximum deflection curves of the three symmetric laminates LC(1), LC(2) and LC(3) for taper configuration F under the action of uni-axial compression. It is observed that the largest stiffness is exhibited by the lay-up configuration LC(2). It is also observed that the smallest stiffness is exhibited by the lay-up configuration LC(1) within the deflection range $W_m/h \leq 1.62$ and by the lay-up configuration LC(3) for the deflection range $W_m/h > 1.62$.

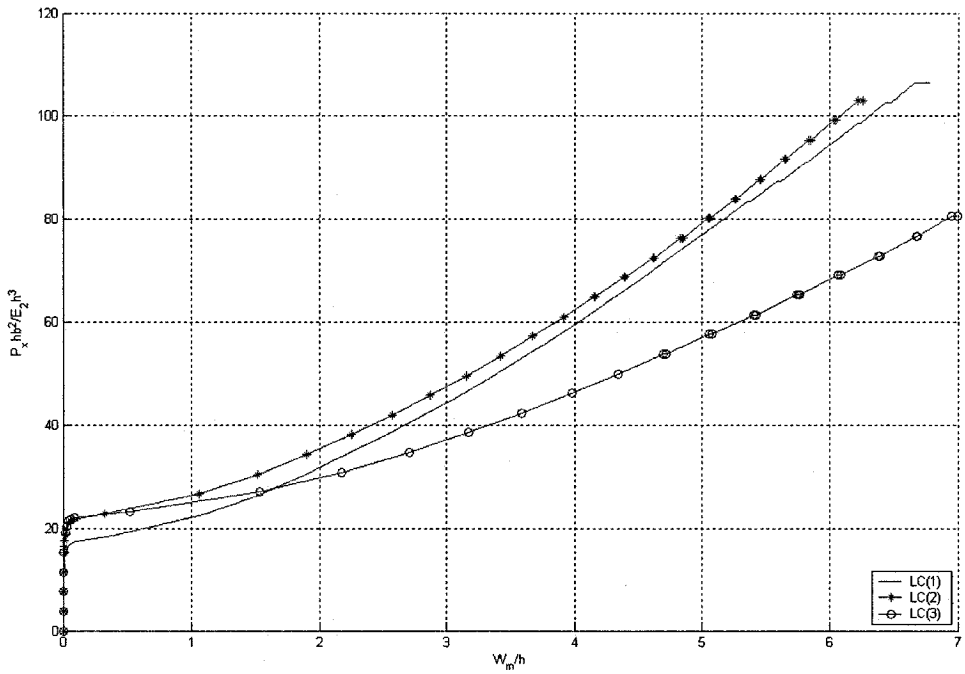

Figure 3.24 Load versus maximum deflection curves of the three symmetric laminates LC(1), LC(2) and LC(3) for taper configuration F under uni-axial compression

Figure 3.25 shows the load versus maximum deflection curves of the six laminates all with taper configuration F and each with a different lay-up configuration under the action of uni-axial compression. Table 14 gives the buckling load, the first-ply failure load and the ultimate failure load for these laminates.

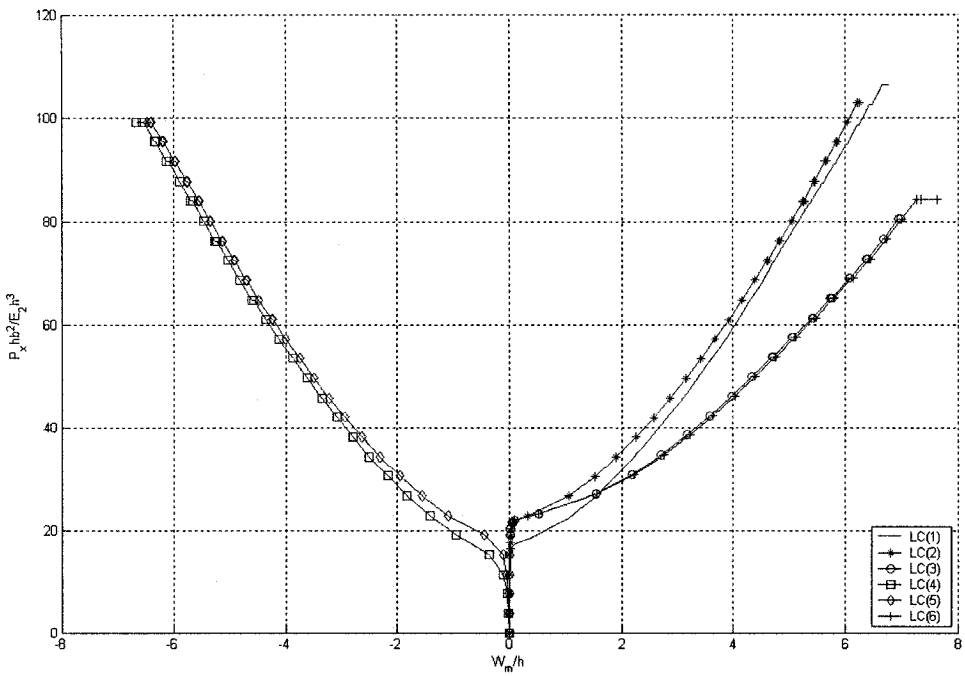

Figure 3.25 Load versus maximum deflection curves of the laminates with taper configuration F for all the six lay-up configurations under uni-axial compression

Table 3.14 Failure data of the laminates with taper configuration F for all the six lay-up configurations under uni-axial compression

Lay-up	Buckling Load (P_xhb^2/E_2h^3)	First-ply failure load (P_xhb^2/E_2h^3)	Ultimate failure load (P_xhb^2/E_2h^3)	$(W_m/h)^*$	Failure location (FL,FE) ♣	First-ply failure mode	Ultimate failure mode
LC(1)	17.989	83.382	106.270	5.360	1,8	T♠	D#
LC(2)	22.798	64.768	102.910	4.15	1,40	T	D
LC(3)	22.619	53.706	80.407	4.692	1,32	T	D
LC(4)	17.565	64.844	99.173	-4.692	10,32	T	D
LC(5)	20.979	61.030	99.171	-4.225	10,8	T	D
LC(6)	22.679	53.706	84.221	4.742	1,32	T	D

For taper configuration F, the lay-up configuration LC(2) is the best choice among all the six lay-up configurations with respect to the buckling load, and the lay-up configuration LC(1) is the best choice with respect to both the first-ply failure load and the ultimate failure load.

Summary

From Figures 3.16 – 3.25 and Table 3.10 – 3.14, the following general observations are also made.

1 For all the five taper configurations, the first-ply failure mode for all the six lay-up configurations is transverse (matrix) failure.

2 For all the five taper configurations, the ultimate failure mode for all the six lay-up configurations is delamination.

3 Locations corresponding to the first-ply failure for all the six lay-up configurations lie near the loaded edge of the plates (i.e. the thin end of the plate). However, for LC(4) and LC(5) lay-up configurations, the failure occurs at the outermost top layer, and for the rest of the lay-up configurations it occurs at the outermost bottom layer.

4 For the lay-up configurations LC(4) and LC(5), the deflections are negative, i.e. downward. But for other lay-up configurations, the deflections are positive, i.e. upward.

5 Variation of the maximum deflection with the load for the symmetric lay-up configuration LC(3) almost coincides with that of the corresponding un-symmetric lay-up configuration LC(6). Therefore, in this case the symmetry in the stacking sequence does not have a strong influence on the progressive failure of the laminate.

3.3.3 Influence of Fiber Orientation

Tapered laminates under uni-axial compression and with lay-up $(\pm\theta)_{4s}$ at the left end are considered. The lay-up at the right (thin) end is $(\pm\theta)_{2s}$ for taper configurations A, B, C and F, and is $(\theta)_8$ for taper configuration D. The variation of buckling load with θ for each taper configuration is determined. The results are plotted in Figure 3.26. A non-

monotonic variation is observed for all taper configurations from this figure. Also the variation is un-symmetric about 45° fiber orientation. Peak values of the buckling loads are predicted to occur for 30° fiber orientation for all taper configurations. From Figure 3.26 it can also be observed that the taper configuration D has the lowest value of buckling load, and the taper configuration F has the highest value of buckling load. The buckling load of the taper configuration C is very close to that of the taper configuration F for $(\pm 0)_{4s}$, $(\pm 15)_{4s}$, $(\pm 30)_{4s}$, $(\pm 45)_{4s}$, and $(\pm 90)_{4s}$ fiber orientations.

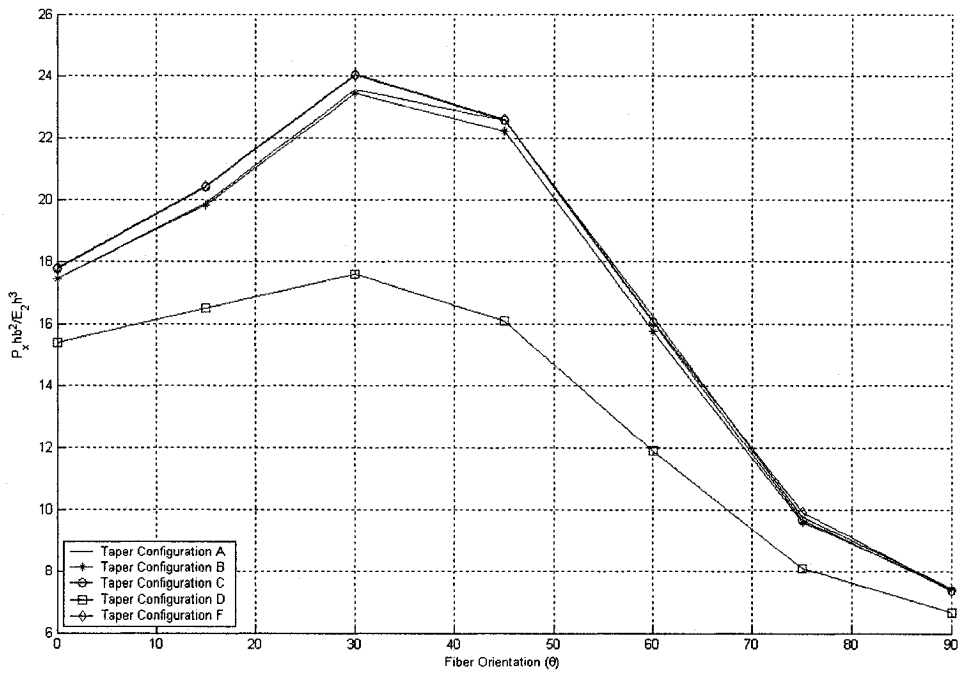

Figure 3.26 Buckling loads of the laminates with $(\pm\theta)_{4s}$ lay-up at the left (thick) end under uni-axial compression

Figure 3.27 shows the variation of the first-ply failure load and the ultimate failure load for laminates with taper configuration A and with lay-up $(\pm\theta)_{4s}$ at the left (thick) end under uni-axial compression. The results show that the variations in response are un-symmetric about 45° fiber orientation. Peak values of the first-ply failure load and

ultimate failure load are predicted to occur for 45° fiber orientation. For $(\pm 0)_{4s}$, $(\pm 15)_{4s}$, $(\pm 75)_{4s}$, and $(\pm 90)_{4s}$ laminates, the value of the first-ply failure load is equal to the value of the ultimate failure load. In the range $15° \leq \theta \leq 45°$ the difference between the ultimate failure load and the first-ply failure load becomes larger, and at θ = 45° the ultimate failure load is 45.91% higher than the first-ply failure load.

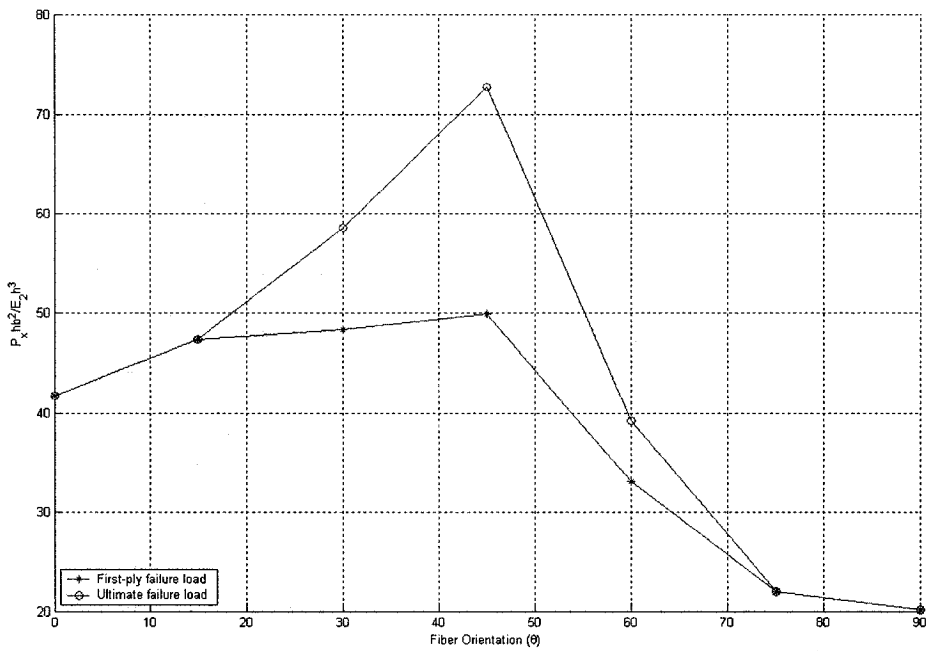

Figure 3.27 Variation of the first-ply and ultimate failure loads of the laminates with taper configuration A and with $(\pm\theta)_{4s}$ lay-up at the left end under uni-axial compression

Figure 3.28 shows the variation of the first-ply failure load and the ultimate failure load for laminates with taper configuration B and with lay-up $(\pm\theta)_{4s}$ at the left (thick) end under uni-axial compression. The results show that the variations in response are un-symmetric about 45° fiber orientation. Peak values of the first-ply failure load and ultimate failure load are predicted to occur for 45° fiber orientation. For $(\pm 0)_{4s}$, $(\pm 75)_{4s}$, and $(\pm 90)_{4s}$ laminates, the value of the first-ply failure load is equal to the value of the

ultimate failure load. In the range $15° \leq \theta \leq 45°$ the difference between the ultimate failure load and the first-ply failure load becomes larger, and at θ = 45° the ultimate failure load is 53.93% higher than the first-ply failure load.

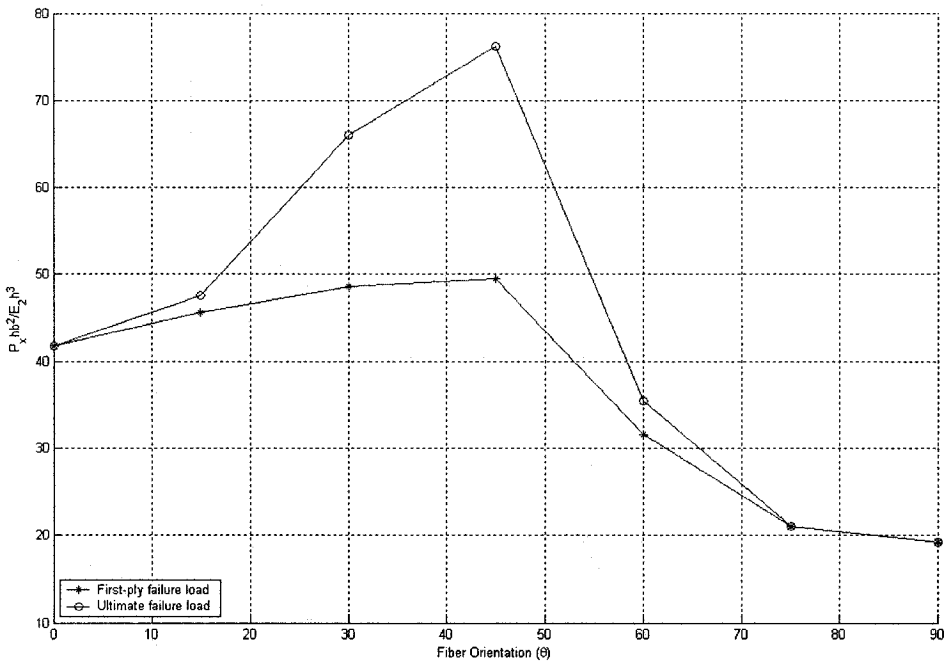

Figure 3.28 Variation of the first-ply and ultimate failure loads of the laminates with taper configuration B and with $(\pm\theta)_{4s}$ lay-up at the left end under uni-axial compression

Figure 3.29 shows the variation of the first-ply failure load and the ultimate failure load for laminates with taper configuration C and with lay-up $(\pm\theta)_{4s}$ at the left (thick) end under uni-axial compression. The results show that the variations in response are un-symmetric about 45° fiber orientation. Peak values of the first-ply failure load and ultimate failure load are predicted to occur for 45° fiber orientation. For $(\pm 0)_{4s}$, $(\pm 75)_{4s}$, and $(\pm 90)_{4s}$ laminates, the value of the first-ply failure load is equal to the value of the ultimate failure load. In the range $15° \leq \theta \leq 45°$ the difference between the ultimate failure load and the first-ply failure load becomes larger, and at θ = 45° the ultimate failure load is 53.56% higher than the first-ply failure load.

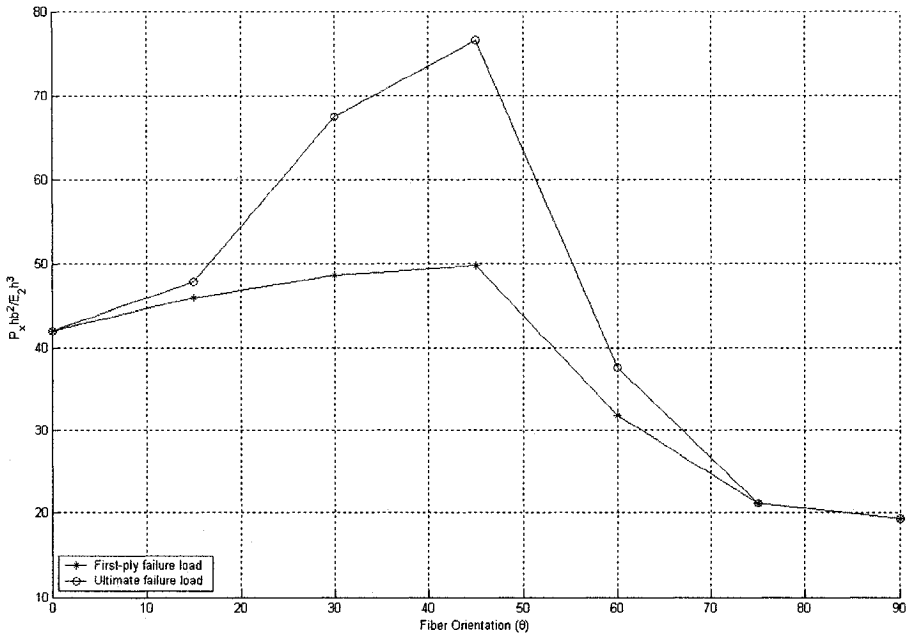

Figure 3.29 Variation of the first-ply and ultimate failure loads of the laminates with taper configuration C and with $(\pm\theta)_{4s}$ lay-up at the left end under uni-axial compression

Figure 3.30 shows the variation of the first-ply failure load and the ultimate failure load for laminates with taper configuration D and with lay-up $(\pm\theta)_{4s}$ at the left (thick) end under uni-axial compression. The results show that the variations in response are un-symmetric about 45° fiber orientation. Peak values of the first-ply failure load and ultimate failure load are predicted to occur for 15° fiber orientation. The value of the first-ply failure load is equal to the value of the ultimate failure load for all the fiber orientation angles.

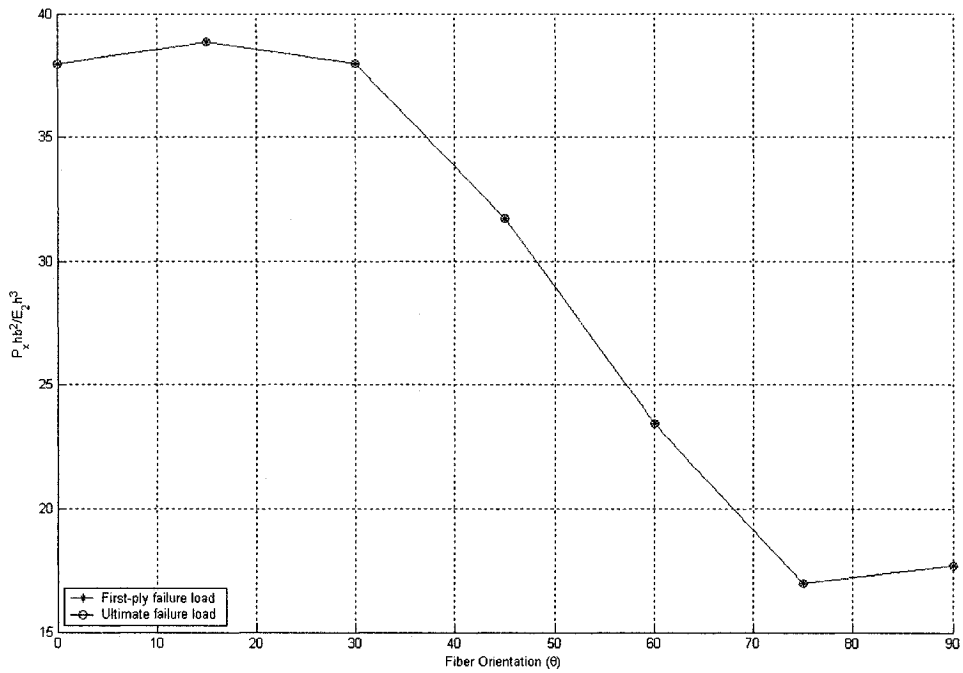

Figure 3.30 Variation of the first-ply and ultimate failure loads of the laminates with taper configuration D and with $(\pm\theta)_{4s}$ lay-up at the left end under uni-axial compression

Figure 3.31 shows the variation of the first-ply failure load and the ultimate failure load for laminates with taper configuration F and with lay-up $(\pm\theta)_{4s}$ at the left (thick) end under uni-axial compression. The results show that the variations in response are un-symmetric about 45° fiber orientation. Peak values of the first-ply failure load and ultimate failure load occur for 45° fiber orientation. For $(\pm 0)_{4s}$, $(\pm 75)_{4s}$, and $(\pm 90)_{4s}$ laminates, the value of the first-ply failure load is equal to the value of the ultimate failure load. In the range $15° \leq \theta \leq 45°$ the difference between the ultimate failure load and the first-ply failure load becomes larger, and at $\theta = 45°$ the ultimate failure load is 49.72% higher than the first-ply failure load.

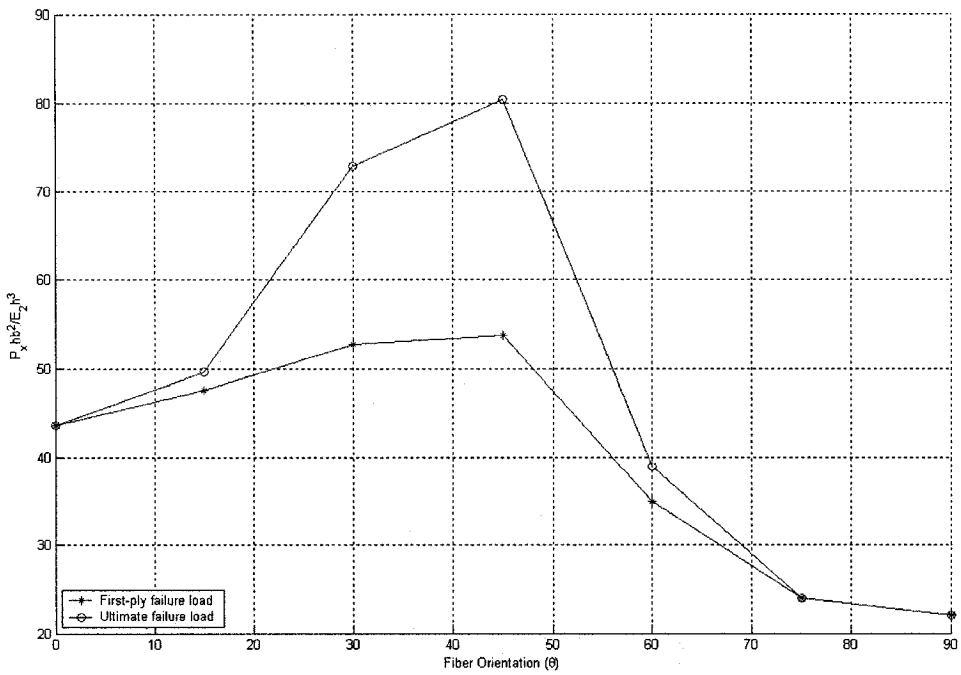

Figure 3.31 Variation of the first-ply and ultimate failure loads of the laminates with taper configuration F and with $(\pm\theta)_{4s}$ lay-up at the left end under uni-axial compression

Figure 3.32 shows the variation of first-ply failure load of tapered laminates with $(\pm\theta)_{4s}$ lay-up at the left (thick) end under uni-axial compression for all the taper configurations. The results show that the variations are un-symmetric about 45° fiber orientation. Peak values of the first-ply failure loads for taper configurations A, B, C, and F are observed at 45° fiber orientation, and for taper configuration D the peak value occurs for 15° fiber orientation. From Figure 3.32 it can be observed that the taper configuration D has the lowest value of first-ply failure load for all fiber orientations, and it is also observed that the taper configuration F has the highest value of first-ply failure load. For $(\pm 0)_{4s}$, the first-ply failure loads of taper configurations A, B, and C are nearly the same. For $(\pm 45)_{4s}$, $(\pm 60)_{4s}$, $(\pm 75)_{4s}$ and $(\pm 90)_{4s}$ laminates, the first-ply failure loads of taper configurations A, B and C are very close to each other. The first-ply failure loads of taper configurations B

and C are close to each other for all fiber orientation angles, except for 30° fiber orientation.

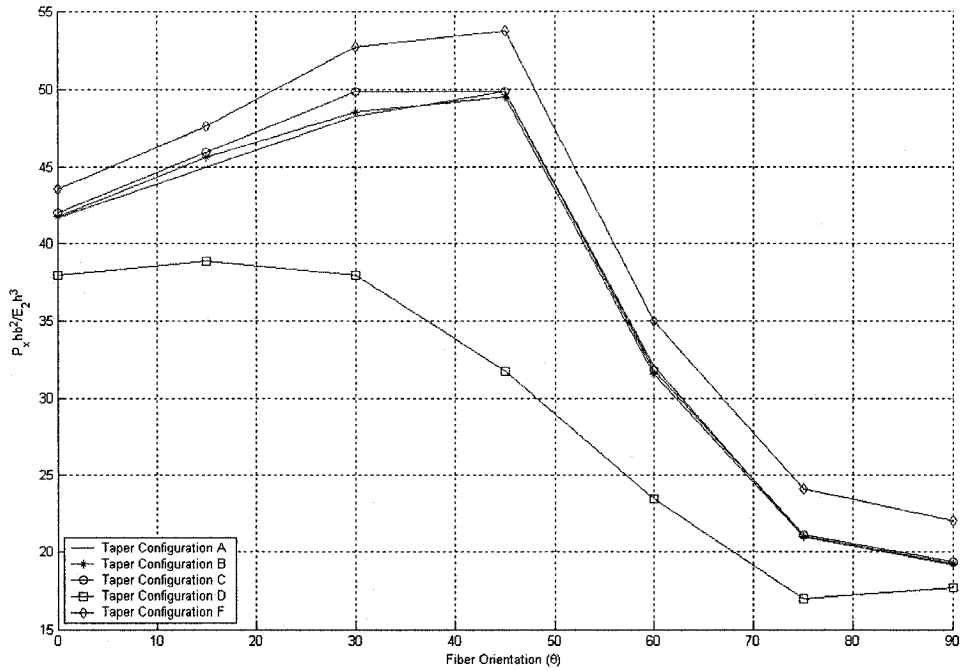

Figure 3.32 First-ply failure load of the laminates with $(\pm\theta)_{4s}$ lay-up at the left (thick) end under uni-axial compression

Figure 3.33 shows the variation of ultimate failure load of tapered laminates with $(\pm\theta)_{4s}$ lay-up at the left (thick) end under uni-axial compression for all the taper configurations. The results show that the variations are un-symmetric about 45° fiber orientation. Peak values of the ultimate failure loads for taper configurations A, B, C, and F correspond to 45° fiber orientation, and for taper configuration D the peak value occurs for 15° fiber orientation. From Figure 3.33 it is observed that the taper configuration D has the lowest value of ultimate failure load for all fiber orientations. It is also observed that the taper configuration F has the highest value of ultimate failure load. For $(\pm0)_{4s}$, $(\pm15)_{4s}$, $(\pm45)_{4s}$,

$(\pm 75)_{4s}$ and $(\pm 90)_{4s}$ laminates, the ultimate failure loads of taper configurations B and C are very close to each other.

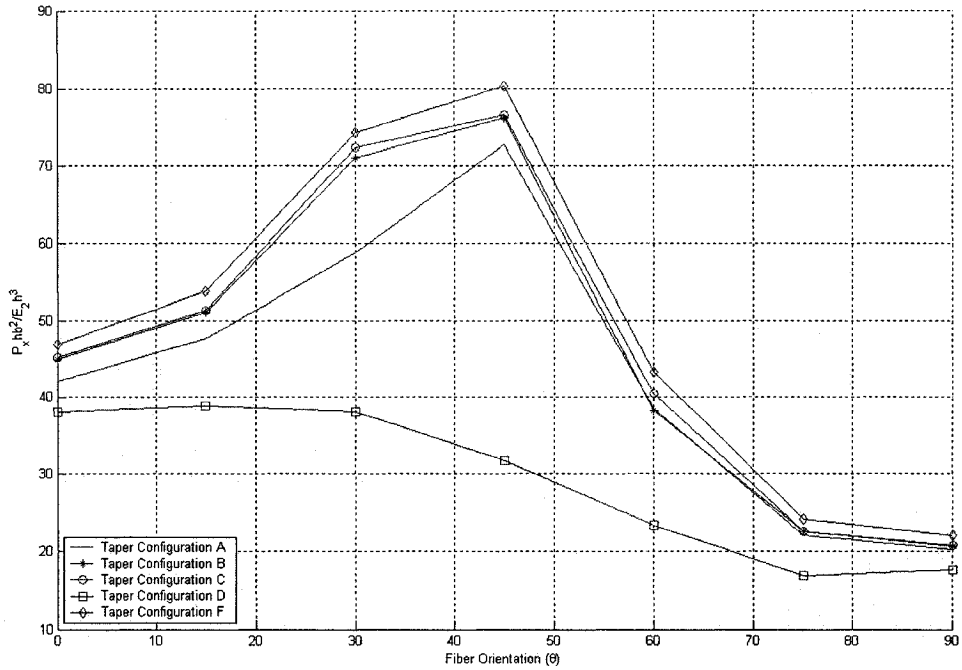

Figure 3.33 Ultimate failure load of the laminates with $(\pm\theta)_{4s}$ lay-up at the left (thick) end under uni-axial compression

3.3.4 Influence of Uniform-thickness Sections

A thick section and a thin section of uniform-thickness laminate are added to the tapered laminate to study their influence on the progressive failure. Taper configuration B is considered for the tapered section of the plate that has $(\pm 45/0/90)_{2s}$ lay-up at the left end. The length of the plate is 0.4185 m. The length of the taper section, L_2, is 0.279 m. The sum of the lengths of thick and thin uniform-thickness sections, L_1+L_3, is 0.1395 m. The width of the plate is 0.279 m. The boundary condition shown in Figure 3.6 is considered. The length of the thick section (L_1) and the length of the thin section (L_3) will be varied

according to the length ratio, i.e. the ratio of the length of thick section (L_1) to the length of thin section (L_3). Figure 3.34 shows the plate with the length ratio that is equal to 1.

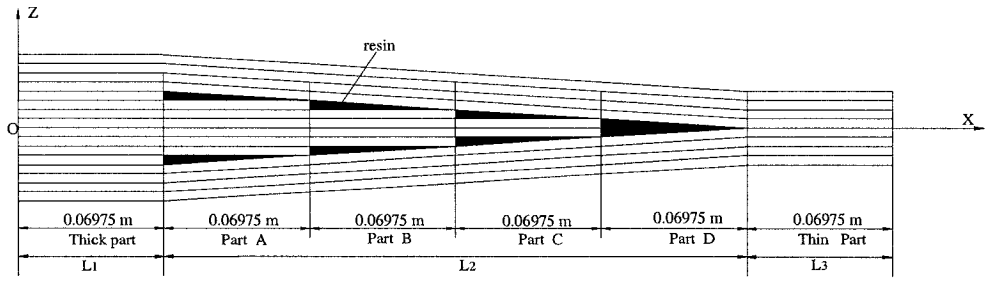

Figure 3.34 Plate with taper configuration B and with thick and thin sections

Figure 3.35 shows the load versus maximum deflection curves of five tapered plates under the action of uni-axial compression. Table 3.15 gives the buckling load, the first-ply failure load and the ultimate failure load for these laminates under the action of uni-axial compression. From Figure 3.35 and Table 3.15, it is observed that the largest stiffness is exhibited by the tapered plate with length ratio 2:1 within the deflection range $W_m/h \leq 1.7$ and by the tapered plate with length ratio 1:2 for the deflection range $W_m/h > 1.7$. The laminate with length ratio 2:1 is the best choice among these five laminates with respect to the buckling load, the laminate with length ratio 1:2 is the best choice with respect to both the first-ply failure load and the ultimate failure load. It is also observed that for all the cases the first-ply failure corresponds to the transverse (matrix) failure, and the ultimate failure corresponds to the delamination failure as in the case of the plate with only the tapered section. Therefore, it is noted that the addition of uniform-thickness sections did not change the modes of failure. However, considerably more resistance to buckling, first-ply and ultimate failures is provided by the addition of uniform-thickness sections.

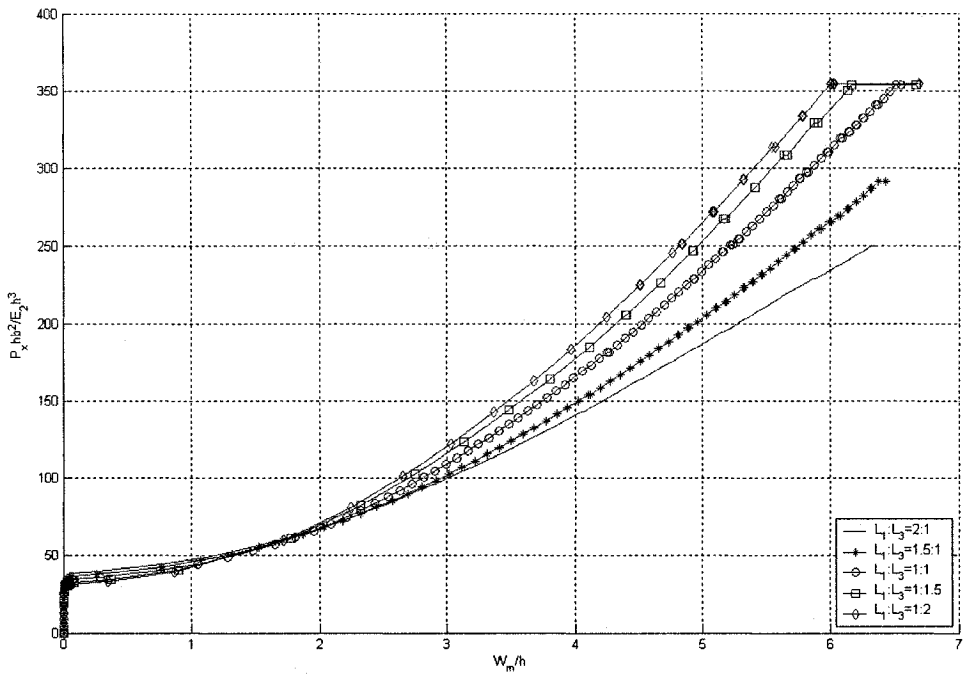

Figure 3.35 Load versus the maximum deflection curves of five tapered plates with different length ratios under the action of uni-axial compression

Table 3.15 Failure data of five tapered plates with different length ratios under the action of uni-axial compression

$L_1:L_3$	Buckling Load (P_xhb^2/E_2h^3)	First-ply failure load (P_xhb^2/E_2h^3)	Ultimate failure load (P_xhb^2/E_2h^3)	$(W_m/h)^*$	Failure location (FL,FE) ♣	First-ply failure mode	Ultimate failure mode
2:1	39.222	142.850	250.130	4.051	1,50	T♠	D#
1.5:1	37.505	154.010	291.330	4.106	1,50	T	D
1:1	35.318	181.860	353.510	4.254	1,50	T	D
1:1.5	33.636	205.520	354.030	4.390	1,50	T	D
1:2	32.318	224.801	354.570	4.502	1,50	T	D

3.3.5 Influence of Boundary Conditions

In this section, the influence of boundary condition on the progressive failure is studied. The laminate with only a tapered section of configuration B and with $(\pm 45/0/90)_{2s}$ lay-up at the left (thick) end is considered. The length and the width of the plate are the same as that given in sub-section 3.3.1. Three boundary conditions have been considered, and

they are, BC1 boundary condition shown in Figure 3.6, BC2 boundary condition shown in Figure 3.36, and BC3 boundary condition shown in Figure 3.37. The results are compared in Figure 3.38 and Table 3.16.

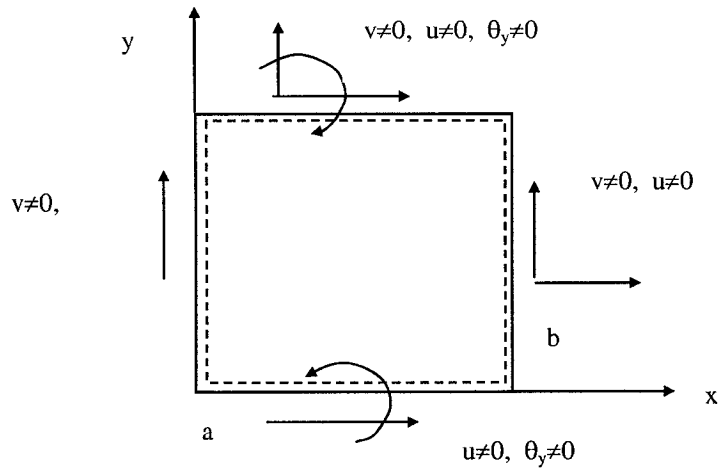

Figure 3.36 BC2 boundary condition

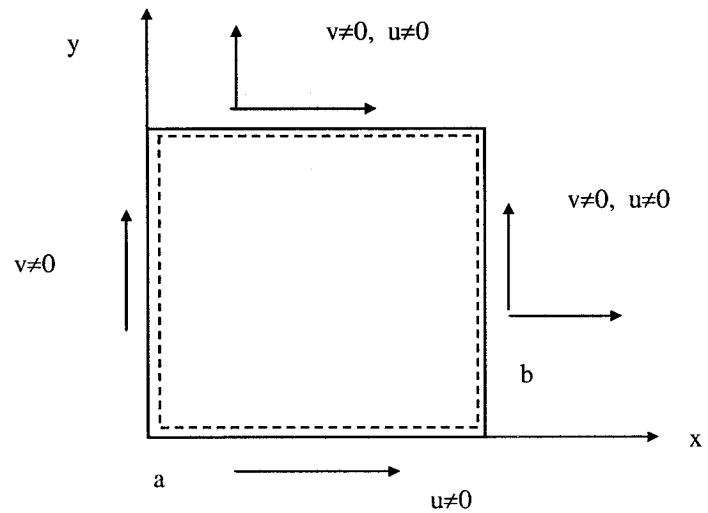

Figure 3.37 BC3 boundary condition

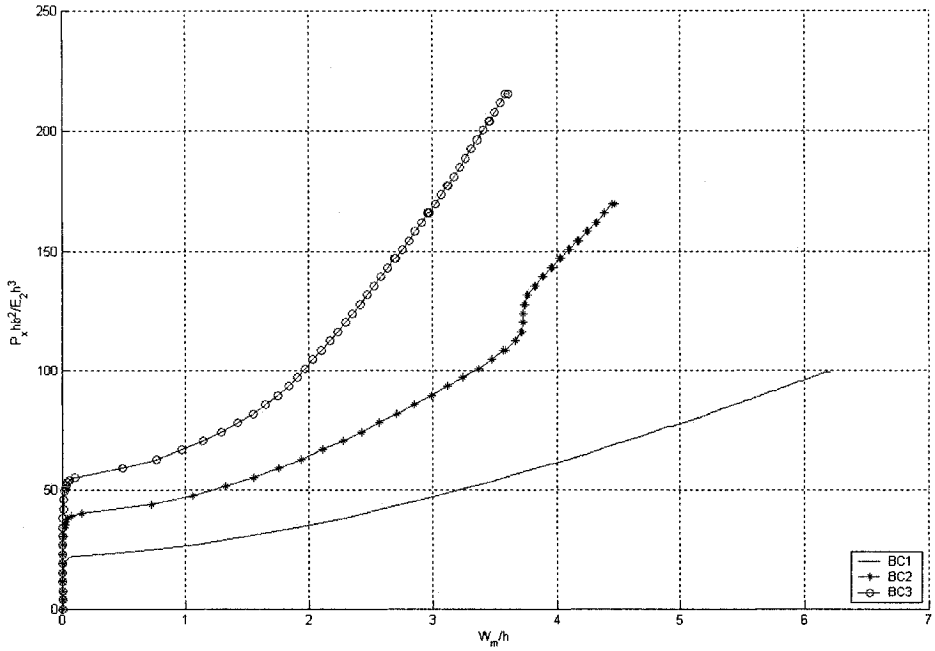

Figure 3.38 Load versus maximum deflection curves of the tapered laminate with taper configuration B corresponding to three boundary conditions under uni-axial compression

Table 3.16 Failure data of the tapered laminate with taper configuration B corresponding to three boundary conditions under uni-axial compression

Boundary condition	Buckling Load (P_xhb^2/E_2h^3)	First-ply failure load (P_xhb^2/E_2h^3)	Ultimate failure load (P_xhb^2/E_2h^3)	$(w_m/h)^*$	Failure location (FL,FE) ♣	First-ply failure mode	Ultimate failure mode
BC1	22.581	61.298	99.440	3.978	1,40	T♠	D#
BC2	41.958	108.710	169.740	3.573	1,24	T	D
BC3	57.216	139.220	215.510	2.581	1,32	T	D

Summary

From Figure 3.38 and Table 3.16, it is observed that the first-ply failure load corresponds to the transverse (matrix) failure, and the ultimate failure corresponds to the delamination failure for all the three boundary conditions. The first-ply failure load is found to be about 2.7 times the buckling load for BC1 boundary condition, 2.6 times for BC2 boundary condition, and 2.4 times for BC3 boundary condition, whereas, the ultimate failure load is

about 4.4 times the buckling load for BC1 boundary condition, 4.0 times for BC2 boundary condition, and 3.8 times for BC3 boundary condition. The ultimate failure load is about 1.6 times the first-ply failure load for BC1 and BC2 boundary conditions, and 1.5 times for BC3 boundary condition. The absolute maximum value of the maximum transverse displacement W_m just before ultimate failure is found to occur in the case of boundary condition BC1 and is equal to 6.16h. The absolute minimum value of the maximum transverse displacement W_m just before the ultimate failure is found to occur in the case of boundary condition BC3 and is equal to 3.59h. It is also noted that the higher the flexural rigidity is, higher are the buckling load and strength for a fixed value of maximum transverse displacement.

3.4 Parametric Study on Bi-axial Compression

Bi-axial compression loadings P_x and P_y are expressed in figures of this sub-section in non-dimensional forms as $P_x hb^2/E_2h^3$ and $P_y hb^2/E_2h^3$, respectively, where P_x is the applied X-direction axial compression loading per unit area, and P_y is the applied Y-direction axial compression loading per unit area. The loadings per unit area in both directions are of the same value, and they are simultaneously increased. The corresponding maximum (transverse) deflection is also expressed in non-dimensional form as W_m/h, where h is the average thickness of the tapered laminate.

3.4.1 Influence of Taper Configuration

Figure 3.39 shows the load versus the maximum deflection curves of the five laminates all with LC(1) lay-up configuration and each with a different taper configuration under the action of bi-axial compression. Table 3.17 gives the buckling load, the first-ply failure load and the ultimate failure load for these laminates.

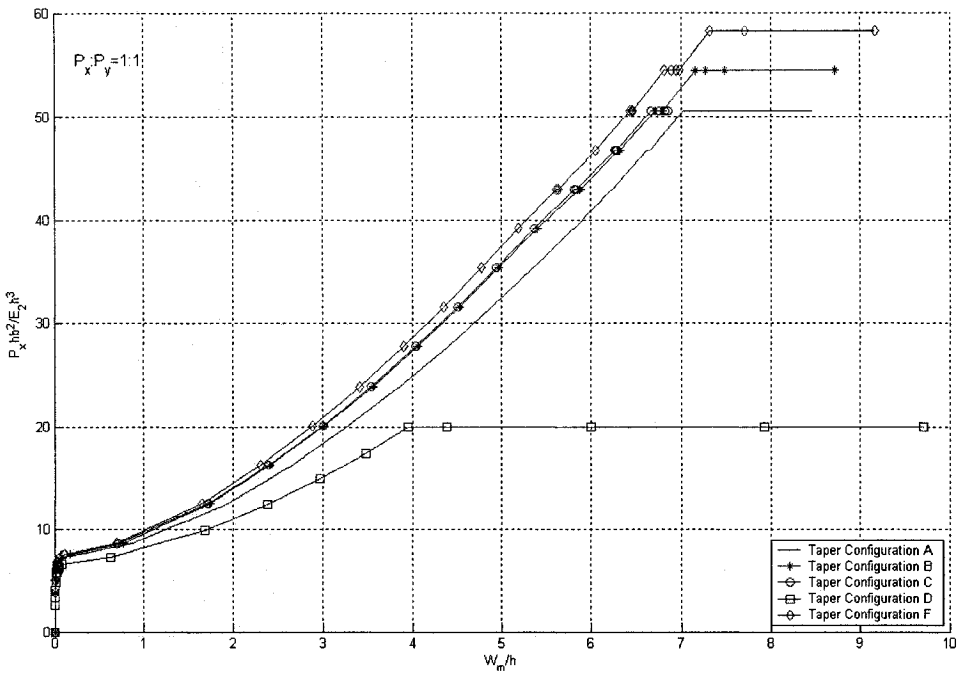

Figure 3.39 Load versus the maximum deflection curves of the laminates with LC(1) lay-up configuration for five taper configurations under bi-axial compression

Table 3.17 Failure data of the laminates with LC(1) lay-up configuration for five taper configurations under bi-axial compression

Taper	Buckling Load (P_xhb^2/E_2h^3)	First-ply failure load (P_xhb^2/E_2h^3)	Ultimate failure load (P_xhb^2/E_2h^3)	$(W_m/h)^*$	Failure location (FL,FE) ♣	First-ply failure mode	Ultimate failure mode
A	8.010	39.097	50.540	5.789	1,40	T♠	D#
B	8.048	39.135	54.393	5.398	1,40	T	D
C	8.048	39.135	50.578	5.365	1,40	T	D
D	6.891	19.987	19.987	3.947	1,32	T	D
F	8.048	42.950	58.207	5.617	1,8	T	D

For lay-up configuration LC(1), both the first-ply failure and the ultimate failure occur at the same value of the loading for taper configuration D. The first-ply failure load is found to be about 4.9 times the buckling load for taper configurations A, B and C, 2.9 times for taper configuration D, and 5.3 times for taper configuration F. The ultimate failure load is about 6.3 times the buckling load for configurations A and C, 6.8 times for configuration

B, 2.9 times for configuration D, and 7.2 times for configuration F. The ultimate failure load is about 1.3 times the first-ply failure load for configurations A and C, 1.4 times for configurations B and F, and 1 time for configuration D. Hence, it can be observed that considerable residual strength exists in the tapered laminates beyond the onset of buckling. Moreover, except the taper configuration D, all other taper configurations can on an average sustain about 35% more loading after first-ply failure until ultimate failure by delaminiation. Locations corresponding to the first-ply failure lie near the loaded edge of the plate (i.e. the thin end of the plate), and at the outermost bottom layer.

Figure 3.40 shows the load versus the maximum deflection curves of the five laminates all with LC(2) lay-up configuration and each with a different taper configuration under the action of bi-axial compression. Table 3.18 gives the buckling load, the first-ply failure load and the ultimate failure load for these laminates.

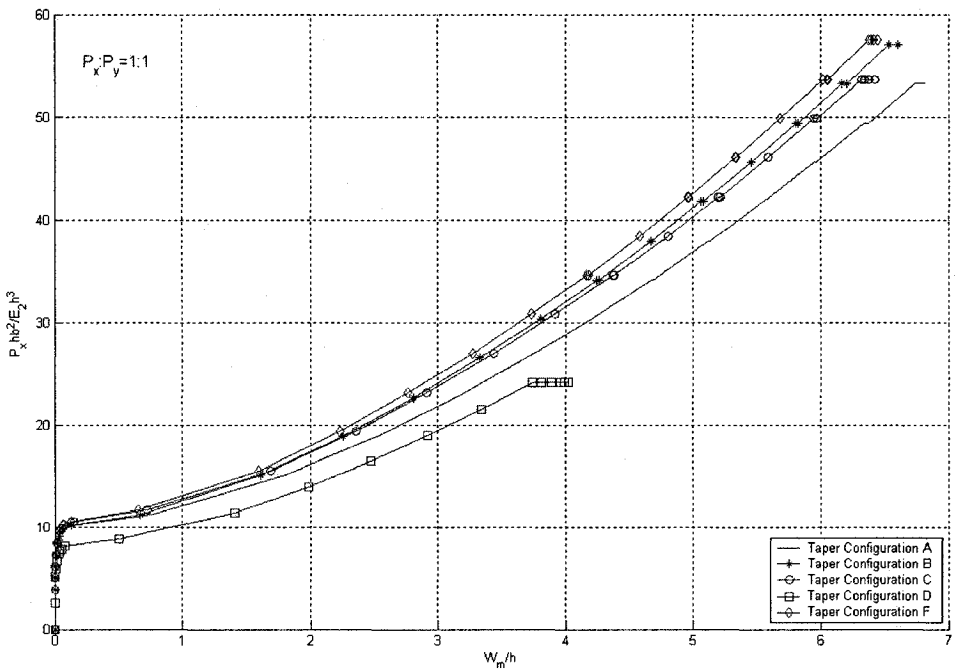

Figure 3.40 Load versus maximum deflection curves of the laminates with LC(2) lay-up configuration for five taper configurations under bi-axial compression

Table 3.18 Failure data of the laminates with LC(2) lay-up configuration for five taper configurations under bi-axial compression

Taper	Buckling Load ($P_x hb^2/E_2h^3$)	First-ply failure load ($P_x hb^2/E_2h^3$)	Ultimate failure load ($P_x hb^2/E_2h^3$)	$(W_m/h)^*$	Failure location (FL,FE) ♣	First-ply failure mode	Ultimate failure mode
A	10.680	34.139	53.210	4.668	1,40	T♠	D#
B	10.680	34.139	57.025	4.244	1,40	T	D
C	11.138	34.596	53.668	4.367	1,40	T	D
D	8.443	24.081	24.081	3.744	1,40	T	D
F	11.138	34.596	57.482	4.166	1,40	T	D

For lay-up configuration LC(2), the values of both the first-ply failure load and the ultimate failure load are the same for taper configuration D. The first-ply failure load is found to be about 3.2 times the buckling load for taper configurations A and B, 2.9 times for taper configuration D, and 3.1 times for taper configurations C and F, whereas, the ultimate failure load is about 5.0 times the buckling load for configuration A, 5.3 times for configuration B, 4.8 times for configuration C, 2.9 times for configuration D, and 5.2 times for configuration F. The ultimate failure load is about 1.6 times the first-ply load for configurations A and C, 1 time for configuration D, and 1.7 times for configurations B and F. Locations corresponding to the first-ply failure lie near the loaded edge of the plate (i.e. the thin end of the plate), and at the outermost bottom layer.

In order to illustrate the positive deflection of the plate under bi-axial compression, a typical deformed configuration is given. Figure 3.41 shows the deformed configuration of the laminate with LC(2) lay-up configuration and with taper configuration B. It is observed that the entire laminate undergoes positive (upward) deflection.

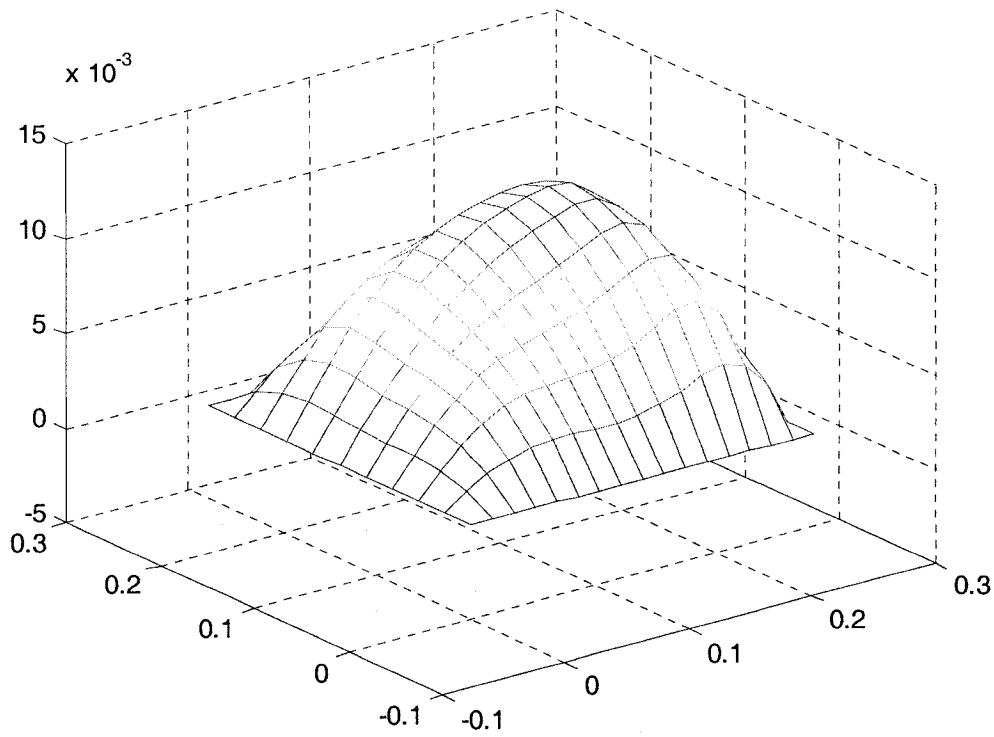

Figure 3.41 The deformed configuration of the laminate with LC(2) lay-up configuration and with taper configuration B under bi-axial compression

Figure 3.42 shows the load versus the maximum deflection curves of the five laminates all with LC(3) lay-up configuration and each with a different taper configuration under the action of bi-axial compression. Table 3.19 gives the buckling load, the first-ply failure load and the ultimate failure load for these laminates.

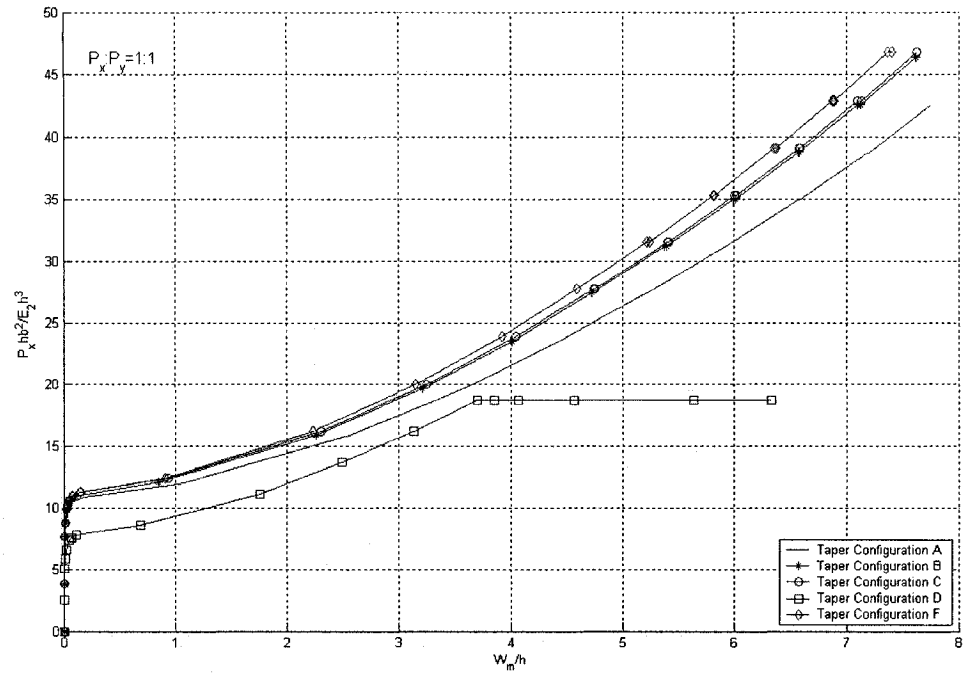

Figure 3.42 Load versus maximum deflection curves of the laminates with LC(3) lay-up configuration for five taper configurations under bi-axial compression

Table 3.19 Failure data of the laminates with LC(3) lay-up configuration for five taper configurations under bi-axial compression

Taper	Buckling Load (P_xhb^2/E_2h^3)	First-ply failure load (P_xhb^2/E_2h^3)	Ultimate failure load (P_xhb^2/E_2h^3)	$(W_m/h)^*$	Failure location (FL,FE) ♣	First-ply failure mode	Ultimate failure mode
A	11.481	27.311	42.568	5.198	1,40	T♠	D#
B	11.520	31.163	46.421	5.379	1,40	T	D
C	11.863	27.692	46.764	4.742	1,40	T	D
D	8.214	18.767	18.767	3.692	1,32	T	D
F	11.863	31.507	46.764	5.221	1,32	T	D

For lay-up configuration LC(3), the values of both the first-ply failure load and the ultimate failure load are the same for taper configuration D. The first-ply failure load is found to be about 2.4 times the buckling load for configuration A, 2.7 times for taper configurations B and F, and 2.3 times for taper configurations C and D, whereas, the ultimate failure load is about 3.7 times the buckling load for configuration A, 4.0 times for configuration B, 3.9 times for configurations C and F, and 2.3 times for configuration

D. The ultimate failure load is about 1.6 times the first-ply failure load for configuration A, 1.5 times for configurations B and F, 1.7 times for configuration C, and 1 time for configuration D. Locations corresponding to the first-ply failure lie near the loaded edge of the plate (i.e. the thin end of the plate), and at the outermost bottom layer.

Figure 3.43 shows the load versus the maximum deflection curves of the five laminates all with LC(4) lay-up configuration and each with a different taper configuration under the action of bi-axial compression. Table 3.20 gives the buckling load, the first-ply failure load and the ultimate failure load for these laminates.

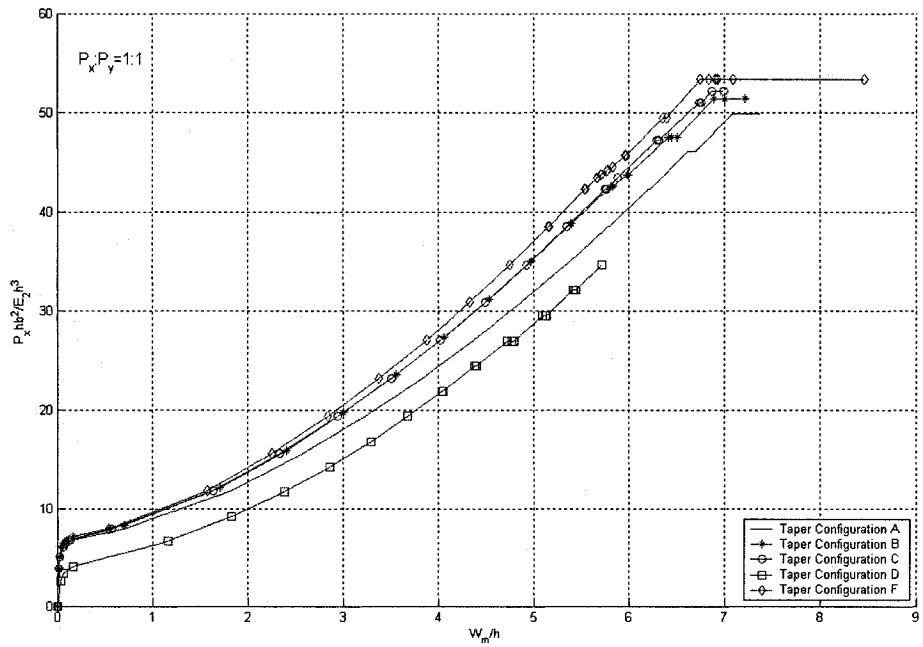

Figure 3.43 Load versus maximum deflection curves of the laminates with LC(4) lay-up configuration for five taper configurations under bi-axial compression

Table 3.20 Failure data of the laminates with LC(4) lay-up configuration for five taper configurations under bi-axial compression

Taper	Buckling Load ($P_x hb^2/E_2h^3$)	First-ply failure load ($P_x hb^2/E_2h^3$)	Ultimate failure load ($P_x hb^2/E_2h^3$)	$(W_m/h)^*$	Failure location (FL,FE) ♣	First-ply failure mode	Ultimate failure mode
A	7.362	34.634	49.892	5.338	10,40	T♠	D#
B	7.705	34.978	51.379	4.971	10,40	T	D
C	7.362	38.449	52.181	5.342	1,40	T	D
D	5.340	21.869	34.584	4.035	10,40	T	D
F	7.362	38.449	53.313	5.153	10,40	T	D

For lay-up configuration LC(4), the first-ply and ultimate failures do not occur at the same load value for taper configuration D, unlike LC(1), LC(2) and LC(3) lay-up configurations that are symmetric. The first-ply failure load is found to be about 4.7 times the buckling load for configuration A, 4.5 times for taper configuration B, 5.2 times for configurations C and F, and 4.1 times for configuration D, whereas, the ultimate failure load is about 6.8 times the buckling load for configuration A, 6.7 times for configuration B, 7.1 times for configuration C, 6.5 times for configuration D, and 7.2 times for configuration F. The ultimate failure load is about 1.4 times the first-ply failure load for configurations A and C, 1.5 times for configuration B, 1.4 times for configurations C and F, and 1.6 times for configuration D. Locations corresponding to the first-ply failure lie near the loaded edge of the plate (i.e. the thin end of the plate). For configurations A, B, D and F, it is at the outermost top layer. But for configuration C, it is at the outermost bottom layer.

Figure 3.44 shows the load versus the maximum deflection curves of the five laminates all with LC(5) lay-up configuration and each with a different taper configuration under

the action of bi-axial compression. Table 3.21 gives the buckling load, the first-ply failure load and the ultimate failure load for these laminates.

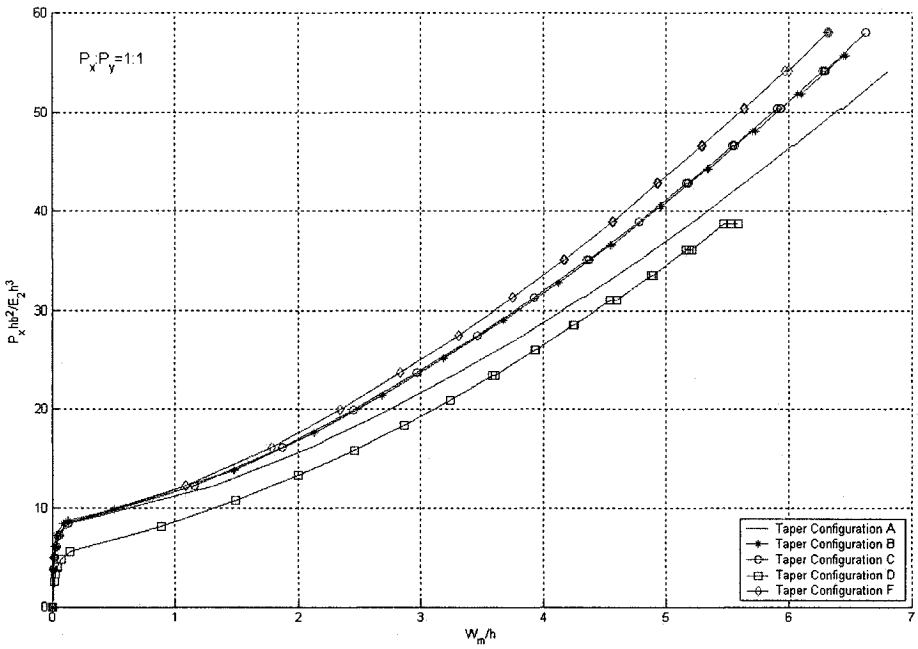

Figure 3.44 Load versus maximum deflection curves of the laminates with LC(5) lay-up configuration for five taper configurations under bi-axial compression

Table 3.21 Failure data of the laminates with LC(5) lay-up configuration for five taper configurations under bi-axial compression

Taper	Buckling Load (P_xhb^2/E_2h^3)	First-ply failure load (P_xhb^2/E_2h^3)	Ultimate failure load (P_xhb^2/E_2h^3)	$(W_m/h)^*$	Failure location (FL,FE) ♣	First-ply failure mode	Ultimate failure mode
A	10.299	31.278	54.164	4.318	1,40	T♠	D#
B	9.307	36.580	55.652	4.542	1,40	T	D
C	10.299	35.092	57.978	4.356	1,40	T	D
D	6.866	23.395	38.652	3.584	1,40	T	D
F	10.299	35.092	57.978	4.162	1,40	T	D

For lay-up configuration LC(5), the first-ply failure load is found to be about 3.0 times the buckling load for configuration A, 3.9 times for configuration B, and 3.4 times for taper configurations C, D and F, whereas, the ultimate failure load is about 5.3 times the

buckling load for configuration A, 6.0 times for configuration B, and 5.6 times for configurations C, D and F. The ultimate failure load is about 1.5 times the first-ply failure load for configuration B, and 1.7 times for configurations A, C, D and F. Locations corresponding to the first-ply failure lie near the loaded edge of the plate (i.e. the thin end of the plate), and at the outermost top layer.

Figure 3.45 shows the load versus the maximum deflection curves of the five laminates all with LC(6) lay-up configuration and each with a different taper configuration under the action of bi-axial compression. Table 3.22 gives the buckling load, the first-ply failure load and the ultimate failure load for these laminates.

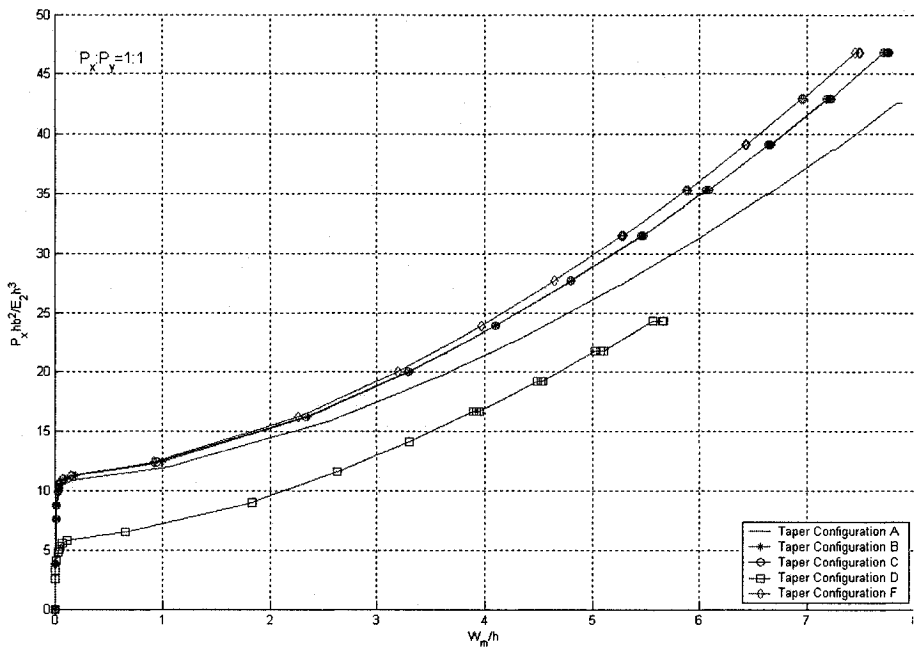

Figure 3.45 Load versus maximum deflection curves of the laminates with LC(6) lay-up configuration for five taper configurations under bi-axial compression

Table 3.22 Failure data of the laminates with LC(6) lay-up configuration for five taper configurations under bi-axial compression

Taper	Buckling Load ($P_x hb^2/E_2h^3$)	First-ply failure load ($P_x hb^2/E_2h^3$)	Ultimate failure load ($P_x hb^2/E_2h^3$)	$(W_m/h)^*$	Failure location (FL,FE) ♣	First-ply failure mode	Ultimate failure mode
A	11.481	27.311	42.568	5.235	1,40	T♠	D#
B	11.863	31.507	46.764	5.457	1,40	T	D
C	11.863	31.507	46.764	5.450	1,40	T	D
D	6.128	16.681	24.310	3.893	1,40	T	D
F	11.863	31.507	46.764	5.274	1,40	T	D

For lay-up configuration LC(6), the values of buckling loads, first-ply failure loads and ultimate failure loads are same for taper configurations B, C and F, but configuration F has less deflection than that of other two configurations, indicating that, it has more stiffness. The taper configuration D is the weakest one. The first-ply failure load is found to be about 2.4 times the buckling load for configuration A, and 2.7 times for configurations B, C, D and F, whereas, the ultimate failure load is about 3.7 times the buckling load for configuration A, 3.9 times for configurations B, C and F, and 4.0 times for configuration D. The ultimate failure load is about 1.6 times the first-ply failure load for configuration A, and 1.5 times for configurations B, C, D and F. Locations corresponding to the first-ply failure lie near the loaded edge of the plate (i.e. the thin end of the plate), and at the outermost bottom layer.

Summary

From Figures 3.39 – 3.45 and Tables 3.17 – 3.22, the following general observations are also made.

1. For all the six lay-up configurations, the taper configuration F (Mid-plane taper) is the strongest one, and the taper configuration D (Continuous plies interspersed) is the

weakest one among all taper configurations with respect to the first-ply failure load, the ultimate failure load and the buckling load.

2. For the three symmetric lay-up configurations LC(1), LC(2) and LC(3), the first-ply failure load and the ultimate failure load are the same for the taper configuration D (Continuous plies interspersed). But for the three un-symmetric lay-up configurations LC(4), LC(5) and LC(6), the first-ply failure load and the ultimate failure load are different. Considerable residual strength exists in these laminates after first-ply failure until the occurrence of ultimate failure.
3. For all the five taper configurations, the deflections are all positive, that is, upward.

3.4.2 Influence of Lay-up Configuration

Figure 3.46 shows the load versus maximum deflection curves of the six laminates all with taper configuration A and each with a different lay-up configuration under the action of bi-axial compression. Table 3.23 gives the buckling load, the first-ply failure load and the ultimate failure load for these laminates.

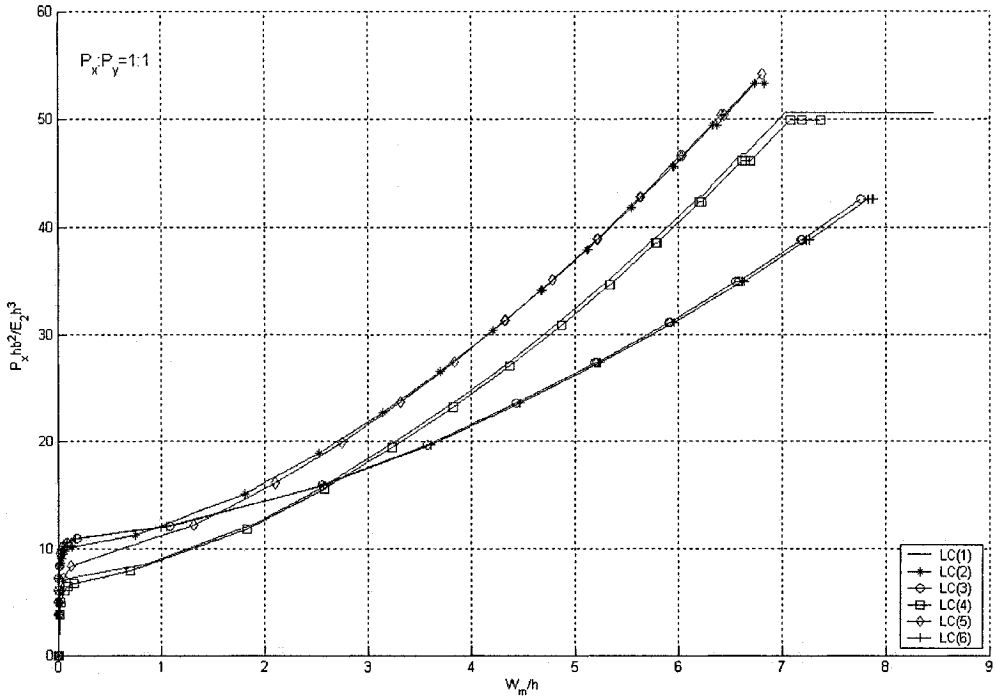

Figure 3.46 Load versus maximum deflection curves of the laminates with taper configuration A for all the six lay-up configurations under bi-axial compression

Table 3.23 Failure data of the laminates with taper configuration A for all the six lay-up configurations under bi-axial compression

Lay-up	Buckling Load (P_xhb^2/E_2h^3)	First-ply failure load (P_xhb^2/E_2h^3)	Ultimate failure load (P_xhb^2/E_2h^3)	$(W_m/h)^*$	Failure location (FL,FE) ♣	First-ply failure mode	Ultimate failure mode
LC(1)	8.010	39.097	50.540	5.789	1,40	T♠	D#
LC(2)	10.680	34.139	53.210	4.668	1,40	T	D
LC(3)	11.481	27.311	42.568	5.198	1,40	T	D
LC(4)	7.362	34.634	49.892	5.338	10,40	T	D
LC(5)	10.299	31.278	54.164	4.318	1,40	T	D
LC(6)	11.481	27.311	42.568	5.235	1,40	T	D

For taper configuration A, the lay-up configurations LC(3) and LC(6) are the best choice among all the six lay-up configurations with respect to the buckling load, the lay-up configuration LC(1) is the best choice with respect to the first-ply failure load, and the lay-up configuration LC(5) is the best choice with respect to the ultimate failure load.

Figure 3.47 shows the load versus maximum deflection curves of the six laminates all with taper configuration B and each with a different lay-up configuration under the action of bi-axial compression. Table 3.24 gives the buckling load, the first-ply failure load and the ultimate failure load for these laminates.

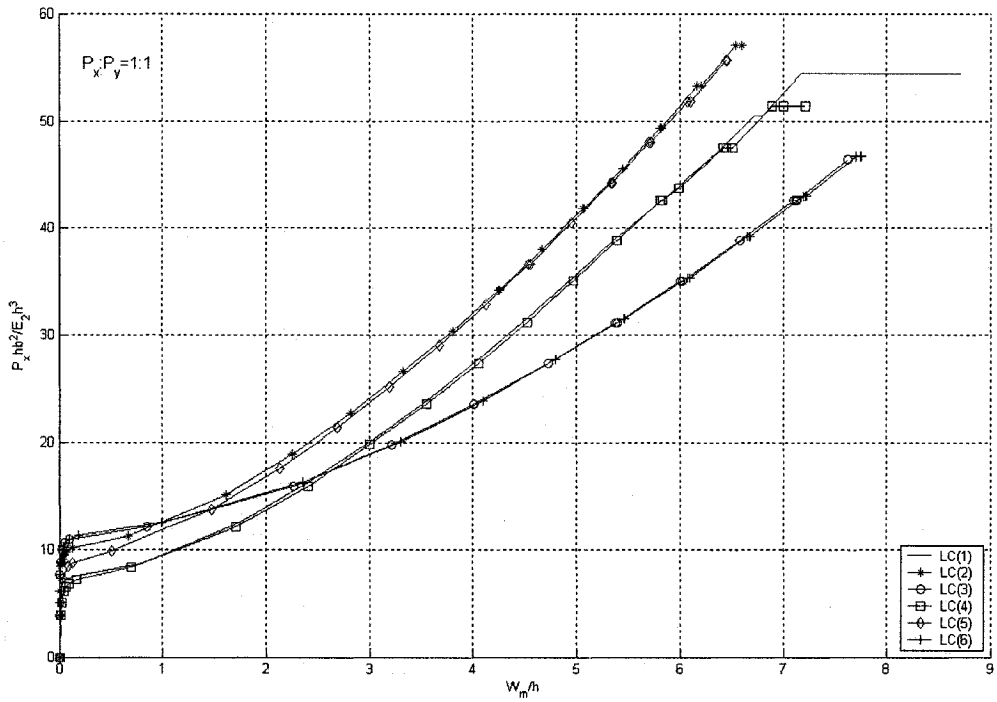

Figure 3.47 Load versus maximum deflection curves of the laminates with taper configuration B for all the six lay-up configurations under bi-axial compression

Table 3.24 Failure data of the laminates with taper configuration B for all the six lay-up configurations under bi-axial compression

Lay-up	Buckling Load (P_xhb^2/E_2h^3)	First-ply failure load (P_xhb^2/E_2h^3)	Ultimate failure load (P_xhb^2/E_2h^3)	$(W_m/h)^*$	Failure location (FL,FE) ♣	First-ply failure mode	Ultimate failure mode
LC(1)	8.048	39.135	54.393	5.398	1,40	T♠	D#
LC(2)	10.680	34.139	57.025	4.244	1,40	T	D
LC(3)	11.520	31.163	46.421	5.379	1,40	T	D
LC(4)	7.705	34.978	51.379	4.971	10,40	T	D
LC(5)	9.307	36.580	55.652	4.542	1,40	T	D
LC(6)	11.863	31.507	46.764	5.457	1,40	T	D

For taper configuration B, the lay-up configuration LC(6) is the best choice among all six lay-up configurations with respect to the buckling load, the lay-up configuration LC(1) is the best choice with respect to the first-ply failure load, and the lay-up configuration LC(2) is the best choice with respect to the ultimate failure load.

Figure 3.48 shows the load versus maximum deflection curves of the six laminates all with taper configuration C and each with a different lay-up configuration under the action of bi-axial compression. Table 3.25 gives the buckling load, the first-ply failure load and the ultimate failure load for these laminates.

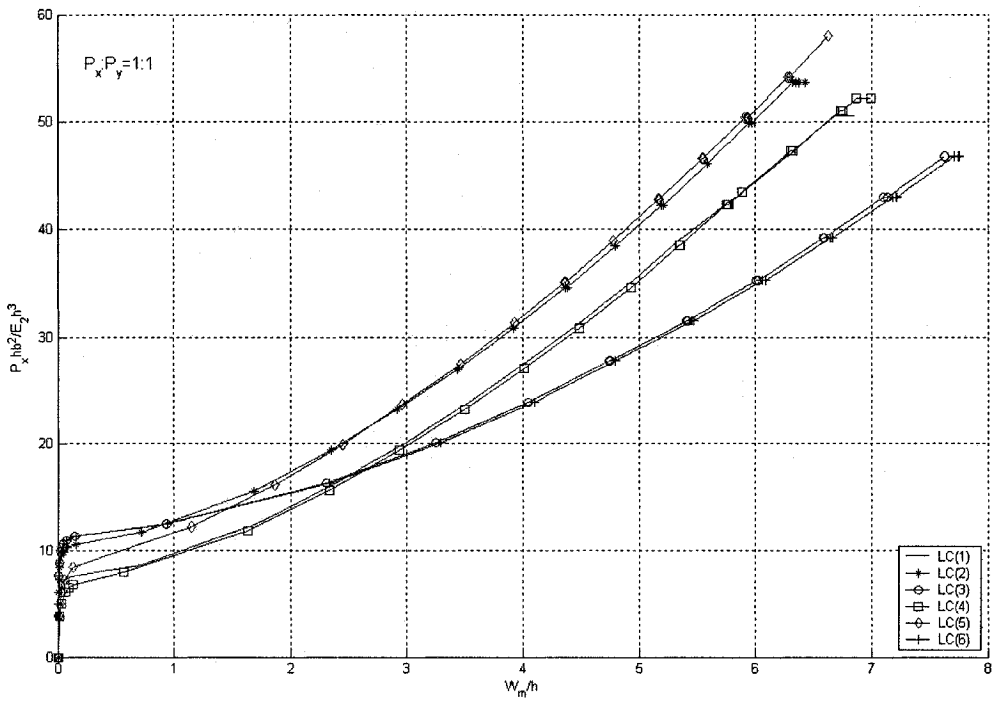

Figure 3.48 Load versus maximum deflection curves of the laminates with taper configuration C for all the six lay-up configurations under bi-axial compression

Table 3.25 Failure data of the laminates with taper configuration C for all the six lay-up configurations under bi-axial compression

Lay-up	Buckling Load ($P_x hb^2/E_2h^3$)	First-ply failure load ($P_x hb^2/E_2h^3$)	Ultimate failure load ($P_x hb^2/E_2h^3$)	$(W_m/h)^*$	Failure location (FL,FE) ♣	First-ply failure mode	Ultimate failure mode
LC(1)	8.048	39.135	50.578	5.365	1,40	T♠	D#
LC(2)	11.138	34.596	53.668	4.367	1,40	T	D
LC(3)	11.863	27.692	46.764	4.742	1,40	T	D
LC(4)	7.362	38.449	52.181	5.342	1,40	T	D
LC(5)	10.299	35.092	57.978	4.356	1,40	T	D
LC(6)	11.863	31.507	46.764	5.450	1,40	T	D

For taper configuration C, the lay-up configurations LC(3) and LC(6) are the best choice among all six lay-up configurations with respect to the buckling load, the lay-up configuration LC(1) is the best choice with respect to the first-ply failure load, and the lay-up configuration LC(5) is the best choice with respect to the ultimate failure load.

Figure 3.49 shows the load versus maximum deflection curves of the six laminates all with taper configuration D and each with a different lay-up configuration under the action of bi-axial compression. Table 3.26 gives the buckling load, the first-ply failure load and the ultimate failure load for these laminates.

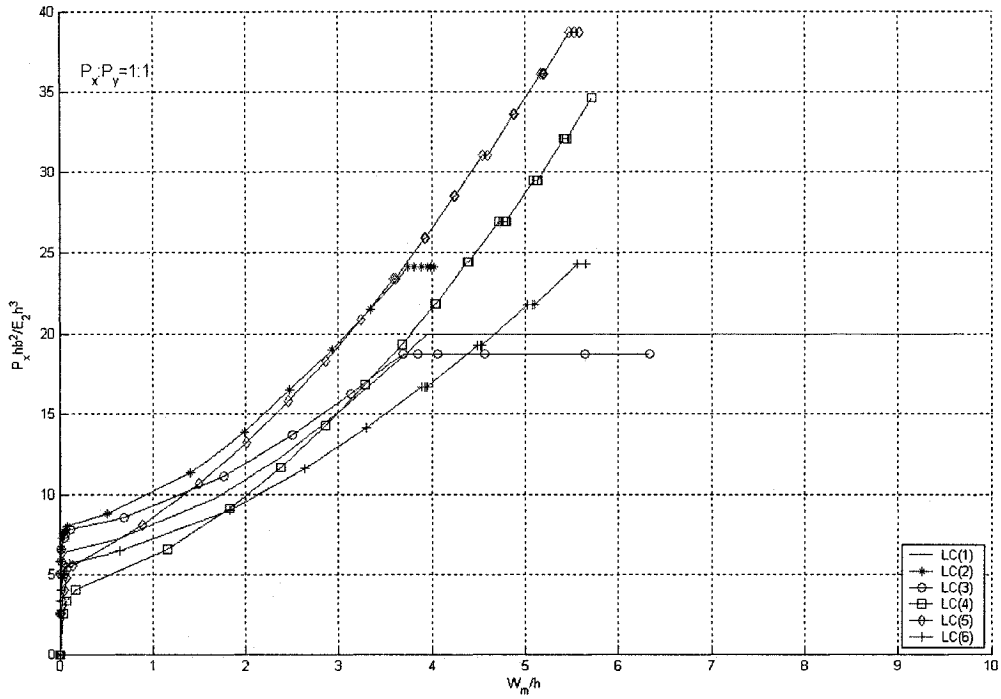

Figure 3.49 Load versus maximum deflection curves of the laminates with taper configuration D for all the six lay-up configurations under bi-axial compression

Table 3.26 Failure data of the laminates with taper configuration D for all the six lay-up configurations under bi-axial compression

Lay-up	Buckling Load (P_xhb^2/E_2h^3)	First-ply failure load (P_xhb^2/E_2h^3)	Ultimate failure load (P_xhb^2/E_2h^3)	$(W_m/h)^*$	Failure location (FL,FE) ♣	First-ply failure mode	Ultimate failure mode
LC(1)	6.891	19.987	19.987	3.947	1,32	T♠	D#
LC(2)	8.443	24.081	24.081	3.744	1,40	T	D
LC(3)	8.214	18.767	18.767	3.692	1,32	T	D
LC(4)	5.340	21.869	34.584	4.035	10,40	T	D
LC(5)	6.866	23.395	38.652	3.584	1,40	T	D
LC(6)	6.128	16.681	24.310	3.893	1,40	T	D

For taper configuration D, the lay-up configuration LC(2) is the best choice among all six lay-up configurations with respect to both the buckling load and the first-ply failure load, and the lay-up configuration LC(5) is the best choice with respect to the ultimate failure load.

Figure 3.50 shows the load versus maximum deflection curves of the six laminates all with taper configuration F and each with a different lay-up configuration under the action of bi-axial compression. Table 3.27 gives the buckling load, the first-ply failure load and the ultimate failure load for these laminates.

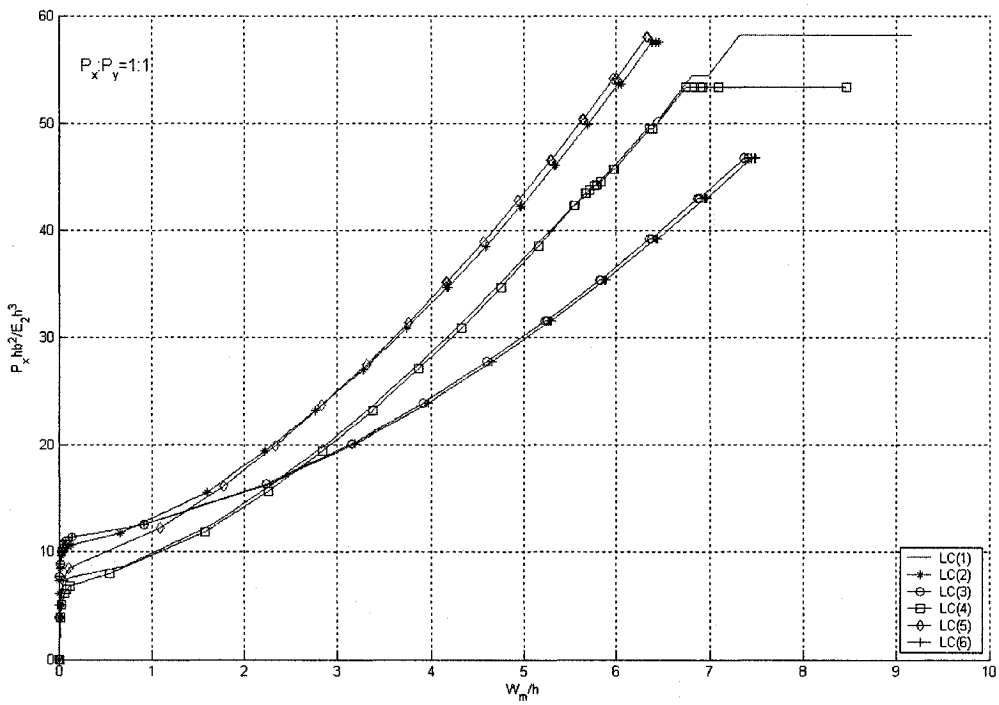

Figure 3.50 Load versus maximum deflection curves of the laminates with taper configuration F for all the six lay-up configurations under bi-axial compression

Table 3.27 Failure data of the laminates with taper configuration F for all the six lay-up configurations under bi-axial compression

Lay-up	Buckling Load (P_xhb^2/E_2h^3)	First-ply failure load (P_xhb^2/E_2h^3)	Ultimate failure load (P_xhb^2/E_2h^3)	$(W_m/h)^*$	Failure location (FL,FE) ♣	First-ply failure mode	Ultimate failure mode
LC(1)	8.048	42.950	58.207	5.617	1,8	T♠	D#
LC(2)	11.138	34.596	57.482	4.166	1,40	T	D
LC(3)	11.863	31.507	46.764	5.221	1,32	T	D
LC(4)	7.362	38.449	53.313	5.153	10,40	T	D
LC(5)	10.299	35.092	57.978	4.162	1,40	T	D
LC(6)	11.863	31.507	46.764	5.274	1,40	T	D

For taper configuration F, lay-up configurations LC(3) and LC(6) are the best choice among all six lay-up configurations with respect to the buckling load, the lay-up configuration LC(1) is the best choice with respect to both the first-ply failure load and the ultimate failure load.

Summary

From Figures 3.46 – 3.50 and Table 3.23 – 3.27, the following general observations are also made.

1. For all the five taper configurations, the first-ply failure mode for all the six lay-up configurations is transverse (matrix) failure.
2. For all the five taper configurations, the ultimate failure mode for all the six lay-up configurations is delamination.
3. Locations corresponding to the first-ply failure for all the six lay-up configurations lie near the loaded edges of the plates (i.e. the thin end of the plate). However, for the laminate with LC(4) and with taper configurations A, B, D or F, the failure occurs at the outermost top layer, and for the rest of the cases it occurs at the outermost bottom layer.
4. For all the lay-up configurations and taper configurations, the deflections are positive, i.e. upward.
5. Except taper configuration D, variations of the maximum deflection with the load for the symmetric lay-up configuration and the corresponding un-symmetric lay-up configuration basically coincide with each other, and it shows that in these cases the symmetry in the stacking sequence does not have a strong influence on the progressive failure of the laminate.

3.4.3 Influence of Uniform-thickness Sections

Except that the loading is bi-axial compression, the study cases are the same as those given in sub-section 3.3.4. Figure 3.51 shows the load versus maximum deflection curves of five tapered plates under the action of bi-axial compression. Table 3.28 gives the buckling load, the first-ply failure load and the ultimate failure load for these laminates under the action of bi-axial compression.

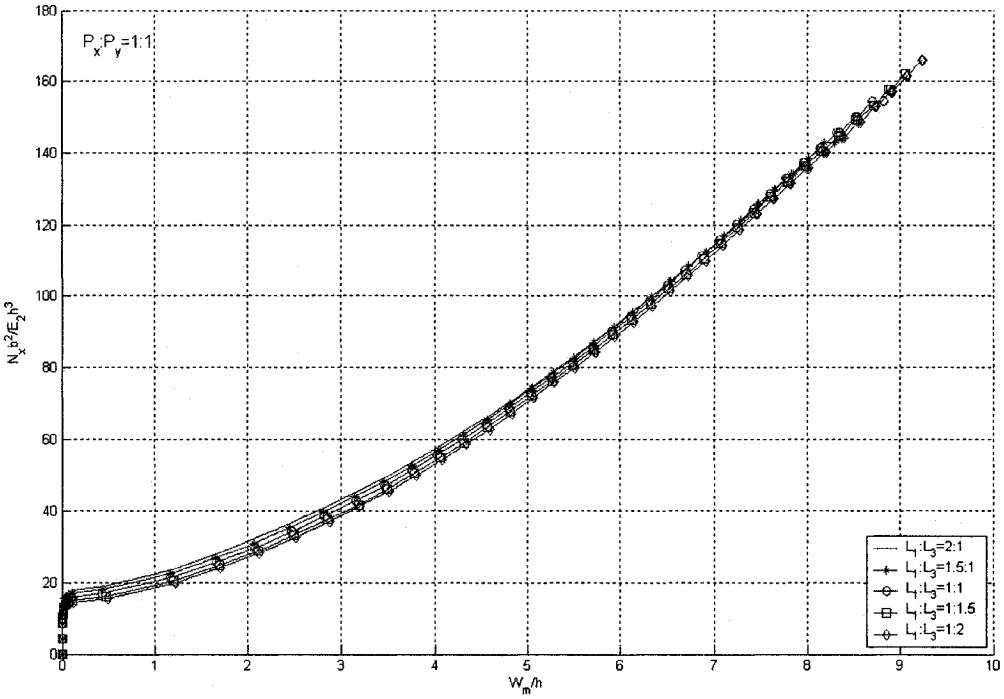

Figure 3.51 Load versus the maximum deflection curves of five tapered plates with different length ratios under the action of bi-axial compression

Table 3.28 Failure data of five tapered plates with different length ratios under the action of bi-axial compression

L_1:L_3	Buckling Load (P_xhb^2/E_2h^3)	First-ply failure load (P_xhb^2/E_2h^3)	Ultimate failure load (P_xhb^2/E_2h^3)	$(W_m/h)^*$	Failure location (FL,FE) ♣	First-ply failure mode	Ultimate failure mode
2:1	18.538	70.675	130.750	4.820	1,50	T♠	D#
1.5:1	17.637	74.065	142.720	5.042	1,50	T	D
1:1	16.435	77.155	154.400	5.257	1,50	T	D
1:1.5	15.534	84.836	162.080	5.705	1,50	T	D
1:2	15.019	84.321	165.850	5.725	1,50	T	D

The laminate with length ratio 2:1 is the best choice among these five laminates with respect to the buckling load, the laminate with length ratio 1:1.5 is the best choice with respect to the first-ply failure load, and the laminate with length ratio 1:2 is the best choice with respect to the ultimate failure load. Locations corresponding to the first-ply failure all lie near the loaded edge of the plate (i.e. the thin end of the plate), and at the outermost bottom layer. The first-ply failure load corresponds to the transverse (matrix) failure, and the ultimate failure corresponds to the delamination failure. However, considerably more resistance to buckling, first-ply and ultimate failures is provided by the addition of uniform-thickness sections.

3.4.4 Influence of Boundary Conditions

Except that the loading is bi-axial compression, the study cases are the same as those given in sub-section 3.3.5. The results are compared in Figure 3.52 and Table 3.29.

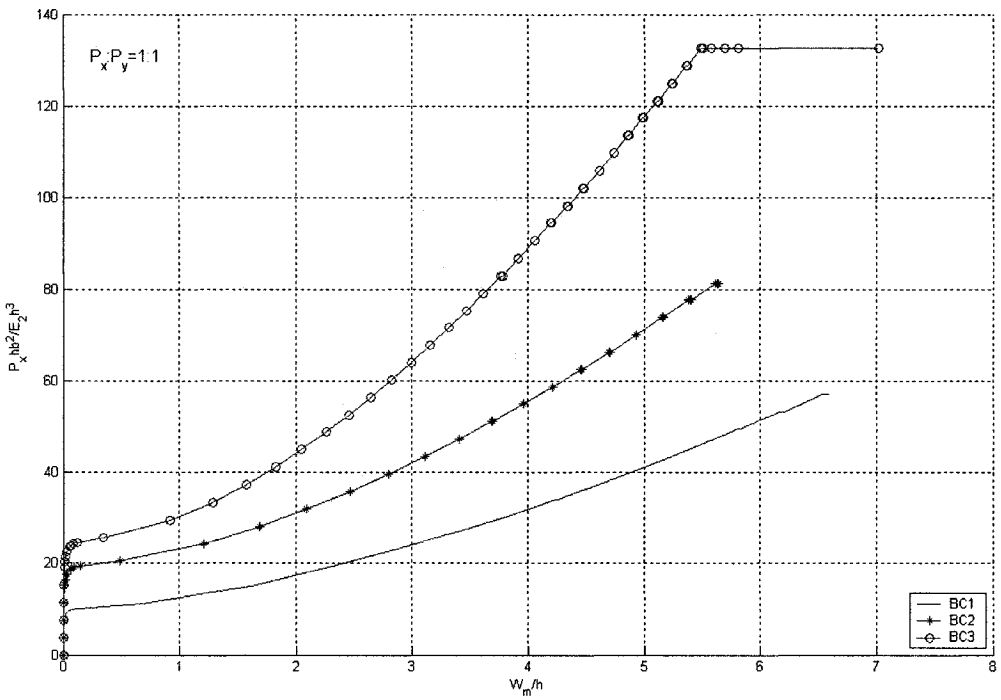

Figure 3.52 Load versus maximum deflection curves of the laminates with three boundary conditions under the action of bi-axial compression

Table 3.29 Failure data of the laminates with three boundary conditions under the action of bi-axial compression

Boundary condition	Buckling Load ($P_x hb^2/E_2h^3$)	First-ply failure load ($P_x hb^2/E_2h^3$)	Ultimate failure load ($P_x hb^2/E_2h^3$)	$(W_m/h)^*$	Failure location (FL,FE) ♣	First-ply failure mode	Ultimate failure mode
BC1	10.680	34.139	57.025	4.244	1,40	T♠	D#
BC2	19.949	51.036	81.551	3.686	1,40	T	D
BC3	25.251	83.039	132.630	3.763	10,24	T	D

From Figure 3.52 and Table 3.29, it is observed that the first-ply failure load corresponds to the transverse (matrix) failure, and the ultimate failure corresponds to the delamination failure for all the three boundary conditions. The first-ply failure load is found to be about 3.2 times the buckling load for BC1 boundary condition, 2.6 times for BC2 boundary condition, and 3.2 times for BC3 boundary condition, whereas, the ultimate failure load is about 5.3 times the buckling load for BC1 and BC3 boundary conditions, and 4.1 times for BC2 boundary condition. The ultimate failure load is about 1.5 times the first-ply failure load for BC1 boundary condition, and 1.6 times for BC2 and BC3 boundary conditions. The absolute maximum value of the maximum transverse displacement W_m just before ultimate failure is found to occur in the case of boundary condition BC1 and is equal to 6.54h. The absolute minimum value of the maximum transverse displacement W_m just before the ultimate failure is found to occur in the case of boundary condition BC3 and is equal to 5.48h. It is also noted that the higher the flexural rigidity is, higher are the buckling load and strength for a fixed value of maximum transverse displacement.

3.4.5 Influence of Load Ratio

The tapered laminate with taper configuration B and with $(\pm 45/0/90)_{2s}$ lay-up at the left (thick) end is considered. The length, the width and the boundary condition of the plate

are the same as that given in sub-section 3.3.1. Figure 3.53 shows the load versus maximum deflection curves for this laminate under the action of bi-axial compression for different load ratio values. Table 3.30 gives the buckling load, the first-ply failure load and the ultimate failure load for all the cases.

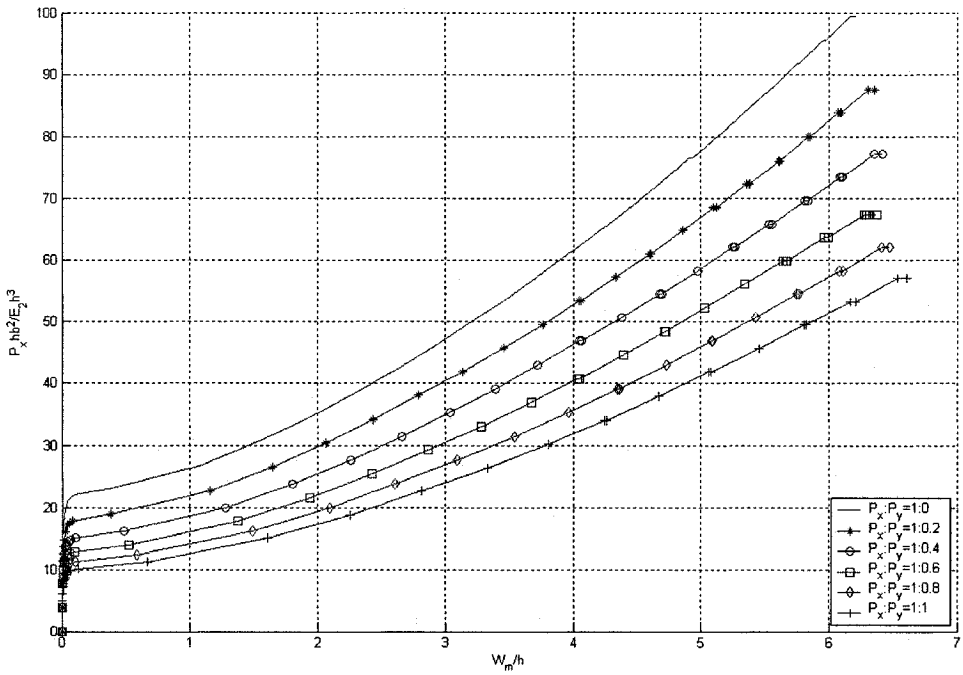

Figure 3.53 The load versus maximum deflection curves of the LC(2) laminate for different load ratio values under bi-axial compression

Table 3.30 Failure data of the LC(2) laminate for different load ratio values under bi-axial compression

Load Ratio $P_x:P_y$	Buckling Load (P_xhb^2/E_2h^3)	First-ply failure load (P_xhb^2/E_2h^3)	Ultimate failure load (P_xhb^2/E_2h^3)	$(W_m/h)^*$	Failure location (FL,FE) ♣	First-ply failure mode	Ultimate failure mode
1:0	22.581	61.297	99.440	3.978	1,40	T♠	D#
1:0.2	18.424	53.325	87.654	4.044	1,40	T	D
1:0.4	15.677	46.764	77.279	4.047	1,40	T	D
1:0.6	13.465	40.737	67.438	4.034	1,40	T	D
1:0.8	11.863	39.135	62.022	4.348	1,40	T	D
1:1	10.680	34.139	57.025	4.244	1,40	T	D

With increasing proportion of P_y in the bi-axial compression, the first-ply failure load and the ultimate failure load decrease monotonically. At $P_x : P_y = 1:1$, the percentage losses in the buckling load, first-ply failure load and the ultimate failure load are 52.7, 44.3 and 42.6 respectively.

3.5 Comparison of Responses to Bi-axial and Uni-axial Compressive Loadings

From Figures 3.10, 3.13 and 3.41, it is observed that the peak value of transverse displacement under uni-axial compression is close to the thin end of the plate. When the compression in the y-direction is added, the location of the peak value of transverse displacement under bi-axial compression shift towards the center of the plate, and becomes closer to it.

For LC(1) lay-up configuration, the buckling load under bi-axial compression with load ratio 1:1 is found to be about 45.5% of the buckling load under uni-axial compression for taper configurations A and C, 45.2% for configuration B, 41.0% for configuration D, and 44.7% for configuration F. The first-ply failure load under bi-axial compression is found to be about 50.0% of the first-ply failure load under uni-axial compression for taper configuration A, 49.4% for configuration B, 49.7% for configuration C, 39.5% for configuration D, and 51.5% for configuration F. The ultimate failure load under bi-axial compression is found to be about 51.4% of the ultimate failure load under uni-axial compression for taper configuration A, 53.3% for configuration B, 49.9% for configuration C, 39.5% for configuration D, and 54.8% for configuration F. For LC(1) lay-up configuration, it is observed that the lowest values of the buckling load, the first-ply failure load and the ultimate failure load correspond to taper configuration D, which

means that taper configuration D is the most sensitive configuration in a relative sense, to multi-axial nature of loadings. The magnitudes of buckling load, first-ply failure load and ultimate failure load for taper configuration D are the lowest in case of uni-axial compression. Because it suffers 59% reduction for buckling load and 60.5% for both first-ply failure load and ultimate failure load when the loading becomes bi-axial, the magnitudes of buckling load, first-ply failure load and ultimate failure load become the lowest for taper configuration D. In a similar manner, it is observed that the taper configuration F is the least sensitive configuration considering both the first-ply failure load and the ultimate failure load. It is also observed that taper configurations A and C are the least sensitive configurations considering the buckling load.

For LC(2) lay-up configuration, the buckling load under bi-axial compression is found to be about 48.8% of the buckling load under uni-axial compression for taper configuration A, 47.3% for configuration B, 49.4% for configuration C, 40.0% for configuration D, and 48.9% for configuration F. The first-ply failure load under bi-axial compression is found to be about 56.0% of the first-ply failure load under uni-axial compression for taper configuration A, 55.7% for configuration B, 56.7% for configuration C, 49.3% for configuration D, and 53.4% for configuration F. The ultimate failure load under bi-axial compression is found to be about 55.8% of the ultimate failure load under uni-axial compression for taper configuration A, 57.3% for configuration B, 54.2% for configuration C, 49.3% for configuration D, and 55.9% for configuration F. For LC(2) lay-up configuration, it is observed that taper configuration D is the most sensitive configuration in a relative sense, to multi-axial nature of loadings. The magnitudes of buckling load, first-ply failure load and ultimate failure load for taper configuration D are

the lowest in case of uni-axial compression. Because it suffers 60% reduction for buckling load and 50.7% for both first-ply failure load and ultimate failure load when the loading becomes bi-axial, the magnitudes of buckling load, first-ply failure load and ultimate failure load become the lowest for taper configuration D. In a similar manner, it is observed that the taper configuration C is the least sensitive configuration considering both the buckling load and the first-ply failure load. It is also observed that taper configuration B is the least sensitive configuration considering the ultimate failure load.

For LC(3) lay-up configuration, the buckling load under bi-axial compression is found to be about 51.8% of the buckling load under uni-axial compression for taper configurations A and B, 52.5% for configuration C, 51.1 for configuration D, and 52.4% for configuration F. The first-ply failure load under bi-axial compression is found to be about 54.8% of the first-ply failure load under uni-axial compression for taper configuration A, 62.9% for configuration B, 55.5% for configuration C, 59.2% for configuration D, and 58.7% for configuration F. The ultimate failure load under bi-axial compression is found to be about 58.5% of the ultimate failure load under uni-axial compression for taper configuration A, 60.9% for configuration B, 61.1% for configuration C, 59.2% for configuration D, and 58.2% for configuration F. For LC(3) lay-up configuration, it is observed that taper configuration D is the most sensitive configuration to multi-axial nature of loadings considering buckling load, the taper configuration A considering first-ply failure load, and the taper configuration F considering ultimate failure load. It is also observed that the taper configuration C is the least sensitive configuration considering both the buckling load and the ultimate failure load, and taper configuration B considering first-ply failure load.

For LC(4) lay-up configuration, the buckling load under bi-axial compression is found to be about 43.1% of the buckling load under uni-axial compression for taper configuration A, 44.9% for configuration B, 42.9% for configuration C, 60.0% for configuration D, and 41.9% for configuration F. The first-ply failure load under bi-axial compression is found to be about 56.8% of the first-ply failure load under uni-axial compression for taper configuration A, 57.3% for configuration B, 63.0% for configuration C, 71.7% for configuration D, and 59.3% for configuration F. The ultimate failure load under bi-axial compression is found to be about 54.5% of the ultimate failure load under uni-axial compression for taper configuration A, 53.9% for configuration B, 54.7% for configuration C, 61.8% for configuration D, and 53.8% for configuration F. For LC(4) lay-up configuration, it is observed that taper configuration F is the most sensitive configuration to multi-axial nature of loadings considering both buckling load and ultimate failure load, and the taper configuration A considering first-ply failure load. It is also observed that the taper configuration D is the least sensitive configuration considering the buckling load, the first-ply failure load and the ultimate failure load.

For LC(5) lay-up configuration, the buckling load under bi-axial compression is found to be about 53.9% of the buckling load under uni-axial compression for taper configuration A, 47.8% for configuration B, 49.1% for configuration C, 60.0% for configuration D, and 49.1% for configuration F. The first-ply failure load under bi-axial compression is found to be about 53.6% of the first-ply failure load under uni-axial compression for taper configuration A, 61.5% for configuration B, 57.5% for configurations C and F, and 70.8% for configuration D. The ultimate failure load under bi-axial compression is found to be about 60.9% of the ultimate failure load under uni-axial compression for taper

configuration A, 59.3% for configuration B, 60.8% for configuration C, 66.1% for configuration D, and 58.5% for configuration F. Fro LC(5) lay-up configuration, it is observed that taper configuration B is the most sensitive configuration to multi-axial nature of loadings considering buckling load, the taper configuration A considering first-ply failure load, and the taper configuration F considering ultimate failure load. It is also observed that the taper configuration D is the least sensitive configuration considering the buckling load, the first-ply failure load and the ultimate failure load.

For LC(6) lay-up configuration, the buckling load under bi-axial compression is found to be about 50.9% of the buckling load under uni-axial compression for taper configuration A, 52.5% for configurations B and C, 54.8% for configuration D, and 52.3% for configuration F. The first-ply failure load under bi-axial compression is found to be about 51.4% of the first-ply failure load under uni-axial compression for taper configuration A, 58.7% for configurations B, C and F, and 60.2% for configuration D. The ultimate failure load under bi-axial compression is found to be about 58.5% of the ultimate failure load under uni-axial compression for taper configuration A, 61.1% for configurations B and C, 60.1% for configuration D, and 55.5% for configuration F. For LC(6) lay-up configuration, it is observed that taper configuration A is the most sensitive configuration to multi-axial nature of loadings considering both buckling load and first-ply failure load, and the taper configuration F considering ultimate failure load. It is also observed that the taper configuration D is the least sensitive configuration considering the buckling load, the first-ply failure load and the ultimate failure load.

3.6 Conclusion

In this chapter, a detailed parametric study on tapered composite plates under the action of uni-axial and bi-axial compression is conducted. Nonlinear finite element formulation and the progressive failure simulation methodology developed in Chapter 2 are used. The first-ply failure load, the ultimate failure load, the buckling load, the associated maximum transverse displacements, the locations and modes of failure including the onset of delamination of tapered laminated plate under the action of uni-axial and bi-axial compression have been calculated and given.

The results of the present study predict that the maximum difference between the buckling loads, the first-ply failure loads and the ultimate failure loads are strongly dependent on the type of laminate lay-up, the type of boundary condition and the type of taper configuration. The failure mode corresponding to the first-ply failure is associated with the localized matrix cracking irrespective of the lay-up configuration, taper configuration, addition of uniform-thickness sections and boundary condition. The failure occurs primarily due to the in-plane normal stresses acting in the direction transverse to the fiber direction. The most critical points corresponding to the first-ply failure lie near the loaded edge of the plate (i.e. the thin end of the plate). The failure mode corresponding to the ultimate failure is associated with delamination irrespective of the lay-up configuration, taper configuration, addition of uniform-thickness sections and boundary condition. The maximum deflection is upward for bi-axial compression for all lay-up configurations considered, and it is also upward for uni-axial compression for lay-up configurations LC(1), LC(2), LC(3) and LC(6). For lay-up configurations LC(4) and LC(5) under uni-axial compression, it is negative, that is, downward.

For LC(1) lay-up configuration, it is observed that the lowest values of the buckling load, the first-ply failure load and the ultimate failure load correspond to taper configuration D, which means that taper configuration D is the most sensitive configuration in a relative sense, to multi-axial nature of loadings. The magnitudes of buckling load, first-ply failure load and ultimate failure load for taper configuration D are the lowest in case of uni-axial compression. Because it suffers 59% reduction for buckling load and 60.5% for both first-ply failure load and ultimate failure load when the loading becomes bi-axial, the magnitudes of buckling load, first-ply failure load and ultimate failure load become the lowest for taper configuration D. In a similar manner, it is observed that the taper configuration F is the least sensitive configuration considering both the first-ply failure load and the ultimate failure load. It is also observed that taper configurations A and C are the least sensitive configurations considering the buckling load.

For LC(2) lay-up configuration, it is observed that taper configuration D is the most sensitive configuration in a relative sense, to multi-axial nature of loadings. The magnitudes of buckling load, first-ply failure load and ultimate failure load for taper configuration D are the lowest in case of uni-axial compression. Because it suffers 60% reduction for buckling load and 50.7% for both first-ply failure load and ultimate failure load when the loading becomes bi-axial, the magnitudes of buckling load, first-ply failure load and ultimate failure load become the lowest for taper configuration D. In a similar manner, it is observed that the taper configuration C is the least sensitive configuration considering both the buckling load and the first-ply failure load. It is also observed that taper configuration B is the least sensitive configuration considering the ultimate failure load.

For LC(3) lay-up configuration, it is observed that taper configuration D is the most sensitive configuration to multi-axial nature of loadings considering buckling load, the taper configuration A considering first-ply failure load, and the taper configuration F considering ultimate failure load. It is also observed that the taper configuration C is the least sensitive configuration considering both the buckling load and the ultimate failure load, and taper configuration B considering first-ply failure load.

For LC(4) lay-up configuration, it is observed that taper configuration F is the most sensitive configuration to multi-axial nature of loadings considering both buckling load and ultimate failure load, and the taper configuration A considering first-ply failure load. It is also observed that the taper configuration D is the least sensitive configuration considering the buckling load, the first-ply failure load and the ultimate failure load.

Fro LC(5) lay-up configuration, it is observed that taper configuration B is the most sensitive configuration to multi-axial nature of loadings considering buckling load, the taper configuration A considering first-ply failure load, and the taper configuration F considering ultimate failure load. It is also observed that the taper configuration D is the least sensitive configuration considering the buckling load, the first-ply failure load and the ultimate failure load.

For LC(6) lay-up configuration, it is observed that taper configuration A is the most sensitive configuration to multi-axial nature of loadings considering both buckling load and first-ply failure load, and the taper configuration F considering ultimate failure load. It is also observed that the taper configuration D is the least sensitive configuration considering the buckling load, the first-ply failure load and the ultimate failure load.

In general, under the action of uni-axial and bi-axial compression, for the lay-up and taper configurations and the boundary conditions considered, the ultimate failure load is about 2.0 - 7.2 times the buckling load, the first-ply failure load is about 2.0 – 5.3 times the buckling load, and the ultimate failure load is about 1.0 - 1.8 times the first-ply failure load. The largest difference between the buckling load and the first-ply failure load corresponds to the tapered laminate under bi-axial compression with the lay-up configuration LC(1), the boundary condition BC1 and the taper configuration F . For this case, the first-ply failure load is about 5.3 times the buckling load. As for the difference between the buckling load and the ultimate failure load, the largest difference corresponds to the tapered laminate with the lay-up configuration LC(1), the boundary condition BC1 and the taper configuration F under the action of bi-axial compression. For this case, the ultimate failure load is about 6.3 times the buckling load. As for the difference between the first-ply failure load and the ultimate failure load, the largest difference corresponds to the tapered laminate with the lay-up configuration LC(4), the boundary condition BC1 and the taper configuration D under the action of uni-axial compression. For this case, the ultimate failure load is about 1.8 times the first-ply failure load. Hence, it can be seen that considerable residual strength is available for these laminates in the post-buckling stage under the action of uni-axial and bi-axial compression.

Chapter 4

Progressive Failure and Post-buckling Response under In-plane Shear

4.1 Introduction

Three symmetric and three un-symmetric lay-up configurations that were defined in Table 3.1, and for each lay-up configuration, five taper configurations shown in Figure 3.1 to Figure 3.5 respectively, are considered. In addition to the above mentioned six lay-up configurations, tapered laminates with $(\pm\theta)_{4s}$ lay-up at the left (thick) end are also considered to understand the influence of fiber orientation on the failure strength of the laminate. The boundary condition, the material properties, the dimension of the plate and the finite element mesh used are the same as those given in sub-section 3.2 of Chapter 3. The objective is to predict the first-ply failure load, the ultimate failure load, the buckling load, the associated maximum transverse displacements, and locations and modes of failure of tapered laminated plates under the action of in-plane positive and negative shear loadings.

Instead of using the tensor polynomial form of the maximum stress failure criterion which is used for the cases of uni-axial compression and bi-axial compression, the tensor polynomial form of the 3D Tsai-Hill criterion is used as the failure criterion for a lamina failure and resin failure in the case of in-plane shear, and the terms associated with the normal stress component in the third principal material direction are omitted.

Figure 4.1 and Figure 4.2 show the direction of the applied shear loading.

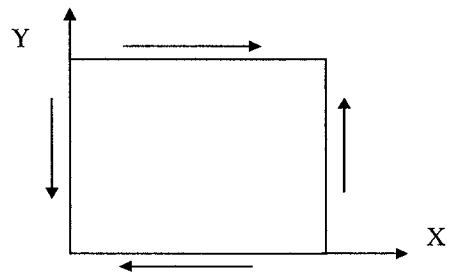

Figure 4.1 Notation for the positive shear

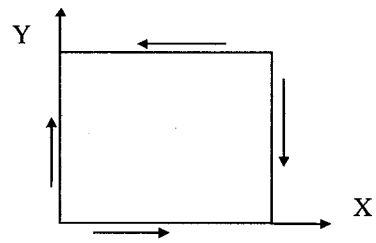

Figure 4.2 Notation for the negative shear

4.2 Parametric Study on In-plane Positive Shear

4.2.1 Influence of Taper Configuration

Figure 4.3 shows the load versus the maximum deflection curves of the five laminates all with LC(1) lay-up configuration and each with a different taper configuration under the action of in-plane positive shear. Table 4.1 gives the buckling load, the first-ply failure load and the ultimate failure load for these laminates. The in-plane shear loading is expressed in figures in non-dimensional form as $P_{xy}hb^2/E_2h^3$, where P_{xy} is the applied in-plane shear loading per unit area. The corresponding maximum (transverse) deflection is also expressed in non-dimensional form as W_m/h, where h is the average thickness of the tapered laminate.

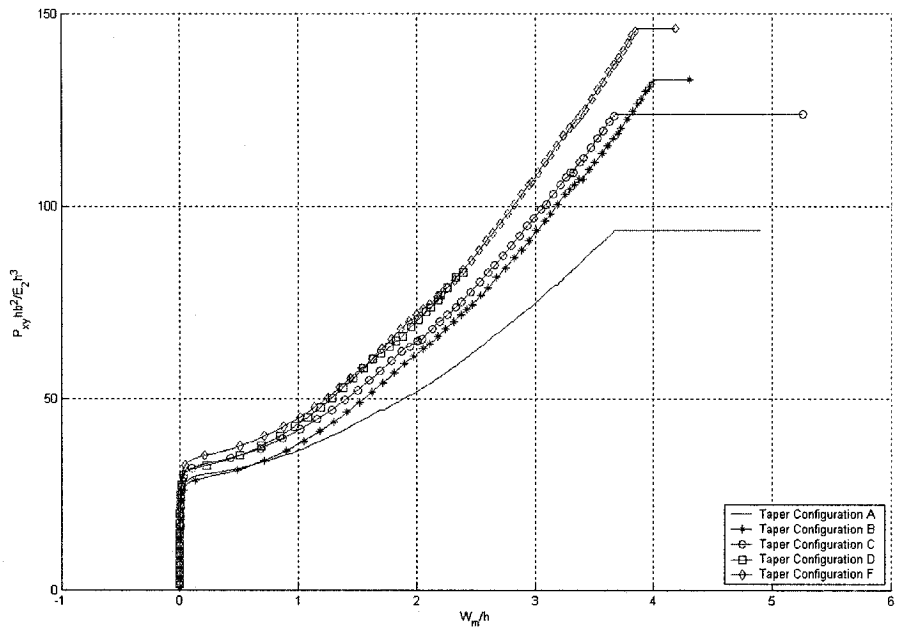

Figure 4.3 Load versus the maximum deflection curves of the laminates with LC(1) lay-up configuration for five taper configurations under in-plane positive shear

Table 4.1 Failure data of the laminates with LC(1) lay-up configuration for five taper configurations under in-plane positive shear

Taper	Buckling Load ($P_{xy}hb^2/E_2h^3$)	First-ply failure load ($P_{xy}hb^2/E_2h^3$)	Ultimate failure load ($P_{xy}hb^2/E_2h^3$)	$(W_m/h)^*$	Failure location (FL,FE) ♣	First-ply failure mode	Ultimate failure mode
A	30.197	47.045	93.452	1.691	1,1	T♠	D#
B	29.562	60.395	132.867	1.941	1,1	T	D
C	32.741	63.573	123.968	1.914	1,1	T	D
D	32.105	61.031	82.644	1.651	1,1	T	D
F	35.283	69.930	146.217	1.923	1,1	T	D

* Non-dimensionalized maximum deflection at first-ply failure

♣ FL and FE are the failed layer number and failed element number at first-ply failure

♠ Transverse mode of failure refers to the matrix failure

Delamination failure

For lay-up configuration LC(1), the first-ply failure load is found to be about 1.6 times the buckling load for taper configuration A, 2.0 times for configurations B and F, and 1.9

times for configurations C and D. The ultimate failure load is about 3.1 times the buckling load for configuration A, 4.5 times for configuration B, 3.8 times for configuration C, 2.6 times for configuration D, and 4.1 times for configuration F. The ultimate failure load is about 2.0 times the first-ply failure load for configurations A and C, 2.2 times for configuration B, 1.4 times for configuration D, and 2.1 times for configuration F. Hence, it can be observed that considerable residual strength exists in the tapered laminates beyond the onset of buckling. Moreover, all the taper configurations can on an average sustain about 95% more loading after first-ply failure until ultimate failure by delaminiation.

Figure 4.4 shows the pre-buckling load-deflection path of the laminates with LC(1) lay-up configuration for five taper configurations under in-plane positive shear. It can be observed that unlike other taper configurations the maximum deflection for taper configuration D changes from negative to positive when the non-dimensional loading reaches a value of about 7.

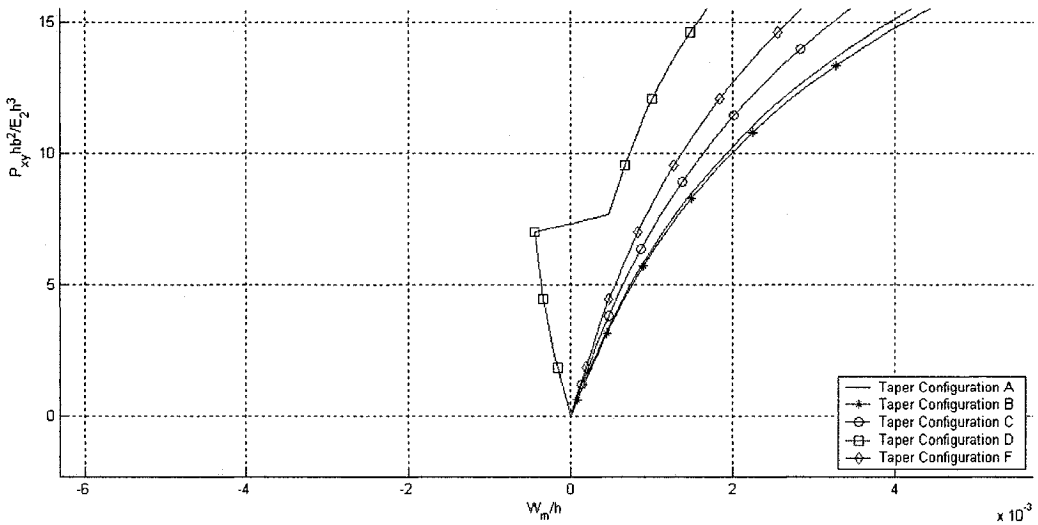

Figure 4.4 The pre-buckling load-deflection path of the laminates with LC(1) lay-up configuration for five taper configurations under in-plane positive shear

Figure 4.5 shows the load versus the maximum deflection curves of the five laminates all with LC(2) lay-up configuration and each with a different taper configuration under the action of in-plane positive shear. Table 4.2 gives the buckling load, the first-ply failure load and the ultimate failure load for these laminates.

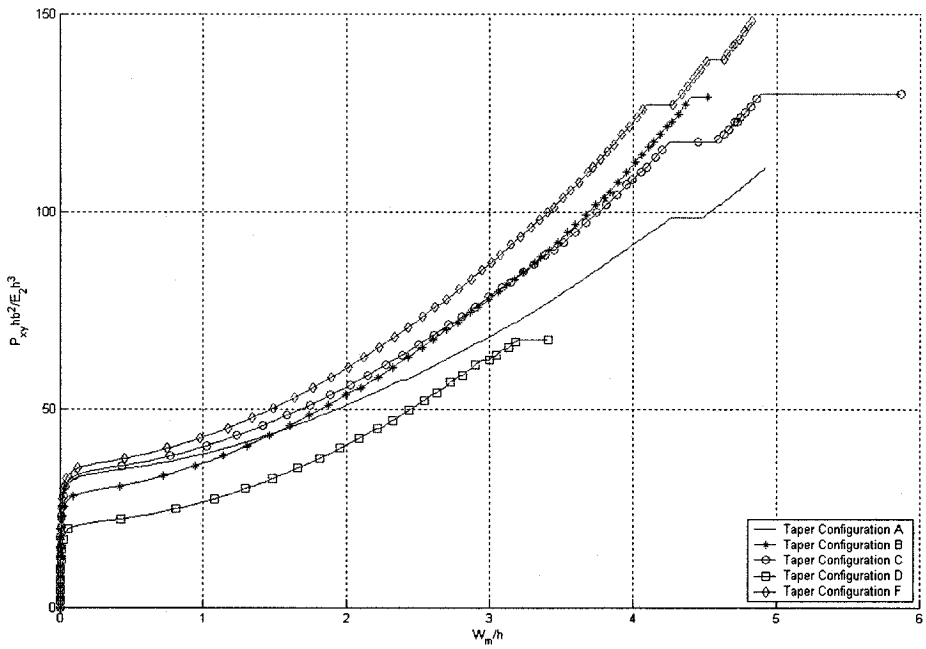

Figure 4.5 Load versus maximum deflection curves of the laminates with LC(2) lay-up configuration for five taper configurations under in-plane positive shear

Table 4.2 Failure data of the laminates with LC(2) lay-up configuration for five taper configurations under in-plane positive shear

Taper	Buckling Load ($P_{xy}hb^2/E_2h^3$)	First-ply failure load ($P_{xy}hb^2/E_2h^3$)	Ultimate failure load ($P_{xy}hb^2/E_2h^3$)	$(W_m/h)^*$	Failure location (FL,FE) ♣	First-ply failure mode	Ultimate failure mode
A	34.647	57.216	111.252	2.383	1,1	T♠	D#
B	29.562	54.672	129.053	1.955	1,1	T	D
C	35.283	71.837	129.689	2.737	1,1	T	D
D	21.933	45.137	67.388	2.211	1,1	T	D
F	36.555	76.287	148.125	2.640	1,1	T	D

For lay-up configuration LC(2), the first-ply failure load is found to be about 1.7 times the buckling load for taper configuration A, 1.8 times for configuration B, 2.0 times for configuration C, and 2.1 times for configurations D and F. The ultimate failure load is about 3.2 times the buckling load for configuration A, 4.4 times for configuration B, 3.7 times for configuration C, 3.1 times for configuration D, and 4.1 times for configuration F. The ultimate failure load is about 1.9 times the first-ply failure load for configuration A, 2.4 times for configuration B, 1.8 times for configuration C, 1.5 times for configuration D, and 1.9 times for configuration F.

In order to illustrate the positive maximum deflection of the plate under in-plane positive shear, a typical deformed configuration is given. Figure 4.6 shows the deformed configuration of the laminate with LC(2) lay-up configuration and with taper configuration B under in-plane positive shear. It is observed that the maximum deflection is positive (upward), but the deflections of the entire laminate are not all positive. The deformed configuration has a large peak, which is positive (upward), and two small peaks, which are negative (downward).

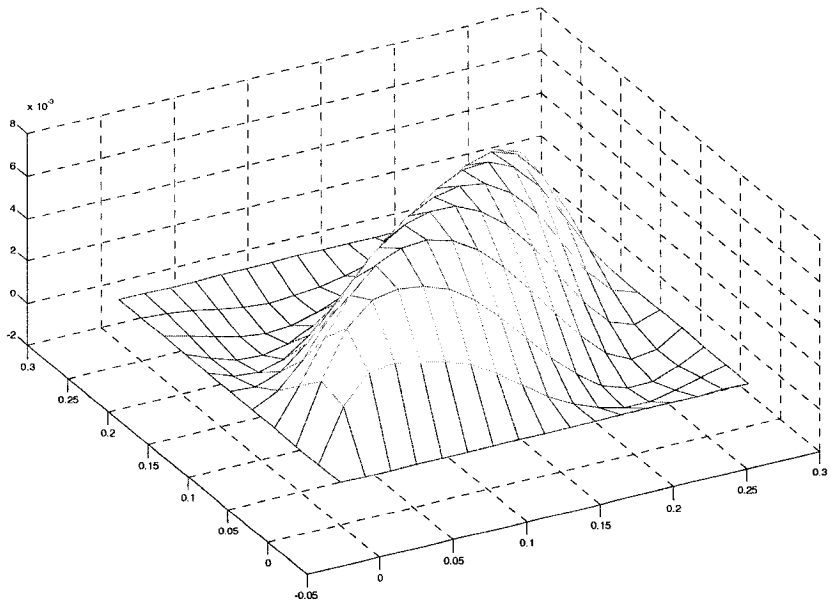

Figure 4.6 The deformed configuration of the laminate with LC(2) lay-up configuration and with taper configuration B under in-plane positive shear

Figure 4.7 shows the load versus the maximum deflection curves of the five laminates all with LC(3) lay-up configuration and each with a different taper configuration under the action of in-plane positive shear. Table 4.3 gives the buckling load, the first-ply failure load and the ultimate failure load for these laminates.

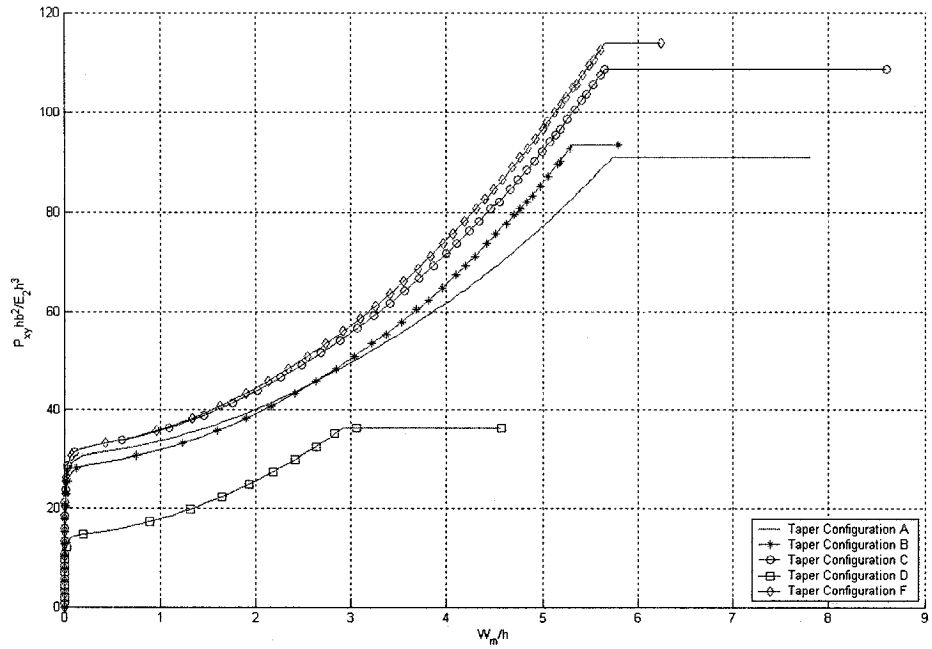

Figure 4.7 Load versus maximum deflection curves of the laminates with LC(3) lay-up configuration for five taper configurations under in-plane positive shear

Table 4.3 Failure data of the laminates with LC(3) lay-up configuration for five taper configurations under in-plane positive shear

Taper	Buckling Load ($P_{xy}hb^2/E_2h^3$)	First-ply failure load ($P_{xy}hb^2/E_2h^3$)	Ultimate failure load ($P_{xy}hb^2/E_2h^3$)	$(W_m/h)^*$	Failure location (FL,FE) ♣	First-ply failure mode	Ultimate failure mode
A	31.469	61.031	90.909	3.932	1,1	T♠	D#
B	29.561	55.308	93.452	3.347	1,1	T	D
C	33.376	71.837	108.710	3.996	1,1	T	D
D	14.940	36.237	36.237	2.922	1,40	T	D
F	33.526	75.651	113.795	4.056	1,1	T	D

For lay-up configuration LC(3), the first-ply failure load is found to be about 1.9 times the buckling load for taper configurations A and B, 2.2 times for configuration C, 2.4 times for configuration D, and 2.3 times for configuration F. The ultimate failure load is about 2.9 times the buckling load for configuration A, 3.2 times for configuration B, 3.3 times for configuration C, 2.4 times for configuration D, and 3.4 times for configuration

F. The ultimate failure load is about 1.5 times the first-ply failure load for configurations A, C and F, 1.7 times for configuration B, and 1.0 time for configuration D.

Figure 4.8 shows the load versus the maximum deflection curves of the five laminates all with LC(4) lay-up configuration and each with a different taper configuration under the action of in-plane positive shear. Table 4.4 gives the buckling load, the first-ply failure load and the ultimate failure load for these laminates.

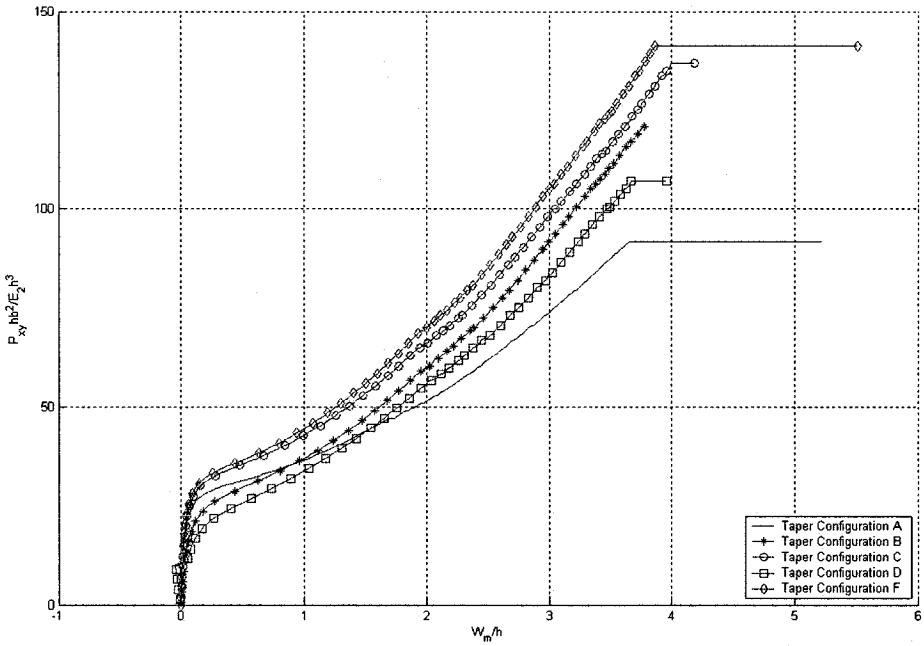

Figure 4.8 Load versus maximum deflection curves of the laminates with LC(4) lay-up configuration for five taper configurations under in-plane positive shear

Table 4.4 Failure data of the laminates with LC(4) lay-up configuration for five taper configurations under in-plane positive shear

Taper	Buckling Load ($P_{xy}hb^2/E_2h^3$)	First-ply failure load ($P_{xy}hb^2/E_2h^3$)	Ultimate failure load ($P_{xy}hb^2/E_2h^3$)	$(W_m/h)^*$	Failure location (FL,FE) ♣	First-ply failure mode	Ultimate failure mode
A	30.833	47.045	91.545	1.696	1,1	T♠	D#
B	28.926	59.123	120.788	1.950	1,1	T	D
C	34.011	64.844	136.682	1.929	1,1	T	D
D	10.490	56.580	106.802	2.020	1,1	T	D
F	34.647	69.294	141.132	1.950	1,1	T	D

For lay-up configuration LC(4), the first-ply failure load is found to be about 1.5 times the buckling load for taper configuration A, 2.0 times for configurations B and F, 1.9 times for configuration C, and 5.4 times for configuration D. The ultimate failure load is about 3.0 times the buckling load for configuration A, 4.2 times for configuration B, 4.0 times for configuration C, 10.2 times for configuration D, and 4.1 times for configuration F. The ultimate failure load is about 1.9 times the first-ply failure load for configurations A and D, 2.0 times for configuration B, 2.1 times for configuration C, and 2.0 times for configuration F.

Figure 4.9 shows the pre-buckling load-deflection path of the laminates with LC(4) lay-up configuration for five taper configurations under in-plane positive shear. It can be observed that unlike other taper configurations, the maximum deflection for taper configuration D changes from negative to positive when the non-dimensional loading reaches a value of about 10.

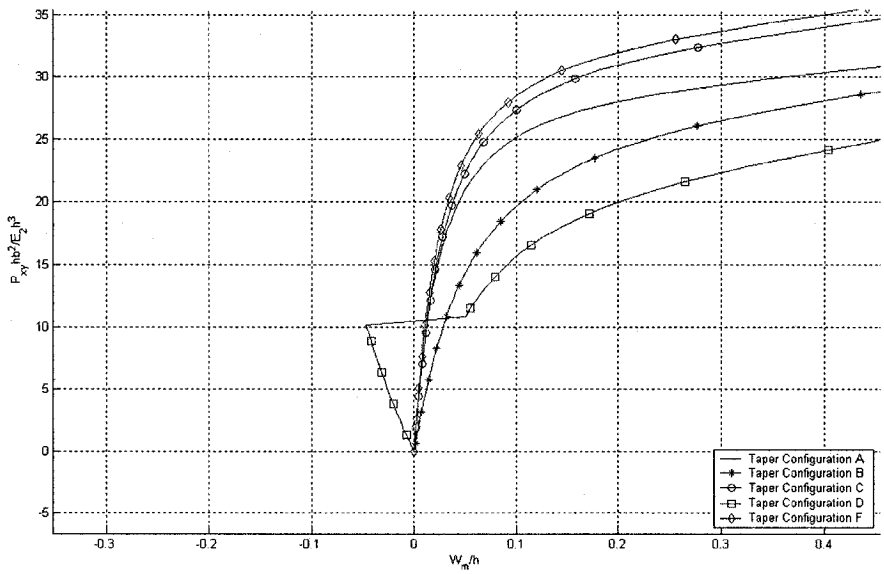

Figure 4.9 The pre-buckling load deflection path of the laminate with LC(4) lay-up configuration for five taper configurations under in-plane positive shear

Figure 4.10 shows the load versus the maximum deflection curves of the five laminates all with LC(5) lay-up configuration and each with a different taper configuration under the action of in-plane positive shear. Table 4.5 gives the buckling load, the first-ply failure load and the ultimate failure load for these laminates.

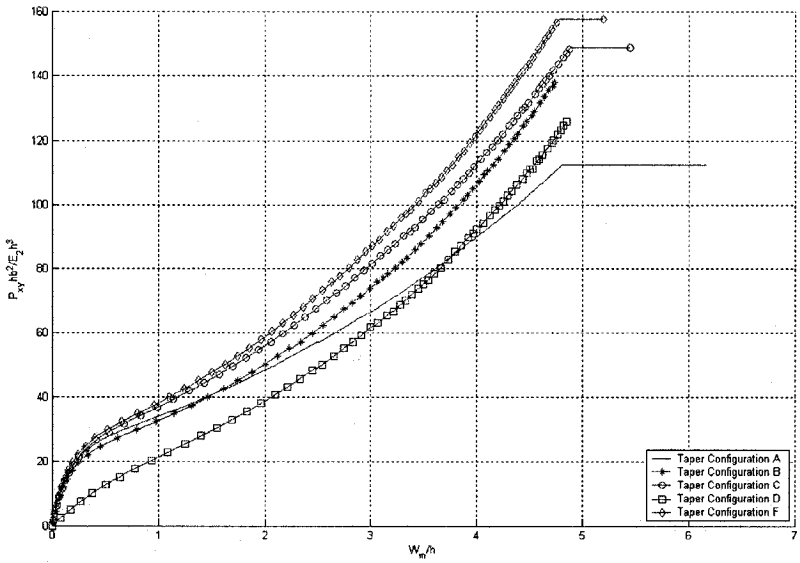

Figure 4.10 Load versus maximum deflection curves of the laminates with LC(5) lay-up configuration for five taper configurations under in-plane positive shear

Table 4.5 Failure data of the laminates with LC(5) lay-up configuration for five taper configurations under in-plane positive shear

Taper	Buckling Load ($P_{xy}hb^2/E_2h^3$)	First-ply failure load ($P_{xy}hb^2/E_2h^3$)	Ultimate failure load ($P_{xy}hb^2/E_2h^3$)	$(W_m/h)^*$	Failure location (FL,FE) ♣	First-ply failure mode	Ultimate failure mode
A	34.011	57.216	112.524	2.497	1,1	T♠	D#
B	32.741	55.308	137.954	2.233	1,1	T	D
C	34.647	72.473	148.760	2.675	1,1	T	D
D	23.840	48.951	125.874	2.471	1,1	T	D
F	35.283	75.651	157.665	2.633	1,1	T	D

For lay-up configuration LC(5), the first-ply failure load is found to be about 1.7 times the buckling load for taper configurations A and B, and 2.1 times for configurations B, C, D and F. The ultimate failure load is about 3.3 times the buckling load for configuration A, 4.2 times for configuration B, 4.3 times for configuration C, 5.3 times for

configuration D, and 4.5 times for configuration F. The ultimate failure load is about 2.0 times the first-ply failure load for configurations A, 2.5 times for configuration B, 2.1 times for configuration C, 2.6 times for configuration D, and 2.1 times for configuration F.

Figure 4.11 shows the load versus the maximum deflection curves of the five laminates all with LC(6) lay-up configuration and each with a different taper configuration under the action of in-plane positive shear. Table 4.6 gives the buckling load, the first-ply failure load and the ultimate failure load for these laminates.

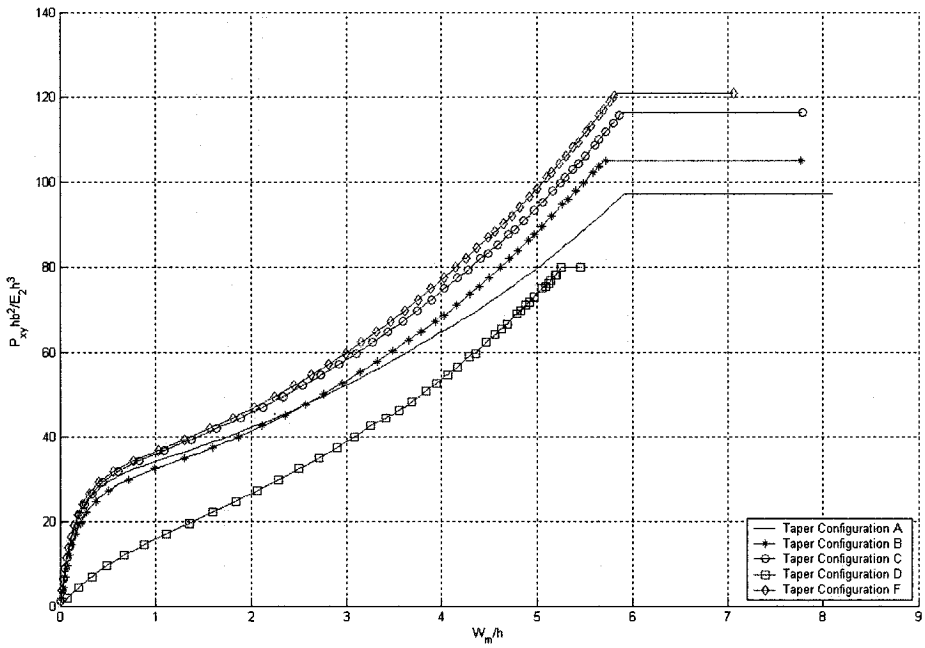

Figure 4.11 Load versus maximum deflection curves of the laminates with LC(6) lay-up configuration for five taper configurations under in-plane positive shear

Table 4.6 Failure data of the laminates with LC(6) lay-up configuration for five taper configurations under in-plane positive shear

Taper	Buckling Load ($P_{xy}hb^2/E_2h^3$)	First-ply failure load ($P_{xy}hb^2/E_2h^3$)	Ultimate failure load ($P_{xy}hb^2/E_2h^3$)	$(W_m/h)^*$	Failure location (FL,FE) ♣	First-ply failure mode	Ultimate failure mode
A	36.555	64.844	97.266	3.988	1,1	T♠	D#
B	35.283	64.209	104.895	3.727	1,1	T	D
C	37.826	78.195	116.339	4.199	1,1	T	D
D	18.755	43.865	80.102	3.340	1,40	T	D
F	37.826	82.010	120.788	4.242	1,1	T	D

For lay-up configuration LC(6), the first-ply failure load is found to be about 1.8 times the buckling load for taper configurations A and B, 2.1 times for configuration C, 2.3 times for configuration D, and 2.2 times for configuration F. The ultimate failure load is about 2.7 times the buckling load for configuration A, 3.0 times for configuration B, 3.1 times for configuration C, 4.3 times for configuration D, and 3.2 times for configuration F. The ultimate failure load is about 1.5 times the first-ply failure load for configurations A, C and F, 1.6 times for configuration B, and 1.8 times for configuration D.

Summary

From Figures 4.3 – 4.11 and Tables 4.1 – 4.6, the following general observations are also made.

1 Among all the six lay-up configurations, the taper configuration F (Mid-plane taper) is the strongest one with respect to the first-ply failure load, the ultimate failure load and the buckling load. However, taper configuration F is not easy to manufacture compared to other taper configurations. Considering this, the next strongest taper configuration is identified. For the lay-up configurations LC(2), LC(3), LC(4), LC(5) and LC(6), the taper configuration C (Overlapping dropped plies) is the best choice among all taper configurations considering the first-ply failure load, the ultimate

failure load and the buckling load. For the lay-up configuration LC(1), taper configuration B is the best choice in terms of the buckling load and the first-ply failure load, whereas, taper configuration C is the best choice in terms of the ultimate failure load.

2 Only for the laminate with LC(3) lay-up configuration for the taper configuration D (Continuous plies interspersed), the first-ply failure load and the ultimate failure load are equal to each other. For all other cases, considerable residual strength exists after the first-ply failure until ultimate failure.

3 For symmetric lay-up configuration LC(3) and the corresponding un-symmetric lay-up configuration LC(6), locations corresponding to the first-ply failure lie near the thin end of the plate for configuration D and at the outermost bottom layer. Whereas, for all other cases, they lie near the thick end of the plate and at the outermost bottom layer.

4 For symmetric lay-up configuration LC(1) and the corresponding un-symmetric lay-up configuration LC(4), maximum deflections change form negative to positive for taper configuration D. For the rest of the cases, the maximum deflections are always positive.

4.2.2 Influence of Lay-up Configuration

Figure 4.12 shows the load versus maximum deflection curves of the six laminates all with taper configuration A and each with a different lay-up configuration under the action of in-plane positive shear. Table 4.7 gives the buckling load, the first-ply failure load and the ultimate failure load for these laminates.

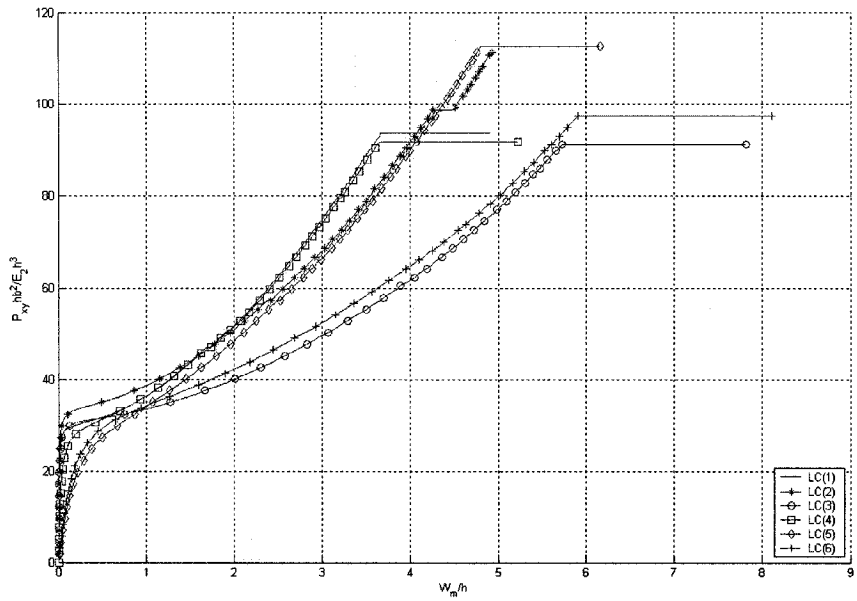

Figure 4.12 Load versus maximum deflection curves of the laminates with taper configuration A for all the six lay-up configurations under in-plane positive shear

Table 4.7 Failure data of the laminates with taper configuration A for all the six lay-up configurations under in-plane positive shear

Lay-up	Buckling Load ($P_{xy}hb^2/E_2h^3$)	First-ply failure load ($P_{xy}hb^2/E_2h^3$)	Ultimate failure load ($P_{xy}hb^2/E_2h^3$)	$(W_m/h)^*$	Failure location (FL,FE) ♣	First-ply failure mode	Ultimate failure mode
LC(1)	30.197	47.045	93.452	1.691	1,1	T♠	D#
LC(2)	34.647	57.216	111.252	2.383	1,1	T	D
LC(3)	31.469	61.031	90.909	3.932	1,1	T	D
LC(4)	30.833	47.045	91.545	1.696	1,1	T	D
LC(5)	34.011	57.216	112.524	2.497	1,1	T	D
LC(6)	36.555	64.844	97.266	3.988	1,1	T	D

For taper configuration A, the lay-up configuration LC(6) is the best choice among all the six lay-up configurations with respect to both the buckling load and the first-ply failure load, and lay-up configuration LC(5) is the best choice with respect to the ultimate failure load.

Figure 4.13 shows the load versus maximum deflection curves of the six laminates all with taper configuration B and each with a different lay-up configuration under the action

of in-plane positive shear. Table 4.8 gives the buckling load, the first-ply failure load and the ultimate failure load for these laminates.

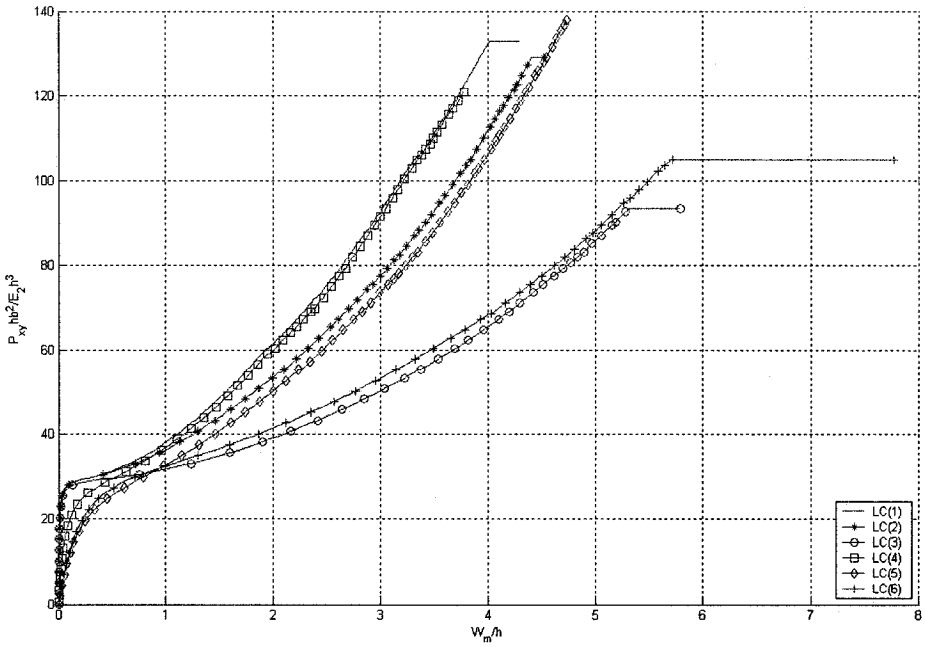

Figure 4.13 Load versus maximum deflection curves of the laminates with taper configuration B for all the six lay-up configurations under in-plane positive shear

Table 4.8 Failure data of the laminates with taper configuration B for all the six lay-up configurations under in-plane positive shear

Lay-up	Buckling Load ($P_{xy}hb^2/E_2h^3$)	First-ply failure load ($P_{xy}hb^2/E_2h^3$)	Ultimate failure load ($P_{xy}hb^2/E_2h^3$)	$(W_m/h)^*$	Failure location (FL,FE) ♣	First-ply failure mode	Ultimate failure mode
LC(1)	29.562	60.395	132.867	1.941	1,1	T♠	D#
LC(2)	29.562	54.672	129.053	1.955	1,1	T	D
LC(3)	29.561	55.308	93.452	3.347	1,1	T	D
LC(4)	28.926	59.123	120.788	1.950	1,1	T	D
LC(5)	32.741	55.308	137.954	2.233	1,1	T	D
LC(6)	35.283	64.209	104.895	3.727	1,1	T	D

For taper configuration B, the lay-up configuration LC(6) is the best choice among all the six lay-up configurations with respect to both the buckling load and the first-ply failure

load, and lay-up configuration LC(5) is the best choice with respect to the ultimate failure load.

Figure 4.14 shows the load versus maximum deflection curves of the six laminates all with taper configuration C and each with a different lay-up configuration under the action of in-plane positive shear. Table 4.9 gives the buckling load, the first-ply failure load and the ultimate failure load for these laminates.

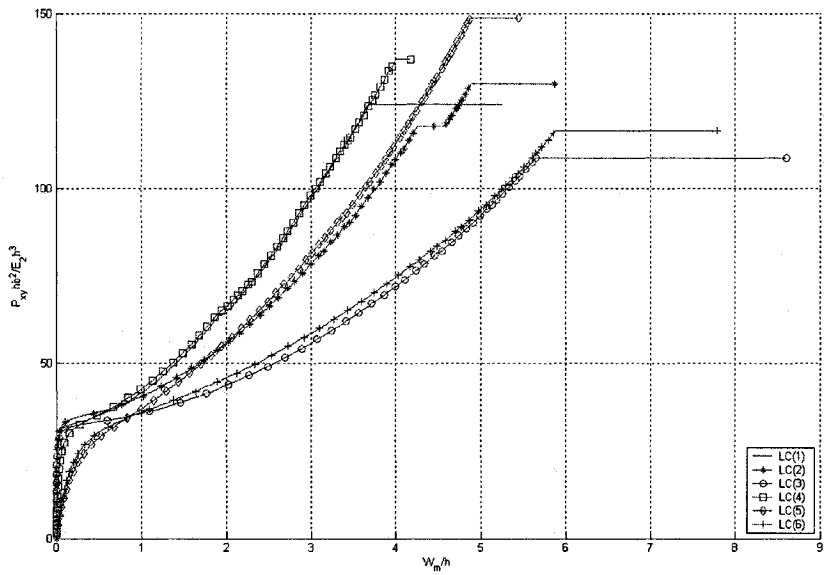

Figure 4.14 Load versus maximum deflection curves of the laminates with taper configuration C for all the six lay-up configurations under in-plane positive shear

Table 4.9 Failure data of the laminates with taper configuration C for all the six lay-up configurations under in-plane positive shear

Lay-up	Buckling Load ($P_{xy}hb^2/E_2h^3$)	First-ply failure load ($P_{xy}hb^2/E_2h^3$)	Ultimate failure load ($P_{xy}hb^2/E_2h^3$)	$(W_m/h)^*$	Failure location (FL,FE) ♣	First-ply failure mode	Ultimate failure mode
LC(1)	32.741	63.573	123.968	1.914	1,1	T♠	D#
LC(2)	35.283	71.837	129.689	2.737	1,1	T	D
LC(3)	33.376	71.837	108.710	3.996	1,1	T	D
LC(4)	34.011	64.844	136.682	1.929	1,1	T	D
LC(5)	34.647	72.473	148.760	2.675	1,1	T	D
LC(6)	37.826	78.195	116.339	4.199	1,1	T	D

For taper configuration C, the lay-up configuration LC(6) is the best choice among all the six lay-up configurations with respect to both the buckling load and the first-ply failure load, and lay-up configuration LC(5) is the best choice with respect to the ultimate failure load.

Figure 4.15 shows the load versus maximum deflection curves of the six laminates all with taper configuration D and each with a different lay-up configuration under the action of in-plane positive shear. Table 4.10 gives the buckling load, the first-ply failure load and the ultimate failure load for these laminates.

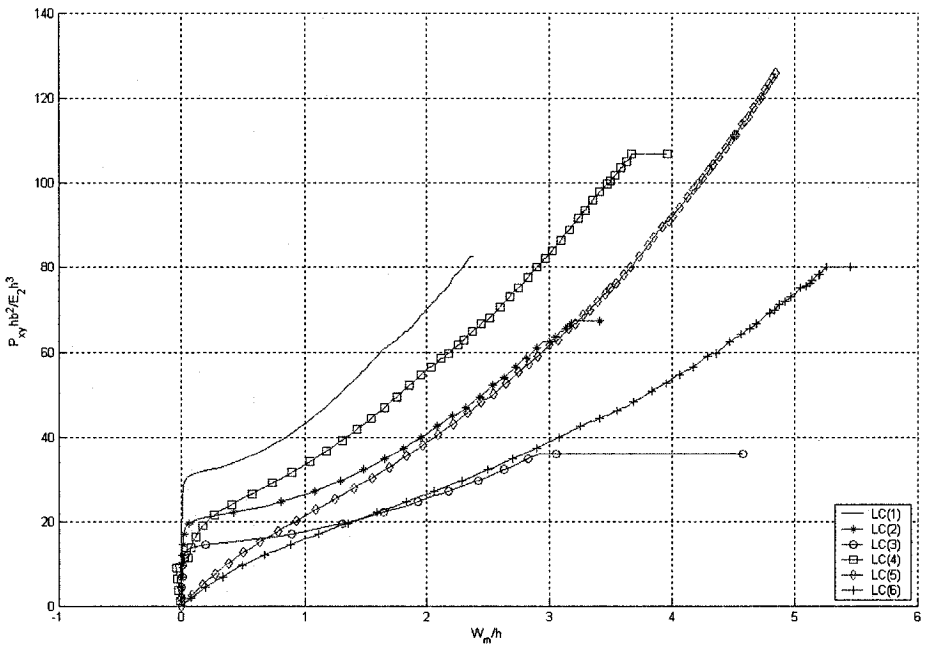

Figure 4.15 Load versus maximum deflection curves of the laminates with taper configuration D for all the six lay-up configurations under in-plane positive shear

Table 4.10 Failure data of the laminates with taper configuration D for all the six lay-up configurations under in-plane positive shear

Lay-up	Buckling Load ($P_{xy}hb^2/E_2h^3$)	First-ply failure load ($P_{xy}hb^2/E_2h^3$)	Ultimate failure load ($P_{xy}hb^2/E_2h^3$)	$(W_m/h)^*$	Failure location (FL,FE) ♣	First-ply failure mode	Ultimate failure mode
LC(1)	32.105	61.031	82.644	1.651	1,1	T♠	D#
LC(2)	21.933	45.137	67.388	2.211	1,1	T	D
LC(3)	14.940	36.237	36.237	2.922	1,40	T	D
LC(4)	10.490	56.580	106.802	2.020	1,1	T	D
LC(5)	23.840	48.951	125.874	2.471	1,1	T	D
LC(6)	18.755	43.865	80.102	3.340	1,40	T	D

For taper configuration D, the lay-up configuration LC(1) is the best choice among all the six lay-up configurations with respect to both the buckling load and the first-ply failure load, and the lay-up configuration LC(5) is the best choice with respect to the ultimate failure load.

Figure 4.16 shows the load versus maximum deflection curves of the six laminates all with taper configuration F and each with a different lay-up configuration under the action of in-plane positive shear. Table 4.11 gives the buckling load, the first-ply failure load and the ultimate failure load for these laminates.

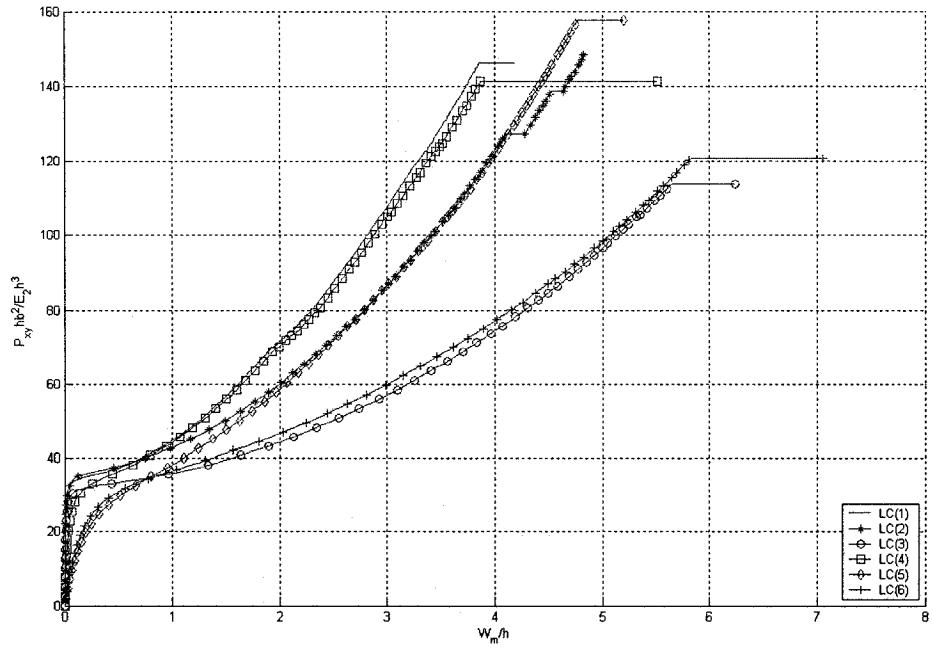

Figure 4.16 Load versus maximum deflection curves of the laminates with taper configuration F for all the six lay-up configurations under in-plane positive shear

Table 4.11 Failure data of the laminates with taper configuration F for all the six lay-up configurations under in-plane positive shear

Lay-up	Buckling Load ($P_{xy}hb^2/E_2h^3$)	First-ply failure load ($P_{xy}hb^2/E_2h^3$)	Ultimate failure load ($P_{xy}hb^2/E_2h^3$)	$(W_m/h)^*$	Failure location (FL,FE) ♣	First-ply failure mode	Ultimate failure mode
LC(1)	35.283	69.930	146.217	1.923	1,1	T♠	D#
LC(2)	36.555	76.287	148.125	2.640	1,1	T	D
LC(3)	33.526	75.651	113.795	4.056	1,1	T	D
LC(4)	34.647	69.294	141.132	1.950	1,1	T	D
LC(5)	35.283	75.651	157.665	2.633	1,1	T	D
LC(6)	37.826	82.010	120.788	4.242	1,1	T	D

For taper configuration F, the lay-up configuration LC(6) is the best choice among all the six lay-up configurations with respect to both the buckling load and the first-ply failure load, and the lay-up configuration LC(5) is the best choice with respect to the ultimate failure load.

Summary

From Figures 4.12 – 4.16 and Tables 4.7 – 4.11, the following general observations are made.

1 For all the five taper configurations, the first-ply failure mode for all the six lay-up configurations is transverse (matrix) failure.

2 For all the five taper configurations, the ultimate failure mode for all the six lay-up configurations is delamination.

3 Locations corresponding to the first-ply failure for all the six lay-up configurations lie at the outermost bottom layer. However, for taper configuration D for LC(3) and LC(6) lay-up configurations, it is near the thin end of the plate. Whereas, for all other cases, it is near the thick end of the plate.

4 Variations of the maximum deflection with the load for the symmetric lay-up configuration basically coincides with that of the corresponding un-symmetric lay-up configuration for taper configurations A (Basic taper), B (Staircase arrangement), C (Overlapping dropped plies) and F (Mid-plane taper). Therefore, in these cases the symmetry in the stacking sequence does not have a strong influence on the progressive failure of the laminate.

4.2.3 Influence of Fiber Orientation

Tapered laminates under the action of in-plane positive shear and with lay-up $(\pm\theta)_{4s}$ at the left end are considered. The lay-up at the right (thin) end is $(\pm\theta)_{2s}$ for taper configurations A, B, C and F, and is $(\theta)_8$ for taper configuration D. The variation of buckling load with θ for each taper configuration is determined. The results are plotted in Figure 4.17. A non-monotonic variation is observed for all taper configurations from this figure. Also the

variation is un-symmetric about 45° fiber orientation. Peak values of the buckling loads are predicted to occur for 90° fiber orientation for all taper configurations. The taper configuration D has the lowest value of buckling load, and the taper configuration F has the highest value of buckling load. Also, for taper configuration D, for all off-axis fiber orientations, the buckling load is significantly less than that of all other taper configurations. The buckling load of the taper configuration C is very close to that of the taper configuration F for $(\pm 15)_{4s}$, $(\pm 30)_{4s}$, $(\pm 45)_{4s}$, and $(\pm 60)_{4s}$ fiber orientations.

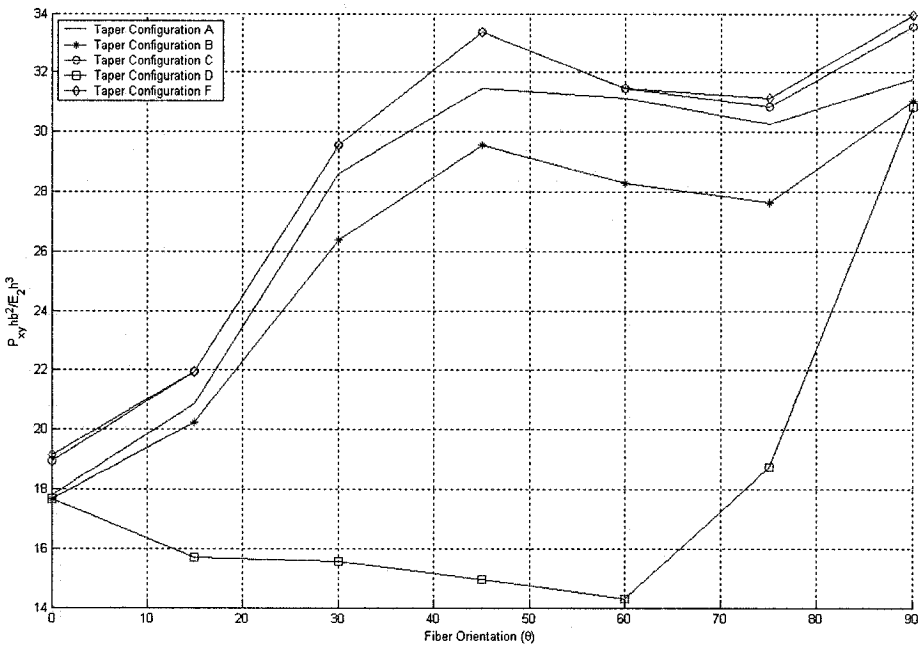

Figure 4.17 Buckling loads of the laminates with $(\pm\theta)_{4s}$ lay-up at the left (thick) end under in-plane positive shear

Figure 4.18 shows the variation of the first-ply failure load and the ultimate failure load for laminates with taper configuration A and with lay-up $(\pm\theta)_{4s}$ at the left (thick) end under the action of in-plane positive shear. The results show that the variations in response are un-symmetric about 45° fiber orientation. Peak values of the first-ply failure load and ultimate failure load are predicted to occur for 45° fiber orientation. In the range $15° \leq \theta \leq 45°$ the difference between the ultimate failure load and the first-ply failure load

becomes larger, and at θ = 45° the ultimate failure load is 48.96% higher than the first-ply failure load.

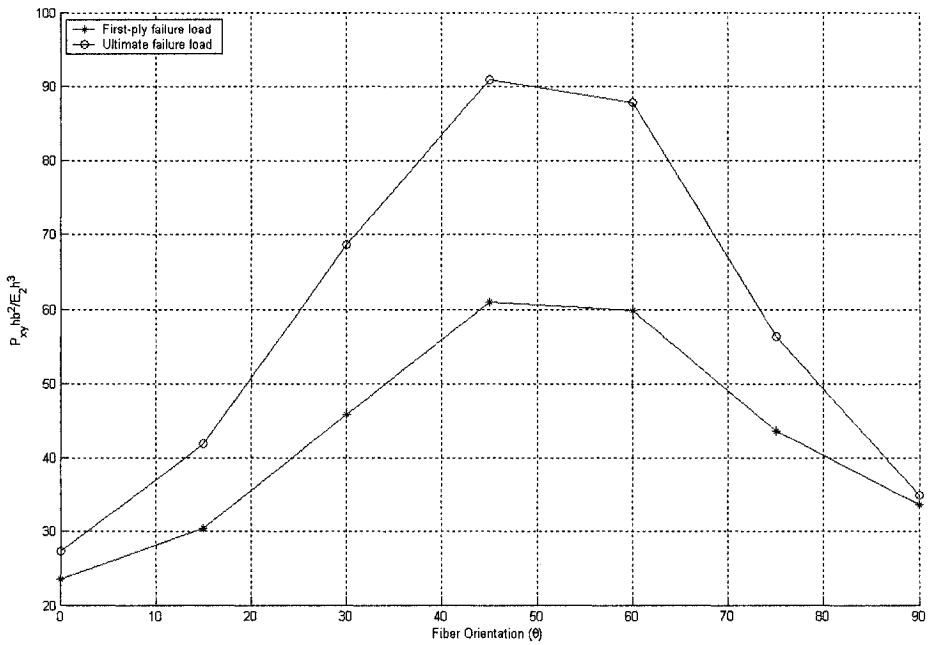

Figure 4.18 Variation of the first-ply and ultimate failure loads of the laminates with taper configuration A and with $(\pm\theta)_{4s}$ lay-up at the left end under in-plane positive shear

Figure 4.19 shows the variation of the first-ply failure load and the ultimate failure load for laminates with taper configuration B and with lay-up $(\pm\theta)_{4s}$ at the left (thick) end under the action of in-plane positive shear. The results show that the variations in response are un-symmetric about 45° fiber orientation. Peak values of the first-ply failure load and ultimate failure load are predicted to occur for 45° fiber orientation. For laminate with $(\pm 0)_{4s}$ lay-up configuration at the thick end, the value of the first-ply failure load is equal to the value of the ultimate failure load. In the range $15° \leq \theta \leq 45°$ the difference between the ultimate failure load and the first-ply failure load becomes larger, and at θ = 45° the ultimate failure load is 68.97% higher than the first-ply failure load.

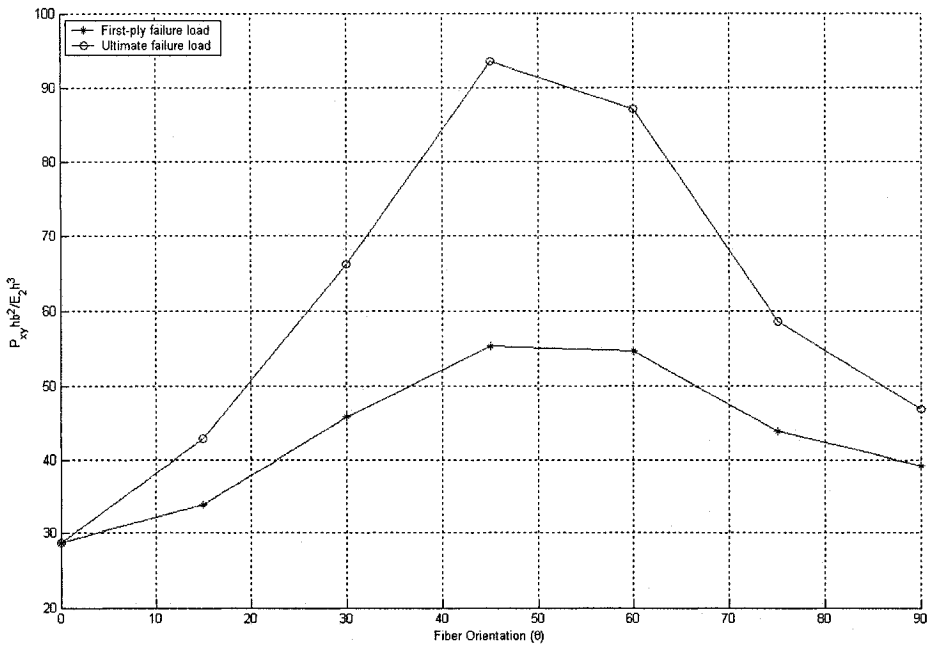

Figure 4.19 Variation of the first-ply and ultimate failure loads of the laminates with taper configuration B and with $(\pm\theta)_{4s}$ lay-up at the left end under in-plane positive shear

Figure 4.20 shows the variation of the first-ply failure load and the ultimate failure load for laminates with taper configuration C and with lay-up $(\pm\theta)_{4s}$ at the left (thick) end under the action of in-plane positive shear. The results show that the variations in response are un-symmetric about 45° fiber orientation. Peak values of the first-ply failure load and ultimate failure load are predicted to occur for 45° fiber orientation. For $(\pm 0)_{4s}$ and $(\pm 90)_{4s}$ laminates, the value of the first-ply failure load is equal to the value of the ultimate failure load. In the range $15° \leq \theta \leq 45°$ the difference between the ultimate failure load and the first-ply failure load becomes larger, and at $\theta = 45°$ the ultimate failure load is 51.33% higher than the first-ply failure load.

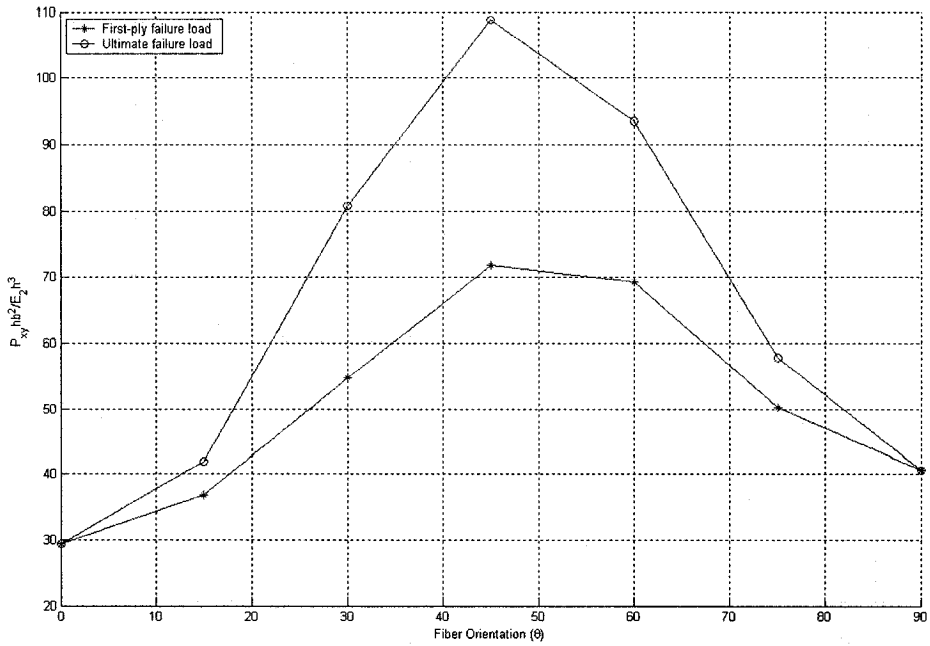

Figure 4.20 Variation of the first-ply and ultimate failure loads of the laminates with taper configuration C and with $(\pm\theta)_{4s}$ lay-up at the left end under in-plane positive shear

Figure 4.21 shows the variation of the first-ply failure load and the ultimate failure load for laminates with taper configuration D and with lay-up $(\pm\theta)_{4s}$ at the left (thick) end under the action of in-plane positive shear. The results show that the variations in response are un-symmetric about 45° fiber orientation. Peak values of the first-ply failure load and ultimate failure load are predicted to occur for 60° fiber orientation. The value of the first-ply failure load is equal to the value of the ultimate failure load for all the fiber orientation angles except for 30° fiber orientation. At $\theta = 30^{\circ}$ the ultimate failure load is 8.62% higher than the first-ply failure load.

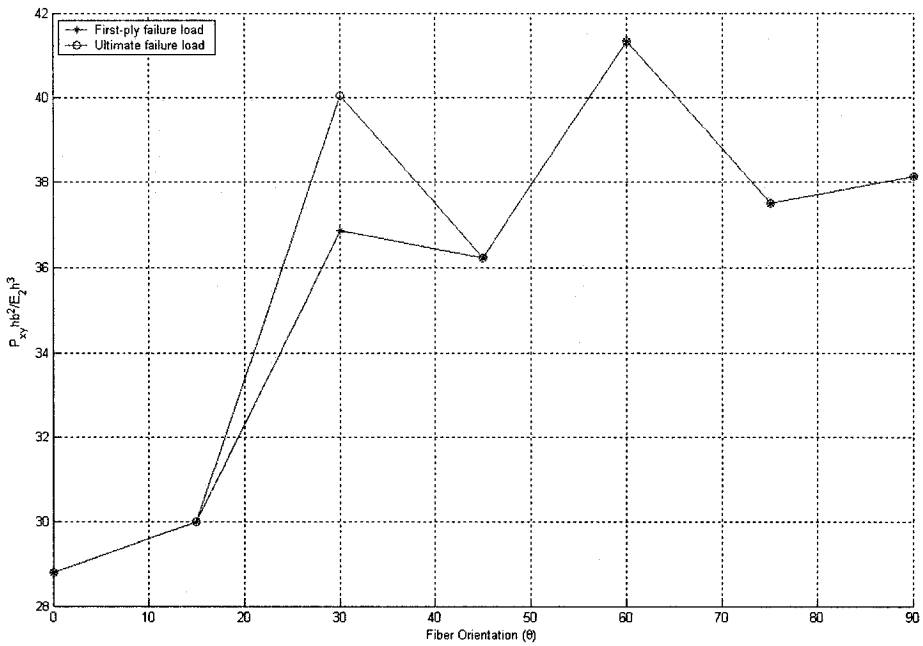

Figure 4.21 Variation of the first-ply and ultimate failure loads of the laminates with taper configuration D and with $(\pm\theta)_{4s}$ lay-up at the left end under in-plane positive shear

Figure 4.22 shows the variation of the first-ply failure load and the ultimate failure load for laminates with taper configuration F and with lay-up $(\pm\theta)_{4s}$ at the left (thick) end under the action of in-plane positive shear. The results show that the variations in response are un-symmetric about 45° fiber orientation. Peak values of the first-ply failure load and ultimate failure load occur for 45° fiber orientation. For $(\pm 0)_{4s}$ and $(\pm 90)_{4s}$ laminates, the value of the first-ply failure load is equal to the value of the ultimate failure load. In the range $15° \leq \theta \leq 45°$ the difference between the ultimate failure load and the first-ply failure load becomes larger, and at $\theta = 45°$ the ultimate failure load is 50.42% higher than the first-ply failure load.

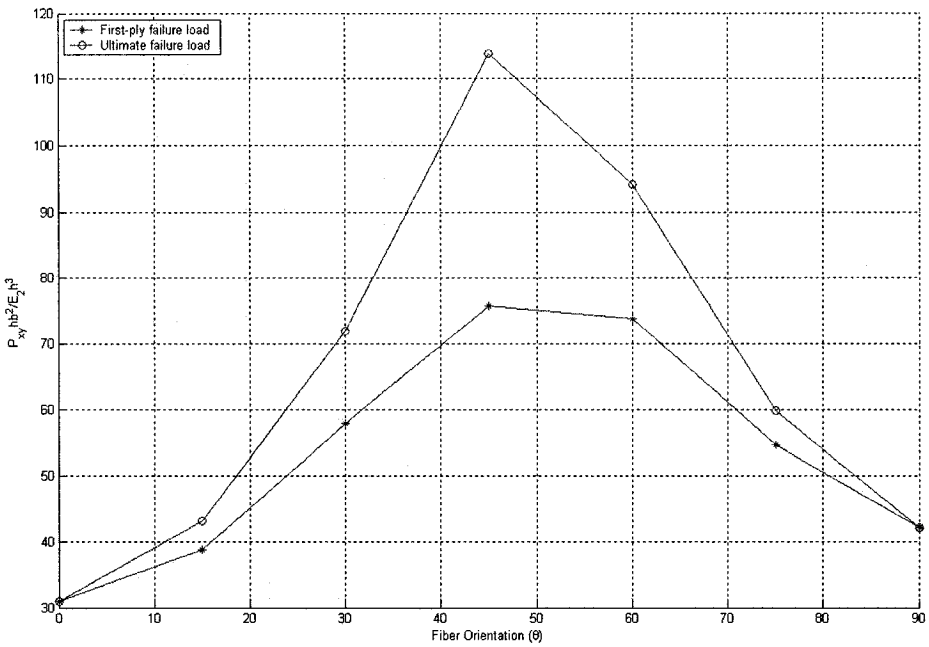

Figure 4.22 Variation of the first-ply and ultimate failure loads of the laminates with taper configuration F and with $(\pm\theta)_{4s}$ lay-up at the left end under in-plane positive shear

Figure 4.23 shows the variation of first-ply failure load of tapered laminates with $(\pm\theta)_{4s}$ lay-up at the left (thick) end under the action of in-plane positive shear for all the taper configurations. The results show that the variations are un-symmetric about 45° fiber orientation. Peak values of the first-ply failure loads for taper configurations A, B, C, and F are observed at 45° fiber orientation, and for taper configuration D the peak value occurs for 60° fiber orientation. The taper configuration F has the highest value of first-ply failure load, and the lowest value of first-ply failure load occurs for configuration A at 0° and 90° fiber orientations, and for configuration D at 15°, 30°, 45°, 60° and 75° fiber orientations.

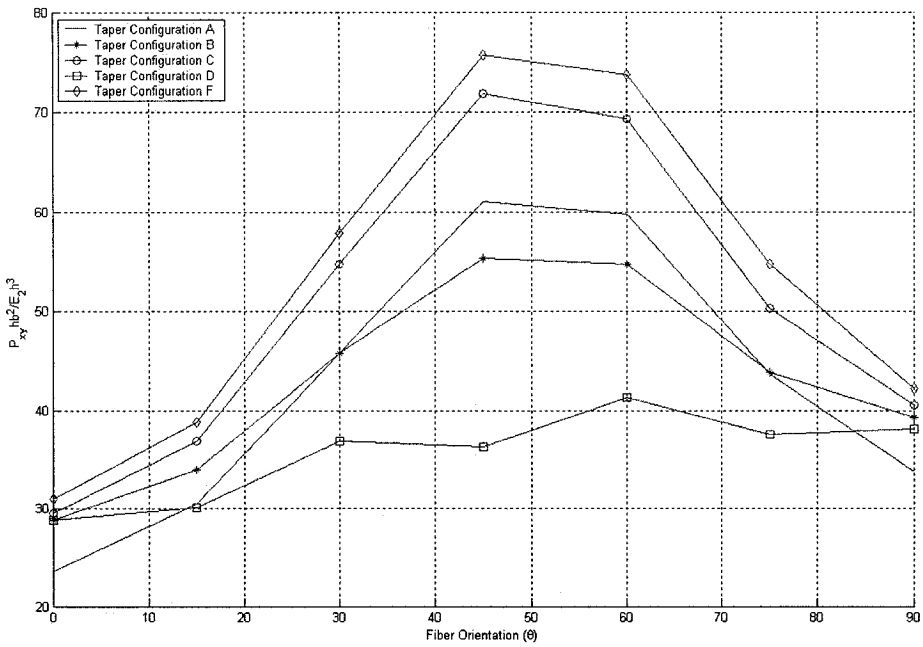

Figure 4.23 First-ply failure load of the laminates with $(\pm\theta)_{4s}$ lay-up at the left (thick) end under in-plane positive shear

Figure 4.24 shows the variation of ultimate failure load of tapered laminates with $(\pm\theta)_{4s}$ lay-up at the left (thick) end under the action of in-plane positive shear for all the taper configurations. The results show that the variations are un-symmetric about 45° fiber orientation. Peak values of the ultimate failure loads for taper configurations A, B, C, and F correspond to 45° fiber orientation, and for taper configuration D the peak value occurs for 60° fiber orientation. The lowest value of first-ply failure load occurs for configuration A at 0° and 90° fiber orientations, and for configuration D at 15°, 30°, 45°, 60° and 75° fiber orientations. The highest value of first-ply failure load occurs for configuration F at 0°, 15°, 45°, 60° and 75° fiber orientations, for configuration C at 30° fiber orientation, and for configuration B at 90° fiber orientation.

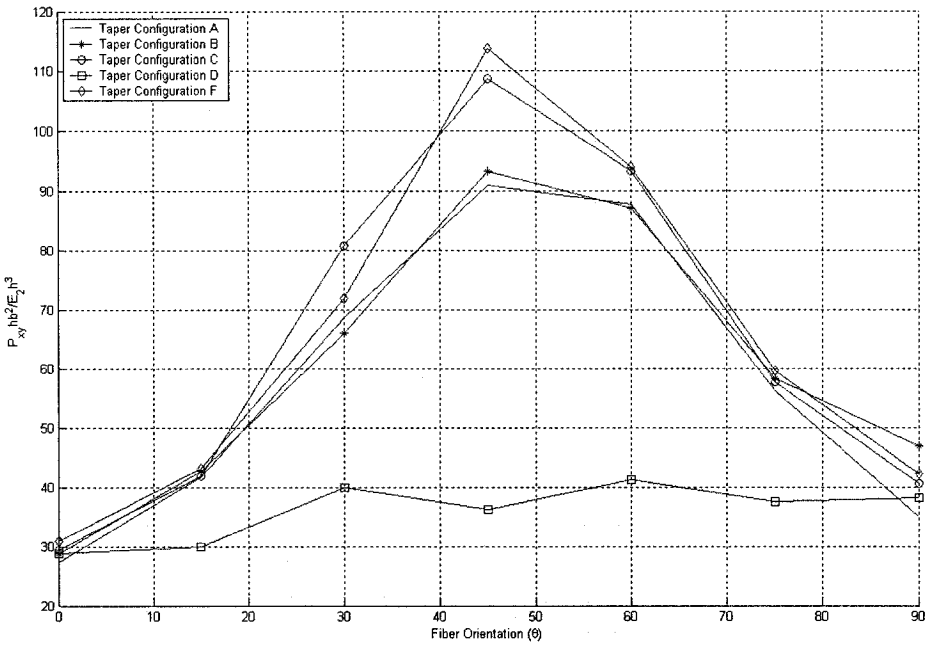

Figure 4.24 Ultimate failure load of the laminates with $(\pm\theta)_{4s}$ lay-up at the left (thick) end under in-plane positive shear

4.2.4 Influence of Uniform-thickness Sections

As in the cases considered in sub-section 3.3.4 of Chapter 3, a thick section and a thin section of uniform-thickness laminate are added to the tapered laminate to study their influence on the progressive failure. Taper configuration B is considered for the tapered section of the plate that has $(\pm 45/0/90)_{2s}$ lay-up at the left end. The length of the plate is 0.4185 m. The length of the taper section, L_2, is 0.279 m. The sum of the lengths of thick and thin uniform-thickness sections, L_1+L_3, is 0.1395 m. The width of the plate is 0.279 m. The length of the thick section (L_1) and the length of the thin section (L_3) will be varied according to the length ratio, i.e. the ratio of the length of thick section (L_1) to the length of thin section (L_3). Figure 3.32 shows the plate with the length ratio that is equal to 1. The boundary condition shown in Figure 3.6 is considered.

Figure 4.25 shows the load versus maximum deflection curves of five tapered plates under the action of in-plane positive shear. Table 4.12 gives the buckling load, the first-ply failure load and the ultimate failure load for these laminates under the action of in-plane positive shear. The laminate with length ratio 2:1 is the best choice among these five laminates with respect to both the buckling load and the first-ply failure load, and the laminate with length ratio 1:1 is the best choice with respect to the ultimate failure load. It is also observed that for all the cases the first-ply failure corresponds to the transverse (matrix) failure, and the ultimate failure corresponds to the delamination failure as in the case of the plate with only the tapered section. Therefore, it is noted that the addition of uniform-thickness sections did not change the modes of failure. However, considerably more resistance to buckling, first-ply failure and ultimate failure is provided by the addition of uniform-thickness sections.

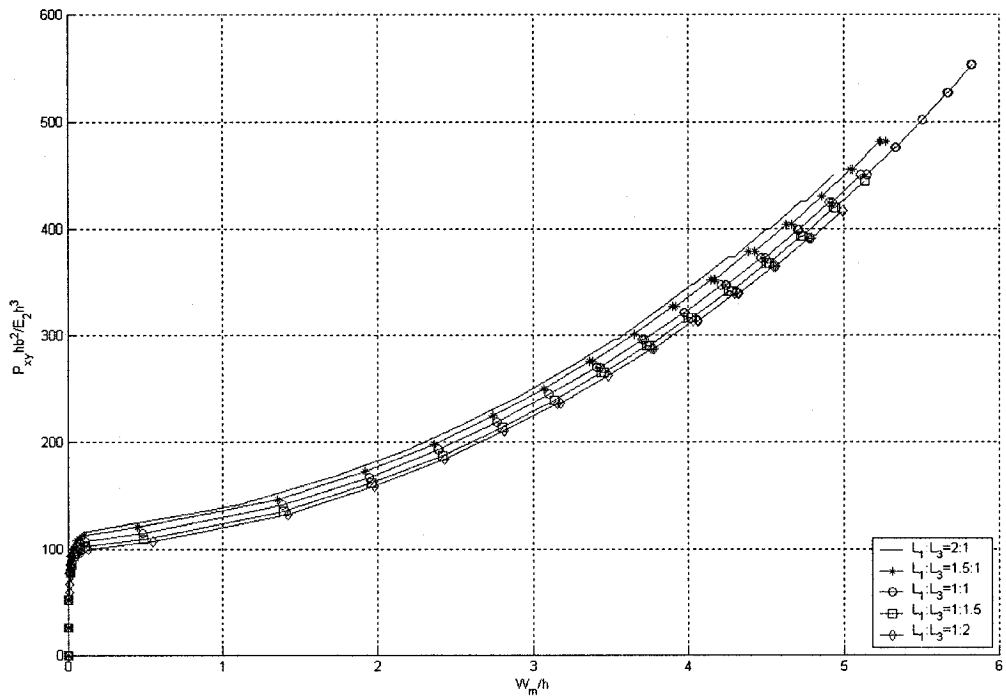

Figure 4.25 Load versus the maximum deflection curves of five tapered plates with different length ratios under the action of in-plane positive shear

Table 4.12 Failure data of five tapered plates with different length ratios under the action of in-plane positive shear

L_1:L_3	Buckling Load ($P_{xy}hb^2/E_2h^3$)	First-ply failure load ($P_{xy}hb^2/E_2h^3$)	Ultimate failure load ($P_{xy}hb^2/E_2h^3$)	$(W_m/h)^*$	Failure location (FL,FE) ♣	First-ply failure mode	Ultimate failure mode
2:1	128.736	296.085	450.570	3.520	1,1	T♠	D#
1.5:1	116.634	274.980	480.960	3.363	1,1	T	D
1:1	111.228	269.565	552.780	3.406	1,1	T	D
1:1.5	105.821	264.165	444.390	3.438	1,1	T	D
1:2	103.247	235.845	416.070	3.155	1,1	T	D

4.2.5 Influence of Boundary Condition

Except that the loading is in-plane positive shear, the study cases are the same as those given in sub-section 3.3.5 of Chapter 3. The influence of boundary condition on the progressive failure is studied. The results are compared in Figure 4.26 and Table 4.13.

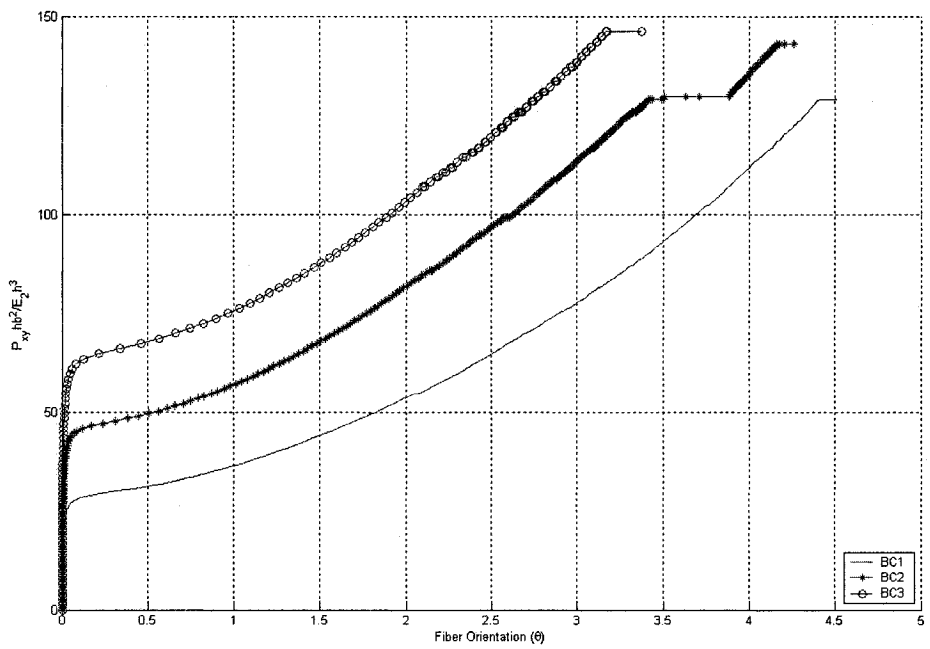

Figure 4.26 Load versus maximum deflection curves of the tapered laminate with taper configuration B corresponding to three boundary conditions under in-plane positive shear

Table 4.13 Failure data of the tapered laminate with taper configuration B corresponding to three boundary conditions under in-plane positive shear

BC	Buckling Load ($P_{xy}hb^2/E_2h^3$)	First-ply failure load ($P_{xy}hb^2/E_2h^3$)	Ultimate failure load ($P_{xy}hb^2/E_2h^3$)	$(W_m/h)^*$	Failure location (FL,FE) ♣	First-ply failure mode	Ultimate failure mode
BC1	29.562	54.672	129.053	2.049	1,1	T♠	D#
BC2	47.363	85.823	143.039	2.134	1,1	T	D
BC3	65.480	106.802	146.211	2.097	16,9	T	D

From Figure 4.26 and Table 4.13, it is observed that the first-ply failure load corresponds to the transverse (matrix) failure, and the ultimate failure corresponds to the delamination failure for all the three boundary conditions. The first-ply failure load is found to be about 1.8 times the buckling load for BC1 and BC2 boundary conditions, and 1.6 times for BC3 boundary condition, whereas, the ultimate failure load is about 4.4 times the buckling load for BC1 boundary condition, 3.0 times the buckling load for BC2 boundary condition, and 2.2 times for BC3 boundary condition. The ultimate failure load is about 2.4 times the first-ply failure load for BC1 boundary condition, 1.7 times for BC2 boundary condition, and 1.4 times for BC3 boundary condition. The absolute maximum value of the maximum transverse displacement W_m just before ultimate failure is found to occur in the case of boundary condition BC1 and is equal to 4.41h. The absolute minimum value of the maximum transverse displacement W_m just before the ultimate failure is found to occur in the case of boundary condition BC3 and is equal to 3.16h. It is also noted that the higher the flexural rigidity is, higher are the buckling load and the strength for a fixed value of maximum transverse displacement.

4.3 Parametric Study on In-plane Negative Shear

4.3.1 Influence of Taper Configuration

Figure 4.27 shows the load versus the maximum deflection curves of the five laminates all with LC(1) lay-up configuration and each with a different taper configuration under the action of in-plane negative shear. Table 4.14 gives the buckling load, the first-ply failure load and the ultimate failure load for these laminates.

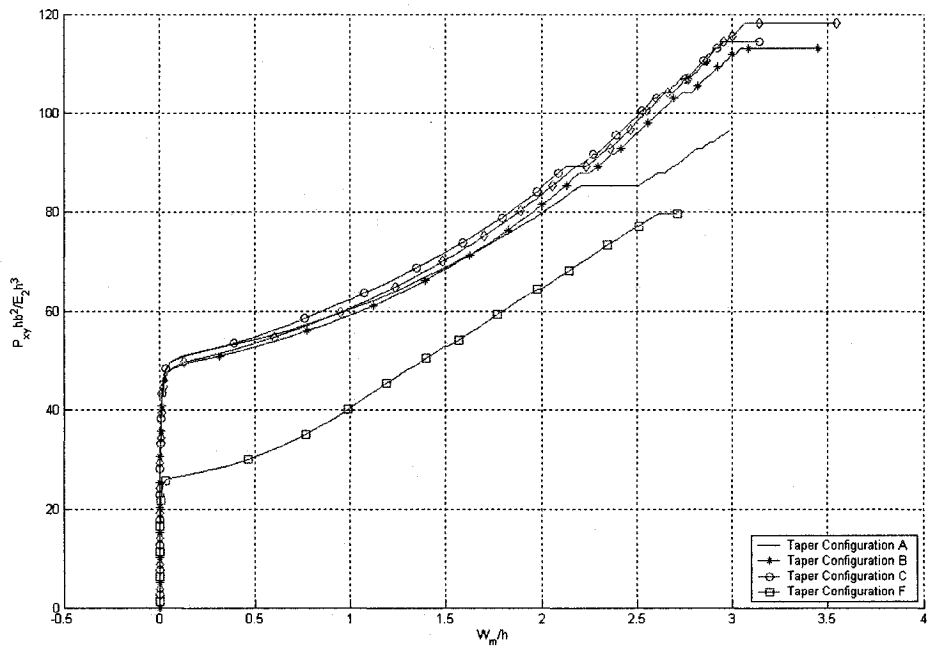

Figure 4.27 Load versus the maximum deflection curves of the laminates with LC(1) lay-up configuration for five taper configurations under in-plane negative shear

Table 4.14 Failure data of the laminates with LC(1) lay-up configuration for five taper configurations under in-plane negative shear

Taper	Buckling Load ($P_{xy}hb^2/E_2h^3$)	First-ply failure load ($P_{xy}hb^2/E_2h^3$)	Ultimate failure load ($P_{xy}hb^2/E_2h^3$)	$(W_m/h)^*$	Failure location (FL,FE) ♣	First-ply failure mode	Ultimate failure mode
A	52.766	55.944	96.630	0.674	1,1	T♠	D#
B	50.223	85.188	113.160	2.128	1,8	T	D
C	51.494	83.916	114.431	1.978	1,1	T	D
D	26.171	52.893	79.565	1.497	1,8	T	D
F	50.223	89.003	118.245	2.176	1,8	T	D

For lay-up configuration LC(1), the first-ply failure load is found to be about 1.1 times the buckling load for taper configurations A and D, 1.7 times for configurations B, 1.6 times for configuration C, and 1.8 times for configuration F. The ultimate failure load is about 1.8 times the buckling load for configuration A, 2.3 times for configuration B, 2.2 times for configuration C, 1.7 times for configuration D, and 2.4 times for configuration F. The ultimate failure load is about 1.7 times the first-ply failure load for configuration A, 1.3 times for configurations B and F, 1.4 times for configuration C, and 1.5 times for configuration D.

Figure 4.28 shows the pre-buckling load deflection path of the laminates with LC(1) lay-up configuration for five taper configurations under in-plane negative shear. It can be observed that at the beginning the maximum deflections for taper configurations A, B, C and F are negative. When the non-dimensional loadings reach certain values, they change to positive.

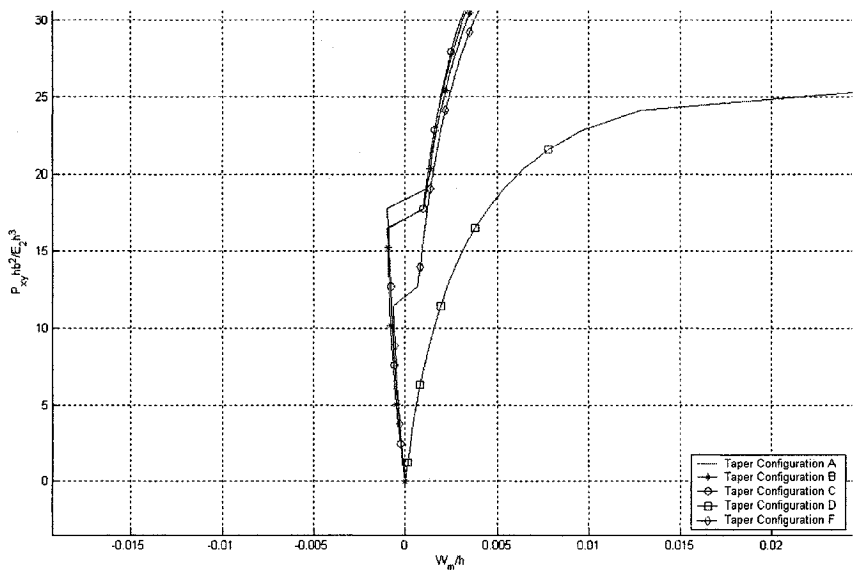

Figure 4.28 The pre-buckling load deflection path of the laminates with LC(1) lay-up configuration for five taper configurations under in-plane negative shear

Figure 4.29 shows the load versus the maximum deflection curves of the five laminates all with LC(2) lay-up configuration and each with a different taper configuration under the action of in-plane negative shear. Table 4.15 gives the buckling load, the first-ply failure load and the ultimate failure load for these laminates.

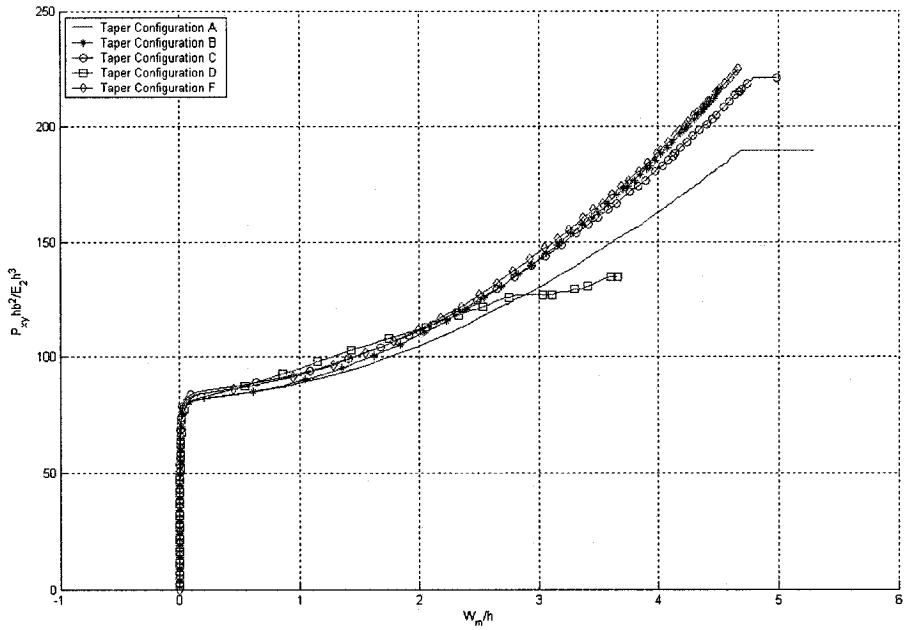

Figure 4.29 Load versus maximum deflection curves of the laminates with LC(2) lay-up configuration for five taper configurations under in-plane negative shear

Table 4.15 Failure data of the laminates with LC(2) lay-up configuration for five taper configurations under in-plane negative shear

Taper	Buckling Load ($P_{xy}hb^2/E_2h^3$)	First-ply failure load ($P_{xy}hb^2/E_2h^3$)	Ultimate failure load ($P_{xy}hb^2/E_2h^3$)	$(W_m/h)^*$	Failure location (FL,FE) ♣	First-ply failure mode	Ultimate failure mode
A	83.280	110.616	189.450	2.256	1,1	T♠	D#
B	83.295	138.588	216.150	2.889	1,8	T	D
C	87.095	142.403	221.235	3.008	1,8	T	D
D	83.280	120.788	134.774	2.456	10,8	T	D
F	85.824	147.489	225.045	3.050	1,8	T	D

For lay-up configuration LC(2), the first-ply failure load is found to be about 1.3 times the buckling load for taper configuration A, 1.7 times for configurations B and F, 1.6

times for configuration C, and 1.5 times for configuration D. The ultimate failure load is about 2.3 times the buckling load for configuration A, 2.6 times for configurations B and F, 2.5 times for configuration C, and 1.6 times for configuration D. The ultimate failure load is about 1.7 times the first-ply failure load for configuration A, 1.6 times for configurations B and C, 1.1 times for configuration D, and 1.5 times for configuration F.

Figure 4.30 shows the pre-buckling load deflection path of the laminates with LC(2) lay-up configuration for five taper configurations under in-plane negative shear. It can be observed that at the beginning the maximum deflections for all taper configurations are negative. When the non-dimensional loadings reach certain values, they change to positive.

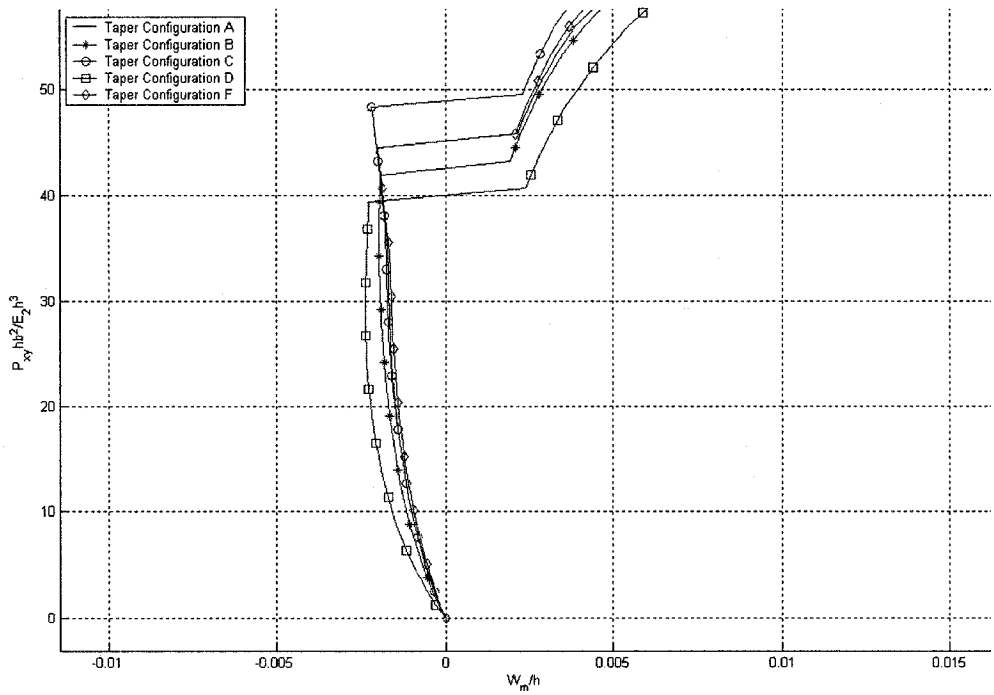

Figure 4.30 The pre-buckling load deflection path of the laminates with LC(1) lay-up configuration for five taper configurations under in-plane negative shear

In order to illustrate the positive maximum deflection of the plate under in-plane negative shear, a typical deformed configuration is given. Figure 4.31 shows the deformed configuration of the laminate with LC(2) lay-up configuration and with taper configuration B under in-plane negative shear. It is observed that the maximum deflection is positive (upward), but the deflections of the entire laminate are not all positive. The deformed configuration has a large peak which is positive (upward), and a small peak which is negative (downward).

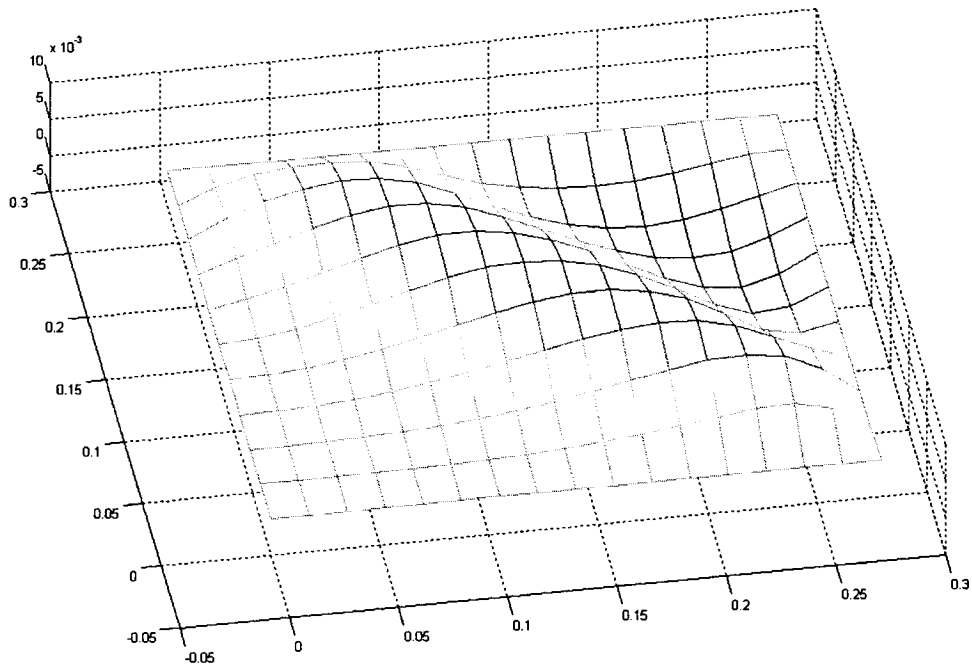

Figure 4.31 The deformed configuration of the laminate with LC(2) lay-up configuration and with taper configuration B under in-plane negative shear

Figure 4.32 shows the load versus the maximum deflection curves of the five laminates all with LC(3) lay-up configuration and each with a different taper configuration under the action of in-plane negative shear. Table 4.16 gives the buckling load, the first-ply failure load and the ultimate failure load for these laminates.

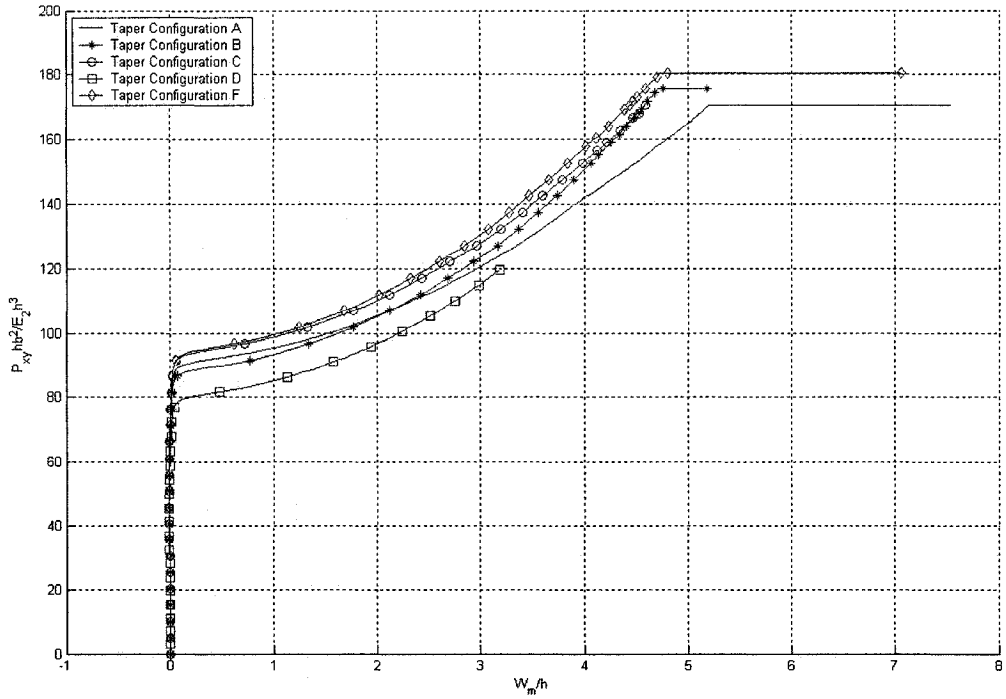

Figure 4.32 Load versus maximum deflection curves of the laminates with LC(3) lay-up configuration for five taper configurations under in-plane negative shear

Table 4.16 Failure data of the laminates with LC(3) lay-up configuration for five taper configurations under in-plane negative shear

Taper	Buckling Load ($P_{xy}hb^2/E_2h^3$)	First-ply failure load ($P_{xy}hb^2/E_2h^3$)	Ultimate failure load ($P_{xy}hb^2/E_2h^3$)	$(W_m/h)^*$	Failure location (FL,FE) ♣	First-ply failure mode	Ultimate failure mode
A	92.181	139.860	170.370	3.908	1,40	T♠	D#
B	89.639	152.580	175.455	4.060	1,8	T	D
C	94.724	156.390	170.370	4.114	1,8	T	D
D	81.055	95.688	119.720	1.934	1,40	T	D
F	95.996	158.925	180.540	4.056	10,8	T	D

For lay-up configuration LC(3), the first-ply failure load is found to be about 1.5 times the buckling load for taper configuration A, 1.7 times for configurations B, C and F, and 1.3 times for configuration F. The ultimate failure load is about 1.8 times the buckling load for configurations A and C, 2.0 times for configuration B, 1.3 times for configuration D, and 1.9 times for configuration F. The ultimate failure load is about 1.2

times the first-ply failure load for configuration A, 1.1 times for configuration B, C and F, and 1.0 time for configuration D.

Figure 4.33 shows the pre-buckling load deflection path of the laminates with LC(3) lay-up configuration for five taper configurations under in-plane negative shear. It can be observed that at the beginning the maximum deflections for all taper configurations are negative. When the non-dimensional loadings reach certain values, they changes to positive.

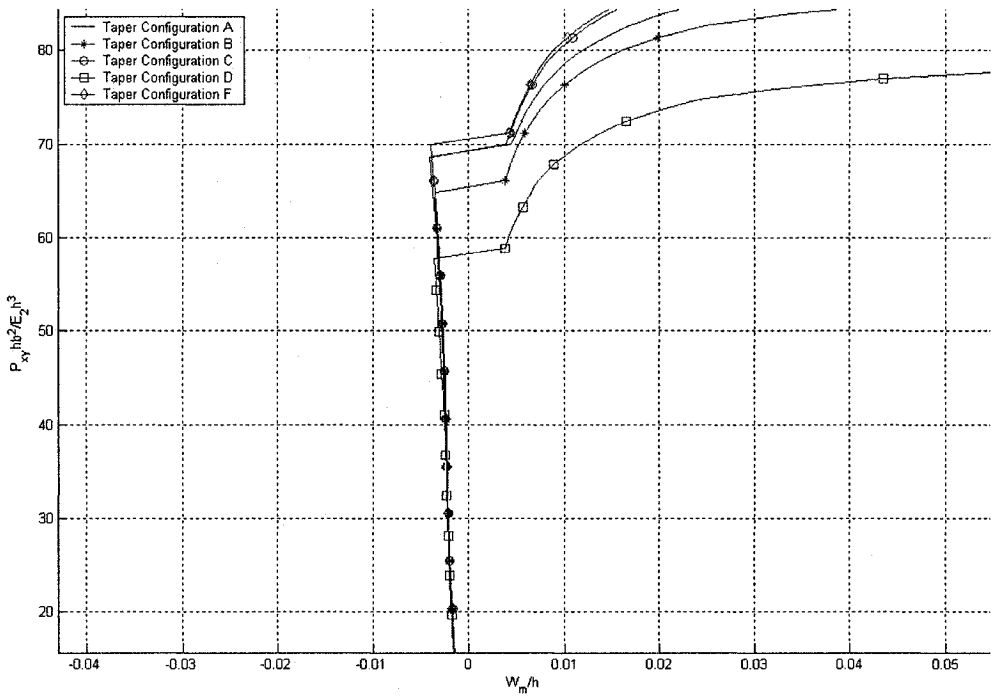

Figure 4.33 The pre-buckling load deflection path of the laminates with LC(3) lay-up configuration for five taper configurations under in-plane negative shear

Figure 4.34 shows the load versus the maximum deflection curves of the five laminates all with LC(4) lay-up configuration and each with a different taper configuration under the action of in-plane negative shear. Table 4.17 gives the buckling load, the first-ply failure load and the ultimate failure load for these laminates.

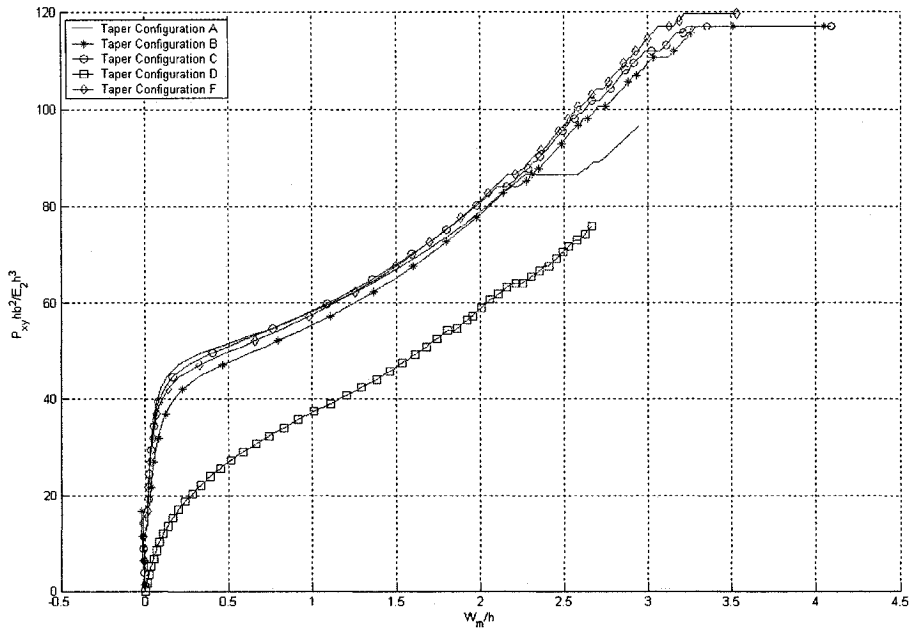

Figure 4.34 Load versus maximum deflection curves of the laminates with LC(4) lay-up configuration for five taper configurations under in-plane negative shear

Table 4.17 Failure data of the laminates with LC(4) lay-up configuration for five taper configurations under in-plane negative shear

Taper	Buckling Load ($P_{xy}hb^2/E_2h^3$)	First-ply failure load ($P_{xy}hb^2/E_2h^3$)	Ultimate failure load ($P_{xy}hb^2/E_2h^3$)	$(W_m/h)^*$	Failure location (FL,FE) ♣	First-ply failure mode	Ultimate failure mode
A	52.766	55.944	96.630	0.856	1,1	T♠	D#
B	50.223	83.916	116.975	2.174	10,8	T	D
C	52.766	83.916	116.975	2.101	1,8	T	D
D	36.660	54.249	75.864	1.805	1,8	T	D
F	50.223	86.459	119.517	2.160	1,8	T	D

For lay-up configuration LC(4), the first-ply failure load is found to be about 1.1 times the buckling load for taper configuration A, 1.7 times for configurations B and F, 1.6 times for configuration C, and 1.5 times for configuration D. The ultimate failure load is about 1.8 times the buckling load for configuration A, 2.3 times for configuration B, 2.2 times for configuration C, 2.1 times for configuration D, and 2.4 times for configuration

F. The ultimate failure load is about 1.7 times the first-ply failure load for configuration A, and 1.4 times for configurations B, C, D and F.

Figure 4.35 shows the pre-buckling load deflection path of the laminates with LC(4) lay-up configuration for five taper configurations under in-plane negative shear. It can be observed that at the beginning the maximum deflections for taper configurations A, B, C and F are negative. When the non-dimensional loadings reach certain values, they change to positive.

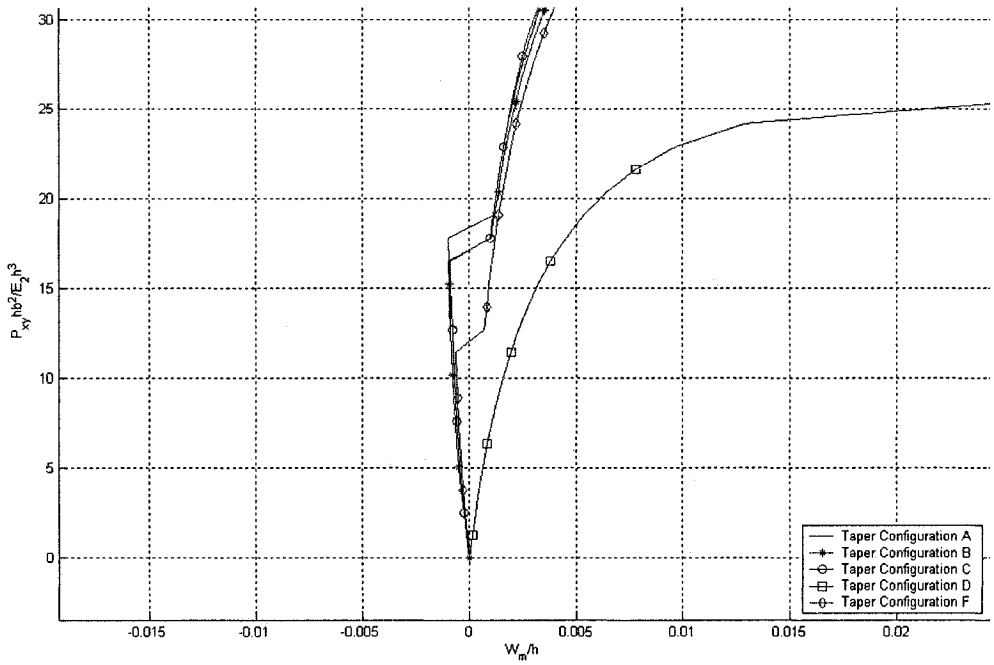

Figure 4.35 The pre-buckling load deflection path of the laminates with LC(4) lay-up configuration for five taper configurations under in-plane negative shear

Figure 4.36 shows the load versus the maximum deflection curves of the five laminates all with LC(5) lay-up configuration and each with a different taper configuration under the action of in-plane negative shear. Table 4.18 gives the buckling load, the first-ply failure load and the ultimate failure load for these laminates.

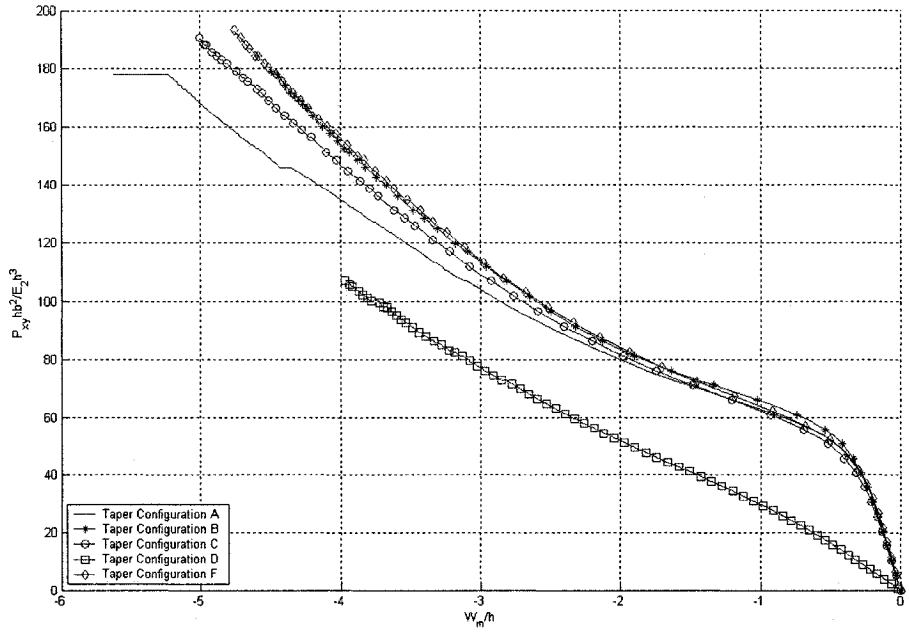

Figure 4.36 Load versus maximum deflection curves of the laminates with LC(5) lay-up configuration for five taper configurations under in-plane negative shear

Table 4.18 Failure data of the laminates with LC(5) lay-up configuration for five taper configurations under in-plane negative shear

Taper	Buckling Load ($P_{xy}hb^2/E_2h^3$)	First-ply failure load ($P_{xy}hb^2/E_2h^3$)	Ultimate failure load ($P_{xy}hb^2/E_2h^3$)	$(W_m/h)^*$	Failure location (FL,FE) ♣	First-ply failure mode	Ultimate failure mode
A	65.480	106.802	178.005	-3.102	10,40	T♠	D#
B	68.024	116.975	179.280	-3.096	1,8	T	D
C	68.024	119.517	190.725	-3.293	10,8	T	D
D	35.390	72.897	106.802	-2.820	10,8	T	D
F	69.294	124.602	193.260	-3.272	10,8	T	D

For lay-up configuration LC(5), the first-ply failure load is found to be about 1.6 times the buckling load for taper configuration A, 1.7 times for configuration B, 1.8 times for configuration C and F, and 2.1 times for configuration D. The ultimate failure load is about 2.7 times the buckling load for configuration A, 2.6 times for configuration B, 2.8 times for configurations C and F, and 3.0 times for configuration D. The ultimate failure

load is about 1.7 times the first-ply failure load for configurations A, 1.5 times for configurations B and D, and 1.6 times for configurations C and F.

In order to illustrate the negative maximum deflection of the plate under in-plane negative shear, a typical deformed configuration is given. Figure 4.37 shows the deformed configuration of the laminate with LC(5) lay-up configuration and with taper configuration B under in-plane negative shear. It is observed that the maximum deflection is negative (downward), but the deflections of the entire laminate are not all negative. The deformed configuration has a large peak which is negative (downward), and a small peak which is positive (upward).

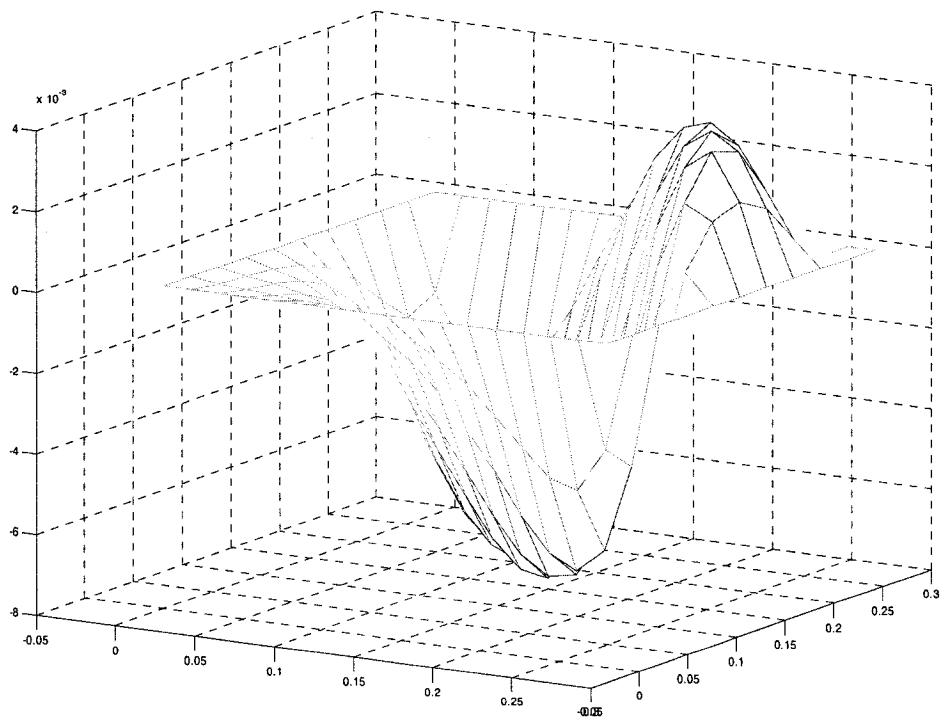

Figure 4.37 The deformed configuration of the laminate with LC(5) lay-up configuration and with taper configuration B under in-plane negative shear

Figure 4.38 shows the load versus the maximum deflection curves of the five laminates all with LC(6) lay-up configuration and each with a different taper configuration under the action of in-plane negative shear. Table 4.19 gives the buckling load, the first-ply failure load and the ultimate failure load for these laminates.

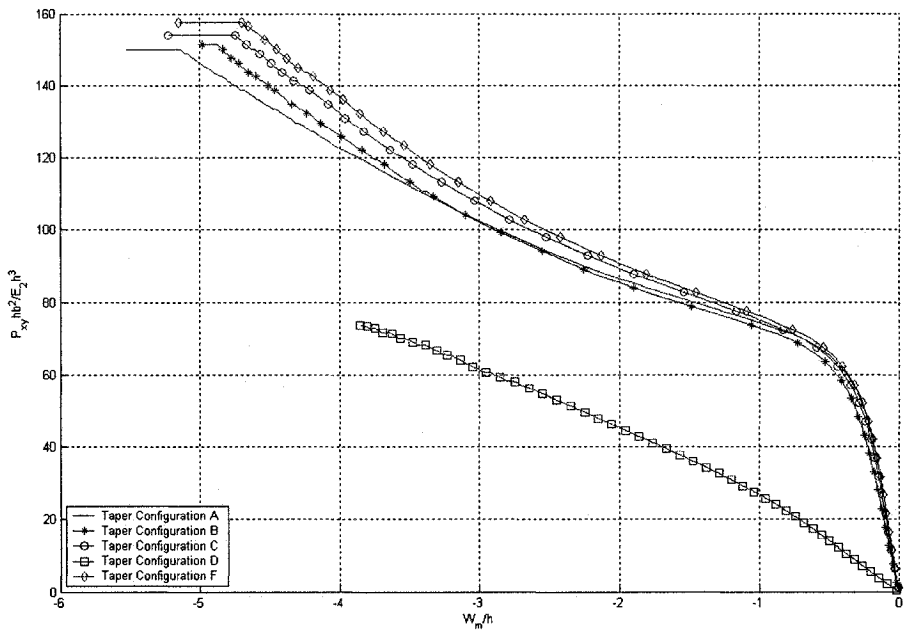

Figure 4.38 Load versus maximum deflection curves of the laminates with LC(6) lay-up configuration for five taper configurations under in-plane negative shear

Table 4.19 Failure data of the laminates with LC(6) lay-up configuration for five taper configurations under in-plane negative shear

Taper	Buckling Load ($P_{xy}hb^2/E_2h^3$)	First-ply failure load ($P_{xy}hb^2/E_2h^3$)	Ultimate failure load ($P_{xy}hb^2/E_2h^3$)	$(W_m/h)^*$	Failure location (FL,FE) ♣	First-ply failure mode	Ultimate failure mode
A	79.466	119.517	150.030	-3.834	10,8	T♠	D#
B	78.195	110.616	151.305	-3.379	10,8	T	D
C	80.738	120.788	153.840	-3.575	10,8	T	D
D	51.071	58.487	73.745	-2.765	10,8	T	D
F	80.738	124.602	157.665	-3.583	10,8	T	D

For lay-up configuration LC(6), the first-ply failure load is found to be about 1.5 times the buckling load for taper configurations A, C and F, 1.4 times for configuration B, and

1.1 times for configuration D. The ultimate failure load is about 1.9 times the buckling load for configurations A, B and C, 1.4 times for configuration D, and 2.0 times for configuration F. The ultimate failure load is about 1.3 times the first-ply failure load for configurations A, C D and F, and 1.4 times for configuration B.

Summary

From Figures 4.27 – 4.38 and Tables 4.14 – 4.19, the following general observations are also made.

1. For all the six lay-up configurations, the taper configuration F (Mid-plane taper) is the strongest one with respect to the first-ply failure load and the ultimate failure load. However, taper configuration F is not easy to manufacture compared to other taper configurations. Considering this, the next strongest taper configuration is identified. For the lay-up configurations LC(2), LC(4), LC(5) and LC(6), the taper configuration C (Overlapping dropped plies) is the best choice among all taper configurations considering the first-ply failure load, the ultimate failure load and the buckling load. For the lay-up configuration LC(1), taper configuration A is the best choice in terms of the buckling load, taper configuration B is the best choice in terms of the first-ply failure load, and taper configuration C is the best choice in terms of the ultimate failure load. For the lay-up configuration LC(3), taper configuration C is the best choice in terms of the buckling load and the first-ply failure load, and taper configuration B is the best choice in terms of the ultimate failure load.
2. Only for the laminate with LC(3) lay-up configuration for the taper configuration D (Continuous plies interspersed), the first-ply failure load and the ultimate failure load

are the same. For all other cases, considerable residual strength exists after the first-ply failure until ultimate failure.

3. For lay-up configuration LC(1), locations corresponding to the first-ply failure lie near the thick end of the plate for configurations A and C, whereas, they lie near the thick end of the plate for all other cases.
4. For lay-up configurations LC(5) and LC(6), the maximum deflections are of the same sense and are negative (downward). For taper configuration D with lay-up configurations LC(1) and LC(4), the maximum deflections are of the same sense and are positive (upward). For the rest of the cases, they all change from negative (downward) to positive (upward).

4.3.2 Influence of Lay-up Configuration

Figure 4.39 shows the load versus maximum deflection curves of the six laminates all with taper configuration A and each with a different lay-up configuration under the action of in-plane negative shear. Table 4.20 gives the buckling load, the first-ply failure load and the ultimate failure load for these laminates.

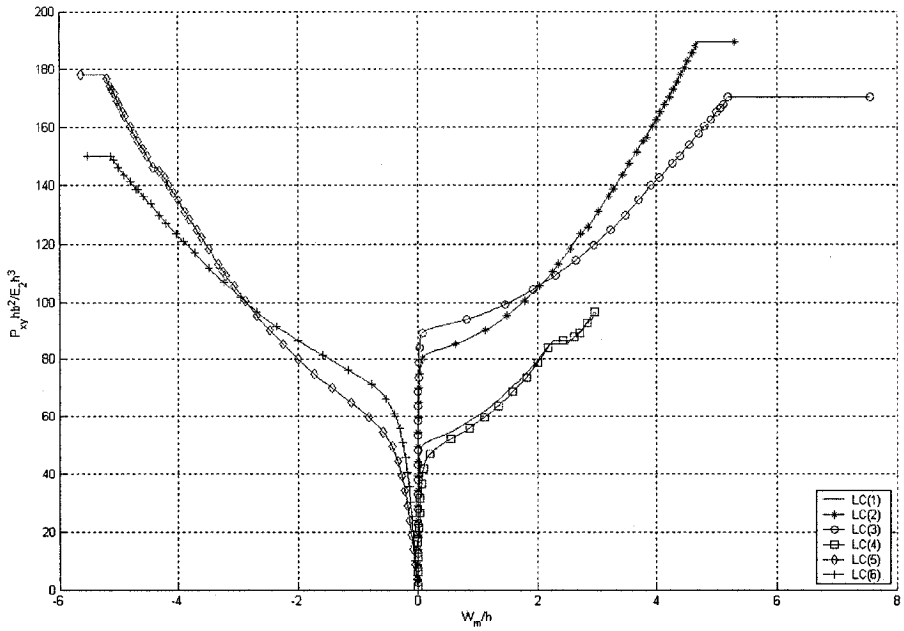

Figure 4.39 Load versus maximum deflection curves of the laminates with taper configuration A for all the six lay-up configurations under in-plane negative shear

Table 4.20 Failure data of the laminates the laminates with taper configuration A for all the six lay-up configurations under in-plane negative shear

Lay-up	Buckling Load ($P_{xy}hb^2/E_2h^3$)	First-ply failure load ($P_{xy}hb^2/E_2h^3$)	Ultimate failure load ($P_{xy}hb^2/E_2h^3$)	$(W_m/h)^*$	Failure location (FL,FE) ♣	First-ply failure mode	Ultimate failure mode
LC(1)	52.766	55.944	96.630	0.674	1,1	T♠	D#
LC(2)	83.280	110.616	189.450	2.256	1,1	T	D
LC(3)	92.181	139.860	170.370	3.908	1,40	T	D
LC(4)	52.766	55.944	96.630	0.856	1,1	T	D
LC(5)	65.480	106.802	178.005	-3.102	10,40	T	D
LC(6)	79.466	119.517	150.030	-3.834	10,8	T	D

For taper configuration A, the lay-up configuration LC(3) is the best choice among all the six lay-up configurations with respect to both the buckling load and the first-ply failure load, and lay-up configuration LC(2) is the best choice with respect to the ultimate failure load.

Figure 4.40 shows the load versus maximum deflection curves of the six laminates all with taper configuration B and each with a different lay-up configuration under the action

of in-plane negative shear. Table 4.21 gives the buckling load, the first-ply failure load and the ultimate failure load for these laminates.

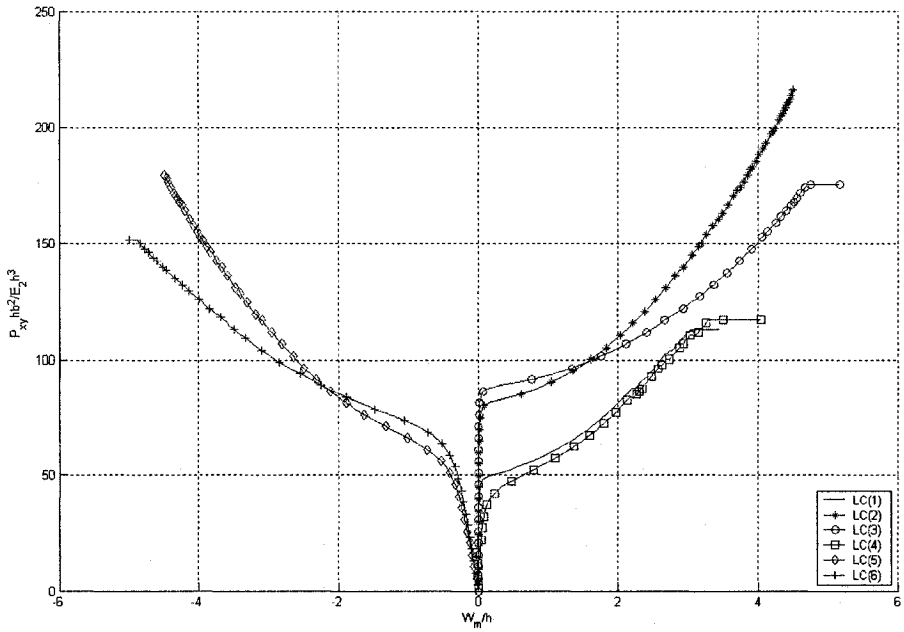

Figure 4.40 Load versus maximum deflection curves of the laminates with taper configuration B for all the six lay-up configurations under in-plane negative shear

Table 4.21 Failure data of the laminates with taper configuration B for all the six lay-up configurations under in-plane negative shear

Lay-up	Buckling Load ($P_{xy}hb^2/E_2h^3$)	First-ply failure load ($P_{xy}hb^2/E_2h^3$)	Ultimate failure load ($P_{xy}hb^2/E_2h^3$)	$(W_m/h)^*$	Failure location (FL,FE) ♣	First-ply failure mode	Ultimate failure mode
LC(1)	50.223	85.188	113.160	2.128	1,8	T♠	D#
LC(2)	83.295	138.588	216.150	2.889	1,8	T	D
LC(3)	89.639	152.580	175.455	4.060	1,8	T	D
LC(4)	50.223	83.916	116.975	2.174	10,8	T	D
LC(5)	68.024	116.975	179.280	-3.096	1,8	T	D
LC(6)	78.195	110.616	151.305	-3.379	10,8	T	D

For taper configuration B, the lay-up configuration LC(3) is the best choice among all the six lay-up configurations with respect to both the buckling load and the first-ply failure load, and lay-up configuration LC(2) is the best choice with respect to the ultimate failure load.

Figure 4.41 shows the load versus maximum deflection curves of the six laminates all with taper configuration C and each with a different lay-up configuration under the action of in-plane negative shear. Table 4.22 gives the buckling load, the first-ply failure load and the ultimate failure load for these laminates.

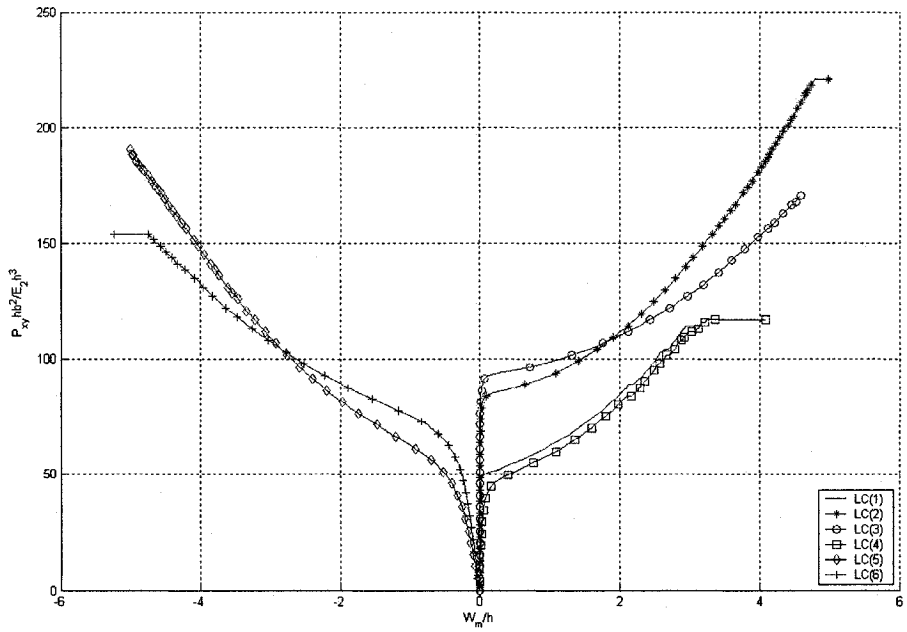

Figure 4.41 Load versus maximum deflection curves of the laminates with taper configuration C for all the six lay-up configurations under in-plane negative shear

Table 4.22 Failure data of the laminates with taper configuration C for all the six lay-up configurations under in-plane negative shear

Lay-up	Buckling Load ($P_{xy}hb^2/E_2h^3$)	First-ply failure load ($P_{xy}hb^2/E_2h^3$)	Ultimate failure load ($P_{xy}hb^2/E_2h^3$)	$(W_m/h)^*$	Failure location (FL,FE) ♣	First-ply failure mode	Ultimate failure mode
LC(1)	51.494	83.916	114.431	1.978	1,1	T♠	D#
LC(2)	87.095	142.403	221.235	3.008	1,8	T	D
LC(3)	94.724	156.390	170.370	4.114	1,8	T	D
LC(4)	52.766	83.916	116.975	2.101	1,8	T	D
LC(5)	68.024	119.517	190.725	-3.293	10,8	T	D
LC(6)	80.738	120.788	153.840	-3.575	10,8	T	D

For taper configuration C, the lay-up configuration LC(3) is the best choice among all the six lay-up configurations with respect to both the buckling load and the first-ply failure load, and lay-up configuration LC(2) is the best choice with respect to the ultimate failure load.

Figure 4.42 shows the load versus maximum deflection curves of the six laminates all with taper configuration D and each with a different lay-up configuration under the action of in-plane negative shear. Table 4.23 gives the buckling load, the first-ply failure load and the ultimate failure load for these laminates.

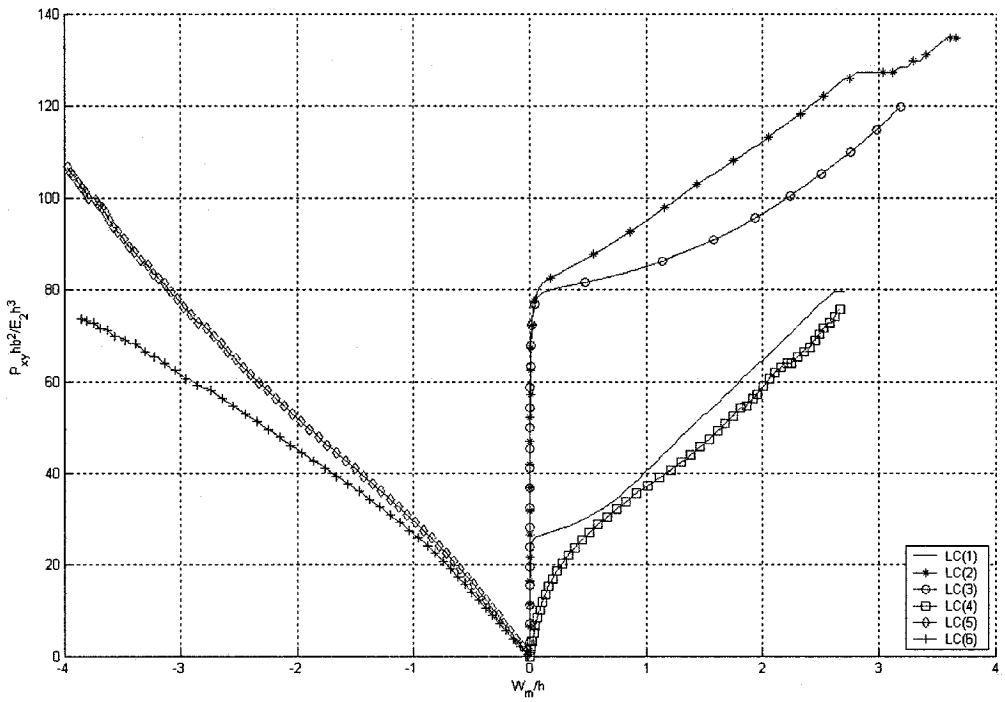

Figure 4.42 Load versus maximum deflection curves of the laminates with taper configuration D for all the six lay-up configurations under in-plane negative shear

Table 4.23 Failure data of the laminates with taper configuration D for all the six lay-up configurations under in-plane negative shear

Lay-up	Buckling Load ($P_{xy}hb^2/E_2h^3$)	First-ply failure load ($P_{xy}hb^2/E_2h^3$)	Ultimate failure load ($P_{xy}hb^2/E_2h^3$)	$(W_m/h)^*$	Failure location (FL,FE) ♣	First-ply failure mode	Ultimate failure mode
LC(1)	26.171	52.893	79.565	1.497	1,8	T♠	D#
LC(2)	83.280	120.788	134.774	2.456	10,8	T	D
LC(3)	81.055	95.688	119.720	1.934	1,40	T	D
LC(4)	36.660	54.249	75.864	1.805	1,8	T	D
LC(5)	35.390	72.897	106.802	-2.820	10,8	T	D
LC(6)	51.071	58.487	73.745	-2.765	10,8	T	D

For taper configuration D, the lay-up configuration LC(3) is the best choice among all the six lay-up configurations with respect to the buckling load, and the lay-up configuration LC(2) is the best choice with respect to both the first-ply failure load and the ultimate failure load.

Figure 4.43 shows the load versus maximum deflection curves of the six laminates all with taper configuration F and each with a different lay-up configuration under the action of in-plane negative shear. Table 3.24 gives the buckling load, the first-ply failure load and the ultimate failure load for these laminates.

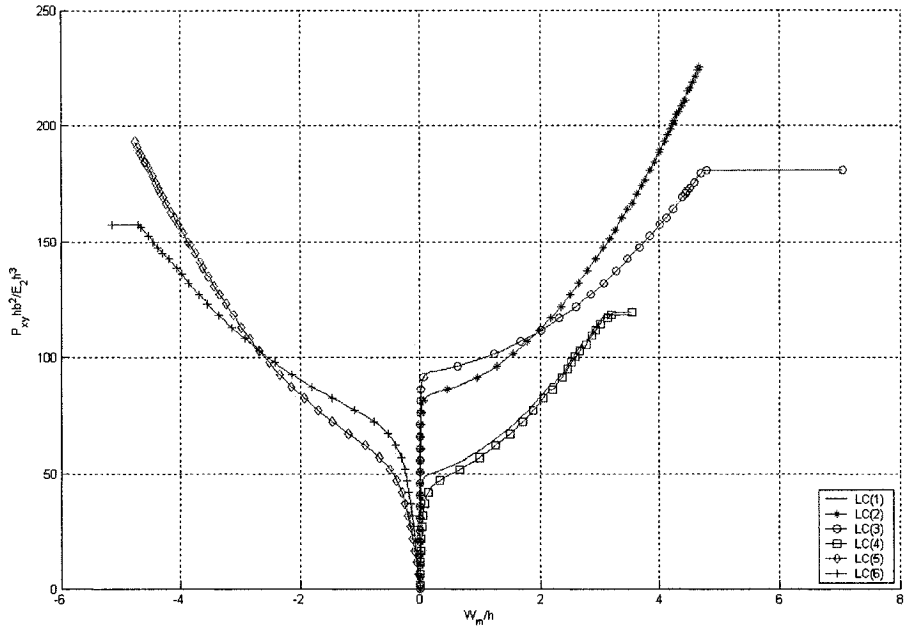

Figure 4.43 Load versus maximum deflection curves of the laminates with taper configuration F for all the six lay-up configurations under in-plane negative shear

Table 4.24 Failure data of the laminates with taper configuration F for all the six lay-up configurations under in-plane negative shear

Lay-up	Buckling Load ($P_{xy}hb^2/E_2h^3$)	First-ply failure load ($P_{xy}hb^2/E_2h^3$)	Ultimate failure load ($P_{xy}hb^2/E_2h^3$)	$(W_m/h)^*$	Failure location (FL,FE) ♣	First-ply failure mode	Ultimate failure mode
LC(1)	50.223	89.003	118.245	2.176	1,8	T♠	D#
LC(2)	85.824	147.489	225.045	3.050	1,8	T	D
LC(3)	95.996	158.925	180.540	4.056	10,8	T	D
LC(4)	50.223	86.459	119.517	2.160	1,8	T	D
LC(5)	69.294	124.602	193.260	-3.272	10,8	T	D
LC(6)	80.738	124.602	157.665	-3.583	10,8	T	D

For taper configuration F, the lay-up configuration LC(3) is the best choice among all the six lay-up configurations with respect to both the buckling load and the first-ply failure load, and lay-up configuration LC(2) is the best choice with respect to the ultimate failure load.

Summary

From Figures 4.39 – 4.43 and Tables 4.20 – 4.24, the following general observations are also made.

1 For all the five taper configurations, the first-ply failure mode for all the six lay-up configurations is transverse (matrix) failure.

2 For all the five taper configurations, the ultimate failure mode for all the six lay-up configurations is delamination.

3 Locations corresponding to the first-ply failure for all the six lay-up configurations lie at the outermost layer and near the loaded edges of the plate.

4 For the un-symmetric lay-up configurations LC(5) and LC(6), the maximum deflections are negative, that is, downward. But for other lay-up configurations including the un-symmetric lay-up configuration LC(4), the maximum deflections are positive, that is, upward.

5 Variation of the maximum deflection with the load for the symmetric lay-up configuration LC(1) basically coincides with that of the corresponding un-symmetric lay-up configuration LC(4). Therefore, in this case the symmetry in the stacking sequence does not have a strong influence on the progressive failure of the laminate. However, for taper configuration D, there exists a difference in early stages of progressive failure.

4.3.3 Influence of Fiber Orientation

Tapered laminates under the action of in-plane negative shear and with lay-up $(\pm\theta)_{4s}$ at the left end are considered. The lay-up at the right (thin) end is $(\pm\theta)_{2s}$ for taper configurations A, B, C and F, and is $(\theta)_8$ for taper configuration D. The variation of

buckling load with θ for each taper configuration is determined. The results are plotted in Figure 4.44. A non-monotonic variation is observed for all taper configurations from this figure. Also the variation is un-symmetric about 45° fiber orientation. Peak values of the buckling loads are predicted to occur for 45° fiber orientation for taper configurations A, B, C and F, to occur for 60° for taper configuration D. The highest value of buckling load occurs for configuration F at 0°, 15°, 45° and 90° fiber orientations, and for configuration D at 30°, 60° and 75° fiber orientations. The lowest value of first-ply failure load occurs for configuration A at 0° and 45°, for configuration A at 15° and 90° fiber orientations, and for configuration B at 30°, 60° and 75° fiber orientations.

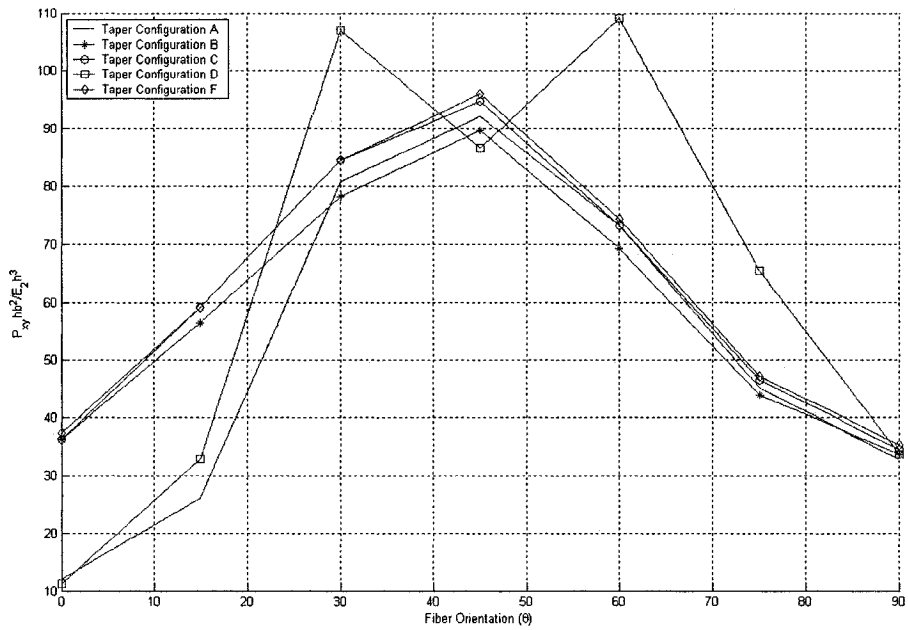

Figure 4.44 Buckling loads of the laminates with $(\pm\theta)_{4s}$ lay-up at the left (thick) end under in-plane negative shear

Figure 4.45 shows the variation of the first-ply failure load and the ultimate failure load for laminates with taper configuration A and with lay-up $(\pm\theta)_{4s}$ at the left (thick) end under the action of in-plane negative shear. The results show that the variations in

response are un-symmetric about 45° fiber orientation. Peak values of the first-ply failure load and ultimate failure load are predicted to occur for 45° fiber orientation. In the range $0° \leq \theta \leq 45°$ the difference between the ultimate failure load and the first-ply failure load becomes larger, and at θ = 45° the ultimate failure load is 21.81% higher than the first-ply failure load.

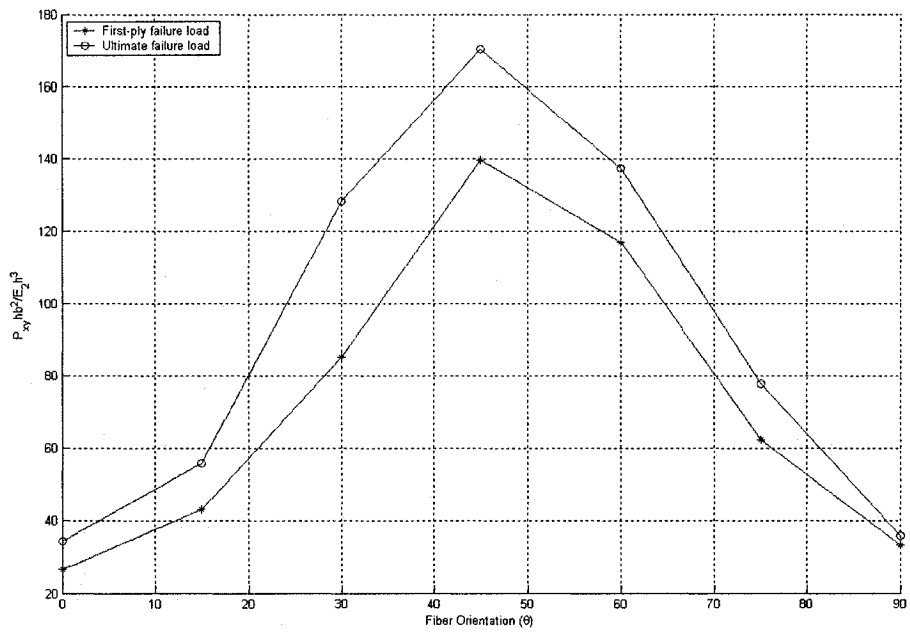

Figure 4.45 Variation of the first-ply and ultimate failure loads of the laminates with taper configuration A and with $(\pm\theta)_{4s}$ lay-up at the left end under in-plane negative shear

Figure 4.46 shows the variation of the first-ply failure load and the ultimate failure load for laminates with taper configuration B and with lay-up $(\pm\theta)_{4s}$ at the left (thick) end under the action of in-plane negative shear. The results show that the variations in response are un-symmetric about 45° fiber orientation. Peak values of the first-ply failure load and ultimate failure load are predicted to occur for 45° fiber orientation. For laminate with $(\pm 90)_{4s}$ lay-up configuration at the thick end, the value of the first-ply failure load is equal to the value of the ultimate failure load. In the range $0° \leq \theta \leq 45°$ the

difference between the ultimate failure load and the first-ply failure load becomes larger, and at $\theta = 45°$ the ultimate failure load is 14.997% higher than the first-ply failure load.

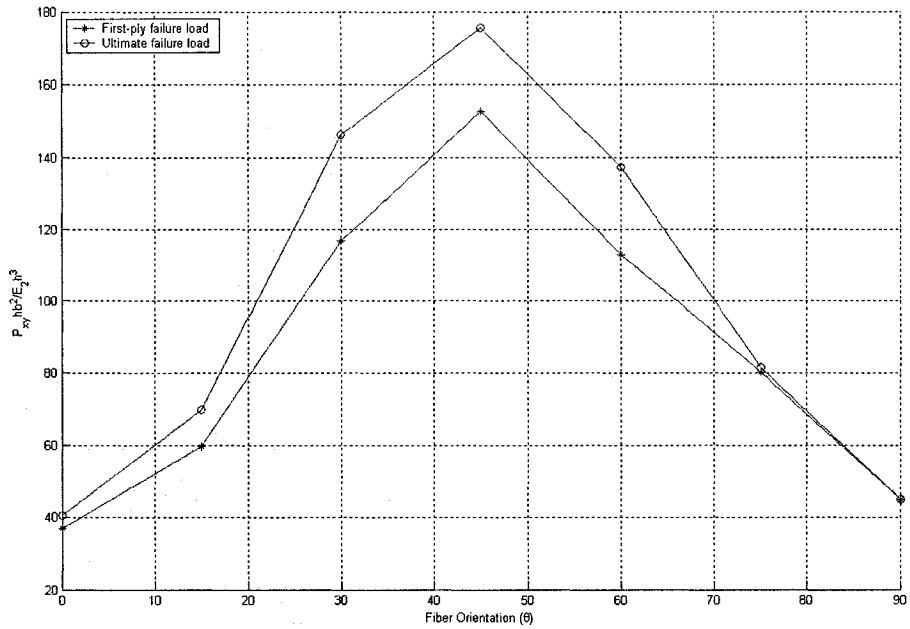

Figure 4.46 Variation of the first-ply and ultimate failure loads of the laminates with taper configuration B and with $(\pm\theta)_{4s}$ lay-up at the left end under in-plane negative shear

Figure 4.47 shows the variation of the first-ply failure load and the ultimate failure load for laminates with taper configuration C and with lay-up $(\pm\theta)_{4s}$ at the left (thick) end under the action of in-plane negative shear. The results show that the variations in response are un-symmetric about 45° fiber orientation. Peak values of the first-ply failure load and ultimate failure load are predicted to occur for 45° fiber orientation. For $(\pm 0)_{4s}$ and $(\pm 90)_{4s}$ laminates, the value of the first-ply failure load is equal to the value of the ultimate failure load. In the range $0° \leq \theta \leq 30°$ the difference between the ultimate failure load and the first-ply failure load becomes larger, and at $\theta = 30°$ the ultimate failure load is 30.10% higher than the first-ply failure load.

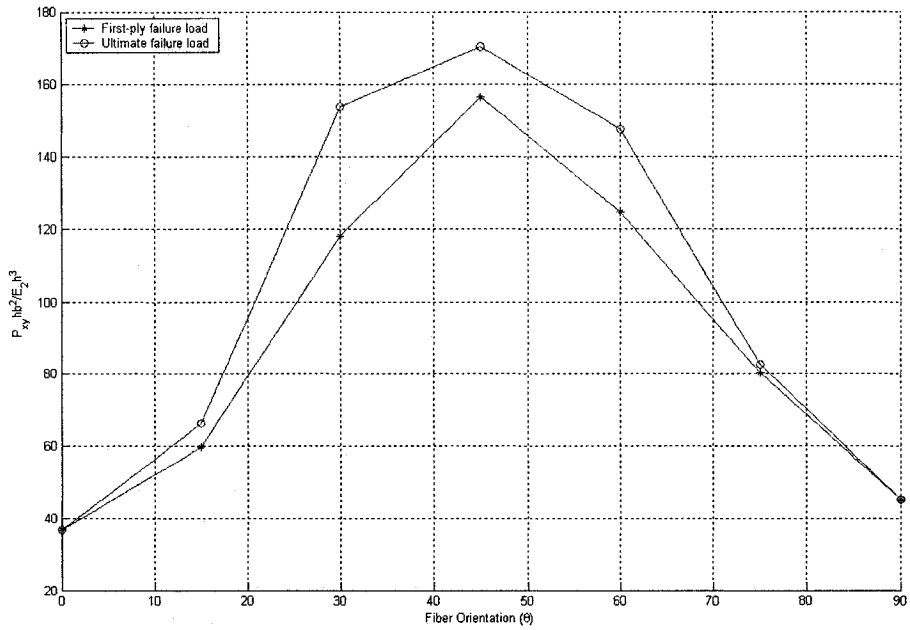

Figure 4.47 Variation of the first-ply and ultimate failure loads of the laminates with taper configuration C and with $(\pm\theta)_{4s}$ lay-up at the left end under in-plane negative shear

Figure 4.48 shows the variation of the first-ply failure load and the ultimate failure load for laminates with taper configuration D and with lay-up $(\pm\theta)_{4s}$ at the left (thick) end under the action of in-plane negative shear. The results show that the variations in response are un-symmetric about 45° fiber orientation. Peak values of the first-ply failure load and ultimate failure load are predicted to occur for 45° fiber orientation. The value of the first-ply failure load is equal to the value of the ultimate failure load for all the fiber orientation angles except for 0°, 30° and 75° fiber orientations. The maximum difference of ultimate failure load and first-ply failure load is found to occur in the case of 15° fiber orientation, and the ultimate failure load is 8.70% higher than the first-ply failure load.

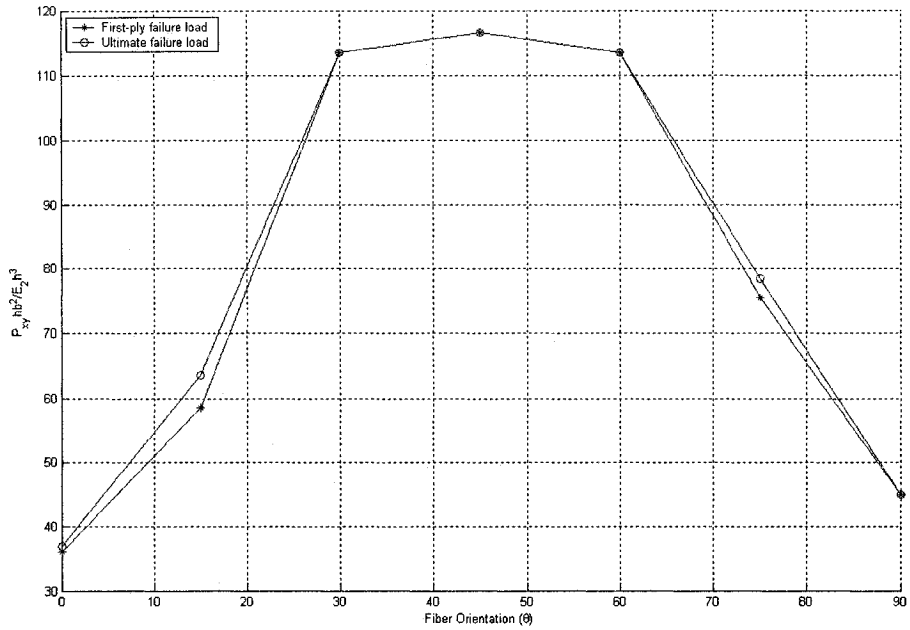

Figure 4.48 Variation of the first-ply and ultimate failure loads of the laminates with taper configuration D and with $(\pm\theta)_{4s}$ lay-up at the left end under in-plane negative shear

Figure 4.49 shows the variation of the first-ply failure load and the ultimate failure load for laminates with taper configuration F and with lay-up $(\pm\theta)_{4s}$ at the left (thick) end under the action of in-plane negative shear. The results show that the variations in response are un-symmetric about 45° fiber orientation. Peak values of the first-ply failure load and ultimate failure load occur for 45° fiber orientation. For $(\pm 0)_{4s}$ and $(\pm 90)_{4s}$ laminates, the value of the first-ply failure load is equal to the value of the ultimate failure load. In the range $0° \leq \theta \leq 30°$ the difference between the ultimate failure load and the first-ply failure load becomes larger, and at θ = 45° the ultimate failure load is 24.75% higher than the first-ply failure load.

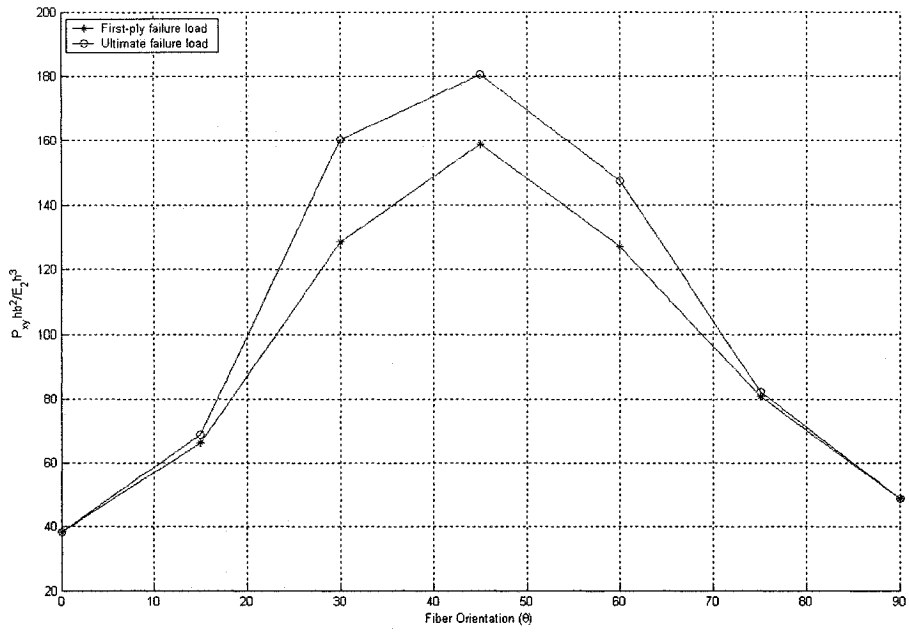

Figure 4.49 Variation of the first-ply and ultimate failure loads of the laminates with taper configuration F and with $(\pm\theta)_{4s}$ lay-up at the left end under in-plane negative shear

Figure 4.50 shows the variation of first-ply failure load of tapered laminates with $(\pm\theta)_{4s}$ lay-up at the left (thick) end under the action of in-plane negative shear for all the taper configurations. The results show that the variations are un-symmetric about 45° fiber orientation. Peak values of the first-ply failure loads for all taper configurations are observed at 45° fiber orientation. The taper configuration F has the highest value of first-ply failure load, and the lowest value of first-ply failure load occurs for configuration A at 0°, 15°, 30°, 75° and 90° fiber orientations, for configuration D at 45° fiber orientation, and for . configuration B at 60° fiber orientation.

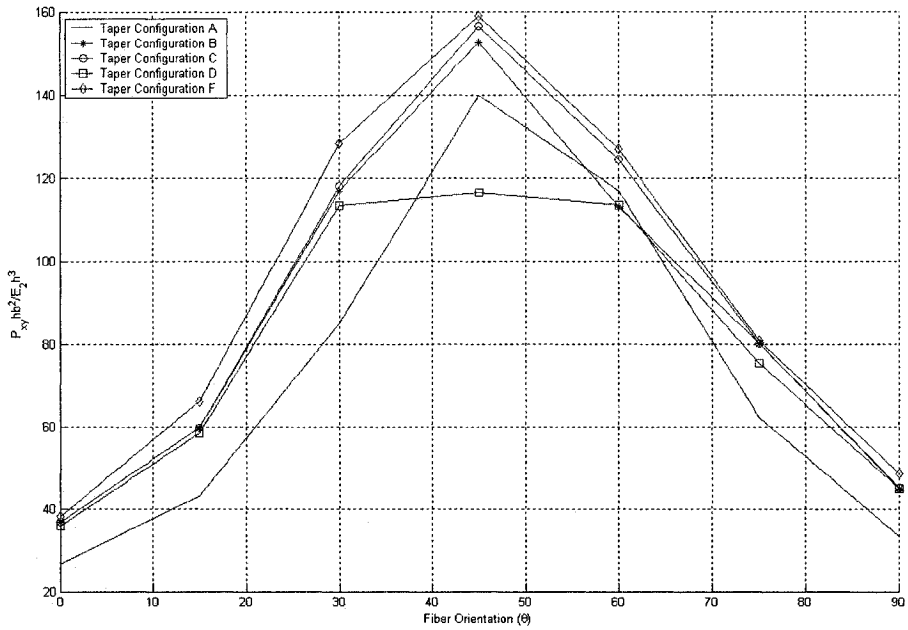

Figure 4.50 First-ply failure load of the laminates with $(\pm\theta)_{4s}$ lay-up at the left (thick) end under in-plane negative shear

Figure 4.51 shows the variation of ultimate failure load of tapered laminates with $(\pm\theta)_{4s}$ lay-up at the left (thick) end under the action of in-plane negative shear for all the taper configurations. The results show that the variations are un-symmetric about 45° fiber orientation. Peak values of the ultimate failure loads for all taper configurations correspond to 45° fiber orientation. The highest value of first-ply failure load occurs for configuration F at 30°, 45°, 60°, 75° and 90° fiber orientations, and for configuration b at 0° and 15° fiber orientations. The lowest value of first-ply failure load occurs for configuration A at 0°, 15°, 75° and 90° fiber orientations, and for configuration D at 30°, 45° and 60° fiber orientations.

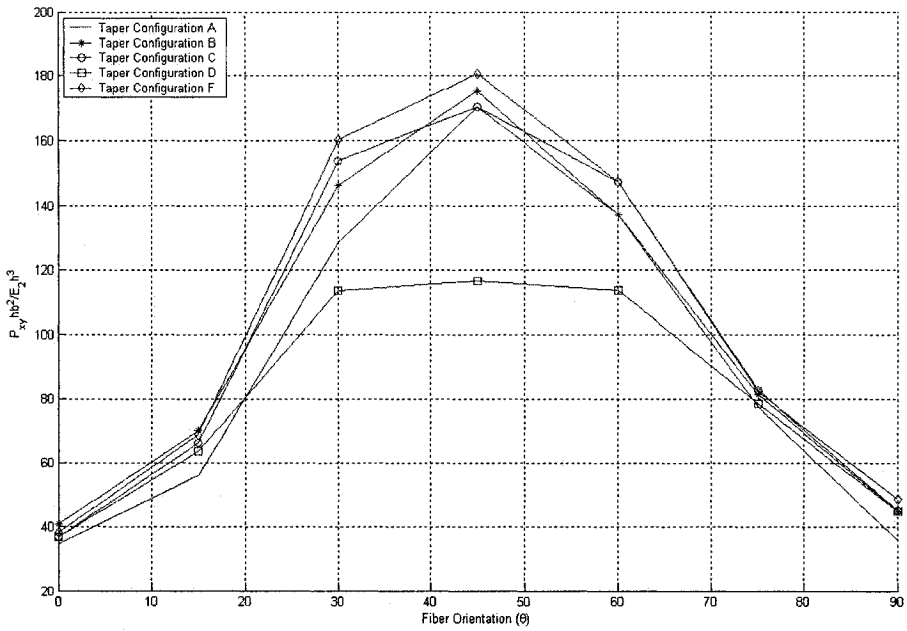

Figure 4.51 Ultimate failure load of the laminates with $(\pm\theta)_{4s}$ lay-up at the left (thick) end under in-plane negative shear

4.3.4 Influence of Uniform-thickness Section

Except that the loading is in-plane negative shear, the study cases are the same as those given in sub-section 4.2.4. Figure 4.52 shows the load versus maximum deflection curves of five tapered plates under the action of in-plane negative shear. Table 4.25 gives the buckling load, the first-ply failure load and the ultimate failure load for these laminates under the action of in-plane negative shear. The laminate with length ratio 2:1 is the best choice among these five laminates with respect to the buckling load, the laminate with length ratio 1:2 is the best choice with respect to and the first-ply failure load, and the laminate with length ratio 1:1 is the best choice with respect to the ultimate failure load. It is also observed that for all the cases the first-ply failure corresponds to the transverse (matrix) failure, and the ultimate failure corresponds to the delamination failure as in the case of the plate with only the tapered section. Therefore, it is noted that the addition of

uniform-thickness sections did not change the modes of failure. However, considerably more resistance to buckling, first-ply failure and ultimate failure is provided by the addition of uniform-thickness sections.

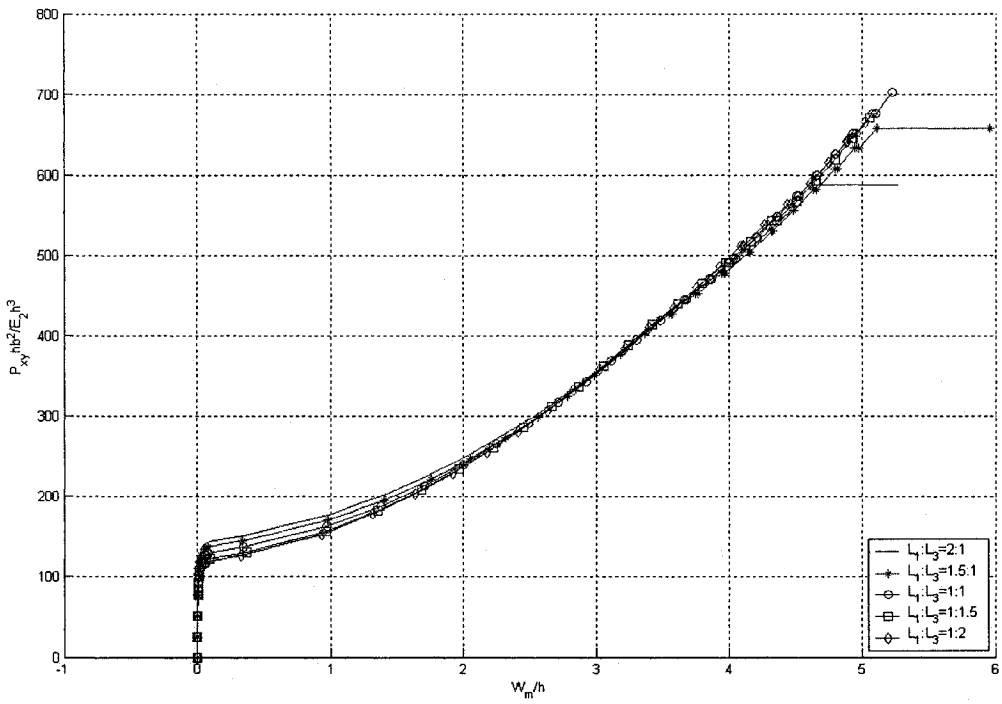

Figure 4.52 Load versus the maximum deflection curves of five tapered plates with different length ratios under in-plane negative shear

Table 4.25 Failure data of five tapered plates with different length ratios under in-plane negative shear

$L_1:L_3$	Buckling Load ($P_{xy}hb^2/E_2h^3$)	First-ply failure load ($P_{xy}hb^2/E_2h^3$)	Ultimate failure load ($P_{xy}hb^2/E_2h^3$)	$(W_m/h)^*$	Failure location (FL,FE) ♣	First-ply failure mode	Ultimate failure mode
2:1	147.012	408.345	588.570	3.377	2,10	T♠	D#
1.5:1	140.064	427.140	658.860	3.544	2,10	T	D
1:1	132.341	445.170	702.630	3.662	2,10	T	D
1:1.5	126.675	490.995	671.220	3.970	2,10	T	D
1:2	122.042	512.100	666.585	4.110	2,10	T	D

4.3.5 Influence of Boundary Conditions

Similar as the cases shown in section 4.2.5, the influence of boundary condition on the progressive failure is studied. The results are compared in Figure 4.53 and Table 4.26.

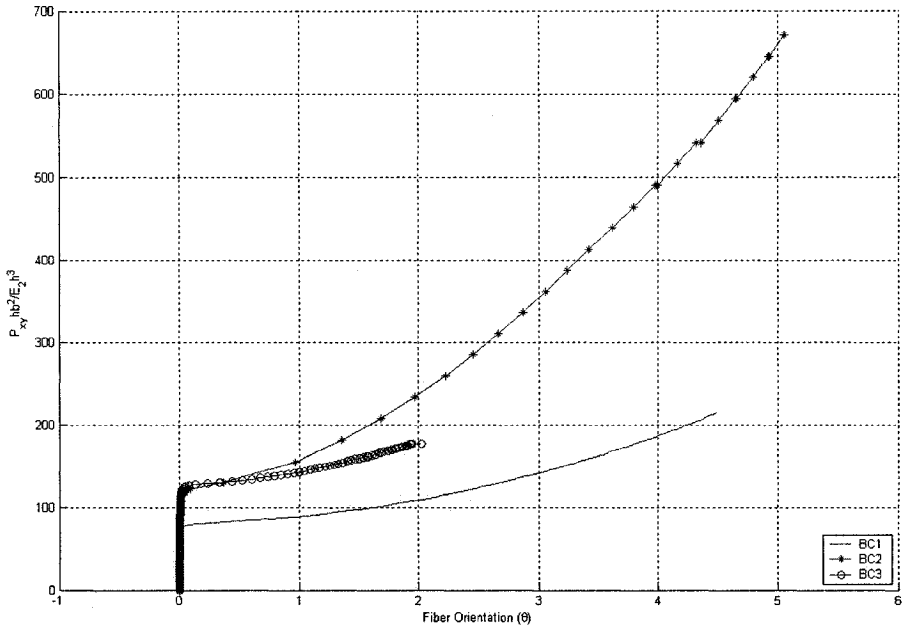

Figure 4.53 Load versus maximum deflection curves of the tapered laminate with taper configuration B corresponding to three boundary conditions under in-plane negative shear

Table 4.26 Failure data of the tapered laminate with taper configuration B corresponding to three boundary conditions under in-plane negative shear

BC	Buckling Load ($P_{xy}hb^2/E_2h^3$)	First-ply failure load ($P_{xy}hb^2/E_2h^3$)	Ultimate failure load ($P_{xy}hb^2/E_2h^3$)	$(W_m/h)^*$	Failure location (FL,FE) ♣	First-ply failure mode	Ultimate failure mode
BC1	83.280	138.588	216.150	2.889	2,8	T♠	D#
BC2	126.675	490.995	671.220	3.970	2,10	T	D
BC3	130.325	143.675	176.730	0.998	16,1	T	D

From Figure 4.53 and Table 4.26, it is observed that the first-ply failure load corresponds to the transverse (matrix) failure, and the ultimate failure corresponds to the delamination failure for all the three boundary conditions. The absolute maximum value of the maximum transverse displacement W_m just before ultimate failure is found to occur in the case of boundary condition BC2 and is equal to 5.05h. The absolute minimum value of

the maximum transverse displacement W_m just before the ultimate failure is found to occur in the case of boundary condition BC3 and is equal to 1.95h.

4.4 Comparison of In-plane Positive Shear and In-plane Negative Shear

For LC(1) lay-up configuration, the buckling load under in-plane negative shear is found to be about 1.75 times the buckling load under in-plane positive shear for taper configuration A, 1.70 times for configuration B, 1.57 times for configuration C, and 1.42 times for configuration F, but for taper configuration D it only about 81.5% of the buckling load under in-plane positive shear. The first-ply failure load under in-plane negative shear is found to be about 1.19 times the first-ply failure load under in-plane positive shear for taper configuration A, 1.41 times for configuration B, 1.32 times for configuration C, and 1.27 times for configuration F, but for taper configuration D it only about 86.7% of the first-ply failure load under in-plane positive shear. The ultimate failure load under in-plane negative shear is found to be about 85.2% of the ultimate failure load under in-plane positive shear for taper configuration B, 92.3% for configuration C, 96.3% for configuration D, 80.9% for configuration F, but for taper configuration A it about 1.03 times the ultimate failure load under in-plane positive shear.

For LC(2) lay-up configuration, the buckling load under in-plane negative shear is found to be about 2.40 times the buckling load under in-plane positive shear for taper configuration A, 2.82 times for configuration B, 2.47 times for configuration C, 3.80 times for configuration D, and 2.35 times for configuration F. The first-ply failure load under in-plane negative shear is found to be about 1.93 times the first-ply failure load under in-plane positive shear for taper configuration A, 2.54 times for configuration B,

1.98 times for configuration C, 2.68 times for configuration D, and 1.93 times for configuration F. The ultimate failure load under in-plane negative shear is found to be about 1.70 times the ultimate failure load under in-plane positive shear for taper configuration A, 1.68 times for taper configuration B, 1.71 times for taper configuration C, 2.00 times for taper configuration D, and 1.52 times for configuration F.

For LC(3) lay-up configuration, the buckling load under in-plane negative shear is found to be about 2.93 times the buckling load under in-plane positive shear for taper configuration A, 3.03 times for configuration B, 2.84 times for configuration C, 5.43 times for configuration D, and 2.86 times for configuration F. The first-ply failure load under in-plane negative shear is found to be about 2.29 times the first-ply failure load under in-plane positive shear for taper configuration A, 2.76 times for configuration B, 2.18 times for configuration C, 2.64 times for configuration D, and 2.10 times for configuration F. The ultimate failure load under in-plane negative shear is found to be about 1.87 times the ultimate failure load under in-plane positive shear for taper configuration A, 1.88 times for taper configuration B, 1.57 times for taper configuration C, 3.30 times for taper configuration D, and 1.59 times for configuration F.

For LC(4) lay-up configuration, the buckling load under in-plane negative shear is found to be about 1.71 times the buckling load under in-plane positive shear for taper configuration A, 1.74 times for configuration B, 1.55 times for configuration C, 3.49 times for configuration D, and 1.45 times for configuration F. The first-ply failure load under in-plane negative shear is found to be about 1.19 times the first-ply failure load under in-plane positive shear for taper configuration A, 1.42 times for configuration B,

1.29 times for configuration C, 1.25 times for configuration F, but for taper configuration D it is only about 95.9% of the first-ply failure load under in-plane positive shear. The ultimate failure load under in-plane negative shear is found to be about 96.8% of the ultimate failure load under in-plane positive shear for taper configuration B, 85.6% for configuration C, 71.0% for configuration D, 84.7% for configuration F, but for taper configuration A it about 1.03 times the ultimate failure load under in-plane positive shear.

For LC(5) lay-up configuration, the buckling load under in-plane negative shear is found to be about 1.93 times the buckling load under in-plane positive shear for taper configuration A, 2.08 times for configuration B, 1.96 times for configuration C, 1.48 times for configuration D, and 1.96 times for configuration F. The first-ply failure load under in-plane negative shear is found to be about 1.87 times the first-ply failure load under in-plane positive shear for taper configuration A, 2.12 times for configuration B, 1.65 times for configuration C, 1.49 times for configuration D, and 1.65 times for configuration F. The ultimate failure load under in-plane negative shear is found to be about 1.58 times the ultimate failure load under in-plane positive shear for taper configuration A, 1.30 times for taper configuration B, 1.28 times for taper configuration C, 1.23 times for taper configuration F, but for taper configuration D it is about 84.8% of the ultimate failure load under in-plane positive shear.

For LC(6) lay-up configuration, the buckling load under in-plane negative shear is found to be about 2.17 times the buckling load under in-plane positive shear for taper configuration A, 2.22 times for configuration B, 2.13 times for configuration C, 2.72 times for configuration D, and 2.13 times for configuration F. The first-ply failure load

under in-plane negative shear is found to be about 1.84 times the first-ply failure load under in-plane positive shear for taper configuration A, 1.72 times for configuration B, 1.55 times for configuration C, 1.33 times for configuration D, and 1.52 times for configuration F. The ultimate failure load under in-plane negative shear is found to be about 1.54 times the ultimate failure load under in-plane positive shear for taper configuration A, 1.44 times for taper configuration B, 1.32 times for taper configuration C, 1.31 times for taper configuration F, but for taper configuration D it is about 92.1% of the ultimate failure load under in-plane positive shear.

4.5 Conclusion

In this chapter, a detailed parametric study on tapered composite plates under the action of in-plane positive and negative shear is conducted. The first-ply failure load, the ultimate failure load, the buckling load, the associated maximum transverse displacements, and the locations and modes of failure including the onset of delamination of tapered laminate plate under the action of in-plane positive and negative shear have been determined and given.

The results of the present study predict that the maximum difference among the buckling loads, the first-ply failure loads and ultimate failure loads are strongly dependent on the type of laminate lay-up, the type of boundary condition and the type of taper configuration. The failure mode corresponding to the first-ply failure is associated with the localized matrix cracking irrespective of the lay-up configuration, taper configuration, addition of uniform-thickness sections and boundary condition. The failure occurs primarily due to the in-plane normal stresses acting in the direction transverse to the fiber

direction. The failure mode corresponding to the ultimate failure is associated with delamination irrespective of the lay-up configuration, taper configuration, addition of uniform-thickness sections and boundary condition.

In general, under the action of in-plane positive and negative shear, for the lay-up and taper configurations and the boundary conditions considered, the ultimate failure load is about 1.3 - 10.2 times the buckling load, the first-ply failure load is about 1.1 – 5.4 times the buckling load, and the ultimate failure load is about 1.0 - 2.6 times the first-ply failure load. The largest difference between the buckling load and the first-ply failure load corresponds to the tapered laminate under in-plane positive shear with the lay-up configuration LC(4), the boundary condition BC1 and the taper configuration D . For this case, the first-ply failure load is about 5.4 times the buckling load. As for the difference between the buckling load and the ultimate failure load, the largest difference corresponds to the tapered laminate with the lay-up configuration LC(4), the boundary condition BC1 and the taper configuration D under the action of in-plane positive shear. For this case, the ultimate failure load is about 10.2 times the buckling load. As for the difference between the first-ply failure load and the ultimate failure load, the largest difference corresponds to the tapered laminate with the lay-up configuration LC(5), the boundary condition BC1 and the taper configuration D under the action of in-plane positive shear. For this case, the ultimate failure load is about 2.6 times the first-ply failure load. Hence, it can be seen that considerable residual strength is available for these laminates in the post-buckling stage under the action of in-plane positive and negative shear.

Chapter 5

Progressive Failure and Post-buckling Response under Bi-axial Compression Combined with In-plane Shear

5.1 Introduction

Six lay-up configurations and five taper configurations that were defined in sub-section 3.2 of Chapter 3 are considered. In addition to the above mentioned six lay-up configurations, tapered laminates with $(\pm\theta)_{4s}$ lay-up at the left (thick) end are also considered to understand the influence of fiber orientation on the failure strength of the laminate. The boundary condition, the material properties, the dimension of the plate and the finite element mesh are the same as those given in sub-section 3.2 of Chapter 3. The objective is to predict the first-ply failure load, the ultimate failure load, the buckling load, the associated maximum transverse displacements, and the locations and modes of failure of tapered laminated plate under the action of bi-axial compression combined with in-plane shear. The tensor polynomial form of the 3D Tsai-Hill criterion is used as the failure criterion for a lamina failure and resin failure, and the terms associated with the normal stress component in the third principal material direction are omitted.

5.2 Parametric Study on Bi-axial Compression Combined with In-plane Positive Shear

5.2.1 Influence of Taper Configuration

Figure 5.1 shows the load versus the maximum deflection curves of the five laminates all with LC(1) lay-up configuration and each with a different taper configuration under the action of bi-axial compression combined with in-plane positive shear. Table 5.1 gives the buckling load, the first-ply failure load and the ultimate failure load for these laminates.

Bi-axial compression loadings P_x and P_y and in-plane shear loading P_{xy} are expressed in figures in non-dimensional forms as P_xhb^2/E_2h^3, P_yhb^2/E_2h^3 and $P_{xy}hb^2/E_2h^3$, respectively, where P_x is the applied X-direction axial compression loading per unit area, P_y is the applied Y-direction axial compression loading per unit area, and P_{xy} is the applied in-plane shear loading per unit area. The corresponding maximum (transverse) deflection is also expressed in non-dimensional form as W_m/h, where h is the average thickness of the tapered laminate.

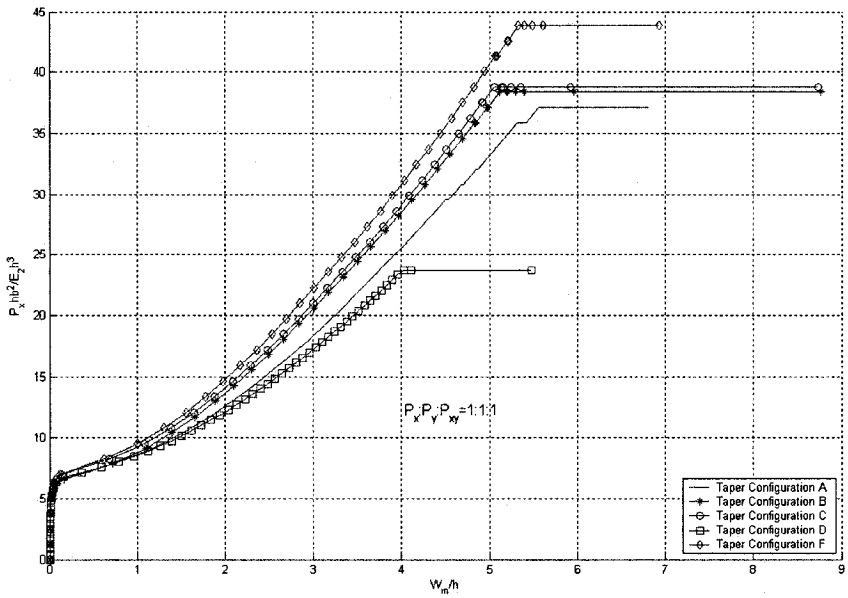

Figure 5.1 Load versus the maximum deflection curves of the laminates with LC(1) lay-up configuration for five taper configurations under bi-axial compression combined with in-plane positive shear

Table 5.1 Failure data of the laminates with LC(1) lay-up configuration for five taper configurations under bi-axial compression combined with in-plane positive shear

Taper	Buckling Load (P_xhb^2/E_2h^3)	First-ply failure load (P_xhb^2/E_2h^3)	Ultimate failure load (P_xhb^2/E_2h^3)	$(W_m/h)^*$	Failure location (FL,FE) ♣	First-ply failure mode	Ultimate failure mode
A	7.248	29.498	37.127	4.503	1,1	T♠	D#
B	7.248	35.855	38.399	4.828	1,1	T	D
C	7.629	37.508	38.780	4.914	1,1	T	D
D	7.418	23.735	23.735	4.028	1,40	T	D
F	7.629	40.052	43.865	4.939	1,40	T	D

For lay-up configuration LC(1), the first-ply failure load is found to be about 4.1 times the buckling load for taper configuration A, 4.9 times for configurations B and C, 3.2 times for configuration D, and 5.2 times for configuration F. The ultimate failure load is about 5.1 times the buckling load for configurations A and C, 5.3 times for configuration B, 3.2 times for configuration D, and 5.7 times for configuration F. The ultimate failure load is about 1.3 times the first-ply failure load for configuration A, 1.1 times for configurations B and F, and 1.0 time for configurations C and D. Hence, it can be observed that considerable residual strength exists in the tapered laminates beyond the onset of buckling.

Figure 5.2 shows the load versus the maximum deflection curves of the five laminates all with LC(2) lay-up configuration and each with a different taper configuration under the action of bi-axial compression combined with in-plane positive shear. Table 5.2 gives the buckling load, the first-ply failure load and the ultimate failure load for these laminates.

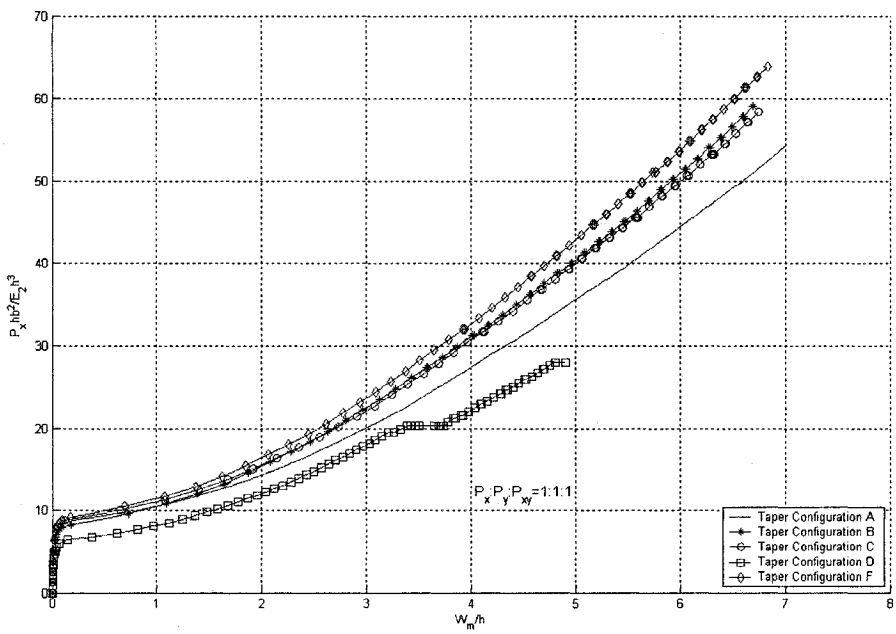

Figure 5.2 Load versus maximum deflection curves of the laminates with LC(2) lay-up configuration for five taper configurations under bi-axial compression combined with in-plane positive shear

Table 5.2 Failure data of the laminates with LC(2) lay-up configuration for five taper configurations under bi-axial compression combined with in-plane positive shear

Taper	Buckling Load ($P_x hb^2/E_2h^3$)	First-ply failure load ($P_x hb^2/E_2h^3$)	Ultimate failure load ($P_x hb^2/E_2h^3$)	$(W_m/h)^*$	Failure location (FL,FE) ♣	First-ply failure mode	Ultimate failure mode
A	9.410	29.117	54.546	4.208	1,40	T♠	D#
B	8.901	27.336	59.123	3.566	1,40	T	D
C	9.410	31.659	58.361	4.106	1,40	T	D
D	6.993	19.496	27.972	3.202	1,40	T	D
F	9.791	32.040	63.827	3.918	1,40	T	D

For lay-up configuration LC(2), the first-ply failure load is found to be about 3.1 times the buckling load for taper configurations A and B, 3.4 times for configuration C, 2.8 times for configuration D, and 3.3 times for configuration F. The ultimate failure load is about 5.8 times the buckling load for configuration A, 6.6 times for configuration B, 6.2 times for configuration C, 4.0 times for configuration D, and 6.5 times for configuration F. The ultimate failure load is about 1.9 times the first-ply failure load for configuration A, 2.2 times for configuration B, 1.8 times for configuration C, 1.4 times for configuration D, and 2.0 times for configuration F.

In order to illustrate the positive deflection of the plate under bi-axial compression combined with in-plane positive shear, a typical deformed configuration is given. Figure 5.3 shows the deformed configuration of the laminate with LC(2) lay-up configuration and with taper configuration B under bi-axial compression combined with in-plane positive shear. It is observed that the entire laminate undergoes positive (upward) deflection.

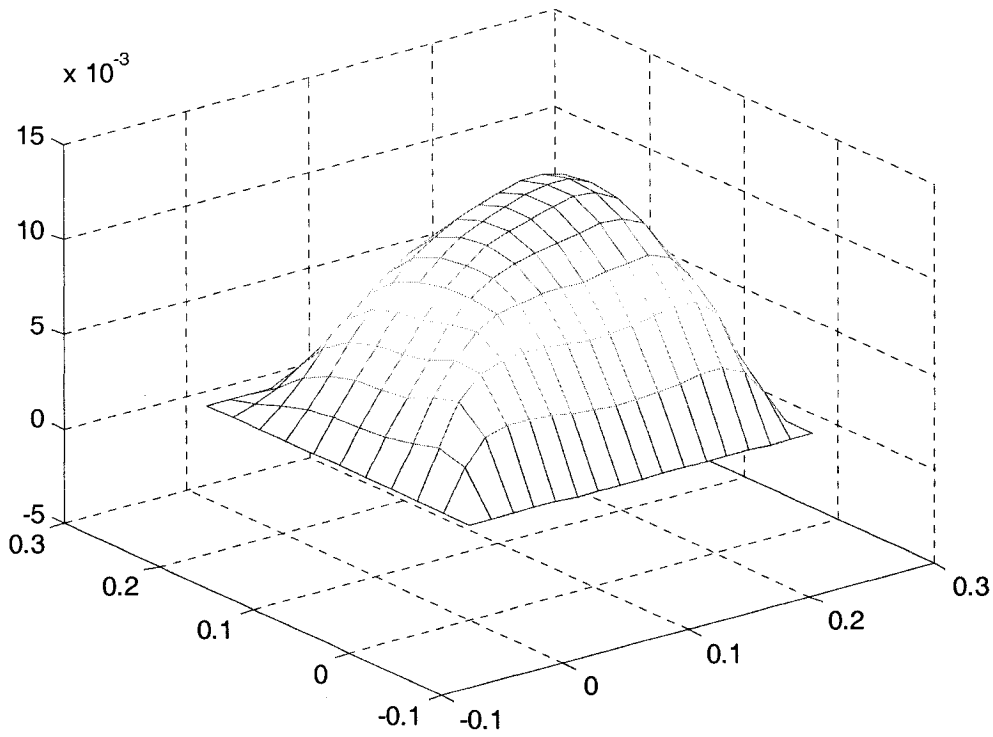

Figure 5.3 The deformed configuration of the laminate with LC(2) lay-up configuration and with taper configuration B under bi-axial compression combined with in-plane positive shear

Figure 5.4 shows the load versus the maximum deflection curves of the five laminates all with LC(3) lay-up configuration and each with a different taper configuration under the action of bi-axial compression combined with in-plane positive shear. Table 5.3 gives the buckling load, the first-ply failure load and the ultimate failure load for these laminates.

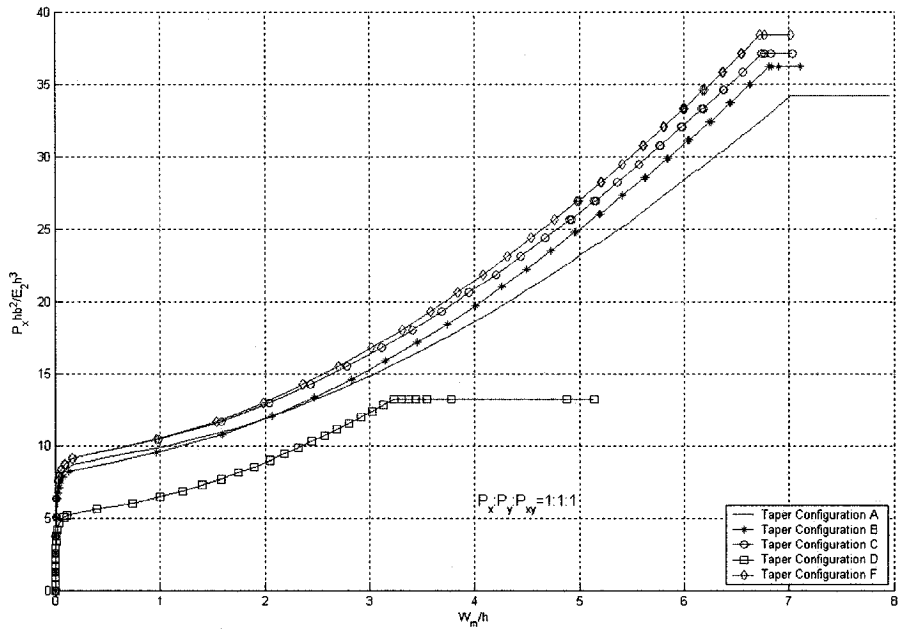

Figure 5.4 Load versus maximum deflection curves of the laminates with LC(3) lay-up configuration for five taper configurations under bi-axial compression combined with in-plane positive shear

Table 5.3 Failure data of the laminates with LC(3) lay-up configuration for five taper configurations under bi-axial compression combined with in-plane positive shear

Taper	Buckling Load (P_xhb^2/E_2h^3)	First-ply failure load (P_xhb^2/E_2h^3)	Ultimate failure load (P_xhb^2/E_2h^3)	$(W_m/h)^*$	Failure location (FL,FE) ♣	First-ply failure mode	Ultimate failure mode
A	9.410	24.030	34.202	5.167	1,40	T♠	D#
B	8.901	24.794	36.237	4.951	1,40	T	D
C	9.791	25.683	37.127	4.900	1,40	T	D
D	5.849	13.266	13.266	3.232	1,40	T	D
F	9.791	26.955	38.399	4.976	1,40	T	D

For lay-up configuration LC(3), the first-ply failure load is found to be about 2.6 times the buckling load for taper configurations A and C, 2.8 times for configurations B and F, and 2.3 times for configuration D. The ultimate failure load is about 3.6 times the buckling load for configuration A, 4.1 times for configuration B, 3.8 times for configuration C, 2.3 times for configuration D, and 3.9 times for configuration F. The

ultimate failure load is about 1.4 times the first-ply failure load for configurations A, C and F, 1.5 times for configuration B, and 1.0 time for configuration D.

Figure 5.5 shows the load versus the maximum deflection curves of the five laminates all with LC(4) lay-up configuration and each with a different taper configuration under the action of bi-axial compression combined with in-plane positive shear. Table 5.4 gives the buckling load, the first-ply failure load and the ultimate failure load for these laminates.

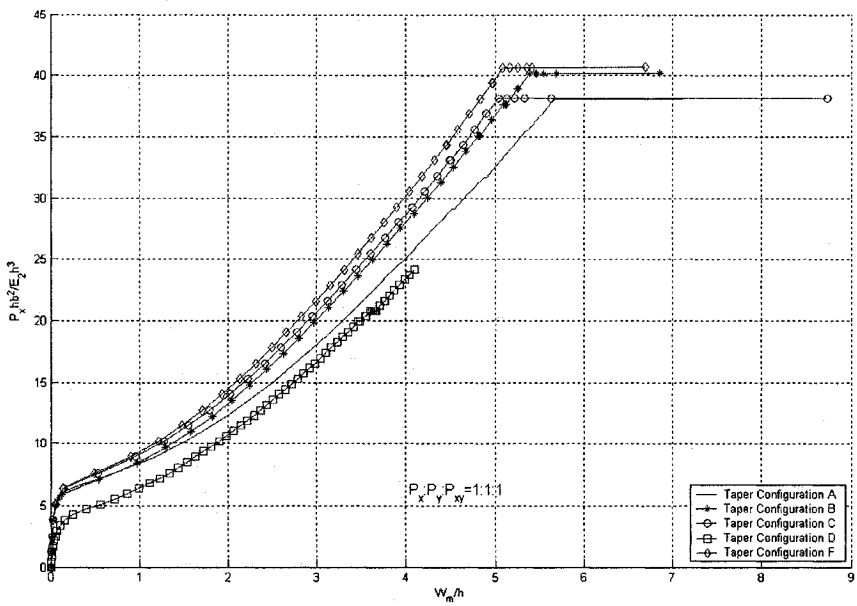

Figure 5.5 Load versus maximum deflection curves of the laminates with LC(4) lay-up configuration for five taper configurations under bi-axial compression combined with in-plane positive shear

Table 5.4 Failure data of the laminates with LC(4) lay-up configuration for five taper configurations under bi-axial compression combined with in-plane positive shear

Taper	Buckling Load (P_xhb^2/E_2h^3)	First-ply failure load (P_xhb^2/E_2h^3)	Ultimate failure load (P_xhb^2/E_2h^3)	$(W_m/h)^*$	Failure location (FL,FE) ♣	First-ply failure mode	Ultimate failure mode
A	6.866	29.117	38.016	4.519	10,40	T♠	D#
B	7.757	32.549	40.178	4.526	10,40	T	D
C	8.265	33.059	38.144	4.491	10,40	T	D
D	4.874	19.920	24.158	3.464	10,40	T	D
F	8.265	34.329	40.686	4.447	10,40	T	D

For lay-up configuration LC(4), the first-ply failure load is found to be about 4.2 times the buckling load for taper configurations A, B and F, 4.0 times for configuration B, and 4.1 times for configuration D. The ultimate failure load is about 5.5 times the buckling load for configuration A, 5.2 times for configuration B, 4.6 times for configuration C, 5.0 times for configuration D, and 4.9 times for configuration F. The ultimate failure load is about 1.3 times the first-ply failure load for configuration A, and 1.2 times for configurations B, C, D and F.

Figure 5.6 shows the load versus the maximum deflection curves of the five laminates all with LC(5) lay-up configuration and each with a different taper configuration under the action of bi-axial compression combined with in-plane positive shear. Table 5.5 gives the buckling load, the first-ply failure load and the ultimate failure load for these laminates.

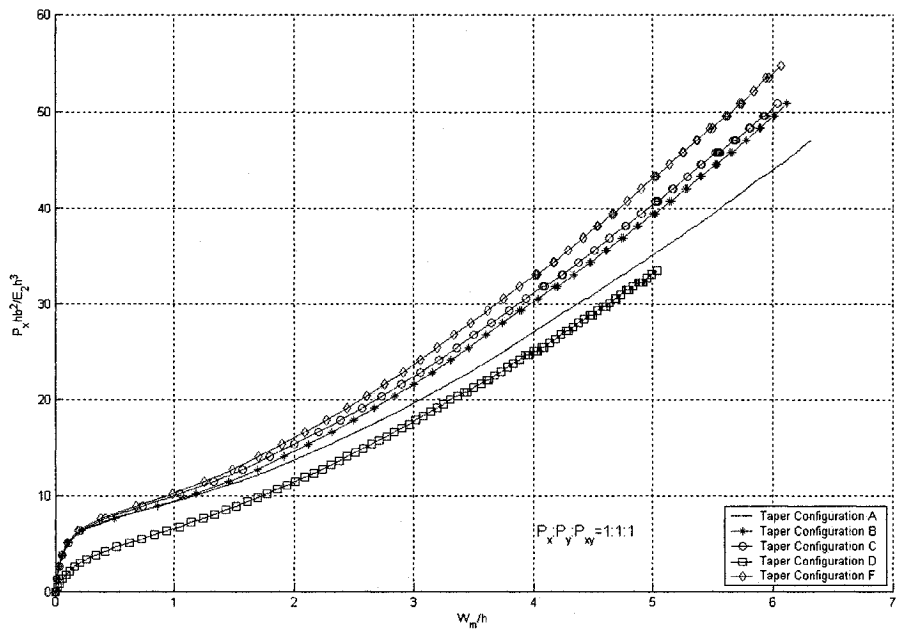

Figure 5.6 Load versus maximum deflection curves of the laminates with LC(5) lay-up configuration for five taper configurations under bi-axial compression combined with in-plane positive shear

Table 5.5 Failure data of the laminates with LC(5) lay-up configuration for five taper configurations under bi-axial compression combined with in-plane positive shear

Taper	Buckling Load ($P_x hb^2/E_2h^3$)	First-ply failure load ($P_x hb^2/E_2h^3$)	Ultimate failure load ($P_x hb^2/E_2h^3$)	$(W_m/h)^*$	Failure location (FL,FE) ♣	First-ply failure mode	Ultimate failure mode
A	8.265	29.244	47.045	4.271	1,40	T♠	D#
B	8.265	29.244	50.858	3.887	1,40	T	D
C	8.265	31.787	50.858	4.079	1,40	T	D
D	5.721	20.768	33.482	3.419	1,40	T	D
F	9.536	33.059	54.672	4.016	1,40	T	D

For lay-up configuration LC(5), the first-ply failure load is found to be about 3.5 times the buckling load for taper configurations A, B and F, 3.8 for configuration C, and 3.6 times for configuration D. The ultimate failure load is about 5.7 times the buckling load for configurations A and F, 6.2 times for configurations B and C, and 5.9 times for configuration D. The ultimate failure load is about 1.6 times the first-ply failure load for configurations A, C, and D, and 1.7 times for configurations B and F.

Figure 5.7 shows the load versus the maximum deflection curves of the five laminates all with LC(6) lay-up configuration and each with a different taper configuration under the action of bi-axial compression combined with in-plane positive shear. Table 5.6 gives the buckling load, the first-ply failure load and the ultimate failure load for these laminates.

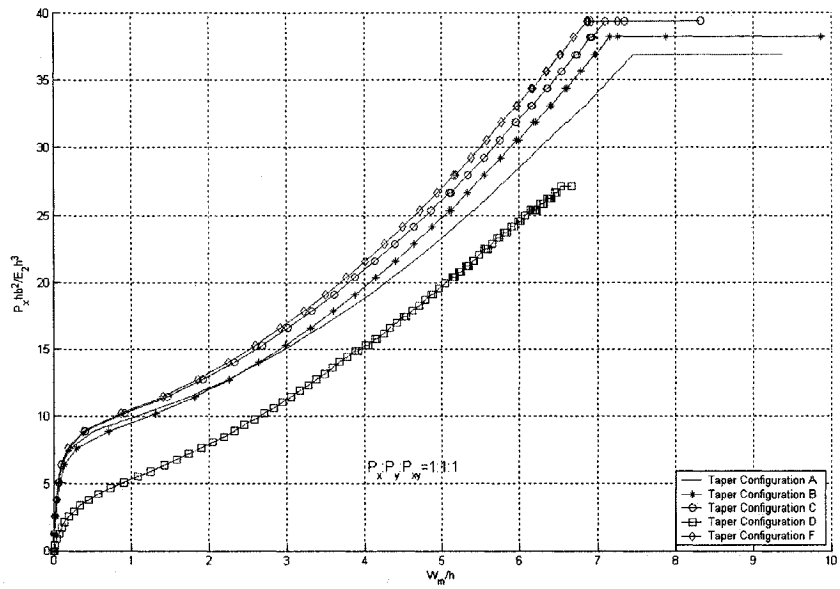

Figure 5.7 Load versus maximum deflection curves of the laminates with LC(6) lay-up configuration for five taper configurations under bi-axial compression combined with in-plane positive shear

Table 5.6 Failure data of the laminates with LC(6) lay-up configuration for five taper configurations under bi-axial compression combined with in-plane positive shear

Taper	Buckling Load (P_xhb^2/E_2h^3)	First-ply failure load (P_xhb^2/E_2h^3)	Ultimate failure load (P_xhb^2/E_2h^3)	$(W_m/h)^*$	Failure location (FL,FE) ♣	First-ply failure mode	Ultimate failure mode
A	9.536	25.430	36.872	5.408	1,40	T♠	D#
B	9.536	25.430	38.144	5.098	1,40	T	D
C	10.808	26.700	39.416	5.095	1,40	T	D
D	5.298	14.834	27.125	3.877	1,40	T	D
F	10.808	27.972	39.416	5.156	1,40	T	D

For lay-up configuration LC(6), the first-ply failure load is found to be about 2.7 times the buckling load for taper configurations A and B, 2.5 times for configuration C, 2.8 times for configuration D, and 2.6 times for configuration F. The ultimate failure load is about 3.9 times the buckling load for configuration A, 4.0 times for configuration B, 3.6 times for configuration C, 5.1 times for configuration D, and 3.6 times for configuration F. The ultimate failure load is about 1.4 times the first-ply failure load for configurations A and F, 1.5 times for configurations B and C, and 1.8 times for configuration D.

Summary

From Figures 5.1– 5.7 and Tables 5.1 – 5.6, the following general observations are also made.

1 Among all the six lay-up configurations, the taper configuration F (Mid-plane taper) is the strongest one with respect to the first-ply failure load, the ultimate failure load and the buckling load. However, taper configuration F is not easy to manufacture compared to other taper configurations. Considering this, the next strongest taper configuration is identified. For the lay-up configurations LC(1), LC(3), LC(5) and LC(6), the taper configuration C (Overlapping dropped plies) is the best choice among all taper configurations considering the first-ply failure load, the ultimate failure load and the buckling load. For the lay-up configurations LC(1) and LC(4), taper configuration B is the best choice in terms of the ultimate failure load, whereas, taper configuration C is the best choice in terms of the buckling load and the first-ply failure load.

2 Only the laminates with LC(1) and LC(3) lay-up configurations for the taper configuration D (Continuous plies interspersed), the first-ply failure load and the ultimate failure load are the same. For all other cases, considerable residual strength exits after the first-ply failure until ultimate failure.

3 For all the types of lay-up configurations and taper configurations considered, the deflections are all positive, that is, upward.

4 Locations corresponding to the first-ply failure lie near the loaded edges of the plate and at the outermost layer.

5.2.2 Influence of Lay-up Configuration

Figure 5.8 shows the load versus maximum deflection curves of the six laminates all with taper configuration A and each with a different lay-up configuration under the action of bi-axial compression combined with in-plane positive shear. Table 5.7 gives the buckling load, the first-ply failure load and the ultimate failure load for these laminates.

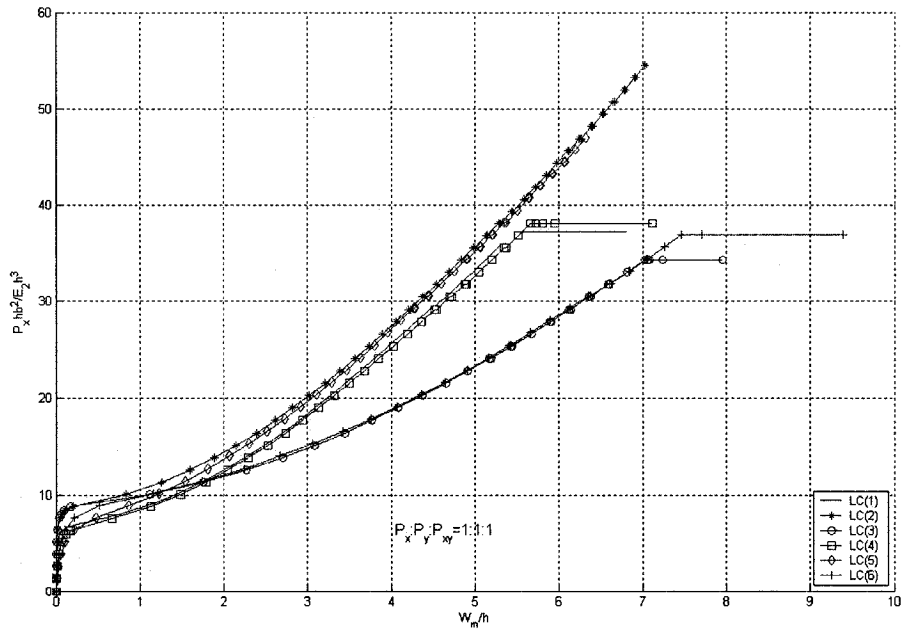

Figure 5.8 Load versus maximum deflection curves of the laminates with taper configuration A for all the six lay-up configurations under bi-axial compression combined with in-plane positive shear

Table 5.7 Failure data of the laminates with taper configuration A for all the six lay-up configurations under bi-axial compression combined with in-plane positive shear

Lay-up	Buckling Load (P_xhb^2/E_2h^3)	First-ply failure load (P_xhb^2/E_2h^3)	Ultimate failure load (P_xhb^2/E_2h^3)	$(W_m/h)^*$	Failure location (FL,FE) ♣	First-ply failure mode	Ultimate failure mode
LC(1)	7.248	29.498	37.127	4.503	1,1	T♠	D#
LC(2)	9.410	29.117	54.546	4.208	1,40	T	D
LC(3)	9.410	24.030	34.202	5.167	1,40	T	D
LC(4)	6.866	29.117	38.016	4.519	10,40	T	D
LC(5)	8.265	29.244	47.045	4.271	1,40	T	D
LC(6)	9.536	25.430	36.872	5.408	1,40	T	D

For taper configuration A, the lay-up configuration LC(6) is the best choice among all the six lay-up configurations with respect to the buckling load, and the lay-up configuration LC(1) is the best choice with respect to the first-ply failure load, and lay-up configuration LC(2) is the best choice with respect to the ultimate failure load.

Figure 5.9 shows the load versus maximum deflection curves of the six laminates all with taper configuration B and each with a different lay-up configuration under the action of bi-axial compression combined with in-plane positive shear. Table 5.8 gives the buckling load, the first-ply failure load and the ultimate failure load for these laminates.

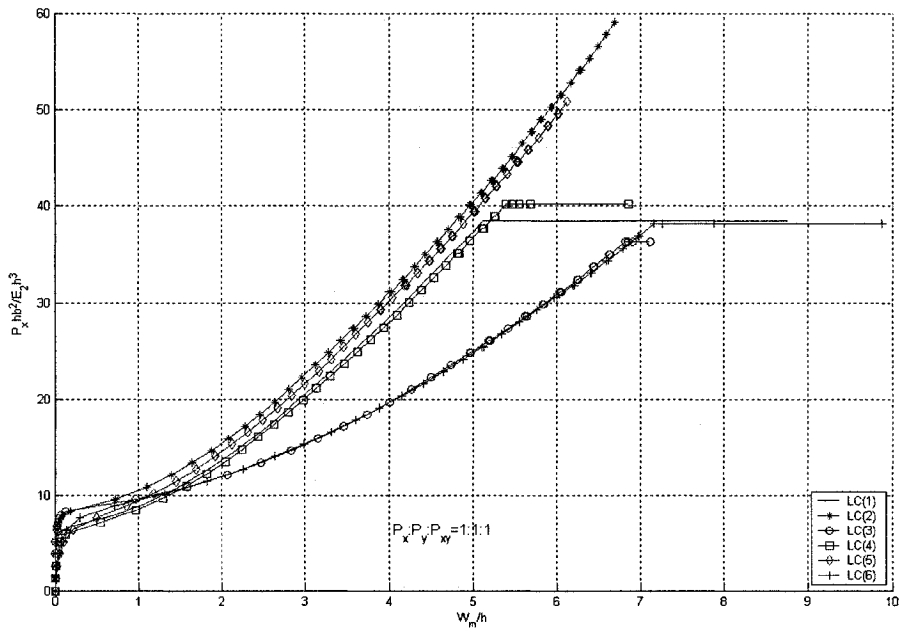

Figure 5.9 Load versus maximum deflection curves of the laminates with taper configuration B for all the six lay-up configurations under bi-axial compression combined with in-plane positive shear

Table 5.8 Failure data of the laminates with taper configuration B for all the six lay-up configurations under bi-axial compression combined with in-plane positive shear

Lay-up	Buckling Load (P_xhb^2/E_2h^3)	First-ply failure load (P_xhb^2/E_2h^3)	Ultimate failure load (P_xhb^2/E_2h^3)	$(W_m/h)^*$	Failure location (FL,FE) ♣	First-ply failure mode	Ultimate failure mode
LC(1)	7.248	35.855	38.399	4.828	1,1	T♠	D#
LC(2)	8.901	27.336	59.123	3.566	1,40	T	D
LC(3)	8.901	24.794	36.237	4.951	1,40	T	D
LC(4)	7.757	32.549	40.178	4.526	10,40	T	D
LC(5)	8.265	29.244	50.858	3.887	1,40	T	D
LC(6)	9.536	25.430	38.144	5.098	1,40	T	D

For taper configuration B, the lay-up configuration LC(6) is the best choice among all the six lay-up configurations with respect to the buckling load, and the lay-up configuration LC(1) is the best choice with respect to the first-ply failure load, and lay-up configuration LC(2) is the best choice with respect to the ultimate failure load.

Figure 5.10 shows the load versus maximum deflection curves of the six laminates all with taper configuration C and each with a different lay-up configuration under the action of bi-axial compression combined with in-plane positive shear. Table 5.9 gives the buckling load, the first-ply failure load and the ultimate failure load for these laminates.

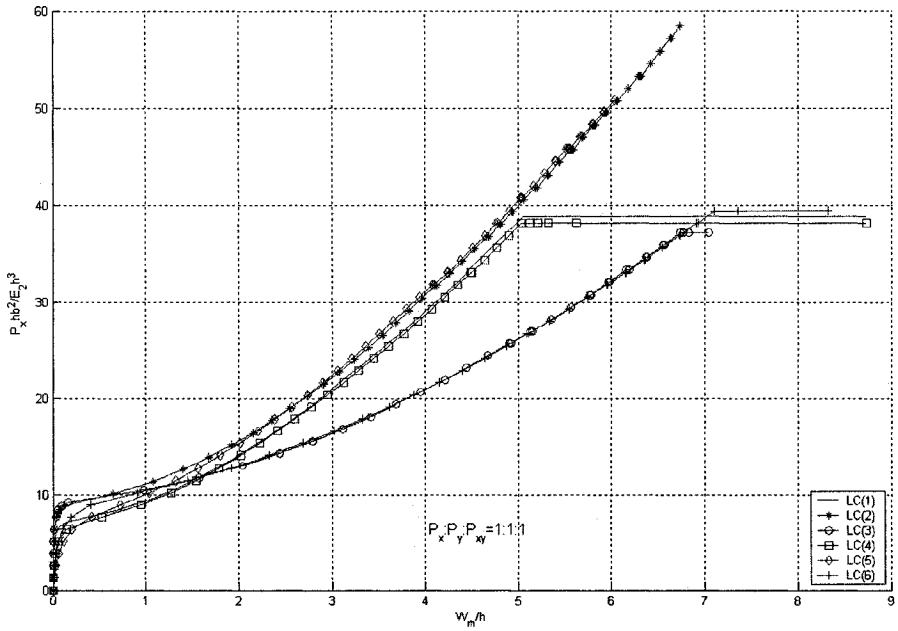

Figure 5.10 Load versus maximum deflection curves of the laminates with taper configuration C for all the six lay-up configurations under bi-axial compression combined with in-plane positive shear

Table 5.9 Failure data of the laminates with taper configuration C for all the six lay-up configurations under bi-axial compression combined with in-plane positive shear

Lay-up	Buckling Load (P_xhb^2/E_2h^3)	First-ply failure load (P_xhb^2/E_2h^3)	Ultimate failure load (P_xhb^2/E_2h^3)	$(W_m/h)^*$	Failure location (FL,FE) ♣	First-ply failure mode	Ultimate failure mode
LC(1)	7.629	37.508	38.780	4.914	1,1	T♠	D#
LC(2)	9.410	31.659	58.361	4.106	1,40	T	D
LC(3)	9.791	25.683	37.127	4.900	1,40	T	D
LC(4)	8.265	33.059	38.144	4.491	10,40	T	D
LC(5)	8.265	31.787	50.858	4.079	1,40	T	D
LC(6)	10.808	26.700	39.416	5.095	1,40	T	D

For taper configuration C, the lay-up configuration LC(6) is the best choice among all the six lay-up configurations with respect to the buckling load, and the lay-up configuration LC(1) is the best choice with respect to the first-ply failure load, and lay-up configuration LC(2) is the best choice with respect to the ultimate failure load.

Figure 5.11 shows the load versus maximum deflection curves of the six laminates all with taper configuration D and each with a different lay-up configuration under the action of bi-axial compression combined with in-plane positive shear. Table 5.10 gives the buckling load, the first-ply failure load and the ultimate failure load for these laminates.

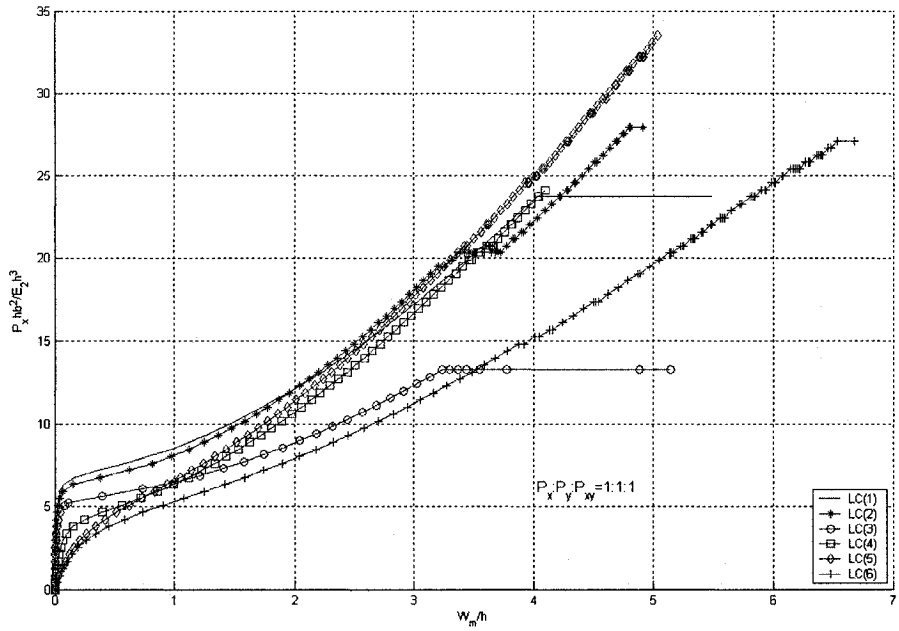

Figure 5.11 Load versus maximum deflection curves of the laminates with taper configuration D for all the six lay-up configurations under bi-axial compression combined with in-plane positive shear

Table 5.10 Failure data of the laminates with taper configuration D for all the six lay-up configurations under bi-axial compression combined with in-plane positive shear

Lay-up	Buckling Load (P_xhb^2/E_2h^3)	First-ply failure load (P_xhb^2/E_2h^3)	Ultimate failure load (P_xhb^2/E_2h^3)	$(W_m/h)^*$	Failure location (FL,FE) ♣	First-ply failure mode	Ultimate failure mode
LC(1)	7.418	23.735	23.735	4.028	1,40	T♠	D#
LC(2)	6.993	19.496	27.972	3.202	1,40	T	D
LC(3)	5.849	13.266	13.266	3.232	1,40	T	D
LC(4)	4.874	19.920	24.158	3.464	10,40	T	D
LC(5)	5.721	20.768	33.482	3.419	1,40	T	D
LC(6)	5.298	14.834	27.125	3.877	1,40	T	D

For taper configuration D, the lay-up configuration LC(1) is the best choice among all the six lay-up configurations with respect to both the buckling load and the first-ply failure load, and the lay-up configuration LC(5) is the best choice with respect to the ultimate failure load.

Figure 5.12 shows the load versus maximum deflection curves of the six laminates all with taper configuration F and each with a different lay-up configuration under the action of bi-axial compression combined with in-plane positive shear. Table 5.11 gives the buckling load, the first-ply failure load and the ultimate failure load for these laminates.

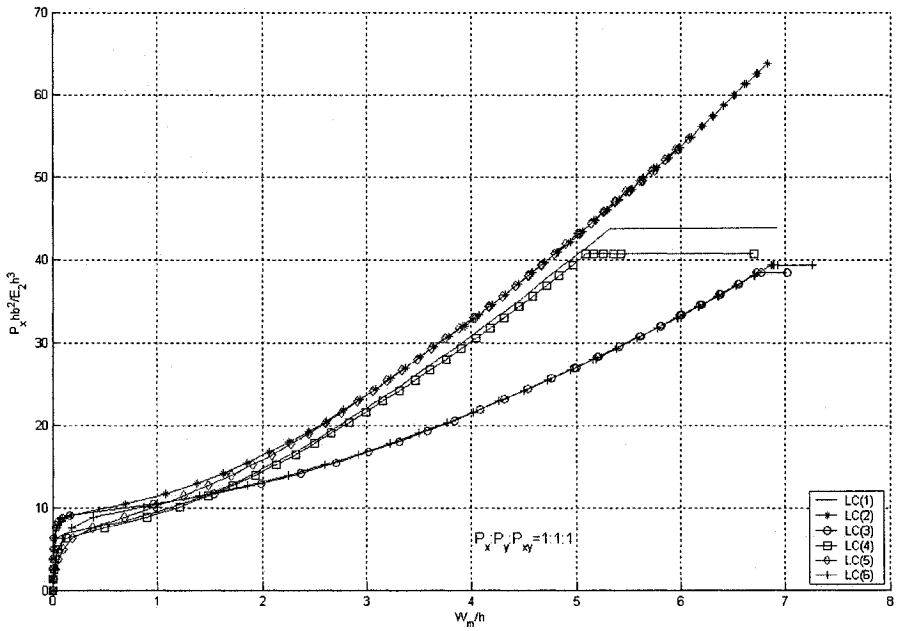

Figure 5.12 Load versus maximum deflection curves of the laminates with taper configuration F for all the six lay-up configurations under bi-axial compression combined with in-plane positive shear

Table 5.11 Failure data of the laminates with taper configuration F for all the six lay-up configurations under bi-axial compression combined with in-plane positive shear

Lay-up	Buckling Load (P_xhb^2/E_2h^3)	First-ply failure load (P_xhb^2/E_2h^3)	Ultimate failure load (P_xhb^2/E_2h^3)	$(W_m/h)^*$	Failure location (FL,FE) ♣	First-ply failure mode	Ultimate failure mode
LC(1)	7.629	40.052	43.865	4.939	1,40	T♠	D#
LC(2)	9.791	32.040	63.827	3.918	1,40	T	D
LC(3)	9.791	26.955	38.399	4.976	1,40	T	D
LC(4)	8.265	34.329	40.686	4.447	10,40	T	D
LC(5)	9.536	33.059	54.672	4.016	1,40	T	D
LC(6)	10.808	27.972	39.416	5.156	1,40	T	D

For taper configuration F, the lay-up configuration LC(6) is the best choice among all the six lay-up configurations with respect to the buckling load, and the lay-up configuration LC(1) is the best choice with respect to the first-ply failure load, and lay-up configuration LC(2) is the best choice with respect to the ultimate failure load.

Summary

From Figures 5.8 – 5.12 and Tables 5.7 – 5.11, the following general observations are also made.

1 For all the five taper configurations, the first-ply failure mode for all the six lay-up configurations is transverse (matrix) failure.

2 For all the five taper configurations, the ultimate failure mode for all the six lay-up configurations is delamination.

3 For all the taper configurations and lay-up configurations, the maximum deflections are positive, i.e. upward.

4 Variations of the maximum deflection with the load for the symmetric lay-up configuration basically coincides with that of the corresponding un-symmetric lay-up configuration for taper configurations A (Basic taper), B (Staircase arrangement),

C (Overlapping dropped plies) and F (Mid-plane taper). Therefore, in these cases the symmetry in the stacking sequence does not have a strong influence on the progressive failure of the laminate.

5.2.3 Influence of Fiber Orientation

Tapered laminates under bi-axial compression combined with in-plane positive shear and with lay-up $(\pm\theta)_{4s}$ at the left end are considered. The lay-up at the right (thin) end is $(\pm\theta)_{2s}$ for taper configurations A, B, C and F, and is $(\theta)_8$ for taper configuration D. The variation of buckling load with θ for each taper configuration is determined. The results are plotted in Figure 5.13. A non-monotonic variation is observed for all taper configurations from this figure. Also the variation is un-symmetric about 45° fiber orientation. Peak values of the buckling loads are predicted to occur at 45° fiber orientation for taper configurations A, B, C and F, and occur at 30° fiber orientation for configuration D. The highest value of buckling load for 0°, 15°, 45°, 60°, and 75° fiber orientations occurs for configuration F, whereas, for 90° fiber orientation, it occurs for configuration B. For taper configuration D and for all off-axis fiber orientations, the buckling load is significantly less than that of all other taper configurations. The buckling load of the taper configuration C is very close to that of the taper configuration F for $(\pm0)_{4s}$, $(\pm15)_{4s}$, $(\pm30)_{4s}$, $(\pm45)_{4s}$, $(\pm60)_{4s}$ and $(\pm75)_{4s}$ fiber orientations.

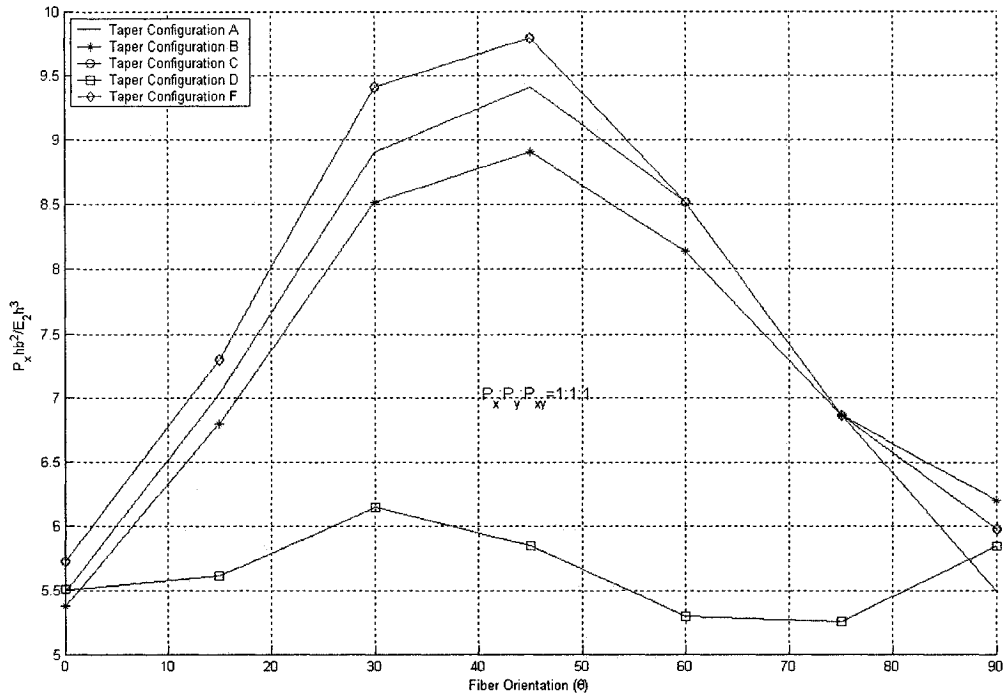

Figure 5.13 Buckling loads of the laminates with $(\pm\theta)_{4s}$ lay-up at the left (thick) end under bi-axial compression combined with in-plane positive shear

Figure 5.14 shows the variation of the first-ply failure load and the ultimate failure load for laminates with taper configuration A and with lay-up $(\pm\theta)_{4s}$ at the left (thick) end under bi-axial compression combined with in-plane positive shear. The results show that the variations in response are un-symmetric about 45° fiber orientation. Peak values of the first-ply failure load and ultimate failure load are predicted to occur for 45° fiber orientation. For laminates with $(\pm 0)_{4s}$, $(\pm 75)_{4s}$ and $(\pm 90)_{4s}$ lay-up configurations at the thick end, the value of the first-ply failure load is equal to the value of the ultimate failure load. In the range $0° \leq \theta \leq 45°$ the difference between the ultimate failure load and the first-ply failure load becomes larger, and at θ = 45° the ultimate failure load is 42.33% higher than the first-ply failure load.

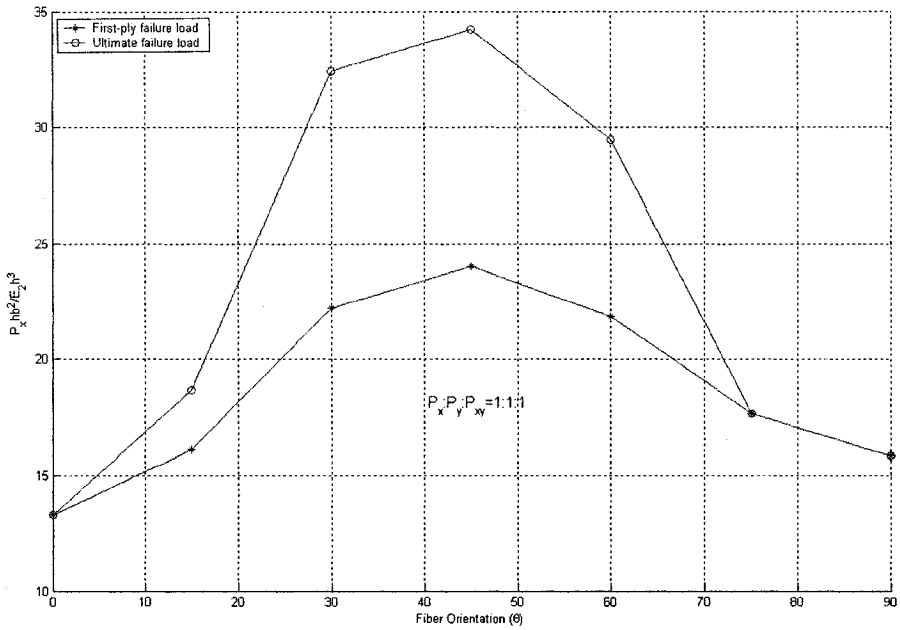

Figure 5.14 Variation of the first-ply and ultimate failure loads of the laminates with taper configuration A and with $(\pm\theta)_{4s}$ lay-up at the left end under bi-axial compression combined with in-plane positive shear

Figure 5.15 shows the variation of the first-ply failure load and the ultimate failure load for laminates with taper configuration B and with lay-up $(\pm\theta)_{4s}$ at the left (thick) end under bi-axial compression combined with in-plane positive shear. The results show that the variations in response are un-symmetric about 45° fiber orientation. Peak values of the first-ply failure load and ultimate failure load are predicted to occur for 45° fiber orientation. For laminates with $(\pm 0)_{4s}$, $(\pm 75)_{4s}$ and $(\pm 90)_{4s}$ lay-up configurations at the thick end, the value of the first-ply failure load is equal to the value of the ultimate failure load. In the range $0° \leq \theta \leq 45°$ the difference between the ultimate failure load and the first-ply failure load becomes larger, and at θ = 45° the ultimate failure load is 46.16% higher than the first-ply failure load.

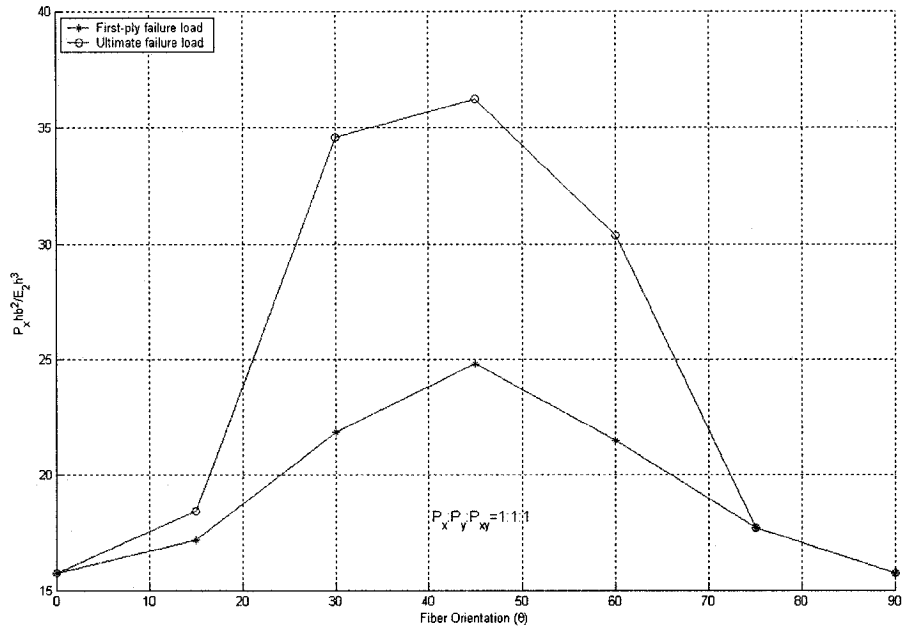

Figure 5.15 Variation of the first-ply and ultimate failure loads of the laminates with taper configuration B and with $(\pm\theta)_{4s}$ lay-up at the left end under bi-axial compression combined with in-plane positive shear

Figure 5.16 shows the variation of the first-ply failure load and the ultimate failure load for laminates with taper configuration C and with lay-up $(\pm\theta)_{4s}$ at the left (thick) end under bi-axial compression combined with in-plane positive shear. The results show that the variations in response are un-symmetric about 45° fiber orientation. Peak values of the first-ply failure load and ultimate failure load are predicted to occur for 45° fiber orientation. For $(\pm 0)_{4s}$, $(\pm 15)_{4s}$, $(\pm 75)_{4s}$ and $(\pm 90)_{4s}$ laminates, the value of the first-ply failure load is equal to the value of the ultimate failure load. In the range $15° \leq \theta \leq 45°$ the difference between the ultimate failure load and the first-ply failure load becomes larger, and at $\theta = 45°$ the ultimate failure load is 44.56 % higher than the first-ply failure load.

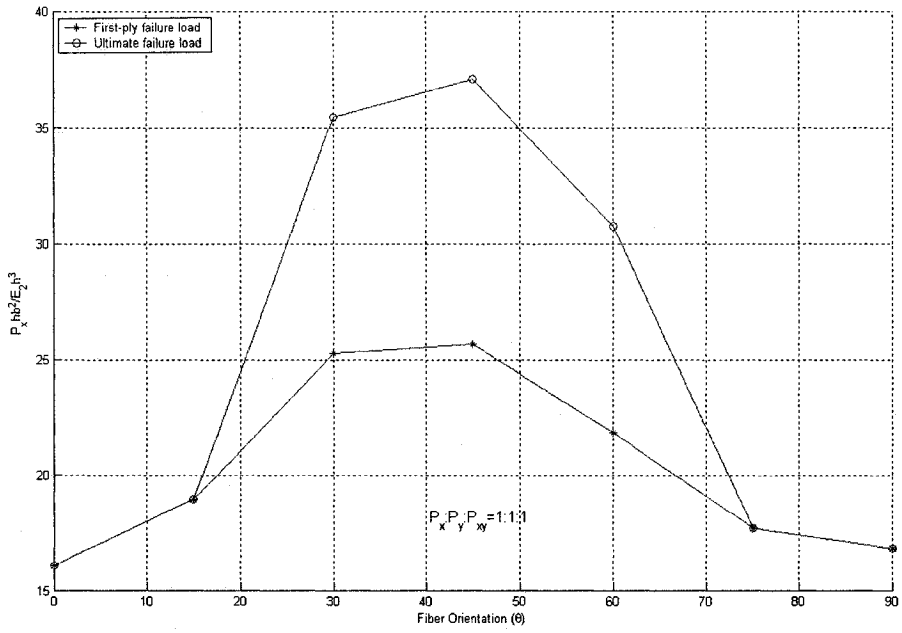

Figure 5.16 Variation of the first-ply and ultimate failure loads of the laminates with taper configuration C and with $(\pm\theta)_{4s}$ lay-up at the left end under bi-axial compression combined with in-plane positive shear

Figure 5.17 shows the variation of the first-ply failure load and the ultimate failure load for laminates with taper configuration D and with lay-up $(\pm\theta)_{4s}$ at the left (thick) end under bi-axial compression combined with in-plane positive shear. The results show that the variations in response are un-symmetric about 45° fiber orientation. Peak values of the first-ply failure load and ultimate failure load are predicted to occur for 15° fiber orientation. The value of the first-ply failure load is equal to the value of the ultimate failure load for all the fiber orientations.

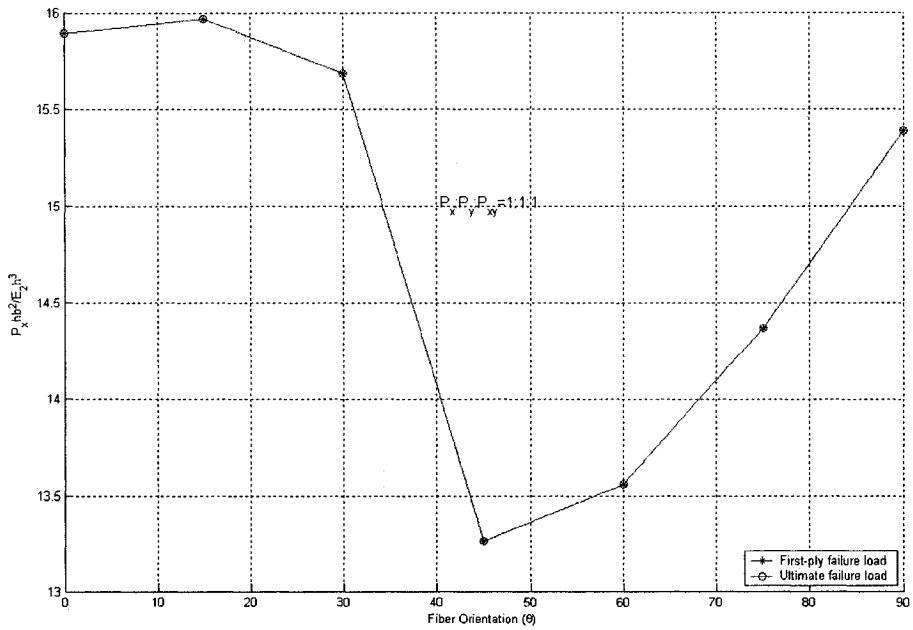

Figure 5.17 Variation of the first-ply and ultimate failure loads of the laminates with taper configuration D and with $(\pm\theta)_{4s}$ lay-up at the left end under bi-axial compression combined with in-plane positive shear

Figure 5.18 shows the variation of the first-ply failure load and the ultimate failure load for laminates with taper configuration F and with lay-up $(\pm\theta)_{4s}$ at the left (thick) end under bi-axial compression combined with in-plane positive shear. The results show that the variations in response are un-symmetric about 45° fiber orientation. Peak values of the first-ply failure load and ultimate failure load occur for 45° fiber orientation. For $(\pm 0)_{4s}$, $(\pm 15)_{4s}$, $(\pm 75)_{4s}$ and $(\pm 90)_{4s}$ laminates, the value of the first-ply failure load is equal to the value of the ultimate failure load. In the range $15° \leq \theta \leq 45°$ the difference between the ultimate failure load and the first-ply failure load becomes larger, and at θ = 45° the ultimate failure load is 42.45% higher than the first-ply failure load.

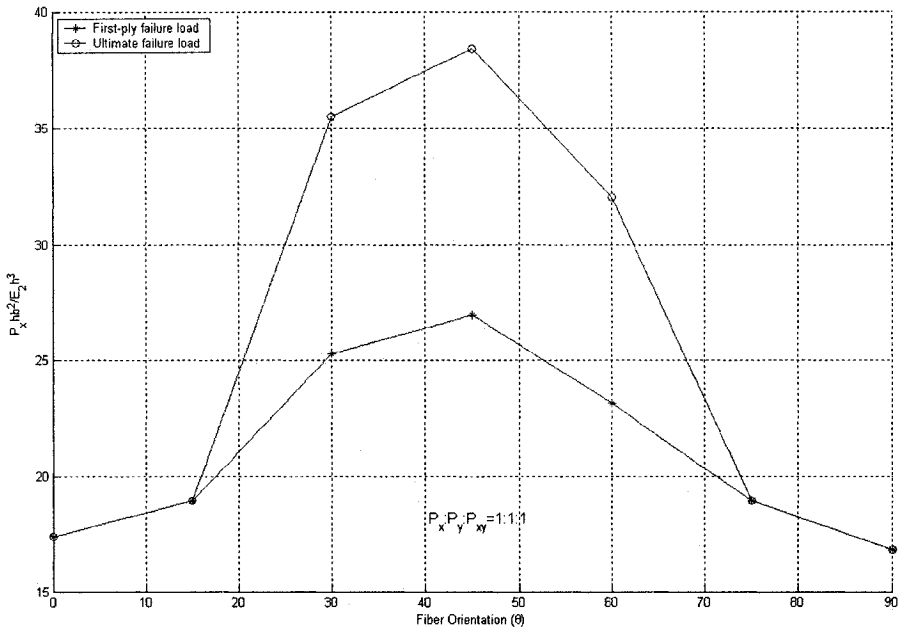

Figure 5.18 Variation of the first-ply and ultimate failure loads of the laminates with taper configuration F and with $(\pm\theta)_{4s}$ lay-up at the left end under bi-axial compression combined with in-plane positive shear

Figure 5.19 shows the variation of first-ply failure load of tapered laminates with $(\pm\theta)_{4s}$ lay-up at the left (thick) end under bi-axial compression combined with in-plane positive shear for all the taper configurations. The results show that the variations are un-symmetric about 45° fiber orientation. Peak values of the first-ply failure loads for taper configurations A, B, C, and F occur at 45° fiber orientation, and the peak value for taper configuration D occurs at 15° fiber orientation. The taper configuration F has the highest value of first-ply failure load for all fiber orientations, and the lowest value of first-ply failure load for 0° fiber orientation occurs for configuration A, whereas, for fiber orientations 15°, 30°, 45°, 60°, 70° and 90° fiber orientations, it occurs for configuration D.

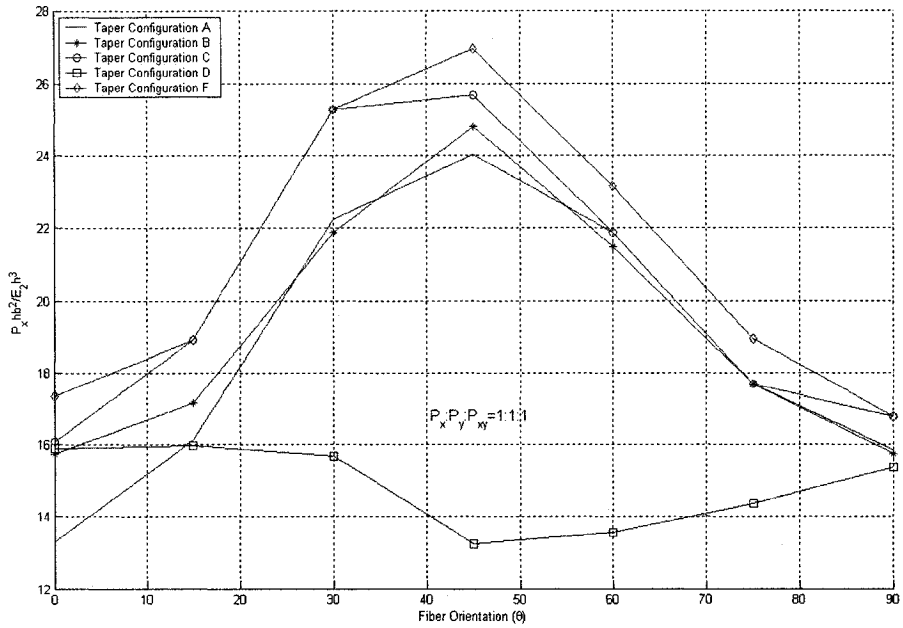

Figure 5.19 First-ply failure load of the laminates with $(\pm\theta)_{4s}$ lay-up at the left (thick) end under bi-axial compression combined with in-plane positive shear

Figure 5.20 shows the variation of ultimate failure load of tapered laminates with $(\pm\theta)_{4s}$ lay-up at the left (thick) end under bi-axial compression combined with in-plane positive shear for all the taper configurations. The results show that the variations are un-symmetric about 45° fiber orientation. Peak values of the ultimate failure loads for taper configurations A, B, C, and F occur at 45° fiber orientation, and the peak value for taper configuration D occurs at 15° fiber orientation. The taper configuration F has the highest value of ultimate failure load for all fiber orientations, and the lowest value of ultimate failure load for 0° fiber orientation occurs for configuration A, whereas, for fiber orientations 15°, 30°, 45°, 60°, 70° and 90° fiber orientations, it occurs for configuration D.

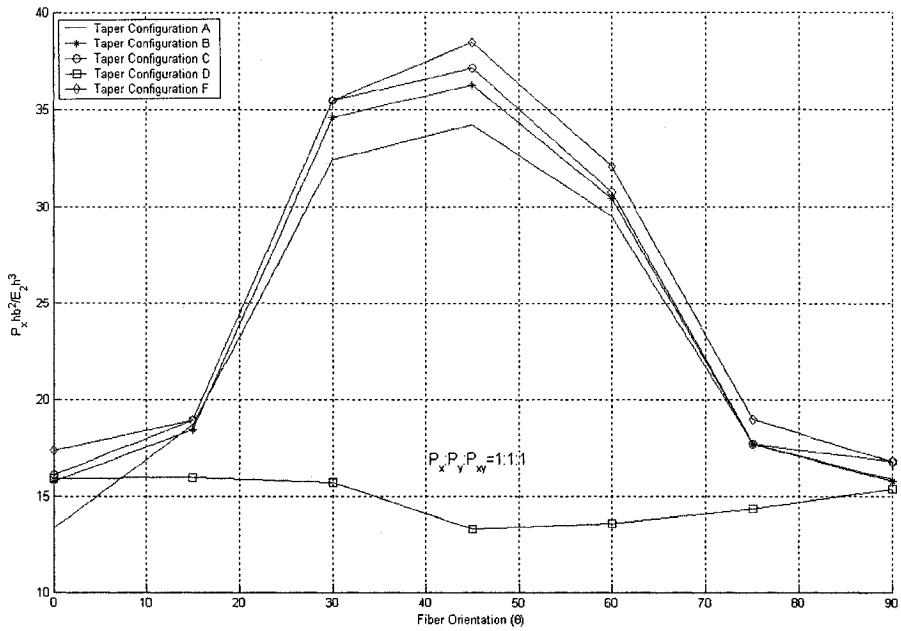

Figure 5.20 Ultimate failure load of the laminates with $(\pm\theta)_{4s}$ lay-up at the left (thick) end under bi-axial compression combined with in-plane positive shear

5.2.4 Influence of Uniform-thickness Section

As in the cases considered in sub-section 3.3.4 of Chapter 3, a thick section and a thin section of uniform-thickness laminate are added to the tapered laminate to study their influence on the progressive failure. Taper configuration B is considered for the tapered section of the plate that has $(\pm 45/0/90)_{2s}$ lay-up at the left end. The length of the plate is 0.4185 m. The length of the taper section, L_2, is 0.279 m. The sum of the lengths of thick and thin uniform-thickness sections, L_1+L_3, is 0.1395 m. The width of the plate is 0.279 m. The length of the thick section (L_1) and the length of the thin section (L_3) will be varied according to the length ratio, i.e. the ratio of the length of thick section (L_1) to the length of thin section (L_3). Figure 3.32 shows the plate with the length ratio that is equal to 1. The boundary condition shown in Figure 3.6 is considered.

Figure 5.21 shows the load versus maximum deflection curves of five tapered plates under the action of bi-axial compression combined with in-plane positive shear. Table 5.12 gives the buckling load, the first-ply failure load and the ultimate failure load for these laminates under the action of bi-axial compression combined with in-plane positive shear. The laminate with length ratio 2:1 is the best choice among these five laminates with respect to both the buckling load and the ultimate failure load, and the laminate with length ratio 1:1 is the best choice with respect to the first-ply failure load. It is also observed that for all the cases the first-ply failure corresponds to the transverse (matrix) failure, and the ultimate failure corresponds to the delamination failure as in the case of the plate with only the tapered section. Therefore, it is noted that the addition of uniform-thickness sections did not change the modes of failure. However, considerably more resistance to buckling, first-ply and ultimate failures is provided by the addition of uniform-thickness sections.

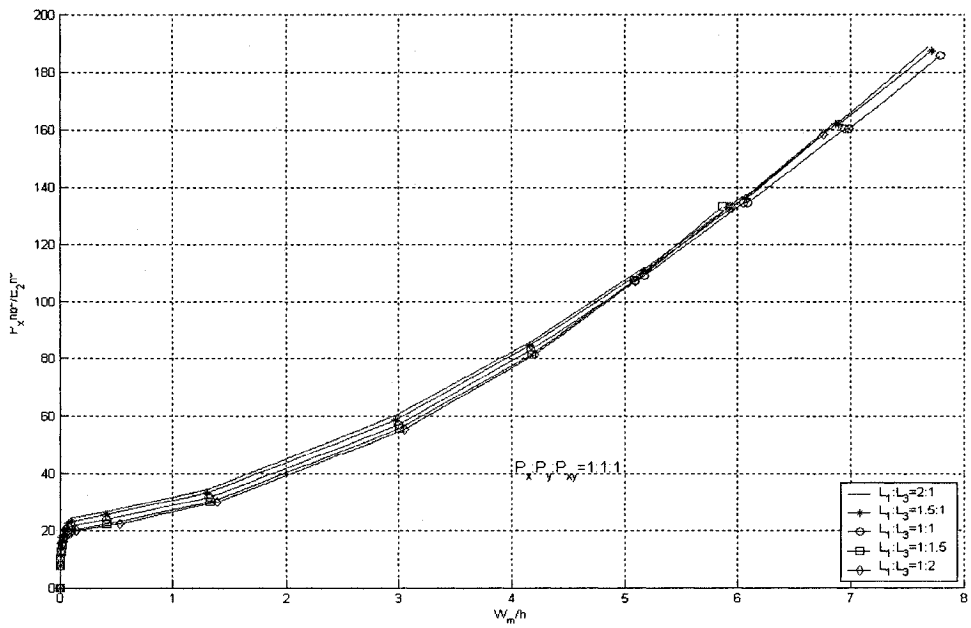

Figure 5.21 Load versus the maximum deflection curves of five tapered plates with different length ratios under the action of bi-axial compression combined with in-plane positive shear

Table 5.12 Failure data of five tapered plates with different length ratios under the action of bi-axial compression combined with in-plane positive shear

L1 :L3	Buckling Load ($P_x hb^2/E_2h^3$)	First-ply failure load ($P_x hb^2/E_2h^3$)	Ultimate failure load ($P_x hb^2/E_2h^3$)	$(W_m/h)^*$	Failure location (FL,FE) ♣	First-ply failure mode	Ultimate failure mode
2:1	25.644	111.768	189.015	5.173	1,50	T♠	D#
1.5:1	24.254	110.378	187.620	5.167	1,50	T	D
1:1	22.632	134.502	186.000	6.052	1,1	T	D
1:1.5	21.165	133.035	133.035	5.861	1,1	T	D
1:2	20.933	132.803	158.550	5.915	1,1	T	D

5.2.5 Influence of Boundary Condition

Except that the loading is bi-axial compression combined with in-plane positive shear, the study cases are the same as those given in sub-section 3.3.5 of Chapter 3. The influence of boundary condition on the progressive failure is studied. The results are compared in Figure 5.22 and Table 5.13.

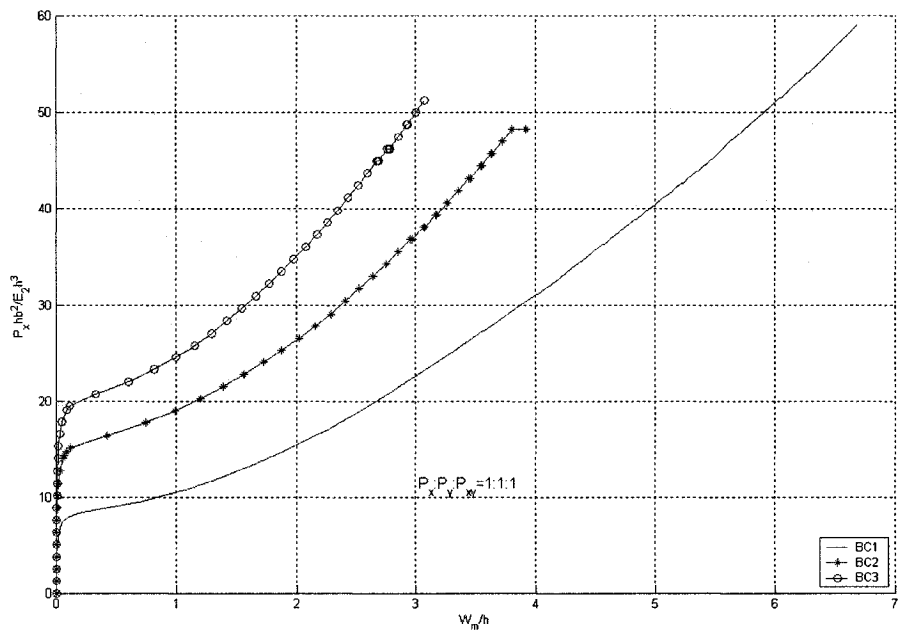

Figure 5.22 Load versus maximum deflection curves of the tapered laminate with taper configuration B corresponding to three boundary conditions under bi-axial compression combined with in-plane positive shear

Table 5.13 Failure data of the tapered laminate with taper configuration B corresponding to three boundary conditions under bi-axial compression combined with in-plane positive shear

BC	Buckling Load ($P_x hb^2/E_2h^3$)	First-ply failure load ($P_x hb^2/E_2h^3$)	Ultimate failure load ($P_x hb^2/E_2h^3$)	$(W_m/h)^*$	Failure location (FL,FE) ♣	First-ply failure mode	Ultimate failure mode
BC1	8.901	27.336	59.123	3.566	1,1	T♠	D#
BC2	17.039	36.746	48.188	2.959	1,40	T	D
BC3	21.360	44.883	51.240	2.679	1,40	T	D

From Figure 5.22 and Table 5.13, it is observed that the first-ply failure load corresponds to the transverse (matrix) failure, and the ultimate failure corresponds to the delamination failure for all the three boundary conditions. The first-ply failure load is found to be about 3.1 times the buckling load for BC1 boundary condition, 2.2 times for BC2 boundary condition, and 2.1 times for BC3 boundary condition, whereas, the ultimate failure load is about 6.6 times the buckling load for BC1 boundary condition, 2.8 times the buckling load for BC2 boundary condition, and 2.4 times for BC3 boundary condition. The ultimate failure load is about 2.2 times the first-ply failure load for BC1 boundary condition, 1.3 times for BC2 boundary condition, and 1.1 times for BC3 boundary condition. The absolute maximum value of the maximum transverse displacement W_m just before ultimate failure is found to occur in the case of boundary condition BC1 and is equal to 6.68h. The absolute minimum value of the maximum transverse displacement W_m just before the ultimate failure is found to occur in the case of boundary condition BC3 and is equal to 3.10h. It is also noted that the higher the flexural rigidity is, the higher are the buckling load, the first-ply failure load and stiffness for a fixed value of maximum transverse displacement. However, this is not the case for ultimate failure load.

5.2.6 Influence of Load Ratio

The tapered laminate with taper configuration B and with LC(2) lay-up configuration is considered. The length, the width and the boundary condition of the plate are the same as that given in sub-section 5.2.1. The ratio of P_x to P_y is set to a value of 1, and the value of P_{xy} is varied. Figure 5.23 shows the load versus maximum deflection curves for the laminate under the action of bi-axial compression combined with in-plane positive shear for different load ratio values (P_x : P_y =1:1, P_{xy} is changed). Table 5.14 gives the buckling load, the first-ply failure load and the ultimate failure load for all the cases.

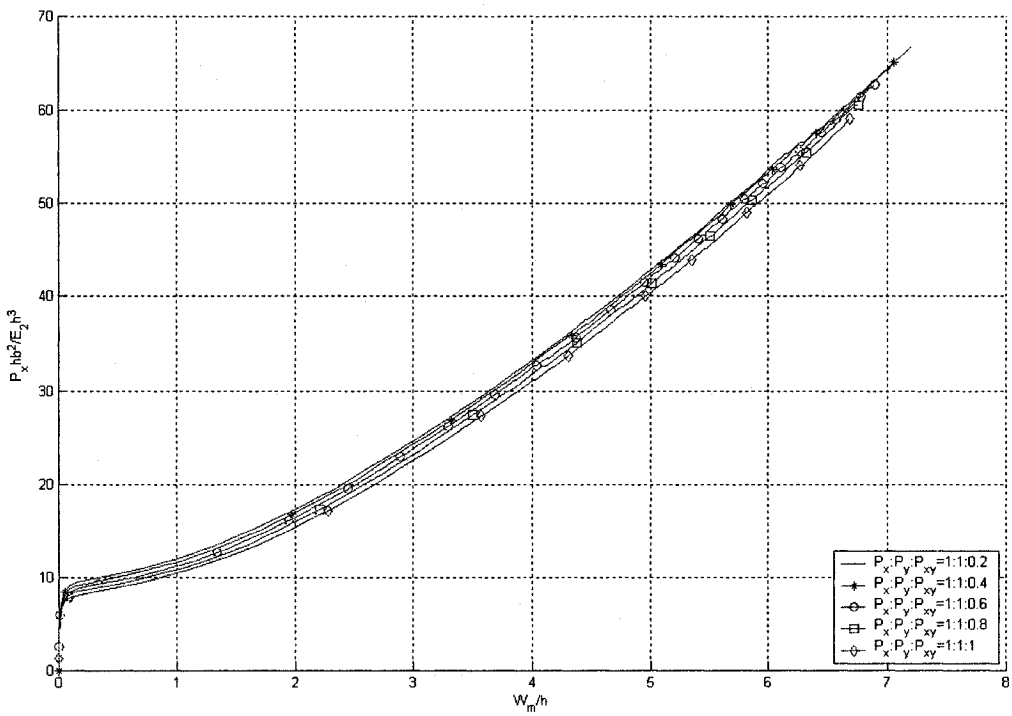

Figure 5.23 Load versus maximum deflection curves of the LC(2) laminate with taper configuration B under bi-axial compression combined with in-plane positive shear for various load ratio values with varying Pxy

Table 5.14 Failure data of the LC(2) laminate with taper configuration B under bi-axial compression combined with in-plane positive shear for various load ratio values with varying P_{xy}

Load Ratio P_x:P_y:P_{xy}	Buckling Load ($P_x hb^2/E_2h^3$)	First-ply failure load ($P_x hb^2/E_2h^3$)	Ultimate failure load ($P_x hb^2/E_2h^3$)	$(W_m/h)^*$	Failure location (FL,FE) ♣	First-ply failure mode	Ultimate failure mode
1:1:0.2	10.172	37.508	66.752	4.448	1,40	T♠	D#
1:1:0.4	9.791	35.855	65.099	4.310	1,40	T	D
1:1:0.6	9.536	32.634	62.726	4.018	1,40	T	D
1:1:0.8	9.027	30.006	60.521	3.793	1,40	T	D
1:1:1	8.901	27.336	59.123	3.566	1,40	T	D

Form Figure 5.23 and Table 5.14, it is observed that with increasing proportion of in-plane positive shear loading in the combined loading, the first-ply failure load and the ultimate failure load are not changed too much. It is also observed that the first-ply failure load corresponds to the transverse (matrix) failure, and the ultimate failure corresponds to the delamination in all the cases. Locations corresponding to the first-ply failure lie near the thin end of the plate and at the outermost bottom layer.

Now, the value of P_{xy} is fixed, and the values of P_x and P_y are changed with 1:1 ratio. Figure 5.24 shows the load versus maximum deflection curves for the laminate under the action of bi-axial compression combined with in-plane positive shear for different load ratio values. Table 5.15 gives the buckling load, the first-ply failure load and the ultimate failure load for all the cases. It is observed that with increasing proportion of bi-axial compression in the combined loading, the first-ply failure load and the ultimate failure load decrease monotonically. At P_x: P_y: P_{xy}=1:1:1, the percentage loss (compared to the case P_x: P_y: P_{xy} =0.2:0.2:1) in the first-ply failure load and ultimate failure load are respectively, 40.28 and 45.93. It is also observed that the first-ply failure load corresponds to the transverse (matrix) failure, and the ultimate failure corresponds to the

delamination in all the cases. Locations corresponding to the first-ply failure lie near the thick end of the plate and at the outermost bottom layer.

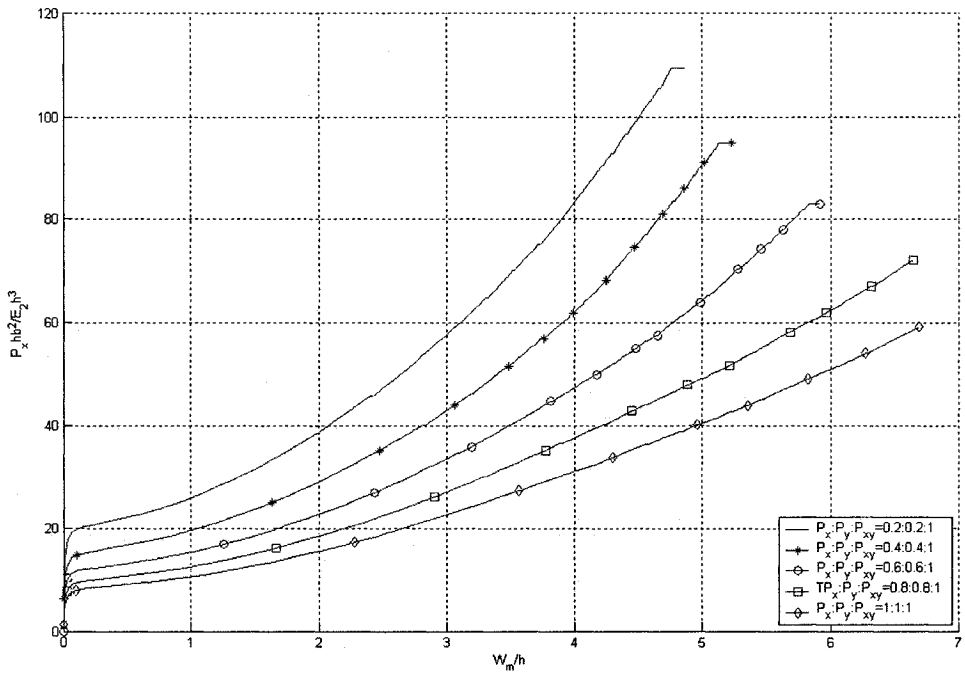

Figure 5.24 Load versus maximum deflection curves of the LC(2) laminate with taper configuration B under bi-axial compression combined with in-plane positive shear for various load ratio values with varying P_x and P_y

Table 5.15 Failure data of the LC(2) laminate with taper configuration B under bi-axial compression combined with in-plane positive shear for various load ratio values with varying P_x and P_y

Load Ratio $P_x:P_y:P_{xy}$	Buckling Load (P_xhb^2/E_2h^3)	First-ply failure load (P_xhb^2/E_2h^3)	Ultimate failure load (P_xhb^2/E_2h^3)	$(W_m/h)^*$	Failure location (FL,FE) ♣	First-ply failure mode	Ultimate failure mode
0.2:0.2:1	20.979	45.773	109.346	2.401	1,1	T♠	D#
0.4:0.4:1	16.656	40.178	94.851	2.811	1,1	T	D
0.6:0.6:1	12.333	34.584	82.899	3.078	1,1	T	D
0.8:0.8:1	10.299	30.006	71.964	3.289	1,1	T	D
1:1:1	8.901	27.336	59.123	3.566	1,1	T	D

The ratio of P_{xy} to P_y is set to a value of 1, and the value of P_x is changed. Figure 5.25 shows the load versus maximum deflection curves for the laminate under the action of bi-axial compression combined with in-plane positive shear for different load ratio values (P_{xy}: P_y =1:1, P_x is changed). Table 5.16 gives the buckling load, the first-ply failure load and the ultimate failure load for these cases. It is observed that with increasing proportion of bi-axial compression in the combined loading, the first-ply failure load and the ultimate failure load decrease monotonically. At P_x: P_y: P_{xy} =1:1:1, the percentage loss (compared to the case P_x: P_y: P_{xy} =0.2:1:1) in the first-ply failure load and ultimate failure load are respectively, 15.13 and 26.58. It is also observed that the first-ply failure load corresponds to the transverse (matrix) failure, and the ultimate failure corresponds to the delamination in all the cases. Locations corresponding to the first-ply failure lie near the thick end of the plate and at the outermost bottom layer.

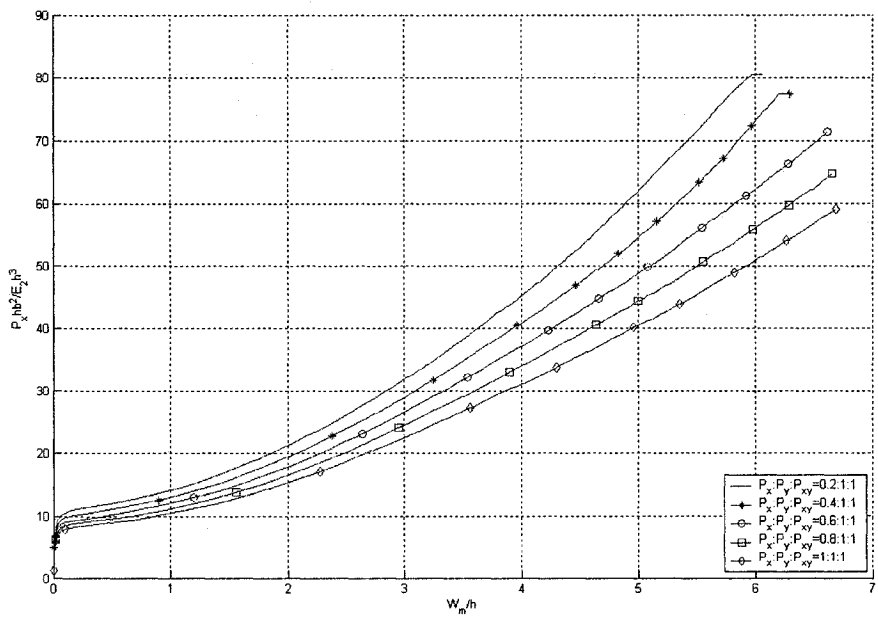

Figure 5.25 Load versus maximum deflection curves of the LC(2) laminate with taper configuration B under bi-axial compression combined with in-plane positive shear for various load ratio values with varying P_x

Table 5.16 Failure data of the LC(2) laminate with taper configuration B under bi-axial compression combined with in-plane positive shear for various load ratio values with varying P_x

Load Ratio $P_x:P_y:P_{xy}$	Buckling Load ($P_x hb^2/E_2h^3$)	First-ply failure load ($P_x hb^2/E_2h^3$)	Ultimate failure load ($P_x hb^2/E_2h^3$)	$(W_m/h)^*$	Failure location (FL,FE) ♣	First-ply failure mode	Ultimate failure mode
0.2:1:1	11.655	32.210	80.526	3.033	1,1	T♠	D#
0.4:1:1	10.680	31.659	77.432	3.234	1,1	T	D
0.6:1:1	9.791	29.498	71.456	3.285	1,1	T	D
0.8:1:1	9.410	29.117	64.718	3.499	1,1	T	D
1:1:1	8.901	27.336	59.123	3.566	1,1	T	D

5.3 Parametric Study on Bi-axial Compression Combined with In-plane Negative Shear

5.3.1 Influence of Taper Configuration

Figure 5.26 shows the load versus the maximum deflection curves of the five laminates all with LC(1) lay-up configuration and each with a different taper configuration under the action of bi-axial compression combined with in-plane negative shear. Table 5.17 gives the buckling load, the first-ply failure load and the ultimate failure load for these laminates.

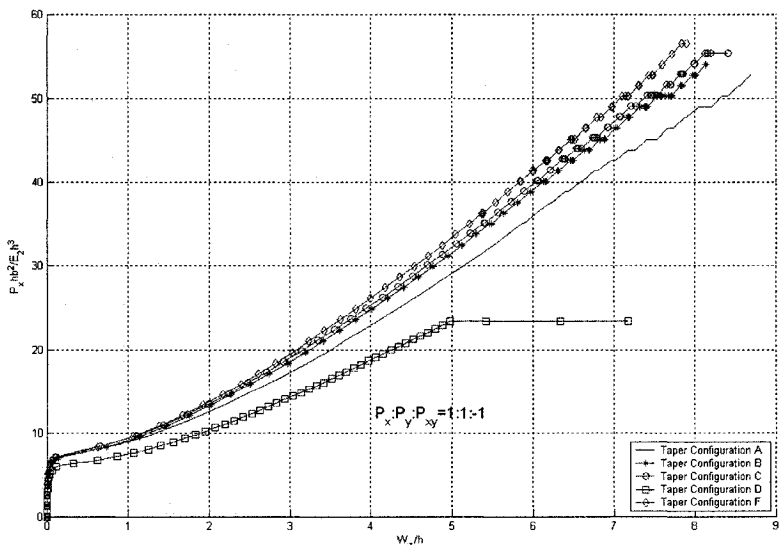

Figure 5.26 Load versus the maximum deflection curves of the laminates with LC(1) lay-up configuration for five taper configurations under bi-axial compression combined with in-plane negative shear

Table 5.17 Failure data of the laminates with LC(1) lay-up configuration for five taper configurations under bi-axial compression combined with in-plane negative shear

Taper	Buckling Load ($P_x hb^2/E_2h^3$)	First-ply failure load ($P_x hb^2/E_2h^3$)	Ultimate failure load ($P_x hb^2/E_2h^3$)	$(W_m/h)^*$	Failure location (FL,FE) ♣	First-ply failure mode	Ultimate failure mode
A	7.609	34.965	52.766	5.864	1,8	T♠	D#
B	7.619	34.965	54.038	5.470	1,8	T	D
C	7.629	35.093	55.436	5.396	1,8	T	D
D	6.570	23.310	23.310	5.396	1,8	T	D
F	7.757	36.237	56.582	5.371	1,8	T	D

For lay-up configuration LC(1), the first-ply failure load is found to be about 4.6 times the buckling load for taper configurations A and B, 4.5 times for configuration C, 3.5 times for configuration D, and 4.7 times for configuration F. The ultimate failure load is about 7.1 times the buckling load for configurations A, B and C, 3.5 times for configuration D, and 6.9 times for configuration F. The ultimate failure load is about 1.5 times the first-ply failure load for configurations A, B and F, 1.6 times for configuration C, and 1.0 time for configuration D.

Figure 5.27 shows the load versus the maximum deflection curves of the five laminates all with LC(2) lay-up configuration and each with a different taper configuration under the action of bi-axial compression combined with in-plane negative shear. Table 5.18 gives the buckling load, the first-ply failure load and the ultimate failure load for these laminates.

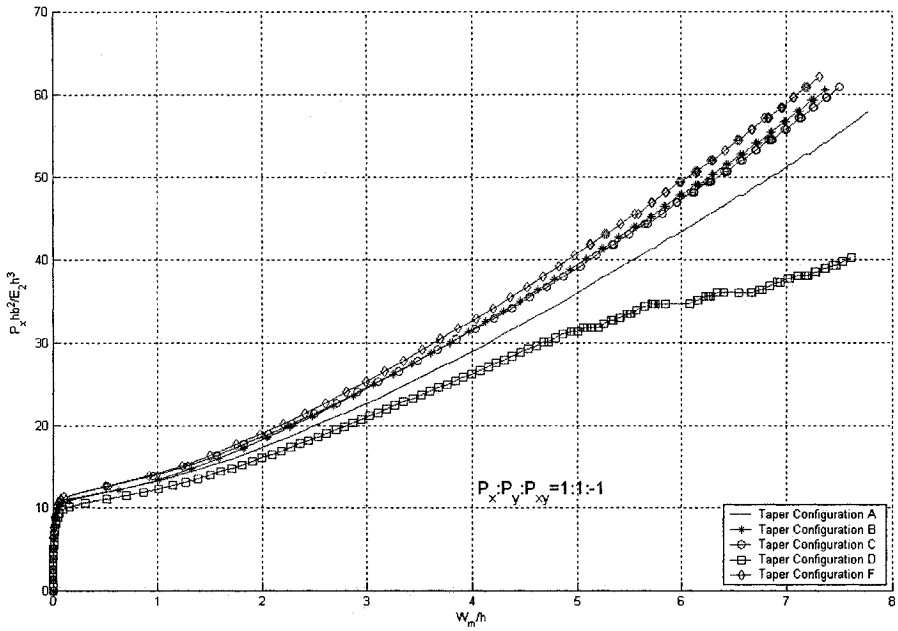

Figure 5.27 Load versus maximum deflection curves of the laminates with LC(2) lay-up configuration for five taper configurations under bi-axial compression combined with in-plane negative shear

Table 5.18 Failure data of the laminates with LC(2) lay-up configuration for five taper configurations under bi-axial compression combined with in-plane negative shear

Taper	Buckling Load (P_xhb^2/E_2h^3)	First-ply failure load (P_xhb^2/E_2h^3)	Ultimate failure load (P_xhb^2/E_2h^3)	$(W_m/h)^*$	Failure location (FL,FE) ♣	First-ply failure mode	Ultimate failure mode
A	11.571	40.178	57.978	5.542	10,8	T♠	D#
B	11.571	41.450	60.521	5.237	10,8	T	D
C	13.223	41.831	60.903	5.337	10,8	T	D
D	10.808	30.092	40.263	4.683	1,40	T	D
F	13.223	41.831	62.174	5.120	10,8	T	D

For lay-up configuration LC(2), the first-ply failure load is found to be about 3.5 times the buckling load for taper configuration A, 3.6 times for configuration B, 3.2 times for configurations C and F, and 2.8 times for configuration D. The ultimate failure load is about 5.0 times the buckling load for configuration A, 5.2 times for configuration B, 4.6 times for configuration C, 3.7 times for configuration D, and 4.7 times for configuration

D. The ultimate failure load is about 1.4 times the first-ply failure load for configuration A, 1.5 times for configurations B, C and F, and 1.3 times for configuration D.

In order to illustrate the positive deflection of the plate under bi-axial compression combined with in-plane negative shear, a typical deformed configuration is given. Figure 5.28 shows the deformed configuration of the laminate with LC(2) lay-up configuration and with taper configuration B under bi-axial compression combined with in-plane negative shear. It is observed that the entire laminate undergoes positive (upward) deflection.

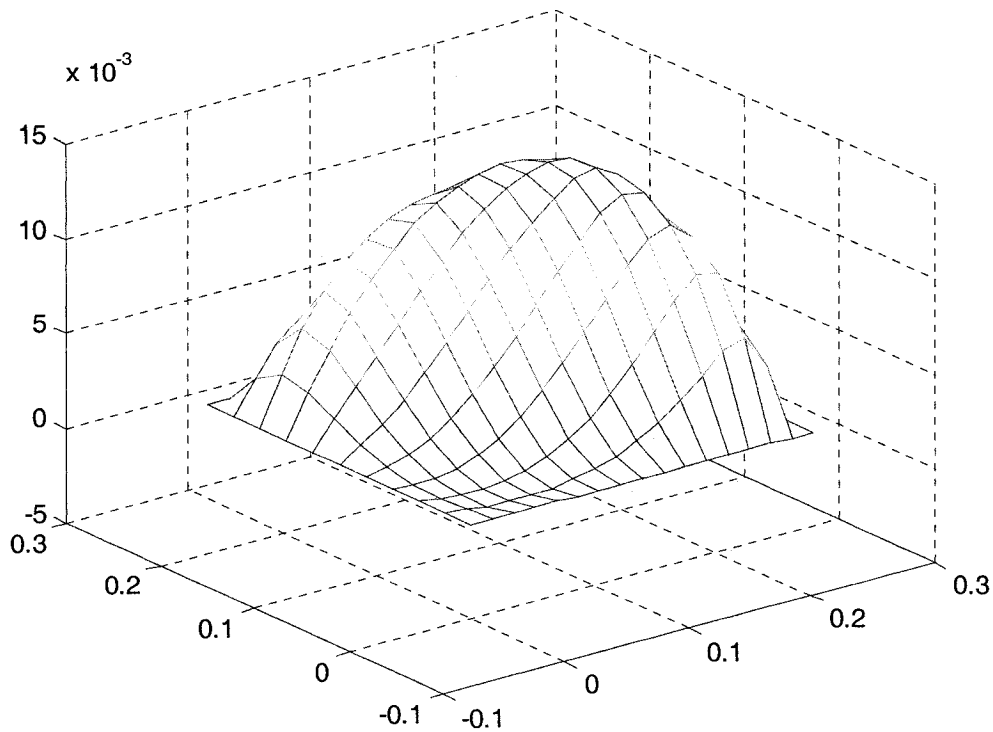

Figure 5.28 The deformed configuration of the laminate with LC(2) lay-up configuration and with taper configuration B under bi-axial compression combined with in-plane negative shear

Figure 5.29 shows the load versus the maximum deflection curves of the five laminates all with LC(3) lay-up configuration and each with a different taper configuration under the action of bi-axial compression combined with in-plane negative shear. Table 5.19

gives the buckling load, the first-ply failure load and the ultimate failure load for these laminates.

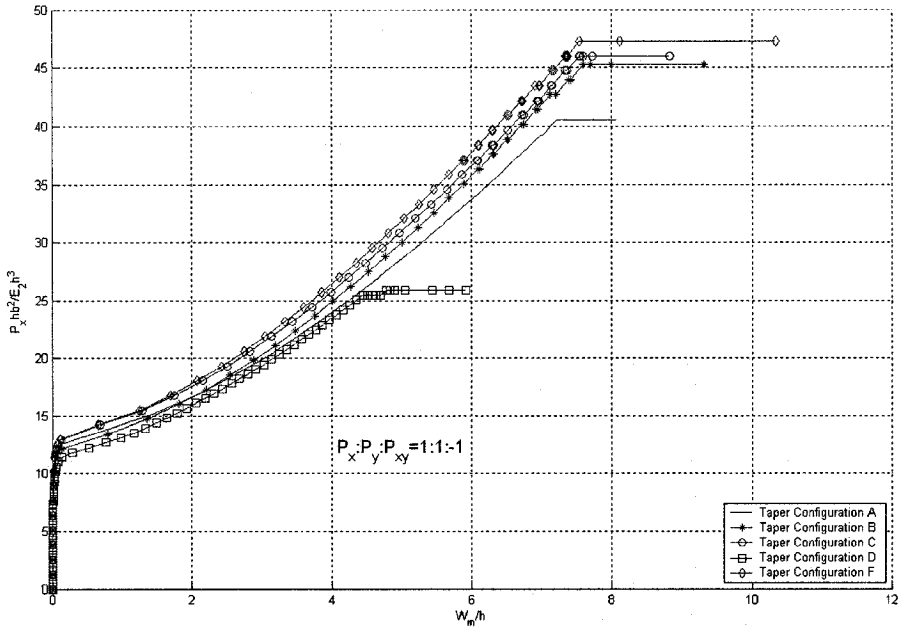

Figure 5.29 Load versus maximum deflection curves of the laminates with LC(3) lay-up configuration for five taper configurations under bi-axial compression combined with in-plane negative shear

Table 5.19 Failure data of the laminates with LC(3) lay-up configuration for five taper configurations under bi-axial compression combined with in-plane negative shear

Taper	Buckling Load (P_xhb^2/E_2h^3)	First-ply failure load (P_xhb^2/E_2h^3)	Ultimate failure load (P_xhb^2/E_2h^3)	$(W_m/h)^*$	Failure location (FL,FE) ♣	First-ply failure mode	Ultimate failure mode
A	13.223	35.474	40.560	6.317	10,8	T♠	D#
B	12.842	36.363	45.264	6.100	10,8	T	D
C	14.876	37.127	46.026	6.077	10,8	T	D
D	12.080	25.430	25.853	4.445	1,40	T	D
F	14.876	37.127	47.298	5.884	10,8	T	D

For lay-up configuration LC(3), the first-ply failure load is found to be about 2.7 times the buckling load for taper configuration A, 2.8 times for configuration B, 2.5 times for configurations C and F, and 2.1 times for configuration D. The ultimate failure load is about 3.1 times the buckling load for configurations A and C, 3.5 times for configuration

B, 2.1 times for configuration D, and 3.2 times for configuration F. The ultimate failure load is about 1.1 times the first-ply failure load for configuration A, 1.2 times for configurations B and C, 1.0 time for configuration D, and 1.3 times for configuration F. Figure 5.30 shows the load versus the maximum deflection curves of the five laminates all with LC(4) lay-up configuration and each with a different taper configuration under the action of bi-axial compression combined with in-plane negative shear. Table 5.20 gives the buckling load, the first-ply failure load and the ultimate failure load for these laminates.

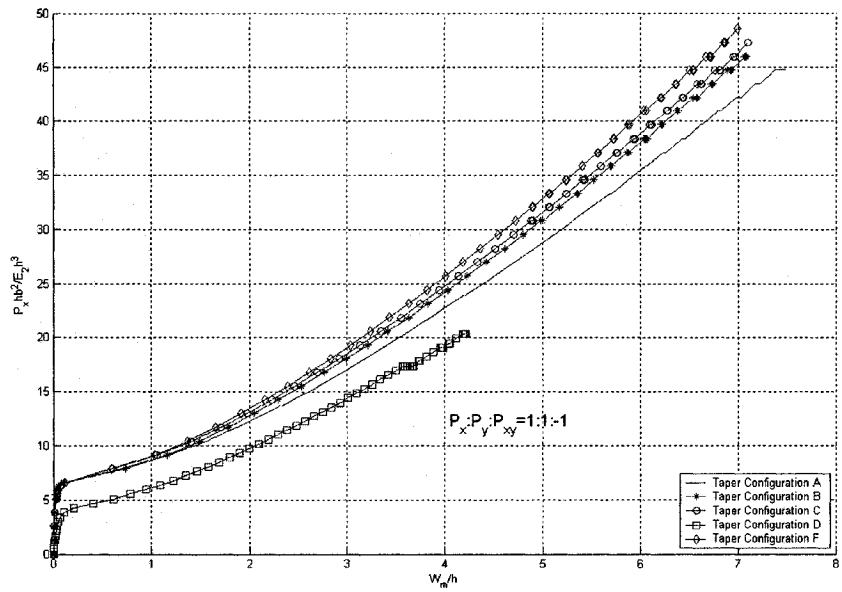

Figure 5.30 Load versus maximum deflection curves of the laminates with LC(4) lay-up configuration for five taper configurations under bi-axial compression combined with in-plane negative shear

Table 5.20 Failure data of the laminates with LC(4) lay-up configuration for five taper configurations under bi-axial compression combined with in-plane negative shear

Taper	Buckling Load (P_xhb^2/E_2h^3)	First-ply failure load (P_xhb^2/E_2h^3)	Ultimate failure load (P_xhb^2/E_2h^3)	$(W_m/h)^*$	Failure location (FL,FE) ♣	First-ply failure mode	Ultimate failure mode
A	7.248	29.498	44.756	5.110	10,8	T♠	D#
B	7.248	30.770	46.026	4.987	10,8	T	D
C	7.248	30.770	47.298	4.888	10,8	T	D
D	4.874	17.376	20.343	3.570	10,8	T	D
F	7.248	32.040	48.570	4.895	10,8	T	D

For lay-up configuration LC(4), the first-ply failure load is found to be about 4.1 times the buckling load for taper configuration A, 4.2 times for configurations B and C, 3.6 times for configuration D, and 4.4 times for configuration F. The ultimate failure load is about 6.2 times the buckling load for configuration A, 6.4 times for configuration B, 6.5 times for configuration C, 4.2 times for configuration D, and 6.7 times for configuration F. The ultimate failure load is about 1.5 times the first-ply failure load for configurations A, B, C and F, and 1.2 times for configuration D.

Figure 5.31 shows the load versus the maximum deflection curves of the five laminates all with LC(5) lay-up configuration and each with a different taper configuration under the action of bi-axial compression combined with in-plane negative shear. Table 5.21 gives the buckling load, the first-ply failure load and the ultimate failure load for these laminates.

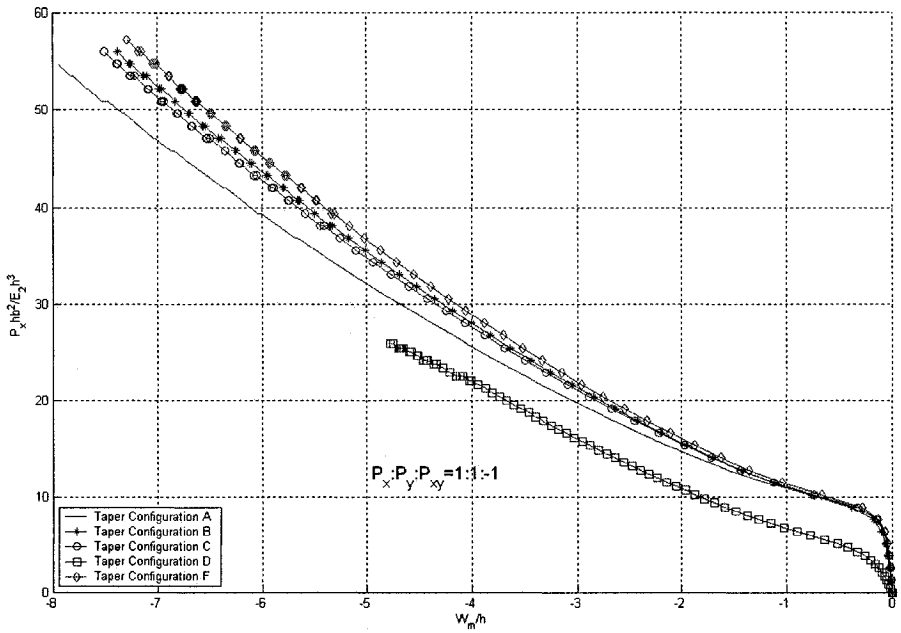

Figure 5.31 Load versus maximum deflection curves of the laminates with LC(5) lay-up configuration for five taper configurations under bi-axial compression combined with in-plane negative shear

Table 5.21 Failure data of the laminates with LC(5) lay-up configuration for five taper configurations under bi-axial compression combined with in-plane negative shear

Taper	Buckling Load (P_xhb^2/E_2h^3)	First-ply failure load (P_xhb^2/E_2h^3)	Ultimate failure load (P_xhb^2/E_2h^3)	$(W_m/h)^*$	Failure location (FL,FE) ♣	First-ply failure mode	Ultimate failure mode
A	9.536	36.872	54.672	-5.676	1,8	T♠	D#
B	9.536	38.144	55.944	-5.323	1,8	T	D
C	9.536	38.144	55.944	-5.410	1,8	T	D
D	5.721	22.038	25.853	-4.009	10,16	T	D
F	9.536	39.416	57.216	-5.311	1,8	T	D

For lay-up configuration LC(5), the first-ply failure load is found to be about 3.9 times the buckling load for taper configurations A and D, 4.0 times for configurations B and C, and 4.1 times for configuration F. The ultimate failure load is about 5.7 times the buckling load for configuration A, 5.9 times for configurations B and C, 4.5 times for configuration D, and 6.0 times for configuration F. The ultimate failure load is about 1.5

times the first-ply failure load for configurations A, B, C and F, and 1.2 times for configuration D.

In order to illustrate the positive deflection of the plate under bi-axial compression combined with in-plane negative shear, a typical deformed configuration is given. Figure 5.32 shows the deformed configuration of the laminate with LC(5) lay-up configuration and with taper configuration B under bi-axial compression combined with in-plane negative shear. It is observed that the entire laminate undergoes negative (downward) deflection.

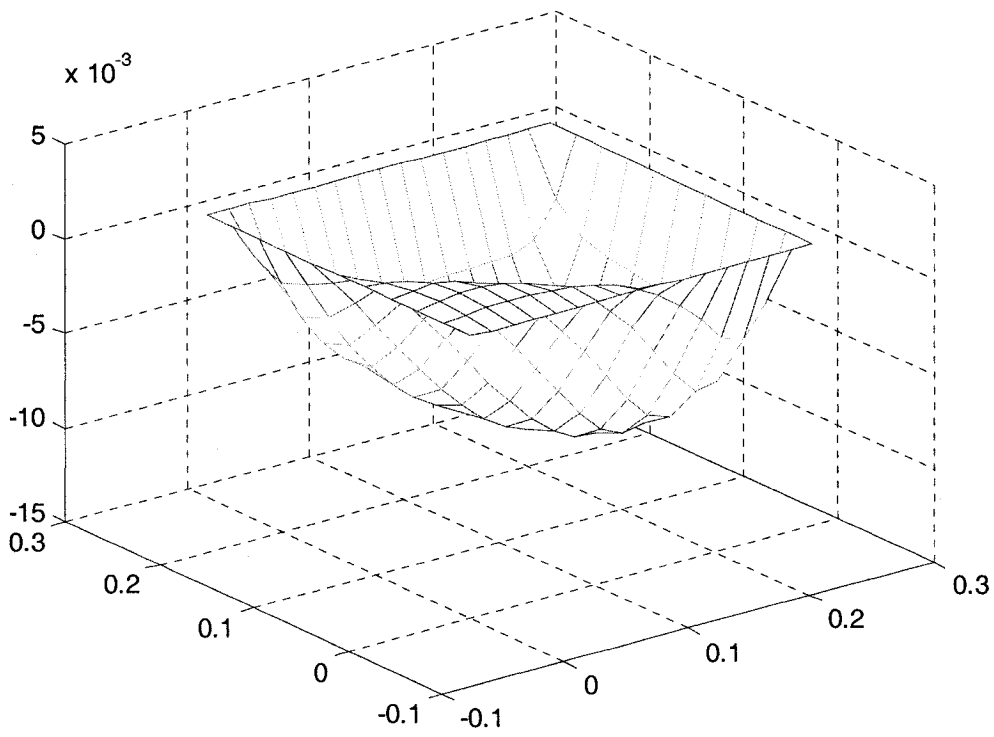

Figure 5.32 The deformed configuration of the laminate with LC(5) lay-up configuration and with taper configuration B under bi-axial compression combined with in-plane negative shear

Figure 5.33 shows the load versus the maximum deflection curves of the five laminates all with LC(6) lay-up configuration and each with a different taper configuration under the action of bi-axial compression combined with in-plane negative shear. Table 5.22 gives the buckling load, the first-ply failure load and the ultimate failure load for these laminates.

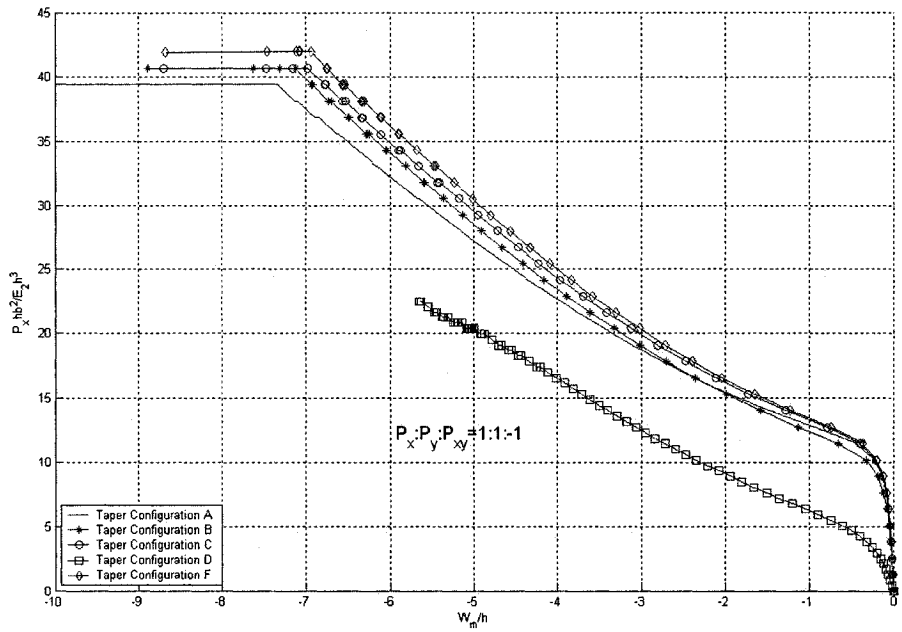

Figure 5.33 Load versus maximum deflection curves of the laminates with LC(6) lay-up configuration for five taper configurations under bi-axial compression combined with in-plane negative shear

Table 5.22 Failure data of the laminates with LC(6) lay-up configuration for five taper configurations under bi-axial compression combined with in-plane negative shear

Taper	Buckling Load ($P_x hb^2/E_2h^3$)	First-ply failure load ($P_x hb^2/E_2h^3$)	Ultimate failure load ($P_x hb^2/E_2h^3$)	$(W_m/h)^*$	Failure location (FL,FE) ♣	First-ply failure mode	Ultimate failure mode
A	13.350	30.515	39.416	-5.652	10,8	T♠	D#
B	12.080	31.787	40.686	-5.588	10,8	T	D
C	13.350	31.787	40.686	-5.411	10,8	T	D
D	6.570	17.376	22.463	-4.207	10,8	T	D
F	13.350	33.059	41.958	-5.455	10,8	T	D

For lay-up configuration LC(6), the first-ply failure load is found to be about 2.3 times the buckling load for taper configuration A, 2.6 times for configurations B and D, 2.4 times for configuration C, and 2.5 times for configuration F. The ultimate failure load is about 3.0 times the buckling load for configurations A and C, 3.4 times for configurations B and D, and 3.1 times for configuration F. The ultimate failure load is about 1.3 times the first-ply failure load for configurations A, B, C, D and F.

Summary

From Figures 5.26 – 5.33 and Tables 5.17 – 5.22, the following general observations are also made.

1. Among all the six lay-up configurations, the taper configuration F (Mid-plane taper) is the strongest one with respect to the buckling load, first-ply failure load and the ultimate failure load. However, taper configuration F is not easy to manufacture compared to other taper configurations. Considering this, the next strongest taper configuration is identified. For the lay-up configurations LC(1), LC(2), LC(3), LC(4) and LC(6), the taper configuration C (Overlapping dropped plies) is the best choice among all taper configurations considering the first-ply failure load, the ultimate failure load and the buckling load. For the lay-up configuration LC(5), taper configuration B and C are same in terms of the buckling load, the first-ply failure load buckling load and the ultimate failure load, so either can be the best choice.
2. Only for the laminate with LC(1) lay-up configuration for the taper configuration D (Continuous plies interspersed), the first-ply failure load and the ultimate failure load are the same. For all other cases, residual strength exits after the first-ply failure until ultimate failure.

3. For lay-up configurations LC(1), LC(2), LC(3) and LC(4), the maximum deflections are all positive, that is, upward. For lay-up configurations LC(5) and LC(6), the maximum deflections are all negative, that is, downward.
4. For all six lay-up configurations considered, Locations corresponding to the first-ply failure lie near the thin end of the plate and at the outermost layer.

5.3.2 Influence of Lay-up Configuration

Figure 5.34 shows the load versus maximum deflection curves of the six laminates all with taper configuration A and each with a different lay-up configuration under the action of bi-axial compression combined with in-plane negative shear. Table 5.23 gives the buckling load, the first-ply failure load and the ultimate failure load for these laminates.

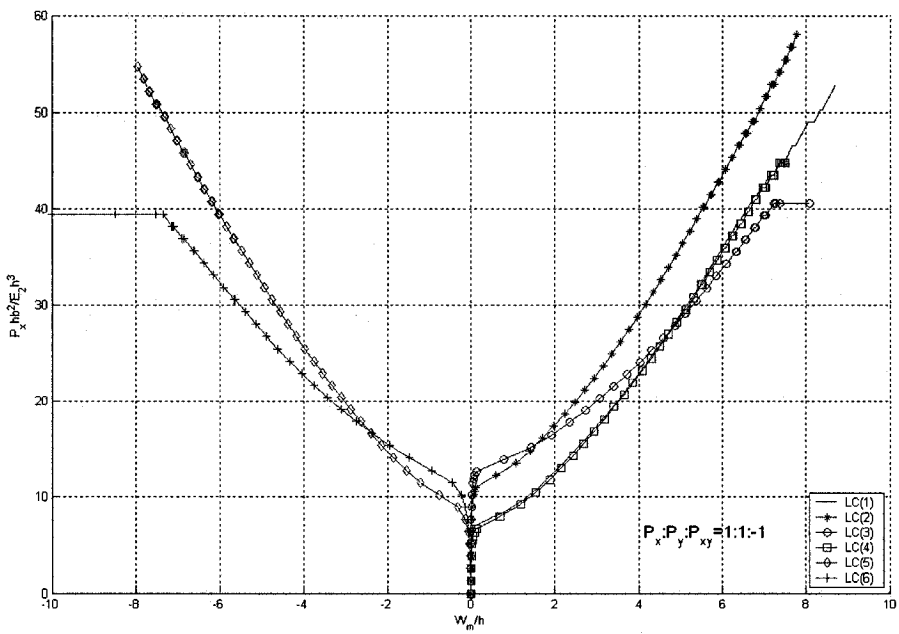

Figure 5.34 Load versus maximum deflection curves of the laminates with taper configuration A for all the six lay-up configurations under bi-axial compression combined with in-plane negative shear

Table 5.23 Failure data of the laminates with taper configuration A for all the six lay-up configurations under bi-axial compression combined with in-plane negative shear

Lay-up	Buckling Load ($P_x hb^2/E_2h^3$)	First-ply failure load ($P_x hb^2/E_2h^3$)	Ultimate failure load ($P_x hb^2/E_2h^3$)	$(W_m/h)^*$	Failure location (FL,FE) ♣	First-ply failure mode	Ultimate failure mode
LC(1)	7.609	34.965	52.766	5.864	1,8	T♠	D#
LC(2)	11.571	40.178	57.978	5.542	10,8	T	D
LC(3)	13.223	35.474	40.560	6.317	10,8	T	D
LC(4)	7.248	29.498	44.756	5.110	10,8	T	D
LC(5)	9.536	36.872	54.672	-5.676	1,8	T	D
LC(6)	13.350	30.515	39.416	-5.652	10,8	T	D

For taper configuration A, the lay-up configuration LC(6) is the best choice among all the six lay-up configurations with respect to the buckling load, and lay-up configuration LC(2) is the best choice with respect to both the first-ply failure load and the ultimate failure load.

Figure 5.35 shows the load versus maximum deflection curves of the six laminates all with taper configuration B and each with a different lay-up configuration under the action of bi-axial compression combined with in-plane negative shear. Table 5.24 gives the buckling load, the first-ply failure load and the ultimate failure load for these laminates.

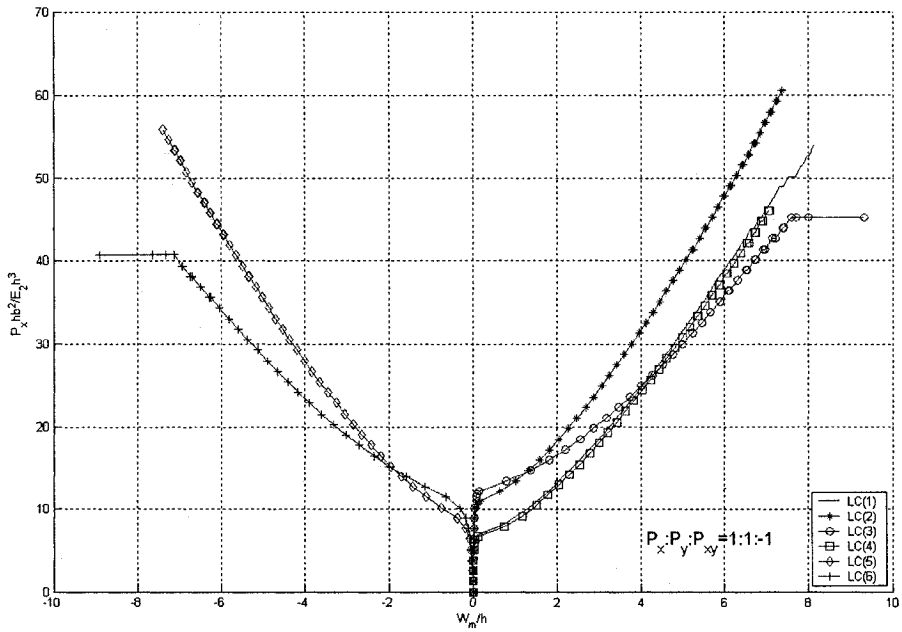

Figure 5.35 Load versus maximum deflection curves of the laminates with taper configuration B for all the six lay-up configurations under bi-axial compression combined with in-plane negative shear

Table 5.24 Failure data of the laminates with taper configuration B for all the six lay-up configurations under bi-axial compression combined with in-plane negative shear

Lay-up	Buckling Load (P_xhb^2/E_2h^3)	First-ply failure load (P_xhb^2/E_2h^3)	Ultimate failure load (P_xhb^2/E_2h^3)	$(W_m/h)^*$	Failure location (FL,FE) ♣	First-ply failure mode	Ultimate failure mode
LC(1)	7.619	34.965	54.038	5.470	1,8	T♠	D#
LC(2)	11.571	41.450	60.521	5.237	10,8	T	D
LC(3)	12.842	36.363	45.264	6.100	10,8	T	D
LC(4)	7.248	30.770	46.026	4.987	10,8	T	D
LC(5)	9.536	38.144	55.944	-5.323	1,8	T	D
LC(6)	12.080	31.787	40.686	-5.588	10,8	T	D

For taper configuration B, the lay-up configuration LC(3) is the best choice among all the six lay-up configurations with respect to the buckling load, and lay-up configuration LC(2) is the best choice with respect to both the first-ply failure load and the ultimate failure load.

Figure 5.36 shows the load versus maximum deflection curves of the six laminates all with taper configuration C and each with a different lay-up configuration under the action of bi-axial compression combined with in-plane negative shear. Table 5.25 gives the buckling load, the first-ply failure load and the ultimate failure load for these laminates.

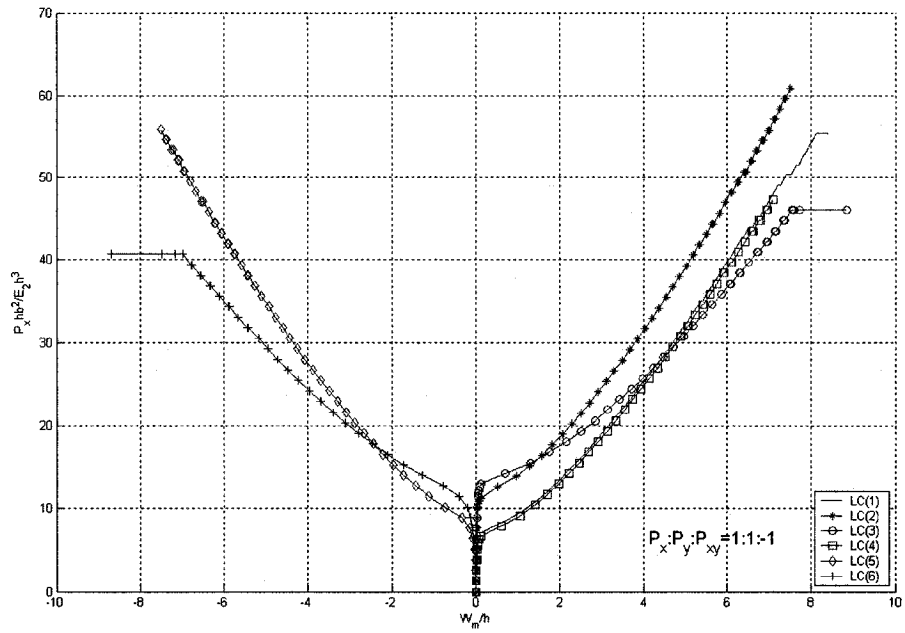

Figure 5.36 Load versus maximum deflection curves of the laminates with taper configuration C for all the six lay-up configurations under bi-axial compression combined with in-plane negative shear

Table 5.25 Failure data of the laminates with taper configuration C for all the six lay-up configurations under bi-axial compression combined with in-plane negative shear

Lay-up	Buckling Load (P_xhb^2/E_2h^3)	First-ply failure load (P_xhb^2/E_2h^3)	Ultimate failure load (P_xhb^2/E_2h^3)	$(W_m/h)^*$	Failure location (FL,FE) ♣	First-ply failure mode	Ultimate failure mode
LC(1)	7.757	35.093	55.436	5.396	1,8	T♠	D#
LC(2)	13.223	41.831	60.903	5.337	10,8	T	D
LC(3)	14.876	37.127	46.026	6.077	10,8	T	D
LC(4)	7.248	30.770	47.298	4.888	10,8	T	D
LC(5)	9.536	38.144	55.944	-5.410	1,8	T	D
LC(6)	13.350	31.787	40.686	-5.411	10,8	T	D

For taper configuration C, the lay-up configuration LC(3) is the best choice among all the six lay-up configurations with respect to the buckling load, and lay-up configuration LC(2) is the best choice with respect to both the first-ply failure load and the ultimate failure load.

Figure 5.37 shows the load versus maximum deflection curves of the six laminates all with taper configuration D and each with a different lay-up configuration under the action of bi-axial compression combined with in-plane negative shear. Table 5.26 gives the buckling load, the first-ply failure load and the ultimate failure load for these laminates.

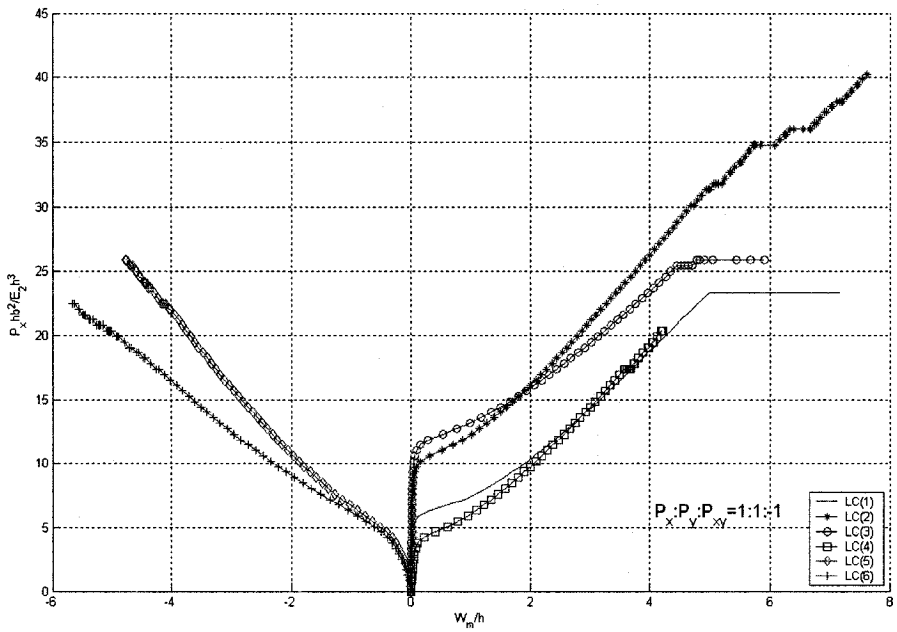

Figure 5.37 Load versus maximum deflection curves of the laminates with taper configuration D for all the six lay-up configurations under bi-axial compression combined with in-plane negative shear

Table 5.26 Failure data of the laminates with taper configuration D for all the six lay-up configurations under bi-axial compression combined with in-plane negative shear

Lay-up	Buckling Load ($P_x hb^2/E_2h^3$)	First-ply failure load ($P_x hb^2/E_2h^3$)	Ultimate failure load ($P_x hb^2/E_2h^3$)	$(W_m/h)^*$	Failure location (FL,FE) ♣	First-ply failure mode	Ultimate failure mode
LC(1)	6.570	23.310	23.310	5.396	1,8	T♠	D#
LC(2)	10.808	30.092	40.263	4.683	1,40	T	D
LC(3)	12.080	25.430	25.853	4.445	1,40	T	D
LC(4)	4.874	17.376	20.343	3.570	10,8	T	D
LC(5)	5.721	22.038	25.853	-4.009	10,16	T	D
LC(6)	6.570	17.376	22.463	-4.207	10,8	T	D

For taper configuration D, the lay-up configuration LC(3) is the best choice among all the six lay-up configurations with respect to the buckling load, and the lay-up configuration LC(2) is the best choice with respect to both the first-ply failure load and the ultimate failure load.

Figure 5.38 shows the load versus maximum deflection curves of the six laminates all with taper configuration F and each with a different lay-up configuration under the action of bi-axial compression combined with in-plane negative shear. Table 5.27 gives the buckling load, the first-ply failure load and the ultimate failure load for these laminates.

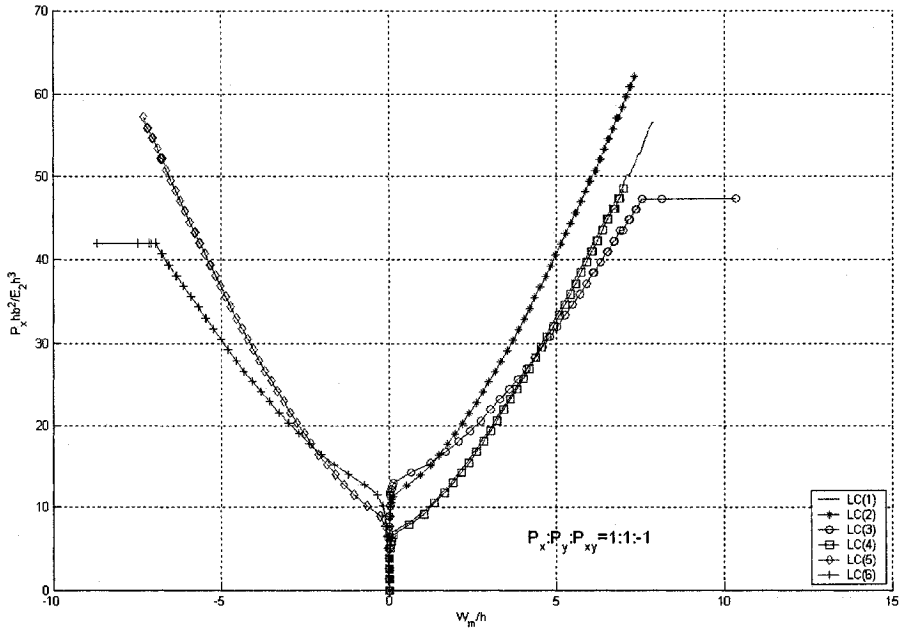

Figure 5.38 Load versus maximum deflection curves of the laminates with taper configuration F for all the six lay-up configurations under bi-axial compression combined with in-plane negative shear

Table 5.27 Failure data of the laminates with taper configuration F for all the six lay-up configurations under bi-axial compression combined with in-plane negative shear

Lay-up	Buckling Load (P_xhb^2/E_2h^3)	First-ply failure load (P_xhb^2/E_2h^3)	Ultimate failure load (P_xhb^2/E_2h^3)	$(W_m/h)^*$	Failure location (FL,FE) ♣	First-ply failure mode	Ultimate failure mode
LC(1)	7.757	36.237	56.582	5.371	1,8	T♠	D#
LC(2)	13.223	41.831	62.174	5.120	10,8	T	D
LC(3)	14.876	37.127	47.298	5.884	10,8	T	D
LC(4)	7.248	32.040	48.570	4.895	10,8	T	D
LC(5)	9.536	39.416	57.216	-5.311	1,8	T	D
LC(6)	13.350	33.059	41.958	-5.455	10,8	T	D

For taper configuration F, the lay-up configuration LC(3) is the best choice among all the six lay-up configurations with respect to both the buckling load, and lay-up configuration LC(2) is the best choice with respect to both the first-ply failure load and the ultimate failure load.

Summary

From Figures 5.34 –5.38 and Tables 5.23 – 5.27, the following general observations are also made.

1. For all the five taper configurations, the first-ply failure mode for all the six lay-up configurations is transverse (matrix) failure.
2. For all the five taper configurations, the ultimate failure mode for all the six lay-up configurations is delamination.
3. For the lay-up configurations LC(5) and LC(6), the maximum deflections are negative, that is, downward. But for other lay-up configurations including the un-symmetric lay-up configuration LC(4), the maximum deflections are positive, that is, upward.
4. Variation of the maximum deflection with the load for the symmetric lay-up configuration LC(1) almost coincides with that of the corresponding un-symmetric lay-up configuration LC(4). Therefore, in this case the symmetry in the stacking sequence does not have a strong influence on the progressive failure of the laminate.

5.3.3 Influence of Fiber Orientation

Tapered laminates under bi-axial compression combined with in-plane negative shear and with lay-up $(\pm\theta)_{4s}$ at the left end are considered. The lay-up at the right (thin) end is $(\pm\theta)_{2s}$ for taper configurations A, B, C and F, and is $(\theta)_8$ for taper configuration D. The variation of buckling load with θ for each taper configuration is determined. The results are plotted in Figure 5.39. A non-monotonic variation is observed for all taper configurations from this figure. Also the variation is un-symmetric about 45° fiber orientation. Peak values of the buckling loads for all the six taper configurations are

predicted to occur at 45° fiber orientation. The highest value of buckling load occurs for configuration F for all fiber orientations. For all fiber orientations except 90° fiber orientation, the buckling load of taper configuration C is very close to that of configuration F.

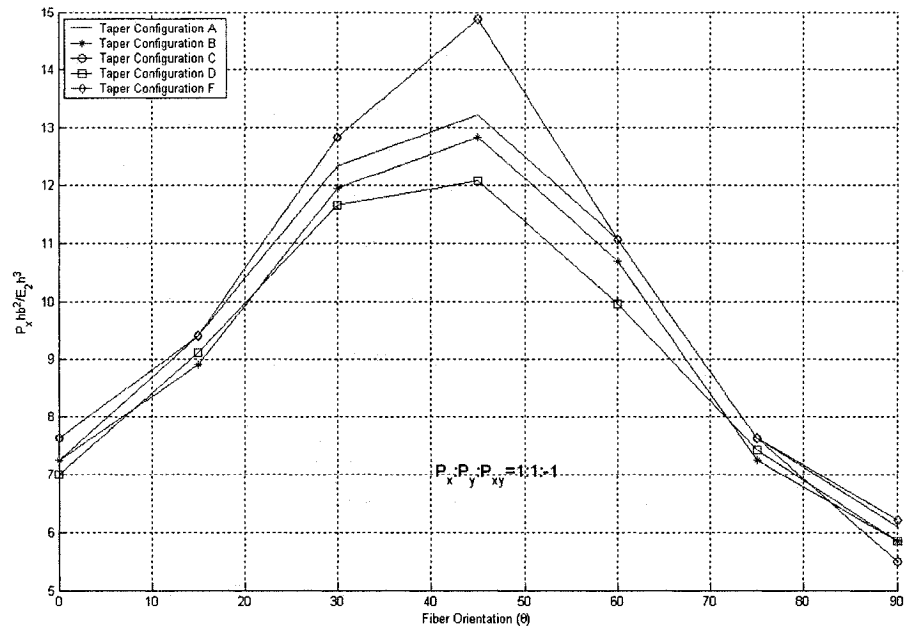

Figure 5.39 Buckling loads of the laminates with $(\pm\theta)_{4s}$ lay-up at the left (thick) end under bi-axial compression combined with in-plane negative shear

Figure 5.40 shows the variation of the first-ply failure load and the ultimate failure load for laminates with taper configuration A and with lay-up $(\pm\theta)_{4s}$ at the left (thick) end under bi-axial compression combined with in-plane negative shear. The results show that the variations in response are un-symmetric about 45° fiber orientation. Peak values of the first-ply failure load and ultimate failure load are predicted to occur for 45° fiber orientation. For laminate with 0°, 15°, 75° and 90° fiber orientations, the value of the first-ply failure load is equal to that of the ultimate failure load. In the range $15° \leq \theta \leq 45°$ the difference between the ultimate failure load and the first-ply failure load becomes

larger, and at θ = 45° the ultimate failure load is 14.34% higher than the first-ply failure load.

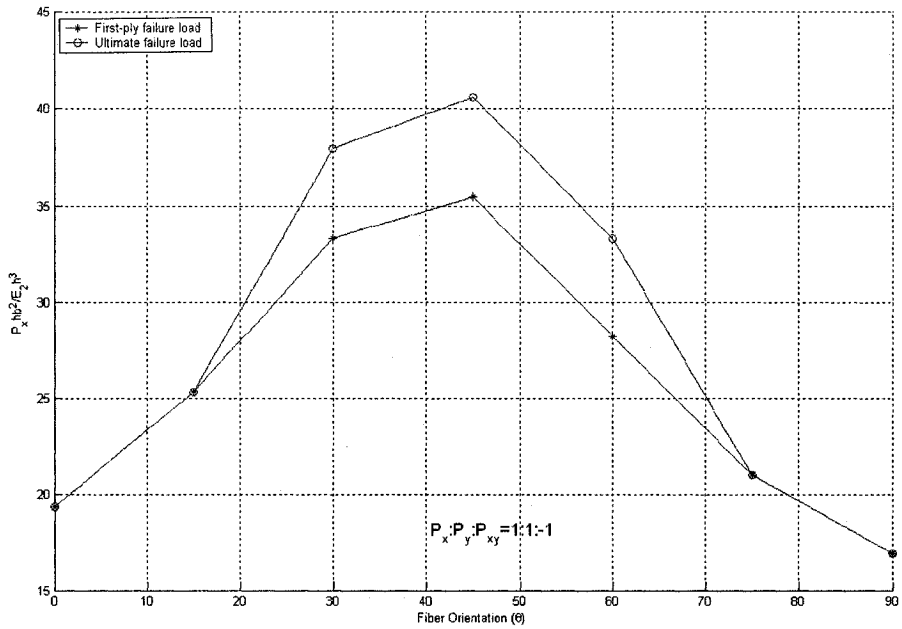

Figure 5.40 Variation of the first-ply and ultimate failure loads of the laminates with taper configuration A and with $(\pm\theta)_{4s}$ lay-up at the left end under bi-axial compression combined with in-plane negative shear

Figure 5.41 shows the variation of the first-ply failure load and the ultimate failure load for laminates with taper configuration B and with lay-up $(\pm\theta)_{4s}$ at the left (thick) end under bi-axial compression combined with in-plane negative shear. The results show that the variations in response are un-symmetric about 45° fiber orientation. Peak values of the first-ply failure load and ultimate failure load are predicted to occur for 45° fiber orientation. For laminate with 0°, 15°, 75° and 90° fiber orientations, the value of the first-ply failure load is equal to that of the ultimate failure load. In the range $15° \leq \theta \leq 45°$ the difference between the ultimate failure load and the first-ply failure load becomes larger, and at θ = 45° the ultimate failure load is 24.48% higher than the first-ply failure load.

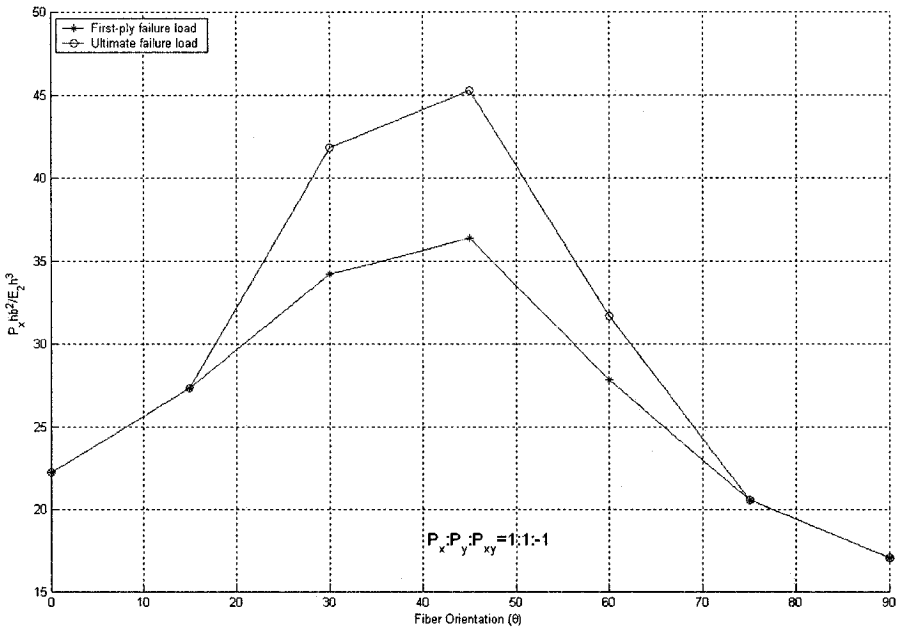

Figure 5.41 Variation of the first-ply and ultimate failure loads of the laminates with taper configuration B and with $(\pm\theta)_{4s}$ lay-up at the left end under bi-axial compression combined with in-plane negative shear

Figure 5.42 shows the variation of the first-ply failure load and the ultimate failure load for laminates with taper configuration C and with lay-up $(\pm\theta)_{4s}$ at the left (thick) end under the action of bi-axial compression combined with in-plane negative shear. The results show that the variations in response are un-symmetric about 45° fiber orientation. Peak values of the first-ply failure load and ultimate failure load are predicted to occur for 45° fiber orientation. For laminate with 0°, 15°, 75° and 90° fiber orientations, the value of the first-ply failure load is equal to that of the ultimate failure load. In the range $15° \leq \theta \leq 45°$ the difference between the ultimate failure load and the first-ply failure load becomes larger, and at $\theta = 30°$ the ultimate failure load is 23.97% higher than the first-ply failure load.

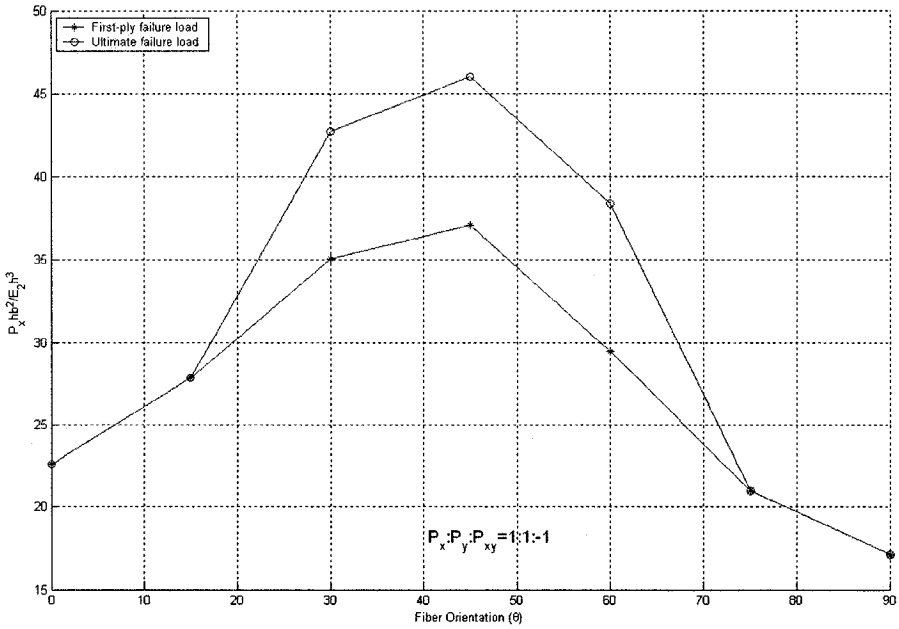

Figure 5.42 Variation of the first-ply and ultimate failure loads of the laminates with taper configuration C and with $(\pm\theta)_{4s}$ lay-up at the left end under bi-axial compression combined with in-plane negative shear

Figure 5.43 shows the variation of the first-ply failure load and the ultimate failure load for laminates with taper configuration D and with lay-up $(\pm\theta)_{4s}$ at the left (thick) end under bi-axial compression combined with in-plane negative shear. The results show that the variations in response are un-symmetric about 45° fiber orientation. Peak values of the first-ply failure load and ultimate failure load are predicted to occur for 30° fiber orientation. The value of the first-ply failure load is equal to the value of the ultimate failure load for all the fiber orientation angles except for 45° and 60° fiber orientations. The maximum difference of ultimate failure load and first-ply failure load is found to occur in the case of 75° fiber orientation, and the ultimate failure load is 3.850% higher than the first-ply failure load.

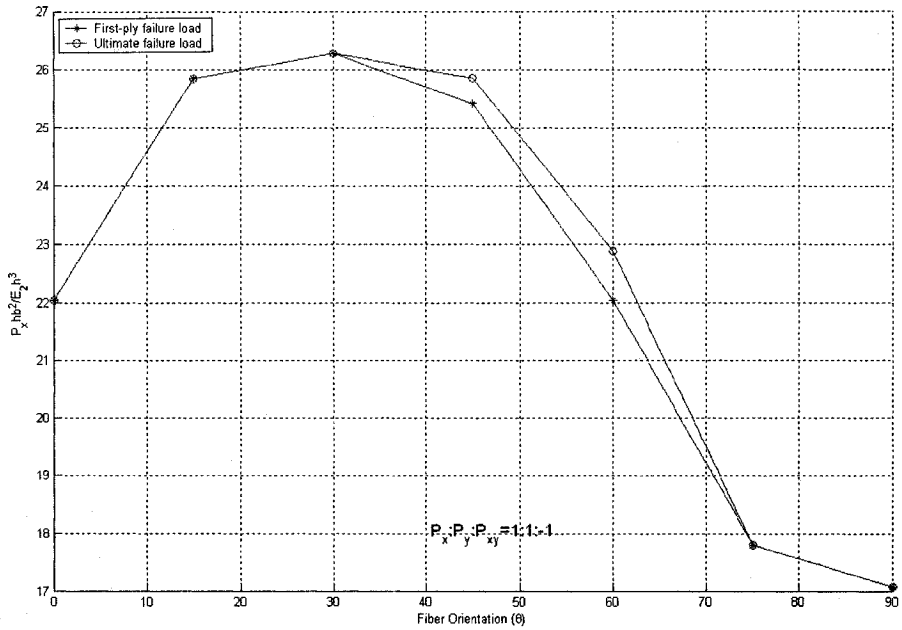

Figure 5.43 Variation of the first-ply and ultimate failure loads of the laminates with taper configuration D and with $(\pm\theta)_{4s}$ lay-up at the left end under bi-axial compression combined with in-plane negative shear

Figure 5.44 shows the variation of the first-ply failure load and the ultimate failure load for laminates with taper configuration F and with lay-up $(\pm\theta)_{4s}$ at the left (thick) end under bi-axial compression combined with in-plane negative shear. The results show that the variations in response are un-symmetric about 45° fiber orientation. Peak values of the first-ply failure load and ultimate failure load occur for 45° fiber orientation. For laminate with 0°, 75° and 90° fiber orientations, the value of the first-ply failure load is equal to that of the ultimate failure load. In the range $0° \leq \theta \leq 45°$ the difference between the ultimate failure load and the first-ply failure load becomes larger, and at $\theta = 45°$ the ultimate failure load is 27.40% higher than the first-ply failure load.

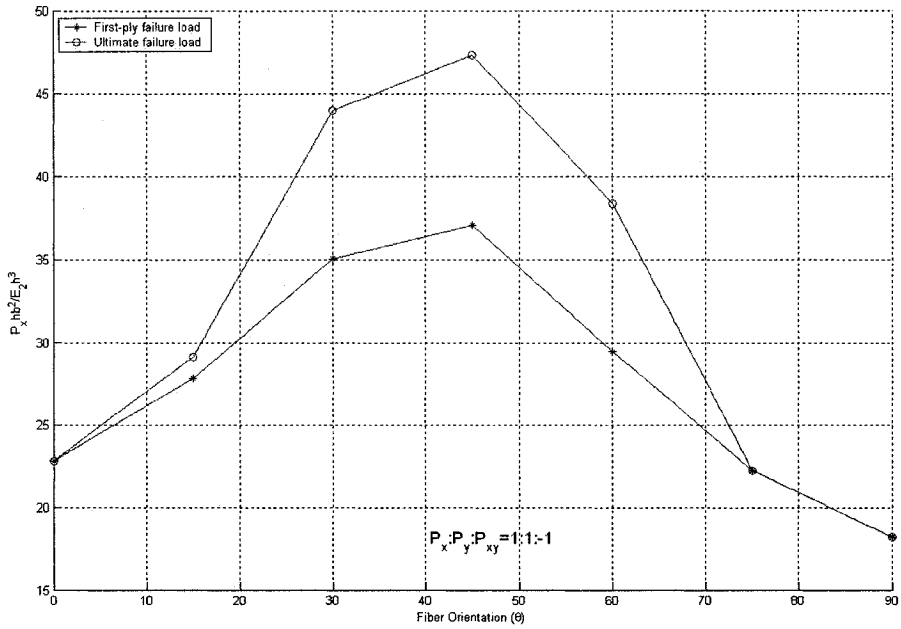

Figure 5.44 Variation of the first-ply and ultimate failure loads of the laminates with taper configuration F and with $(\pm\theta)_{4s}$ lay-up at the left end under bi-axial compression combined with in-plane negative shear

Figure 5.45 shows the variation of first-ply failure load of tapered laminates with $(\pm\theta)_{4s}$ lay-up at the left (thick) end under bi-axial compression combined with in-plane negative shear for all the six taper configurations. The results show that the variations are un-symmetric about 45° fiber orientation. Peak values of the first-ply failure loads for taper configurations A, B, C and F occurs at 45° fiber orientation, whereas, the peak value for taper configuration D occurs at 30° fiber orientation. The taper configuration F has the highest value of first-ply failure load for all fiber orientations. The lowest value of first-ply failure load for 0° fiber orientation occurs for configuration A, whereas, for fiber orientations 15°, 30°, 45°, 60°, 70° and 90° fiber orientations, it occurs for configuration D. For 15°, 30°, 45° and 60° fiber orientations, the first-ply load of taper configuration C is very close to that of configuration F.

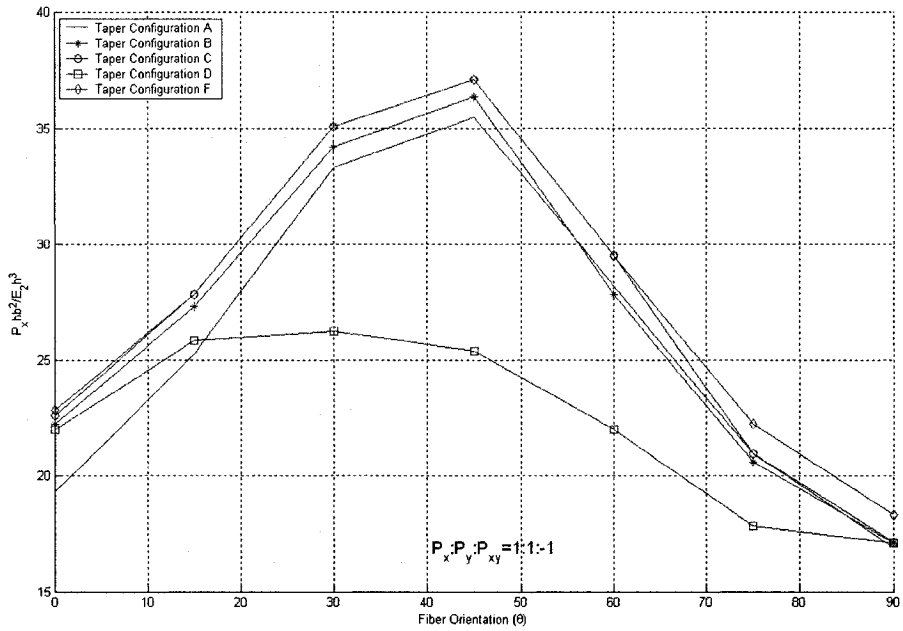

Figure 5.45 First-ply failure load of the laminates with $(\pm\theta)_{4s}$ lay-up at the left (thick) end under bi-axial compression combined with in-plane negative shear

Figure 5.46 shows the variation of ultimate failure load of tapered laminates with $(\pm\theta)_{4s}$ lay-up at the left (thick) end under bi-axial compression combined with in-plane negative shear for all the taper configurations. The results show that the variations are un-symmetric about 45° fiber orientation. Peak values of the first-ply failure loads for taper configurations A, B, C and F occurs at 45° fiber orientation, whereas, the peak value for taper configuration D occurs at 30° fiber orientation. The taper configuration F has the highest value of first-ply failure load for all fiber orientations. The lowest value of first-ply failure load for 0° fiber orientation occurs for configuration A, whereas, for fiber orientations 15°, 30°, 45°, 60°, 70° and 90° fiber orientations, it occurs for configuration D.

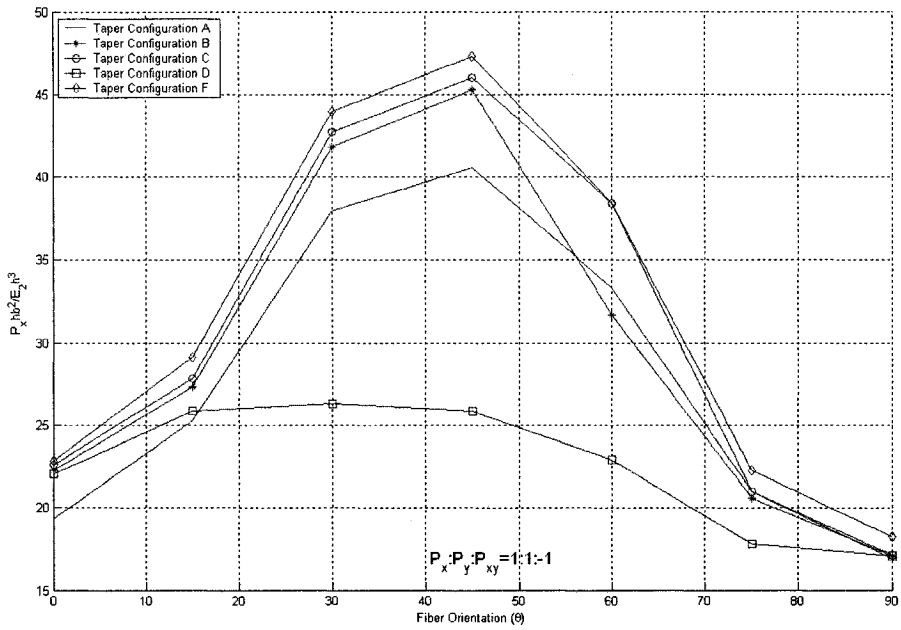

Figure 5.46 Ultimate failure load of the laminates with $(\pm\theta)_{4s}$ lay-up at the left (thick) end under bi-axial compression combined with in-plane negative shear

5.3.4 Influence of Uniform-thickness Sections

Except that the loading is bi-axial compression combined with in-plane negative shear, the study cases are the same as those given in sub-section 4.2.4 of Chapter 4. Figure 5.47 shows the load versus maximum deflection curves of five tapered plates under the action of bi-axial compression combined with in-plane negative shear. Table 5.28 gives the buckling load, the first-ply failure load and the ultimate failure load for these laminates under the action of bi-axial compression combined with in-plane negative shear. The laminate with length ratio 2:1 is the best choice among these five laminates with respect to the buckling load, the laminate with length ratio 1:1.5 is the best choice with respect to the first-ply failure load, and the laminate with length ratio 1.5:1 is the best choice with respect to the ultimate failure load. It is also observed that for all the cases the first-ply failure corresponds to the transverse (matrix) failure, and the ultimate failure corresponds

to the delamination failure as in the case of the plate with only the tapered section. Therefore, it is noted that the addition of uniform-thickness sections did not change the modes of failure. However, considerably more resistance to buckling, first-ply and ultimate failures is provided by the addition of uniform-thickness sections.

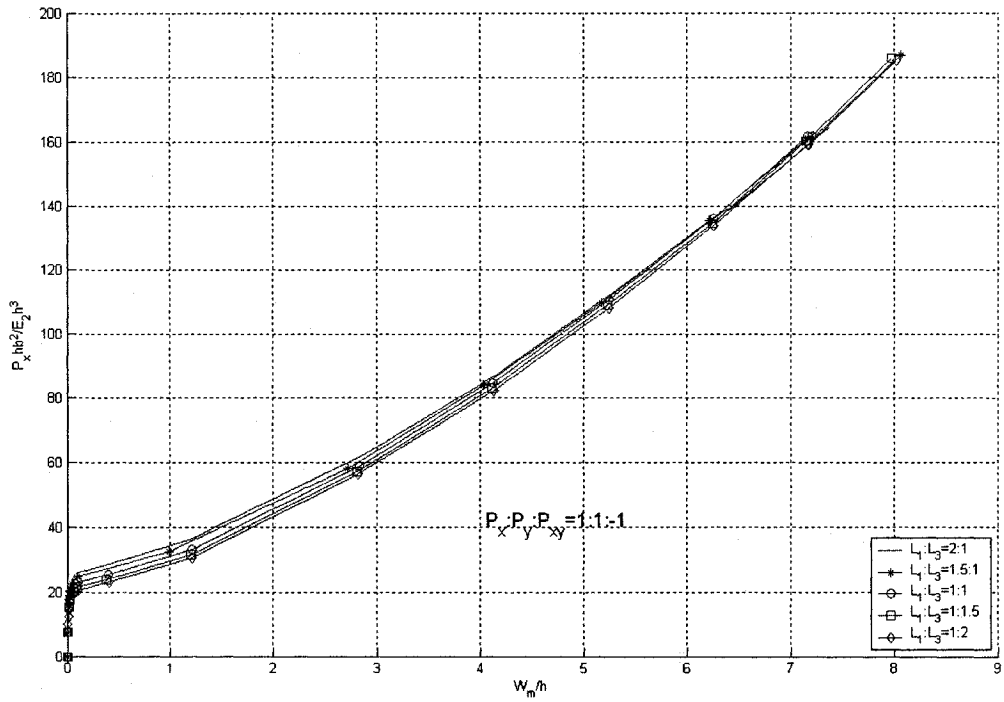

Figure 5.47 Load versus the maximum deflection curves of five tapered plates with different length ratios under the action of bi-axial compression combined with negative shear

Table 5.28 Failure data of five tapered plates with different length ratios under the action of bi-axial compression combined with in-plane negative shear

L1 :L3	Buckling Load ($P_{xy}hb^2/E_2h^3$)	First-ply failure load ($P_{xy}hb^2/E_2h^3$)	Ultimate failure load ($P_{xy}hb^2/E_2h^3$)	$(W_m/h)^*$	Failure location (FL,FE) ♣	First-ply failure mode	Ultimate failure mode
2:1	27.267	139.137	164.880	6.370	2,10	T♠	D#
1.5:1	25.580	135.429	186.930	6.215	1,20	T	D
1:1	24.254	136.124	161.865	6.249	2,20	T	D
1:1.5	22.632	160.245	186.000	7.142	2,10	T	D
1:2	21.860	159.480	185.220	7.157	2,20	T	D

5.3.5 Influence of Boundary Conditions

Except that the loading is in-plane positive shear, the study cases are the same as those given in sub-section 3.3.5 of Chapter 3. The results are compared in Figure 5.48 and Table 5.29.

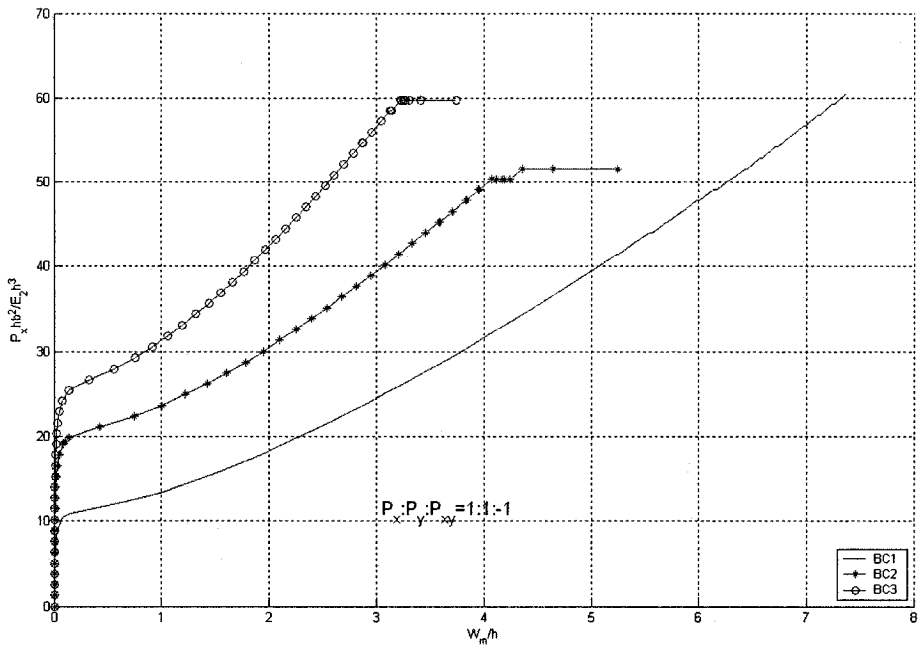

Figure 5.48 Load versus maximum deflection curves of the tapered laminate with taper configuration B corresponding to three boundary conditions under bi-axial compression combined with in-plane negative shear

Table 5.29 Failure data of the tapered laminate with taper configuration B corresponding to three boundary conditions under bi-axial compression combined with in-plane negative shear

BC	Buckling Load ($P_{xy}hb^2/E_2h^3$)	First-ply failure load ($P_{xy}hb^2/E_2h^3$)	Ultimate failure load ($P_{xy}hb^2/E_2h^3$)	$(W_m/h)^*$	Failure location (FL,FE) ♣	First-ply failure mode	Ultimate failure mode
BC1	11.571	41.450	60.521	5.237	10,8	T♠	D#
BC2	21.743	43.992	51.621	3.453	1,8	T	D
BC3	27.336	53.402	59.759	2.777	1,8	T	D

From Figure 5.48 and Table 5.29, it is observed that the first-ply failure load corresponds to the transverse (matrix) failure, and the ultimate failure corresponds to the delamination failure for all the three boundary conditions. The first-ply failure load is found to be about 3.6 times the buckling load for BC1 boundary condition, 2.0 times for BC2 boundary condition, and 2.0 times for BC3 boundary condition, whereas, the ultimate failure load is about 5.2 times the buckling load for BC1 boundary condition, and 2.0 times for BC2 and BC3 boundary conditions. The ultimate failure load is about 5.2 times the first-ply failure load for BC1 boundary condition, 2.4 times for BC2 boundary condition, and 2.2 times for BC3 boundary condition. The absolute maximum value of the maximum transverse displacement W_m just before ultimate failure is found to occur in the case of boundary condition BC1 and is equal to 7.38h. The absolute minimum value of the maximum transverse displacement W_m just before the ultimate failure is found to occur in the case of boundary condition BC3 and is equal to 3.25h. It is also noted that the higher the flexural rigidity is, higher are the buckling load, the first-ply failure load and stiffness for a fixed value of maximum transverse displacement, whereas, it is not the case for ultimate failure load.

5.3.6 Influence of Load Ratio

The tapered laminate with taper configuration B and with LC(2) lay-up configuration is considered. The length, the width and the boundary condition of the plate are the same as that given in sub-section 5.2.1. The ratio of P_x to P_y is set to a value of 1, and the value of P_{xy} is varied. Figure 5.49 shows the load versus maximum deflection curves for the laminate under the action of bi-axial compression combined with in-plane negative shear for different load ratio values ($P_x = P_y = 1$, P_{xy} is changed). Table 5.30 gives the buckling load, the first-ply failure load and the ultimate failure load for all the cases.

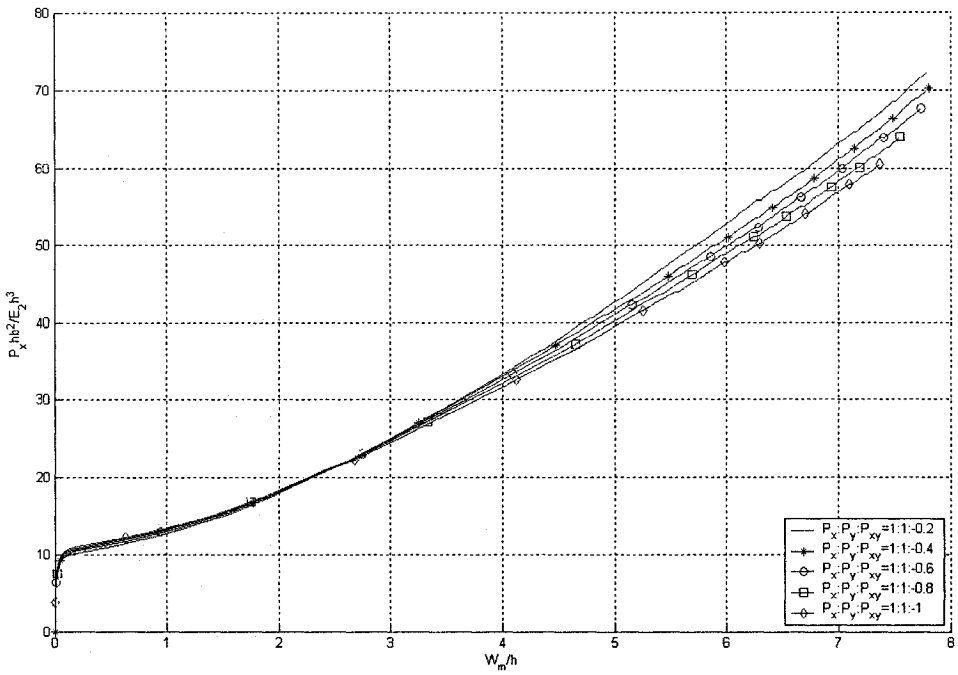

Figure 5.49 Load versus maximum deflection curves of the LC(2) laminate with taper configuration B under bi-axial compression combined with in-plane negative shear for various load ratio values with varying P_{xy}

Table 5.30 Failure data of the LC(2) laminate with taper configuration B under bi-axial compression combined with in-plane negative shear for various load ratio values with varying P_{xy}

Load Ratio $P_x:P_y:P_{xy}$	Buckling Load (P_xhb^2/E_2h^3)	First-ply failure load (P_xhb^2/E_2h^3)	Ultimate failure load (P_xhb^2/E_2h^3)	$(W_m/h)^*$	Failure location (FL,FE) ♣	First-ply failure mode	Ultimate failure mode
1:1:-0.2	12.571	43.611	72.344	4.779	1,40	T♠	D#
1:1:-0.4	12.189	42.213	70.185	4.899	1,40	T	D
1:1:-0.6	12.061	41.450	67.641	4.996	1,40	T	D
1:1:-0.8	11.911	40.941	63.954	5.101	1,40	T	D
1:1:-1	11.571	40.560	60.521	5.237	1,40	T	D

Form Figure 5.49 and Table 5.30, it is observed that with increasing proportion of in-plane positive shear loading in the combined loading, the first-ply failure load and the ultimate failure load are not changed too much. It is also observed that the first-ply failure

load corresponds to the transverse (matrix) failure, and the ultimate failure corresponds to the delamination in all the cases. Locations corresponding to the first-ply failure lie near the thin end of the plate and at the outermost bottom layer.

Now, the value of P_{xy} is fixed, and the values of P_x and P_y are changed with 1:1 ratio. Figure 5.50 shows the load versus maximum deflection curves for the laminate under the action of bi-axial compression combined with in-plane negative shear for different load ratio values (P_{xy}=-1, P_x and P_y are changed). Table 5.31 gives the buckling load, the first-ply failure load and the ultimate failure load for all the cases. It is observed that with increasing proportion of bi-axial compression in the combined loading, the first-ply failure load and the ultimate failure load decrease monotonically. At P_x: P_y: P_{xy} =1:1:-1, the percentage loss (compared to the case P_x: P_y: P_{xy} =0.2:0.2:-1) in the first-ply failure load and ultimate failure load are respectively, 57.44% and 60.53%. It is also observed that the first-ply failure load corresponds to the transverse (matrix) failure, and the ultimate failure corresponds to the delamination in all the cases. Locations corresponding to the first-ply failure lie near the thick end of the plate and at the outermost top layer.

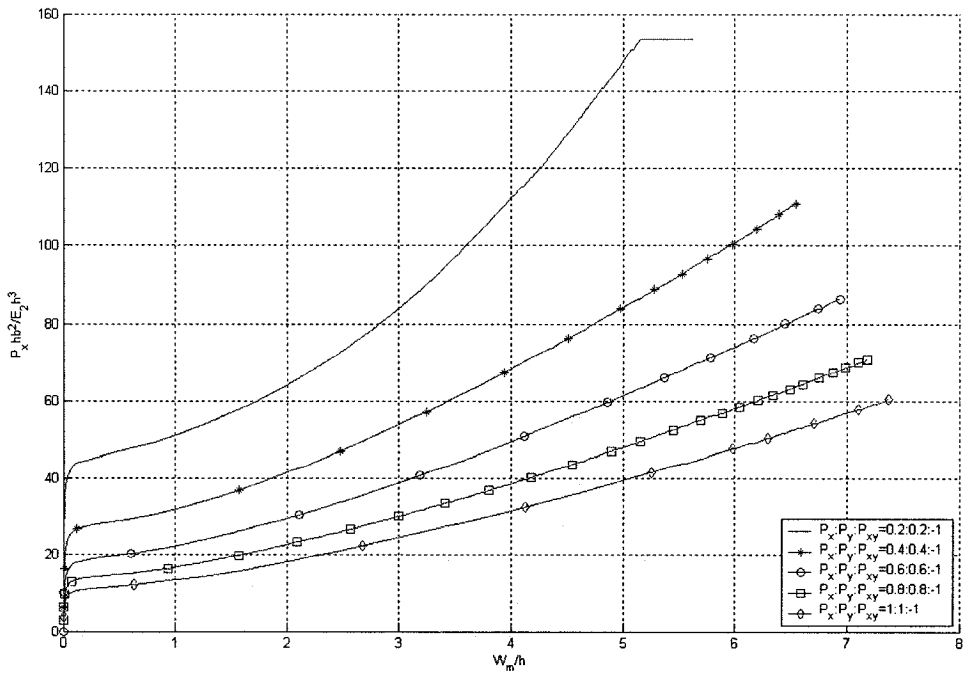

Figure 5.50 Load versus maximum deflection curves of the LC(2) laminate with taper configuration B under bi-axial compression combined with in-plane negative shear for various load ratio values with varying P_x and P_y

Table 5.31 Failure data of the LC(2) laminate with taper configuration B under bi-axial compression combined with in-plane negative shear for various load ratio values with varying P_x and P_y

Load Ratio $P_x:P_y:P_{xy}$	Buckling Load (P_xhb^2/E_2h^3)	First-ply failure load (P_xhb^2/E_2h^3)	Ultimate failure load (P_xhb^2/E_2h^3)	$(W_m/h)^*$	Failure location (FL,FE) ♣	First-ply failure mode	Ultimate failure mode
0.2:0.2:-1	47.807	97.394	153.330	3.504	8,10	T♠	D#
0.4:0.4:-1	28.608	73.745	110.616	4.341	8,10	T	D
0.6:0.6:-1	19.709	58.487	86.459	4.751	8,10	T	D
0.8:0.8:-1	14.622	47.892	70.778	4.977	8,10	T	D
1:1:-1	11.571	41.450	60.521	5.237	8,10	T	D

The ratio of P_{xy} to P_y is set to a value of -1, and the value of P_x is changed. Figure 5.51 shows the load versus maximum deflection curves for the laminate under the action of bi-axial compression combined with in-plane negative shear for different load ratio values

(P_{xy} : P_y =-1:1, P_x ischanged). Table 5.32 gives the buckling load, the first-ply failure load and the ultimate failure load for these cases. It is observed that with increasing proportion of bi-axial compression in the combined loading, the first-ply failure load and the ultimate failure load decrease monotonically. At P_x: P_y: P_{xy} =1:1:-1, the percentage loss (compared to the case P_x: P_y: P_{xy} =0.2:1:-1) in the first-ply failure load and ultimate failure load are respectively, 30.64 and 35.68. It is also observed that the first-ply failure load corresponds to the transverse (matrix) failure, and the ultimate failure corresponds to the delamination in all the cases. Locations corresponding to the first-ply failure lie near the thick end of the plate and at the outermost layer.

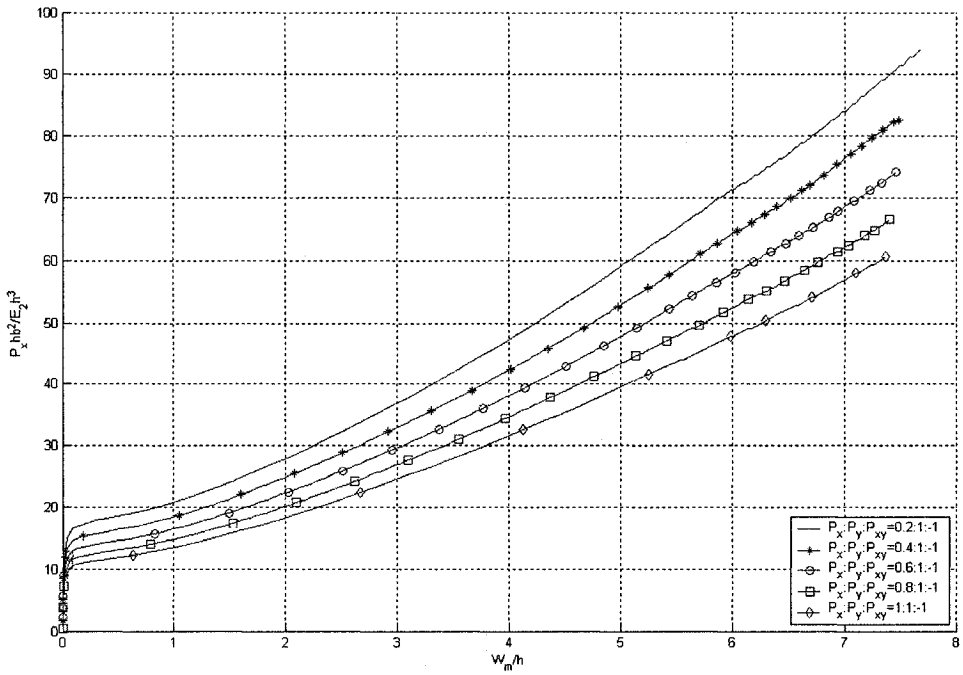

Figure 5.51 Load versus maximum deflection curves of the LC(2) laminate with taper configuration B under bi-axial compression combined with in-plane negative shear for various load ratio values with varying P_x

Table 5.32 Failure data of the LC(2) laminate with taper configuration B under bi-axial compression combined with in-plane netative shear for various load ratio values with varying P_x

Load Ratio P_x:P_y:P_{xy}	Buckling Load ($P_x hb^2/E_2h^3$)	First-ply failure load ($P_x hb^2/E_2h^3$)	Ultimate failure load ($P_x hb^2/E_2h^3$)	$(W_m/h)^*$	Failure location (FL,FE) ♣	First-ply failure mode	Ultimate failure mode
0.2:1:-1	18.437	59.759	94.088	5.060	1,8	T♠	D#
0.4:1:-1	15.894	54.249	82.644	5.126	1,8	T	D
0.6:1:-1	14.198	48.740	74.168	5.099	10,8	T	D
0.8:1:-1	12.927	44.501	66.540	5.136	10,8	T	D
1:1:-1	11.571	41.450	60.521	5.237	10,8	T	D

5.4 Comparison of Responses to Biaxial Compression Combined with In-plane positive shear and to Biaxial Compression Combined with In-plane Negative Shear

For LC(1) lay-up configuration, the buckling load under bi-axial compression combined with in-plane negative shear is found to be about 1.05 times the buckling load under bi-axial compression combined with in-plane positive shear for taper configurations A and B, 1 time for configuration C, and 1.02 times for configuration F, but for taper configuration D it only about 88.6% of the buckling load under bi-axial compression combined with in-plane positive shear. The first-ply failure load under bi-axial compression combined with in-plane negative shear is found to be about 97.5% of the first-ply failure load under bi-axial compression combined with in-plane positive shear for taper configuration B, 93.6% for configuration C, 98.2% for configuration D, and 90.5% for configuration F, but for taper configuration A it about 1.19 times the first-ply failure load under bi-axial compression combined with in-plane positive shear. The ultimate failure load under bi-axial compression combined with in-plane negative shear is found to be about 1.42 times the ultimate failure load under bi-axial compression

combined with in-plane positive shear for taper configuration A, 1.41 times for configuration B, 1.43 times for configuration C, 1.29 times for configuration F, but for taper configuration D it is about 98.2% of the ultimate failure load under bi-axial compression combined with in-plane positive shear.

For LC(2) lay-up configuration, the buckling load under bi-axial compression combined with in-plane negative shear is found to be about 1.23 times the buckling load under bi-axial compression combined with in-plane positive shear for taper configuration A, 1.30 times for configuration B, 1.41 times for configuration C, 1.55 times for configuration D, and 1.35 times for configuration F. The first-ply failure load under bi-axial compression combined with in-plane negative shear is found to be about 1.38 times the first-ply failure load under bi-axial compression combined with in-plane positive shear for taper configuration A, 1.52 times for configuration B, 1.32 times for configuration C, 1.54 times for configuration D, and 1.31 times for configuration F. The ultimate failure load under bi-axial compression combined with in-plane negative shear is found to be about 1.06 times the ultimate failure load under bi-axial compression combined with in-plane positive shear for taper configuration A, 1.02 times for taper configuration B, 1.04 times for taper configuration C, and 1.44 times for taper configuration D, but for configuration F it is only 97.4% of the ultimate failure load under bi-axial compression combined with in-plane positive shear.

For LC(3) lay-up configuration, the buckling load under bi-axial compression combined with in-plane negative shear is found to be about 1.41 times the buckling load under bi-axial compression combined with in-plane positive shear for taper configuration A, 1.44

times for configuration B, 1.52 times for configuration C, 2.07 times for configuration D, and 1.52 times for configuration F. The first-ply failure load under bi-axial compression combined with in-plane negative shear is found to be about 1.48 times the first-ply failure load under bi-axial compression combined with in-plane positive shear for taper configuration A, 1.47 times for configuration B, 1.45 times for configuration C, 1.92 times for configuration D, and 1.38 times for configuration F. The ultimate failure load under bi-axial compression combined with in-plane negative shear is found to be about 1.19 times the ultimate failure load under bi-axial compression combined with in-plane positive shear for taper configuration A, 1.25 times for taper configuration B, 1.24 times for taper configuration C, 1.94 times for taper configuration D, and 1.23 times for configuration F.

For LC(4) lay-up configuration, the buckling load under bi-axial compression combined with in-plane negative shear is found to be about 1.06 times the buckling load under bi-axial compression combined with in-plane positive shear for taper configuration A, and 1 time for configuration D, whereas, it is about 93.4% of the buckling load under bi-axial compression combined with in-plane positive shear for configuration B, and 87.7% for configurations C and F. The first-ply failure load under bi-axial compression combined with in-plane negative shear is found to be about 94.5% of the first-ply failure load under bi-axial compression combined with in-plane positive shear for taper configuration B, 93.1% for configuration C, 87.2% for configuration D, and 93.3 for configuration F, but for taper configuration A it is only about 1.01 times the first-ply failure load under bi-axial compression combined with in-plane positive shear. The ultimate failure load under bi-axial compression combined with in-plane negative shear is found to be about 1.18

times the ultimate failure load under bi-axial compression combined with in-plane positive shear for taper configuration A, 1.45 times for configuration B, 1.24 times for configuration C, 1.19 times for configuration F, but for taper configuration D it is about 84.2% of the ultimate failure load under bi-axial compression combined with in-plane positive shear.

For LC(5) lay-up configuration, the buckling load under bi-axial compression combined with in-plane negative shear is found to be about 1.15 times the buckling load under bi-axial compression combined with in-plane positive shear for taper configurations A, B and C, and 1 time for configurations D and F. The first-ply failure load under bi-axial compression combined with in-plane negative shear is found to be about 1.26 times the first-ply failure load under bi-axial compression combined with in-plane positive shear for taper configuration A, 1.30 times for configuration B, 1.20 times for configuration C, 1.06 times for configuration D, and 1.19 times for configuration F. The ultimate failure load under bi-axial compression combined with in-plane negative shear is found to be about 1.16 times the ultimate failure load under bi-axial compression combined with in-plane positive shear for taper configuration A, 1.10 times for taper configurations B and C, 1.05 times for taper configuration F, but for taper configuration D it is about 77.2% of the ultimate failure load under bi-axial compression combined with in-plane positive shear.

For LC(6) lay-up configuration, the buckling load under bi-axial compression combined with in-plane negative shear is found to be about 1.40 times the buckling load under bi-axial compression combined with in-plane positive shear for taper configuration A, 1.27

times for configuration B, and 1.24 times for configurations C, D and F. The first-ply failure load under bi-axial compression combined with in-plane negative shear is found to be about 1.20 times the first-ply failure load under bi-axial compression combined with in-plane positive shear for taper configuration A, 1.25 times for configuration B, 1.91 times for configuration C, 1.17 times for configuration D, and 1.18 times for configuration F. The ultimate failure load under bi-axial compression combined with in-plane negative shear is found to be about 1.07 times the ultimate failure load under bi-axial compression combined with in-plane positive shear for taper configurations A and B, 1.03 times for taper configuration C, 1.06 times for taper configuration F, but for taper configuration D it is about 82.8% of the ultimate failure load under bi-axial compression combined with in-plane positive shear.

5.5 Conclusion

In this chapter, a detailed parametric study on tapered composite plates under the action of bi-axial compression combined with in-plane shear is conducted. The first-ply failure loads, the ultimate failure load, the buckling load, the associated maximum transverse displacements, and the locations and modes of failure including the onset of delamination of tapered laminate plate under the action of bi-axial compression combined with in-plane shear have been determined and given.

The results of the present study predict that the maximum difference among the buckling loads, the first-ply failure loads and ultimate failure loads are strongly dependent on the type of laminate lay-up, the type of boundary condition and the type of taper configuration. The failure mode corresponding to the first-ply failure is associated with

the localized matrix cracking irrespective of the lay-up configuration, taper configuration, addition of uniform-thickness sections and boundary condition. The failure occurs primarily due to the normal stresses acting in the direction transverse to the fiber direction. The failure mode corresponding to the ultimate failure is associated with delamination irrespective of the lay-up configuration, taper configuration, addition of uniform-thickness sections and boundary condition. The maximum deflection is upward for bi-axial compression combined with in-plane positive shear for all lay-up configurations and all taper configurations considered, and it is upward for bi-axial compression combined with in-plane negative shear for lay-up configurations LC(1), LC(2), LC(3) and LC(4). For lay-up configurations LC(5) and LC(6) under bi-axial compression combined with in-plane negative shear, it is negative, that is, downward.

In general, under the action of bi-axial compression combined with in-plane shear, for the lay-up and taper configurations and the boundary conditions considered, the ultimate failure load is about 2.2 - 7.1 times the buckling load, the first-ply failure load is about 2.1 - 5.2 times the buckling load, and the ultimate failure load is about 1.0 - 2.2 times the first-ply failure load. The largest difference between the buckling load and the first-ply failure load corresponds to the tapered laminate under bi-axial compression combined with in-plane positive shear with the lay-up configuration LC(1), the boundary condition BC1 and the taper configuration F. For this case, the first-ply failure load is about 5.2 times the buckling load. As for the difference between the buckling load and the ultimate failure load, the largest difference corresponds to the tapered laminate with the lay-up configuration LC(1), the boundary condition BC1 and the taper configurations A, B and C under the action of bi-axial compression combined with in-plane negative shear. For

this case, the ultimate failure load is about 7.1 times the buckling load. As for the difference between the first-ply failure load and the ultimate failure load, the largest difference corresponds to the tapered laminate with the lay-up configuration LC(2), the boundary condition BC1 and the taper configuration B under the action of bi-axial compression combined with in-plane positive shear. For this case, the ultimate failure load is about 2.2 times the first-ply failure load. Hence, it can be seen that considerable residual strength is available for these laminates in the post-buckling stage under the action of shear and that the direction of applied shear loading has a strong influence.

Chapter 6

Stochastic Failure Analysis

6.1 Introduction

The reliability of many engineering structures in the presence of uncertainty has been a crucial factor in their analysis and design. Primary and secondary systems related to aerospace structures are quite sensitive to small imperfections in pertinent design variables. Several of these variables are inherently random and can be most appropriately modeled as random processes. They may include quantities such as modulus of elasticity, Poisson ratio, shear strength, and a variety of other physical and mathematical parameters. Clearly, the complexity of these modern structures requires the use of versatile numerical techniques such as the finite element method to obtain accurate mathematical approximations to their physical behavior.

Significant randomness is displayed in the spatial variations in the properties of fibers and of matrix materials, in the properties at interfaces, in the fiber orientation angles of various piles, in the thickness of lamina, and so on. Tests on a single material specimen provide a specific value for each material parameter and mechanical property. However, different randomly distributed values are obtained for the same mechanical property or the material parameter after a number of specimens are tested. Most of the existing techniques are limited to dealing with deterministic loadings and environmental conditions despite the fact that they intrinsically involve randomness and uncertainty to a considerable degree. Therefore, the analysis of laminates should be performed based on a probabilistic approach. In light of this, in this thesis the Markov Model and Stochastic

Finite Element Analysis, which is basically Finite Element Analysis performed on the basis of a stochastic approach, are used.

The following section begins with a description of the analytical modeling of material properties as stochastic processes. The formulations and the associated MATLAB program developed in Chapter 2 are extended so as to incorporate the stochastic description of material properties and stochastic finite element analysis.

6.2 Stochastic Field Modeling of Material Properties

Spatial variations of material properties such as Young's modulus, Poisson's ratio and the shear modulus for both composite and resin materials are in each case considered to constitute a two-dimensional homogeneous stochastic field. Here, the term homogeneous refers to a particular stochastic characteristic. Each material property is expressed as a sum of a mean component and a fluctuating component. The fluctuating component of a material property has a zero mean. For illustrative purposes, first the stochastic field of Young's modulus in the fiber direction (E_1) is described below. A similar procedure is applicable to E_2, E_3, G_{12}, G_{13}, G_{23}, ν_{12}, ν_{23}, and ν_{13} of composite material, and E, ν and G of the resin.

$$E_1 = \overline{E}_1[1 + a(X)] \tag{6.1}$$

$$E[a(X)] = 0 \tag{6.2}$$

The auto-correlation function is given by:

$$R_{aa}(\xi) = E[a(X)a(X+\xi)] \tag{6.3}$$

In the equations (6.1-6.3), $X = [x, y]^T$ indicates the position vector and $\xi = [\xi_x, \xi_y]^T$ represents the separation vector between two points X and $(X + \xi)$. In the present thesis,

it is assumed that each material property varies at each Gauss point of all the finite elements. Thus, if there are a total of n finite elements present in the structure, and m represents the order of Gauss quadrature, then there are N (equal to n*m) material property values associated with the n elements. Consider only the fluctuating component of the homogeneous stochastic field, which models the material property variations around the expected value. These N values $a_i = a(X_i),\ (i = 1,2,3,. \ . \ . \ .,N)$, are random variables with mean zero, but correlated. Here, X_i corresponds to the location of each Gauss point. Their correlation characteristics can be specified in terms of the covariance matrix C_{aa} of order N*N, whose ij^{th} component is given by:

$$c_{ij} = Cov[a_i a_j] = E[[a_i a_j]] = R_{aa}(\xi_{ij}) \qquad i, j = 1,....,N \tag{6.4}$$

in which $\xi_{ij} = (X_j - X_i)$ represents the separation distance between the Gauss points i and j. Then, a vector $\{a\} = [a_1 \quad a_2 \quad a_3 ... \quad a_N]^T$ can be obtained as

$$\{a\} = [L]\{Z\} \tag{6.5}$$

where $\{Z\} = [Z_1 \quad Z_2 \quad Z_3 ... \quad Z_N]^T$ is a matrix consisting of N independent Gaussian random variables with zero mean and unit standard deviation, and $[L]$ is a lower triangular matrix obtained by the Cholesky decomposition of the covariance matrix $[C_{aa}]$. Thus,

$$[L][L^T] = [C_{aa}] \tag{6.6}$$

Once the Cholesky decomposition is accomplished, different sample vectors of $\{a\}$ are obtained by generating different samples for the Gaussian random vectors $\{Z\}$.

The correlation properties of the stochastic field representing the fluctuating components of the material property are expressed using the Markov correlation model, also known as the First-order autoregressive model. The choice of this model in this work is due to its familiarity and wide use.

6.3 Markov Model

The Markov correlation model is given by [82]

$$R_{aa}(\xi) = \sigma_a^2 \exp\left[-\left(\frac{|\xi|}{d}\right)\right] \tag{6.7}$$

in which the correlation length d is a positive parameter such that when it is large the correlation disappears more slowly, and σ_a is the standard deviation of the stochastic field $a(X)$.

The process $a(X)$ is defined as the stochastic field which represents the deviatoric components of the material property with autocorrelation function as given in the Markov model. The basic material properties such as the elastic modulus and Poisson's ratio are assumed to have a Gaussian distribution and are given by:

$E_{1g} = E_{1m}(1 + a_g)$ 1-directional Young's modulus for composite (6.8)

$E_{2g} = E_{2m}(1 + b_g)$ 2-directional Young's modulus for composite (6.9)

$E_{3g} = E_{3m}(1 + c_g)$ 3-directional Young's modulus for composite (6.10)

$v_{12g} = v_{12m}(1 + d_g)$ 1-2 directional Poisson's ratio for composite (6.11)

$v_{13g} = v_{13m}(1 + e_g)$ 1-3 directional Poisson's ratio for composite (6.12)

$v_{23g} = v_{23m}(1 + f_g)$ 2-3 directional Poisson's ratio for composite (6.13)

$$G_{12g} = G_{12m}(1 + g_g) \quad \text{1-2 directional Shear modulus for composite} \quad (6.14)$$

$$G_{13g} = G_{13m}(1 + h_g) \quad \text{1-3 directional Shear modulus for composite} \quad (6.15)$$

$$G_{23g} = G_{23m}(1 + j_g) \quad \text{2-3 directional Shear modulus for composite} \quad (6.16)$$

$$E_g = E_m(1 + k_g) \quad \text{Young's modulus for resin} \quad (6.17)$$

$$v_g = v_m(1 + l_g) \quad \text{Poisson's ratio for resin} \quad (6.18)$$

$$G_g = G_m(1 + m_g) \quad \text{Shear modulus for resin} \quad (6.19)$$

in which a_g, b_g, c_g, d_g, e_g, f_g, g_g, h_g, j_g, k_g, l_g, and m_g, are the values of the stochastic field $a(X)$, $b(X)$, $c(X)$, $d(X)$, $e(X)$, $f(X)$, $g(X)$, $h(X)$, $j(X)$, $k(X)$, $l(X)$ and $m(X)$, respectively, at each Gauss point in the structure. These values also represent the variations in the material properties E_1, E_2, E_3, v_{12}, v_{13}, v_{23}, G_{12}, G_{13}, G_{23}, E, v and G. E_{1m}, E_{2m} and E_{3m} are the mean values of the Young's modulus in directions 1, 2 and 3 for composite material, respectively, and, v_{12m}, v_{13m}, and v_{23m} are the mean values of the 1-2 direction Poisson's ratio, 1-3 direction Poisson's ratio and 2-3 direction Poisson's ratio for composite material. G_{12m}, G_{13m} and G_{23m} are the mean values of the 1-2 direction Shear modulus, 1-3 direction Shear modulus and 2-3 direction Shear modulus for composite material. E_m, v_m and G_m are the mean value of the Young's modulus, the mean value of the Poisson's ratio and the mean value of the Shear modulus for resin material, respectively.

The assumption of Gaussian distribution implies the possibility of generating negative values for the material properties. In order to avoid this difficulty, the values of the random variable a_g in the case of Monte-Carlo simulation are confined to the range

$$-1+\varepsilon \le a_g \le 1-\varepsilon \tag{6.20}$$

where ε is a positive constant introduced to avoid the mathematical complications that would arise if the sum $(1+a_g)$ becomes negative or zero. The other material property values are confined in a similar manner.

6.4 Stochastic simulation methodology

The boundary condition that has been considered in this study is shown in Figure 3.6. Composite material properties and resin material properties used in the present study are given in Table 6.1 and Table 6.2 respectively. There are no actual test data available for these materials that can be used to calculate standard deviation values of material properties. Therefore, representative values are assumed. Dimensions of the plate are: a = 279 mm, b = 279 mm, and ply thickness t = 0.135 mm. The loading considered is bi-axial compression combined with in-plane positive shear, and the direction of the applied positive shear loading is shown in Figure 4.1. The tapered laminate with LC(1) lay-up configuration and with taper configuration B is considered. A 8 by 5 finite element mesh as shown in Figure 3.7 is used in the present analysis.

Table 6.1 Material properties of T300/5208 graphite-epoxy material

Mechanical property	Mean value	Standard deviation	Strength property	Value
E_1	132.58 GPa	2.8719	X_t	1.515 GPa
E_2	10.8 GPa	0.3298	X_c	1.697 GPa
E_3	10.8 GPa	0.3298	$Y_t = Z_t$	43.8 MPa
$G_{12} = G_{13}$	5.7 GPa	0.2366	$Y_c = Z_c$	43.8 MPa
$\nu_{12} = \nu_{13}$	0.24	0.0317	R	67.6 MPa
ν_{23}	0.49	0.0317	S=T	86.9 MPa

In the Table 6.1, ν_{12}, ν_{13} and ν_{23} are the Poisson's ratios in the planes 1-2, 1-3 and 2-3, respectively. E_1, E_2 and E_3 are the Young's moduli in the fiber direction and in the directions transverse to it, respectively. G_{12}, G_{13} and G_{23} are the shear moduli associated

with planes 1-2, 1-3 and 2-3, respectively. X_t is the tensile strength of lamina in fiber direction. X_c is the compressive strength of lamina in fiber direction. Y_t is the tensile strength of lamina in the direction transverse to fiber direction (in plane 1-2). Y_c is the compressive strength of lamina in the same direction. Z_t is the tensile strength of lamina in principal material direction 3. Z_c is the compressive strength of lamina in principal material direction 3. R, S and T are shear strengths of lamina in planes 2-3, 1-3 and 1-2, respectively.

Table 6.2 Material properties of 5208 epoxy material

Mechanical property	Mean value	Standard deviation	Strength property	Value
E	3.8 GPa	0.3171	σ_T	43.8 MPa
ν	0.38	0.0317	σ_C	43.8 MPa
G	1.38 GPa	0.2298	σ_S	67.6 MPa

In Table 6.2, E is the Young's modulus, ν is the Poisson's ratio, and G is the shear modulus. σ_T , σ_C and σ_S denote the tensile strength, compressive strength and shear strength respectively.

Bi-axial compression loadings P_x and P_y, and in-plane shear loading P_{xy} are expressed in Figure 6.2 and tables 6.3 in non-dimensional forms as $P_x hb^2/E_2h^3$, $P_y hb^2/E_2h^3$ and P_{xy} hb^2/E_2h^3 respectively, where P_x is the applied X-direction axial compression loading per unit area, P_y is the applied Y-direction axial compression loading per unit area, and P_{xy} is the applied in-plane shear loading per unit area. The loadings per unit area in both directions are of the same value, and they are simultaneously increased. The corresponding maximum (transverse) deflection is also expressed in non-dimensional form as W_m/h, where h is the average thickness of the tapered laminate.

Using the data on elastic constants of the composite material (given in Table 6-1), resin material (given in Table 6-2), and the generated sample realizations of stochastic and the processes of elastic constants at each Gauss point, the stochastic Young's modulus, Poisson's ratio, and shear modulus are determined according to the equations (6.1-6.20). For each simulation case, the stochastic Young's modulus, Poisson's ratio, and shear modulus at each Gauss point are generated first. Substituting these properties into Equations (2.58-2.60), the extensional stiffness A_{ij}, the bending stiffness D_{ij} and the bending-extensional coupling stiffness B_{ij} are determined. Further, the stochastic laminate elasticity matrix [E] at the corresponding Gauss point is obtained. Once the stochastic laminate elasticity matrix [E] is determined, the analysis procedure will be the same as that described in Chapter 2. The set of sample realizations of failure loads, deflections, etc., will be recorded. Once one simulation is finished, the next simulation will be started, and the same analysis procedure will be repeated but using the newly simulated sample realizations of stochastic material properties.

In practice, a three-point Gauss quadrature is employed as it gives the most accurate results for 9-node element. Sample realizations of Young's moduli, Poisson's ratios, Shear moduli and the stochastic elasticity matrix [E] calculated for element 1 and 13 in the structure of LC(1) tapered laminate are shown in Figure 6.1.

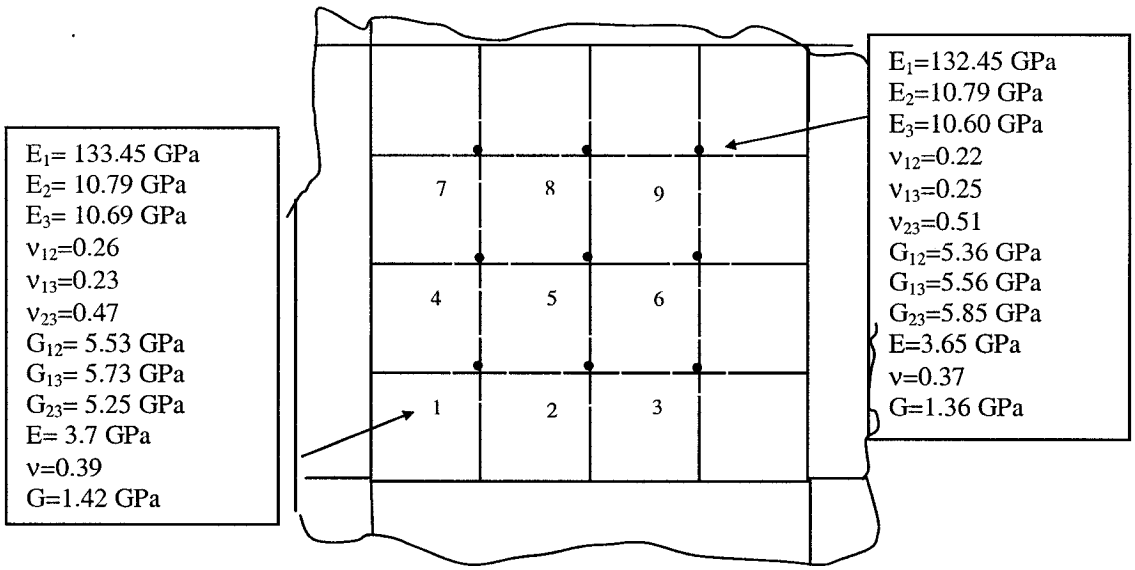

Element 1

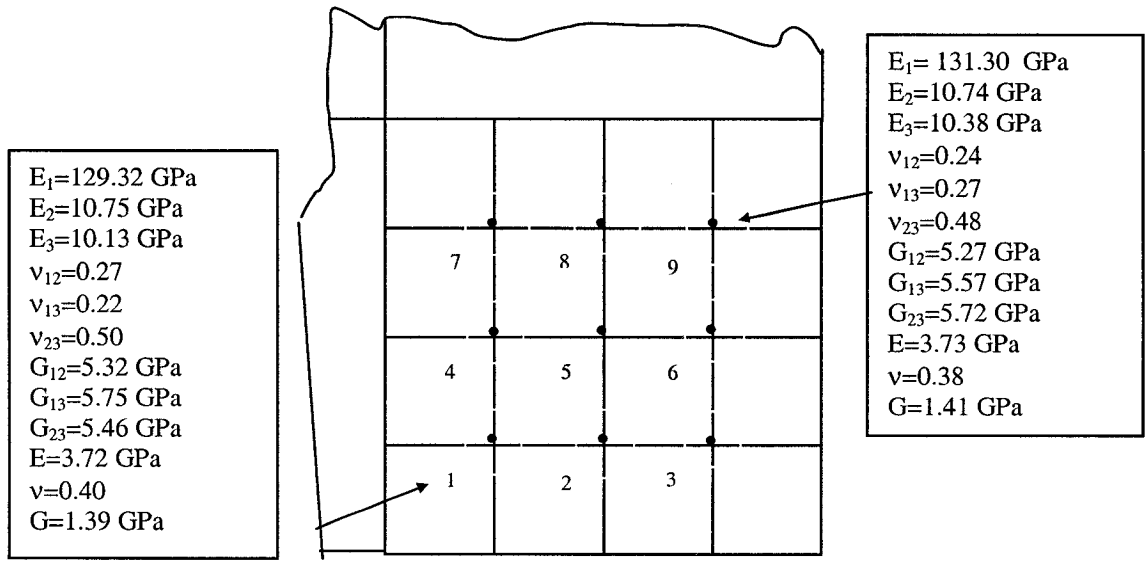

Element 13

Figure 6.1 A set of sample realizations of elastic constants at different Gauss points in element 1 (at the loaded edge) and element 13 (the central element)

6.5 Stochastic Analysis and Results

In order to illustrate the stochastic results, the results of three simulations are given. Figure 6.2 shows the load versus maximum deflection curves of the LC(1) laminate with taper configuration B for three simulations. Table 6.3 shows the failure data for all the cases.

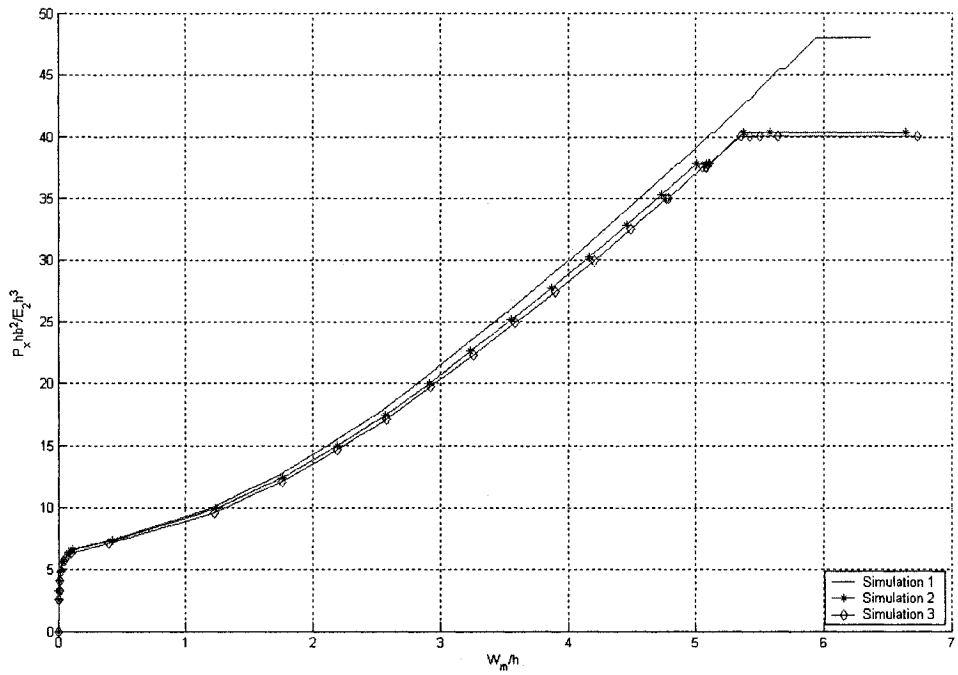

Figure 6.2 The load versus maximum deflection curves of the LC(1) laminate with taper configuration B for three simulations

Table 6.3 Failure data for the LC(1) laminate with taper configuration B for three simulations

Simulation Case	Buckling Load ($P_{xy}hb^2/E_2h^3$)	First-ply failure load ($P_{xy}hb^2/E_2h^3$)	Ultimate failure load ($P_{xy}hb^2/E_2h^3$)	$(W_m/h)^*$	Failure location (FL,FE) ♣	First-ply failure mode	Ultimate failure mode
1	6.534	37.8639	48.0356	4.8525	1,1	T♠	D#
2	6.257	37.5588	40.4068	5.0520	1,1	T	D
3	5.982	35.0159	40.1017	4.7435	1,1	T	D

The mean values of first-ply failure load, ultimate failure load and the corresponding maximum deflections can be determined based on the results of certain number of simulations.

In the stochastic analysis, the number of simulations is kept at 100 considering the computational time taken for the entire stochastic analysis. The mean values and the standard deviation values of both the first-ply failure load and the ultimate failure load for configuration at left end that is subjected to bi-axial compression combined with in-plane positive shear loading are determined. The mean values and the standard deviation values Bi-axial compression loadings P_x and P_y and in-plane shear loading P_{xy} are expressed in figures in non-dimensional forms as $P_x hb^2/E_2h^3$, $P_y hb^2/E_2h^3$ and $P_{xy}hb^2/E_2h^3$, respectively, where P_x is the applied X-direction axial compression loading per unit area, P_y is the applied Y-direction axial compression loading per unit area, and P_{xy} is the applied in-plane shear loading per unit area. The corresponding maximum (transverse) deflection is also expressed in non-dimensional form as W_m/h, where h is the average thickness of the tapered laminate.

The mean values of the first-ply failure load and the corresponding maximum deflection are presented in Figure 6.3. The mean values of the first-ply failure load and the corresponding maximum deflection are both influenced by the number of simulations. Within the range of 1-40 simulations, the mean value of the first-ply failure load decreases. Within the range of 40-50 simulations, the mean value of the first-ply failure load increases. Within the range of 50-90 simulations the mean value decreases again, but the decrease rate is much slower than the first decrease, and within the range of 90-100 simulations, the value nearly becomes steady. Within the range of 1-90 simulations, the

mean values of the corresponding maximum deflection at the first-ply failure decreases, but the decrease rate becomes smaller, and within the range of 90-100 simulations the value nearly becomes steady. It can be observed that between the ranges of 10-40 simulations and 50-90 simulations, the mean values of the first-ply failure load and mean values of the corresponding maximum deflection at the first-ply failure have the same trend of variation.

The variations of the standard deviation values of the first-ply failure load and the corresponding maximum deflection with the number of simulations are presented in Figure 6.4. The standard deviation values of the first-ply failure load and the corresponding maximum deflection are both influenced by the number of simulations. It can be observed that between the ranges of 0-30 simulations and 50-100 simulations, the standard deviation value of the first-ply failure load and the standard deviation value of the corresponding maximum deflection at the first-ply failure have the same trend of variation. The standard deviation value of the first-ply failure load and the standard deviation value of the corresponding maximum deflection at the first-ply failure increase in the range of 50-100.

The mean values of the ultimate failure load and the corresponding maximum deflection are presented in Figure 6.5. The mean value of the ultimate failure load and the mean value of the corresponding maximum deflection are influenced by the number of simulations. The mean value of the ultimate failure load and the mean value of the corresponding maximum deflection have the same trend of variation between the ranges of 0-30 simulations, 50-70 simulations and 60-100 simulations.

The ratio of the mean value of the ultimate failure load to the mean value of the first-ply failure load is calculated. It has been observed that the minimum value of this ratio is 1.129, the maximum value is 1.149, and the average value is 1.1346.

The variations of the standard deviation value of the ultimate failure load and the corresponding maximum deflection with the number of simulations are presented in Figure 6.6. The standard deviation values of the ultimate failure load and the maximum deflection are both influenced by the number of simulations. The standard deviation value of ultimate failure load decreases between the ranges of 20-50 simulations and 60-90 simulations, and increases between the ranges of 10-20 simulations and 50-60 simulations. The standard deviation value of the corresponding maximum deflection decreases between the range of 10-60 simulations, and increases between the range of 60-100 simulations. The standard deviation of the ultimate failure load and the standard deviation of the corresponding maximum deflection have the same trend of variation between the range of 20-50 simulations.

The ratio of the standard deviation of the ultimate failure load to the standard deviation of the first-ply failure load is calculated. It has been observed that the minimum value of this ratio is 3.2455, the maximum value is 11.1467, and the average value is 4.4359. This indicates that the degree of randomness in the ultimate failure is much more than that in the first-ply failure.

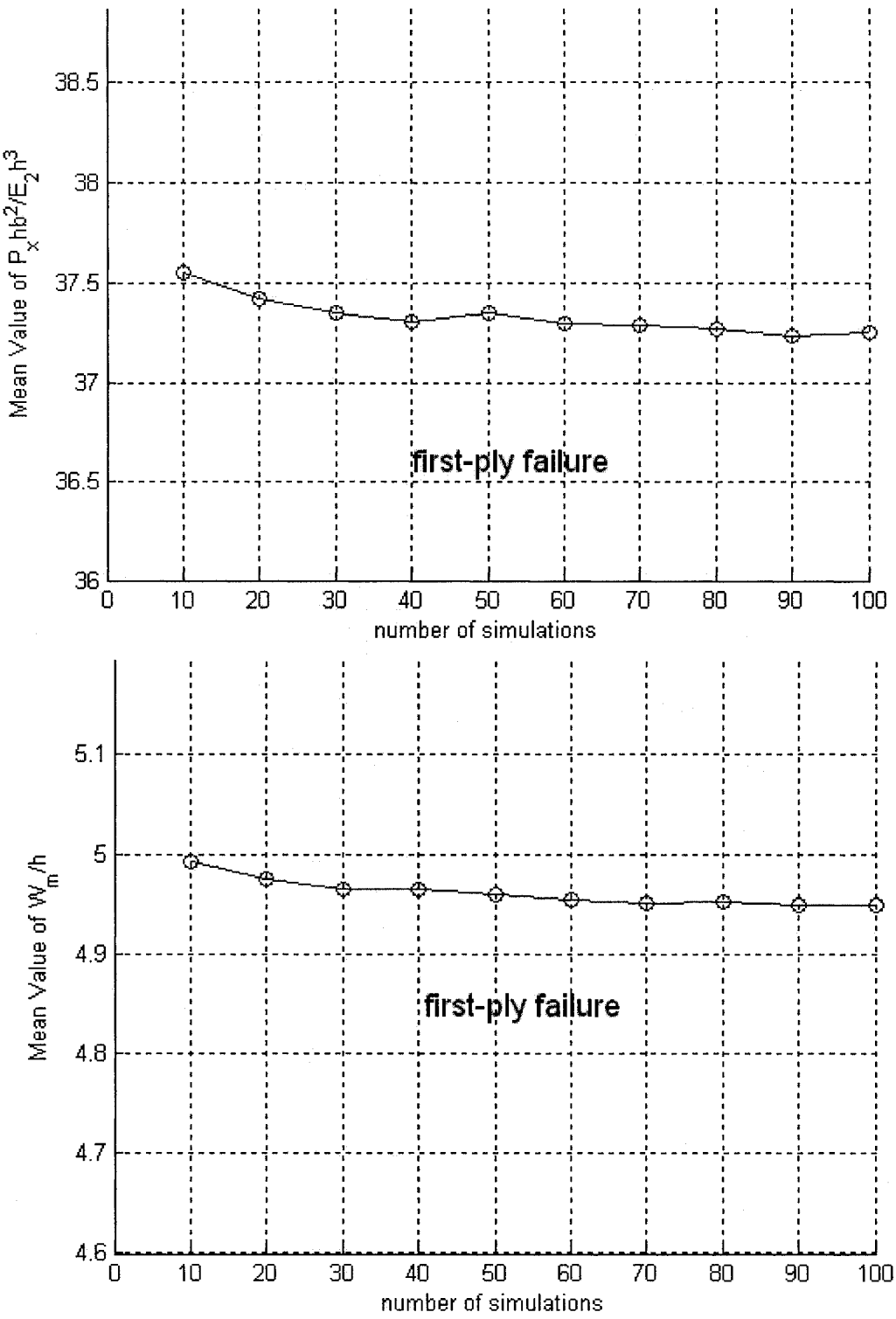

Figure 6.3 The mean values of the first-ply failure load and the corresponding maximum deflection for LC(1) laminate under bi-axial compression combined with in-plane positive shear

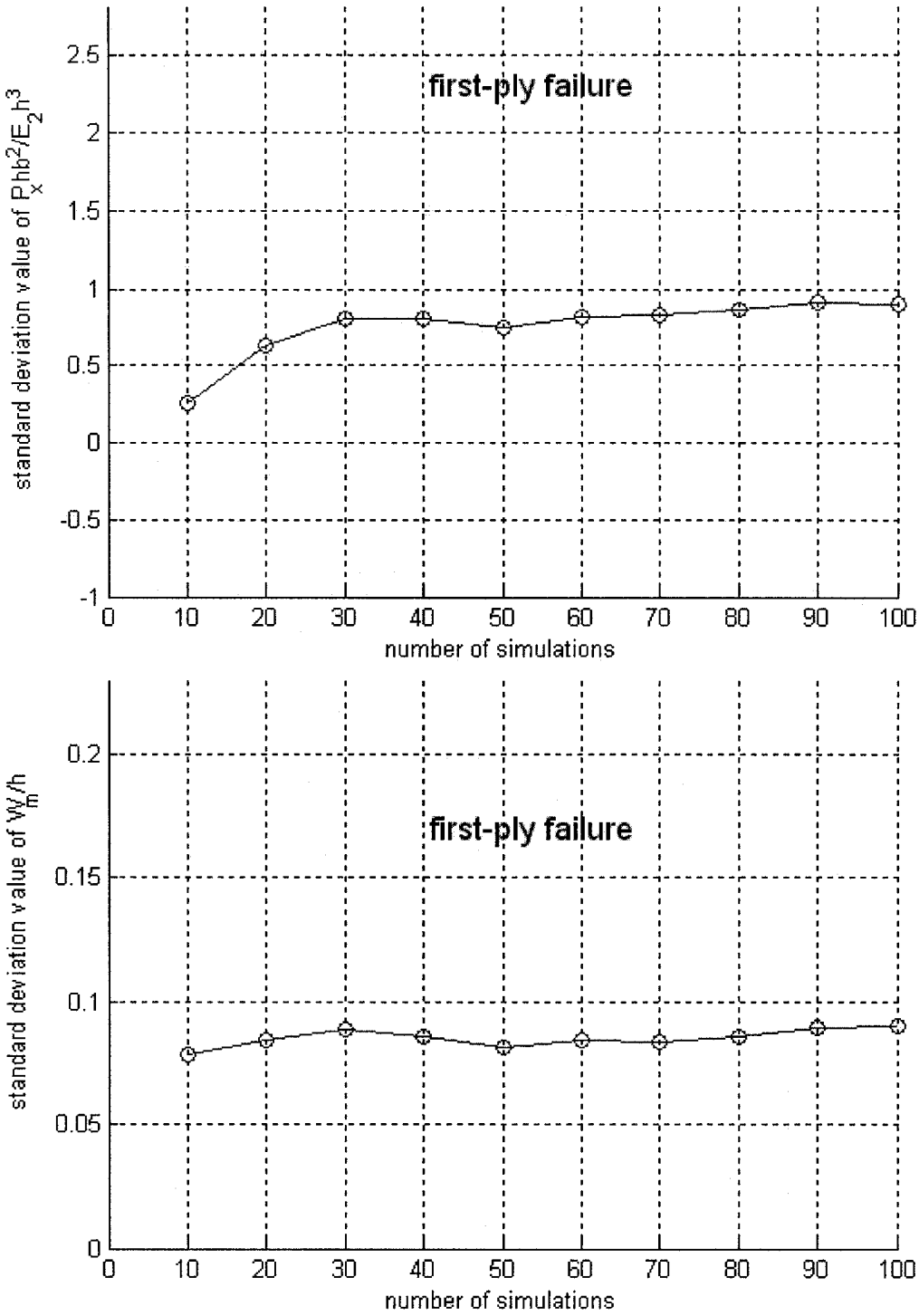

Figure 6.4 The standard deviation values of the first-ply failure load and the corresponding maximum deflection for LC(1) laminate under bi-axial compression combined with in-plane positive shear

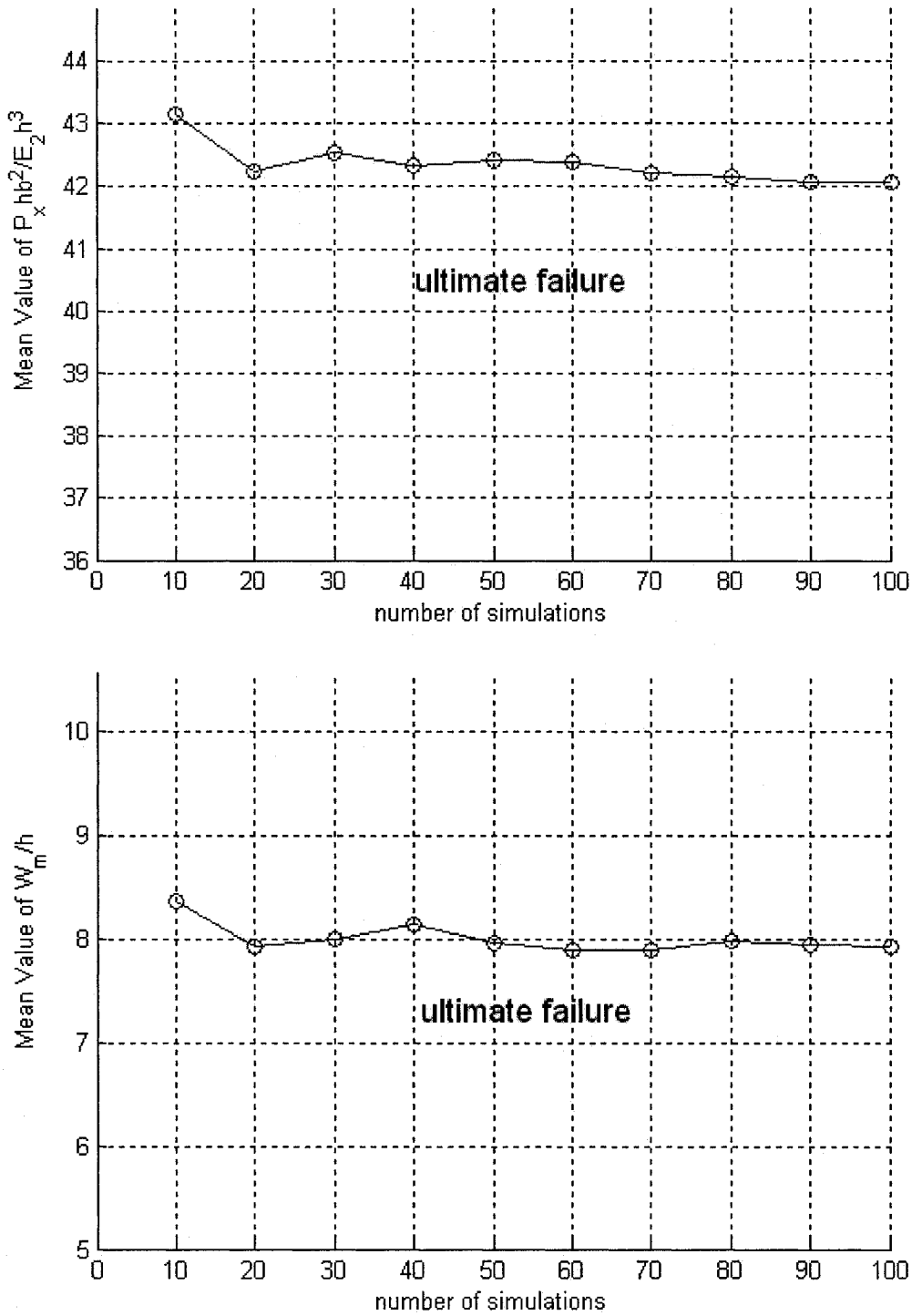

Figure 6.5 The mean values of the ultimate failure load and the corresponding maximum deflection for LC(1) laminate under bi-axial compression combined with in-plane positive shear

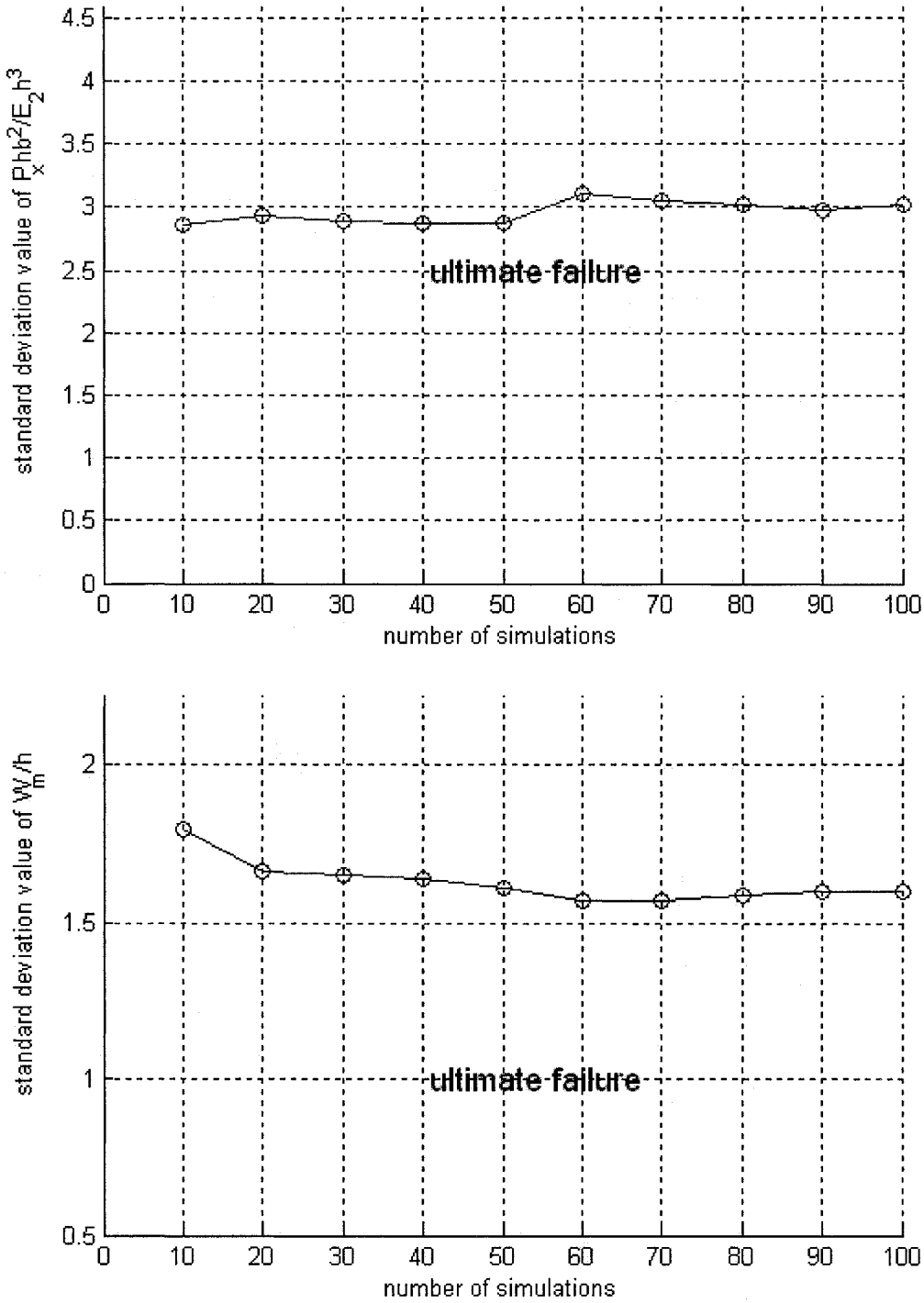

Figure 6.6 The standard deviation values of the ultimate failure load and the corresponding maximum deflection for LC(1) laminate under bi-axial compression combined with in-plane positive shear

6.6 Conclusion

This chapter has investigated the progressive failure of tapered composite laminates using a non-linear finite element formulation that also takes into account the influence of shear deformation. The influences of randomness in the material property values on the first-ply and ultimate failure loads, and the corresponding maximum deflections of the laminate have also been investigated. The number of simulations seems to have a strong influence on the probabilistic characteristics of predicted failure loads and maximum deflection values when the number of simulations is less than 60. Considering the maximum value of the ratio of the mean value of the ultimate failure load to the mean value of the first-ply failure load, it is noted that about 14% more strength is available after the first-ply failure until the ultimate failure. Considering the maximum value of the ratio of the standard deviation of the ultimate failure load to the standard deviation of the first-ply failure load, it is noted that the degree of randomness in the ultimate failure is much higher than that in the first-ply failure.

Chapter 7

Conclusions and Recommendations

In the present thesis, the principle of minimum potential energy, the first-order shear deformation theory and the geometric nonlinearity in the von Karman sense are used to derive the nonlinear finite element formulation for the analysis of tapered laminated plates. The nonlinear finite element formulation employs a nine-node Lagrangian element which has five degrees of freedom (two in-plane displacements, one transverse displacement and two rotational degrees of freedom) per node. A progressive failure simulation methodology for tapered laminates is given. The resulting nonlinear equations are solved using the Newton-Raphson technique.

For the stochastic failure analysis, a nonlinear stochastic finite element methodology for tapered laminates based on the Monte Carlo Simulation is used. The formulations and the associated MATLAB program that has been developed to conduct the non-linear finite element analysis are extended so as to incorporate the stochastic description of material properties and the stochastic finite element analysis. Using the stochastic material properties, the mean values and the standard deviation values of failure loads are calculated.

For the case of uni-axial compression and bi-axial compression, the tensor polynomial form of the maximum stress criterion is used to predict the failure of the lamina. For the case of in-plane shear and bi-axial compression combined with in-plane positive or negative shear loadings, the tensor polynomial form of the 3-D Tsai-Hill criterion is used

to predict the failure of the lamina, and the terms associated with the normal stress component in the third principal material direction are omitted. The maximum stress criterion is used to predict the onset of delamination at the interface between two adjacent layers (including the composite layer and the imagined resin layer). The influences of laminate configurations, taper configurations, fiber orientation angles, boundary conditions, load ratios and addition of uniform-thickness sections on the deflection response, the first-ply failure load, the ultimate failure load, the failure mode and the maximum deflection associated with the failure loads have been determined and given.

Based on the study, the following main concluding remarks can be made:

1. Failure mode of the first-ply failure is associated with the localized matrix cracking and occurs primarily due to in-plane normal stresses acting in the direction transverse to the fiber direction irrespective of lay-up configuration, taper configuration, boundary condition, load ratio and addition of uniform-thickness sections.

2. The first-ply failure locations lie near the loaded edges of the plate, and at the outermost layer.

3. For tapered laminates, the ultimate failure mode is delamination irrespective of lay-up configuration, taper configuration, boundary condition, load ratio and addition of uniform-thickness sections.

4. The maximum difference between the first-ply failure load and the ultimate failure load is strongly dependent on lay-up configuration, taper configuration, boundary condition, load ratio and addition of uniform-thickness sections.

5. The failure loads of laminates under the action of bi-axial compression are considerably lesser than that for the laminates under the action of uni-axial compression. The reduction of the first-ply failure load from that for uni-axial compression to that for bi-axial compression is about 28.3% to 60.5%, and the average reduction is 43.4%. The largest reduction (60.5%) corresponds to the tapered laminate with lay-up configuration LC(1) and with taper configuration D, and the smallest reduction (28.3%) corresponds to the tapered laminate with lay-up configuration LC(4) and with taper configuration D. The reduction of the ultimate failure load from that for uni-axial compression to that for bi-axial compression is about 33.9% - 60.5%, and the average reduction is 43.3%. The largest reduction (60.5%) corresponds to the tapered laminate with lay-up configuration LC(1) and with taper configuration D, and the smallest reduction (33.9%) corresponds to the tapered laminate with lay-up configuration LC(5) and with taper configuration D. However, there is a relatively small change in the first-ply and ultimate failure loads when the bi-axial compression is applied together with the shear load. The change of the first-ply failure load from that for biaxial compression to that for bi-axial compression combined with in-plane positive shear is about -18.8% to 29.3%, and the average reduction is 11.7%. As we can see, in some cases the failure load under bi-axial compression combined with in-plane shear load becomes larger than that under bi-axial compression only. The largest reduction (29.3%) corresponds to the tapered laminate with lay-up configuration LC(3) and with taper configuration D, and the largest enhancement (18.8%) corresponds to the tapered laminate with lay-up configuration LC(1) and with taper configuration D. The change in the ultimate

failure load from that for bi-axial compression to that for bi-axial compression combined with in-plane positive shear is about -18.89% to 30.1%, and the average reduction is 12.1%. The largest reduction (30.1%) corresponds to the tapered laminate with lay-up configuration LC(4) and with taper configuration D, and the largest enhancement (18.8%) corresponds to the tapered laminate with lay-up configuration LC(1) and with taper configuration D.

6. Comparison of the response to bi-axial compression with that for uni-axial compression shows no uniform trend such that an overall conclusion about the nature of the response can be drawn regarding the sensitivity of taper configuration to multi-axial loadings. The trend of the response varies from one lay-up configuration to another lay-up configuration.

7. The deflections under compression and compression combined with in-plane shear are either upward throughout the plate or downward throughout.

8. However, the deflections under in-plane shear are not so uniform. At some parts of the plate, they are positive (upward), but at some parts of the plate, they are negative (downward).

9. The deformed configurations are more complex under in-plane shear than that under bi-axial compression combined with in-plane shear.

10. Generally, taper configuration F is the strongest taper configuration among all the five taper configurations with respect to the first-ply failure load, the ultimate failure load and the buckling load. However, taper configuration F is not practical to

manufacture compared to other taper configurations. As a result, the next strongest taper configuration is either taper configuration B or C, which depends on the lay-up configurations and loadings.

11. Considering the maximum value of the ratio of the mean value of the ultimate failure load to the mean value of the first-ply failure load, it is noted that about 14% more strength is available after the first-ply failure until the ultimate failure for the LC(1) laminate with taper configuration B under bi-axial compression combined with in-plane positive shear.

12. Considering the maximum value of the ratio of the standard deviation of the ultimate failure load to the standard deviation of the first-ply failure load, it is noted that the degree of randomness in the ultimate failure is much higher than that in the first-ply failure for the LC(1) laminate with taper configuration B under bi-axial compression combined with in-plane positive shear.

The contributions made in the thesis are summarized below:

1. The main contribution in the present thesis is a systematic and thorough study of the progressive failure of tapered laminates under compressive and shear loadings, and the pre-buckling, pre-first-ply-failure, post-first-ply-failure, and post-buckling rsponse.

2. In addition, a methodology to quantify the influence of stochastic variability in the material properties on the progressive failure is also developed and applied to the case of combined loadings, which is the most severe loading case.

3. The relative design and performance advantages of different taper configurations and the influences of lay-up configuration, boundary condition, fiber orientations, and addition of uniform-thickness sections on these advantages have been brought out.

4. The availability of considerable residual strength after first-ply and buckling failures in tapered laminates has been confirmed through the present study, and further, the available residual strengths have been quantified. Cost-effective designs can be developed with much confidence based on the results obtained in the present work regarding the residual strength values.

5. The reliability indices needed in the reliability-based design of tapered composite laminates can be calculated based on the stochastic analysis results presented in the thesis. Hence, the results of the present thesis will form the basis for developing cost-effective and high-performance composite structures.

The following recommendations for further study can be considered.

1. Progressive failure under uni-axial compression in the y-direction.

2. Progressive failure analysis using Hashin criterion, using tensor polynomial criteria of maximum strain (Tsai-Wu) criterion or using Hoffman's criterion.

3. Stochastic progressive failure analysis under the action of uni-axial compression, bi-axial compression, in-plane positive and in-plane negative shear.

4. Using other correlation models for stochastic material properties, the laminate progressive failure analysis has to be conducted.

5. Experimental investigation of progressive failure of tapered composite plate.

References

1. He, K., Hoa, S. V. and Ganesan, R., "The Study of Tapered Laminated Composite Structures: a review", Composites Science and Technology, Vol. 60(14), 2000, pp. 2643-2657.

2. Turvey, G.J., "A Study of the Onset of Flexural Failure in Cross-ply Laminated Strips", Fiber Science and Technology, Vol. 13, 1980, pp. 325-356.

3. Turvey, G.J., "Flexural Failure Analysis of Angle-ply Laminates of GTRP and CFRP", Journal of Strain Analysis, Vol. 15, 1980, pp. 43-49.

4. Turvey, G.J., "An Initial Flexural Failure Analysis Symmetrically Laminated Cross-ply Rectangular Plates". International Journal of Solids and Structures, Vol. 16, 1980, pp. 451-463.

5. Turvey, G.J., "Initial Flexural Failure Analysis of Square Simply Supported Angle-ply Plate", Fiber Science and Technology, Vol. 14, 1981, pp. 47-63.

6. Turvey, G.J., "Uniformly Loaded Anti-symmetric Cross-ply Laminated Rectangular Plates: an Initial Flexural Failure Analysis", Fiber Science and Technology, Vol. 15, 1982, pp. 1-10.

7. Turvey, G.J., "Effects of Shear Deformation on the Onset of Flexural Failure in Symmetric Cross-ply Laminated Rectangular Plates", In. Composite Structures III, Editor: I.H. Marshall, Elsevier, London, Vol. 4, 1989, pp. 141-146.

8. Turvey, G.J. and Osman, M.Y., "Exact and Approximate Linear and Nonlinear Failure Analysis of Laminated Mindlin Plates in Flexure", In: Composite Structures

III, Editor: I.H. Marshall, Elsevier, London, Vol. 5, 1989, pp. 133-169.

9. Reddy, J.N. and Pandey, A.K., "A First-ply Failure Analysis of Composite Laminates", Computers and Structures, Vol. 25, 1987, pp. 371-393.

10. Reddy, Y.S. and Reddy, J.N., "Linear and Non-linear Failure Analysis of Composite Laminates with Transverse Shear, Composites Science and Technology, Vol. 44, 1992, pp. 227-255.

11. Lee, J.D., "Three Dimensional Finite element analysis of damaged accumulation in composite laminate", Computers and Structures, Vol. 15, No. 3, pp. 335-250.

12. Ochoa, O.O. and Engblom, J.J., "Analysis of Progressive Failure in Composites", Composite Science and Technology, Vol. 28, 1987, pp. 87-102.

13. Hwang, W.C. and Sun, C.T., "Failure Analysis of Laminated Composites by Using Iterative Three Dimensional Strength Theory", Computers and Structures, Vol. 33, No. 1, 1989, pp. 41-47.

14. Tolson, S. and Zabaras, N., "Finite Element Analysis of Progressive Failure in Laminated Composite Plates", Computers and Structures, Vol. 36, No. 3, 1991, pp. 361-376.

15. Nuismer, R.J. and Tan, S.C., "Constitutive Relations of a Cracked Composite Lamina", Journal of Composite Materials, Vol. 22, 1988, pp. 306-321.

16. Tan, S.C. and Nuismer, R.J., "A Theory for Progressive Matrix Cracking in Composite Laminates", Journal of Composite Materials, Vol. 23, 1989, pp. 1029-1047.

17. Reddy, Y.S. and Reddy, J.N., "Three-dimensional Finite Element Progressive Failure

Analysis of Composite Laminates Under Axial Tension", Journal of Composites Technology and Research, Vol. 15, No. 2, pp. 73-87.

18. Tan, S.C., "A Progressive Failure Model for Composite Laminates Containing Openings", Journal of Composite Materials, Vol. 25, 1991, pp. 556-557.

19. Tan, S.C. and Perez, J., "Progressive Failure of Laminated Composite with a Hole under Compressive Loading", Journal of Reinforced Plastics and Composites, Vol. 12, 1993, pp. 1043-1057

20. Chou, S.C., Opringer, O. and Rainey, J.H., "Post-failure Behavior of Laminates: II-Stress Concentration", Journal of Composite Materials, Vol. 11, 1977, pp. 71-78.

21. Irvine, T.B. and Ginty, C.A., "Progressive Fracture of Fiber Composites", Journal of Composite Materials, Vol. 20, 1986, pp. 166-184.

22. Chang, F.K. and Chang, K.Y., "Post-failure Analysis of Bolted Composite Joints in Tension or Shear-out Mode Failure", Journal of Composite Materials, Vol. 21, 1987, pp. 809-833.

23. Chang, F.K. and Chang, K.Y., "A Progressive Damage Model for Laminated composites Containing Stress Concentrations", Journal of Composite Materials, Vol. 21, 1987, pp. 843-855.

24. Chang, F.K. and Lessard, L.B., "Damage Tolerance of Laminated Composites Containing an Open Hole and Subjected to Compressive Loadings: Part I-Analysis", Journal of Composite Materials, Vol. 25, 1991, pp. 2-43.

25. Lessard, L.B. and Chang. F.K. "Damage Tolerance of Laminated Composites Containing an Open Hole and Subjected to Compressive Loadings: Part II-

Experiment", Journal of Composite Materials, Vol. 25, 1991, pp. 44-64.

26. Lessard, L.B. and Shokrieh, M.M., "Two-dimensional Modeling of Composite Pinned-joint Failure", Journal of Composite Materials, Vol. 29, 1995, pp. 671-679.

27. Shokrieh, M.M. and Lessard, L.B. "Effects of Material Nonlinearity on the Three-dimensional Stress State of Pin-loaded Composite laminates", Journal of Composite Materials, Vol. 30, 1996, pp. 839-861.

28. Kim, Y.S. and Hoa, S.V. "Bi-axial buckling Behavior of Composite Rectangular Plates", Composite Structures, Vol. 31, 1995, pp. 247-252.

29. Roberts, J.C., Bao, G. and White, G.J., "Experimental, Numerical and Analytical Results for Bending and Buckling of Rectangular Orthotropic Plates", Composite Structures, Vol. 43, 1999, pp.289-299.

30. Gu, H.Z. and Chattopadhyay, A., "An Experimental Investigation of Delamination buckling and post-buckling of Composite Laminates", Composites Science and Technology, Vol. 59, 1999, pp. 903-910.

31. Bansal, A. and Kumosa, M., "Experimental and Analytical Studies of Failure Models in Iosipescu Specimens under Biaxial Loadings", Journal of composite Materials, Vol. 26, 1995, pp. 334-358.

32. Grief, R. and Chapon, E., "Investigation of Successive Failure Modes in Graphite/epoxy Laminated Composite Beams", Journal of Reinforced Plastics and Composites, Vol. 12, No. 5, pp. 602-621.

33. Starnes, Jr.J.H. and Rouse, M., "Post-buckling and Failure Characteristics of Selected Flat Rectangular Graphite-epoxy Plates Loaded in Compression", AIAA Journal,

Paper No. 81-0543, 1981.

34. Engelstad, S.P., Reddy, J.N. and Knight, Jr.N.F., "Post-buckling Response and Failure Prediction of Graphite Epoxy Plates Loaded in Compression", AIAA Journal., Vol. 30, 1992, pp. 2106-2113.

35. Lee, H.H. and Hyer, M.W., "Post-buckling Failure of Composite Plates with Holes", AIAA Journal, Vol. 31, 1993, pp. 1293-1298.

36. Kam, T.Y. and Sher, H.F., "Nonlinear and First-ply Failure Analysis of Laminated Composite Cross-ply Plates", Journal of Composite Materials. Vol. 29, 1995, pp. 463-485.

37. Kaminski, B.E. and Ashton, J.E., "Diagonal Tension Behaviour of Boron Epoxy Shear Panels", Journal of Composite Materials, Vol. 5, 1971, pp. 553-558.

38. Kobayashi, S., Sumihara, K. and Koyama, K., "Shear Buckling Strengths of Graphite Epoxy Laminate Panels", In Composite Materials, Proceedings of the Japan-US Conference, Editors: Kawata, K. and Akaska, T.,Tokyo, 1981, pp. 436-445.

39. Agrawal, B.L., "Post-buckling Behavior of Composite Shear Webs", AIAA Journal, Vol. 19, 1981, pp. 933-939.

40. Zhang, Y. and Matthews, F.L., "Post-buckling Behavior of Anisotropic Laminated Plates under Pure Shear and Shear Combined with Compressive Loading", AIAA Journal, Vol. 22, 1984, pp. 281-286.

41. Stein, M., "Post-buckling of Long Orthotropic Plates in Combined Shear and Compression", AIAA Journal, Vol. 23, 1985, pp. 788-794.

42. Prabhakar, M.K. and Kennedy, J.B., "Non-linear Behavior of Un-symmetric Angle-

ply Rectangular Plates Under In-plane Shear Load", Journal of Mechanical Engineering Science, Vol. 21, 1979, pp. 205-212.

43. Kumar, A. and Sindhi, P.R., "Post-buckling Behavior of Rectangular Plates under Pure Shear", Journal of Aeronautical Society of India, Vol. 41, 1992, pp. 191-204.

44. Kosteletos, S., "Post-buckling Response of Laminated Plates under Shear Load", Composite Structures, Vol. 20, 1992, pp. 137-145.

45. Singh, S.B., Kumar, A. and Iyengar, N.G.R., "Progressive Failure of Symmetrically Laminated Plate Under Uni-axial Compression", Structural Engineering and Structural Mechanics, Vol. 5, 1997, pp. 433-450.

46. Singh, S.B., Kumar, A., "Post-buckling Response and Failure of Symmetric Laminates Under In-plane Shear", Composite Science and Technology, Vol. 58, 1998, pp. 1949-1960.

47. Ganesan, R. and Zhang, D., "Progressive Failure Analysis of Composite Laminates Subjected to In-Plane Compressive and Shear Loadings", Journal of Science and Engineering of Composite Materials, Vol. 11, Nos. 2-3, 2004. pp. 79-102.

48. Farghaly, S. H. and Gadelrab, R. M., "Free Vibration of a Stepped Composite Timoshenko Cantilevered Beam", Journal of Sound and Vibration, Vol. 187, No. 5, 1995, pp. 886-896.

49. Rao, S. R. and Ganesan, N., "Dynamic Response of Non-Uniform Composite Beams", Journal of Sound and Vibration, Vol. 200, No.5, 1997, pp. 563-577.

50. Nabi, M. S. and Ganesan, N., "A Generalized Element for the Free Vibration Analysis of Composite Beams", Computers and Structures, Vol. 51(5), 1994, pp.

607-610.

51. Karabelis, D. L. and Beskos, D. E., "Static, Dynamic and Stability Analyses of Structures Composed of Tapered Beams", Computers and Structures, Vol. 16(6), 1983, pp. 731-748.

52. Tong, X., Tabarrok, B. and Yeh, K. Y., "Vibration Analysis of Timoshenko Beams with Non-homogeneity and Varying Cross-section", Journal of Sound and Vibration, Vol. 186 (5), 1995, pp. 821-835.

53. Ganesan, R. and Abd EL-Maksoud, Mohamed A, "Dynamic Response of Variable-Thickness Composite Beams Using Efficient Basis Functions." Third Canadian Int. Composites Conf. CANCOM 2001, Aug. 21-24, 2001, Montreal.

54. Ganesan, R. and Zabihollah, A., "Vibration Analysis of Tapered Composite Beams using a Higher-order Finite Element. Part I: Formulation", Composite Structures, In Press, Corrected Proof, Available online 8 September 2005.

55. Ganesan, R. and Zabihollah, A., "Vibration Analysis of Tapered Composite Beams using a Higher-order Finite Element. Part II: Parametric Study", Composite Structures, In Press, Corrected Proof, Available online 8 September 2005.

56. Ganesan, R. and Chen, L., "Effects of Tapered Configuration and Taper Angle on the Free Vibration Response of Variable-thickness Composite Beams", In: Presentation in the fifth Canadian-international Composites Conference. 16-19 August 2005. Vancouver, Canada.

57. Liu, W.G., "Dynamic Instability Analysis of Tapered Composite Plates using Finite Element and Ritz Methods", M.A.Sc. Thesis, 2005, Concordia University.

58. Adams, D. F., Ramkumar, R.L., and Walrath, D.E., "Analysis of Porous Laminates in the Presence of Ply Drop-offs and Fastener Holes", Northrop Technical Report NOR 84-113, Northrop Corporation, Hawthorne, CA 90250, and the University of Wyoming, laramie, Wyoming 820271, May 1984.

59. Hoa, S.V., Du, B.L., and Vu-Khanh, T., "Interlaminar Stresses in Tapered Laminates", Polymer Composites, October 1988, Vol.9, No. 5, 337-344.

60. Daoust, J. and Hoa, S.V., "Parameters Affecting Interlaminar Stresses in Tapered Laminates under Static Loading Conditions", Polymer Composites, October 1989, Vol. 10, No. 5, 374-383.

61. Curry, J.M., Johnson, E.R., and Starnes Jr, J.H., "Effect of Dropped Plies on the Strength of Graphite-epoxy Laminates", AIAA Journal, Vol. 30, No. 2, February 1992, 449-456.

62. Kemp, B.L., and Johnson, E.R., "Response and Failure Analysis of Graphite-epoxy Laminate Containing Terminating Internal Plies", Proceedings of the AIAA/ASME/ASCE/AHS 26th Structures, Structural Dynamics, and Materials Conference, Pt. 1, AIAA, New York, April 1985, pp.13-24; AIAA Paper 85-0608.

63. Varughese, B., and Mukherjee, A., "Analysis of Tapered Laminated Composites with Non-symmetric Lay-up", Journal of Reinforced Plastics and Composites, Vol. 16, No. 7/1997.

64. Salpekar, S.I., Raju, I.S., and O'Brien, T.K., "Strain-energy-release Rate Analysis of Delamination in a Tapered Laminate Subjected to Tension Load", J. of Composite Materials, Vol. 25, February 1991, pp 118-141.

65. Murri, G.B., O'Brien, T.K., and Salpekar, S.A., "Tension Fatigue of Glass/Epoxy and Graphite/Epoxy Tapered Laminates", American Helicopter Society Journal, Vol. 38, No. 1, 1993, pp. 29-37.

66. Murri, G.B., Salpekar, S.A., and O'Brien, T.K., "Fatigue Delamination Onset Prediction in Unidirectional Tapered Laminates", Composite Materials: Fatigue and Fracture (Third Volume). ASTM STP 1110. T.K. O'Brien, Ed., American Society for Testing and Materials, Philadelphia, 1991, pp312-339.

67. Murri, G.B., O'Brien, T.K., and Rousseau, C.Q., "Fatigue Life Methodology for Tapered Composite Flexbeam Laminates", Journal of the American Helicopter Society, Vol. 43, No. 2, April 1998, pp. 146-155.

68. Fish, J.C. and Lee, S.W., "Delamination of Tapered Composite Structures", Engineering Fracture Mechanics Vol. 34, No. 1, pp43-54, 1989.

69. Vizzini, A.J. and Lee, S.W., "Damage Analysis of Composite Tapered Beams", Journal of the American Helicopter Society, Vol. 40, No. 2, April 1995, pp. 43-49.

70. Llanos, A.S. and Vizzini, A.J., "The Effect of Film Adhesive on the Delamination Strength of Tapered Composites", Journal of Composite Materials, Vol. 26, No. 13, 1992, pp. 1968-1983.

71. Vizzini, A.J., "Influence of Realistic Ply-drop Geometries on Interlaminar Stresses in Tapered Laminates", Composite Materials: Fatigue and Fracture-Fifth Volume, ASTM STP 1230, R.H. Martin, Ed., American Society for Testing and Materials, Philadelphia, 1995, pp.467-485.

72. Vizzini, A.J., "Shear-lag Analysis about an Internally-dropped Ply", Journal of

Reinforced Plastics and Composites, Vol. 16, No. 1/1997.

73. Botting, A.D, Vizzini, A.J., Lee, S.W., "Effect of Ply-drop Configuration on Delamination Strength of Tapered Composite Structures", AIAA J., Vol. 34, No. 8, August 1996, pp. 1650-1656.

74. Fish, J.C. and Vizzini, A.J., "Delamination of Ply-drop Configurations", Composite Materials: Testing and Design (Eleven Volume), ASTM STP 1206. E.T. Camponeschi, Jr., Ed., American Society for Testing and Materials, Philadelphia, 1993, pp. 323-332.

75. Fish, J.C. and Vizzini, A.J., "Tailoring Concepts for Improved Structural Performance of Rotorcraft Flexbeams", Composites Engineering, Vol. 2, No. 5-7, pp. 303-312, 1992.

76. He, K., "Interlaminar Stresses and Fracture Behavior in Thickness-Tapered Composite Laminates", Ph. D. Thesis, 2002, Concordia University.

77. Vizzini, A.J., "Strength of Laminated Composites with Internal Discontinuities Parallel to the Applied Load", AIAA Journal, Vol.30, No. 6, June 1992.

78. Harrison, P.N. and Johnson, E.R., "A Mixed Variational Formulation for Interlaminar Stresses in Thickness-tapered Composite Laminates", Int. J. Solids Structures Vol. 35, No. 16, pp.2377-2399, 1996.

79. Mortensen F. and O.T. Thomsen, " A Simple Approach for the Analysis of Embedded Ply Drops in Composite and Sandwich Laminates", Composite Science and Technology, Vol. 59, 1999, pp. 1213-1226.

80. Stock, T.A., Bellini, P.X., Murthy, L.N. and Chamis, C.C., "Probabilistic Composite

Micromechanics", Proceeding of the AIAA/ASME/ASCE/AHS/ASC 29th Structures, Structural Dynamics and Materials Conference (Williamsburg, VA), AIAA, Washington, DC, April 1988, Pt. 3, pp.1289-1293.

81. Fukuda, H., "Monte Carlo Simulation of the Strength of Hybrid Composite", Journal of Composite Materials, Vol.16, 1982, pp. 371-385.

82. Dzenis, Y.A., Joshi, S.P. and Bogdanocich, A.E., "Damage Evaluation Modeling in Orthotropic Laminated Composites", AIAA Journal, Vol. 32. No. 2, 1994, pp. 357-364.

83. Joshi, S.P. and Frantziskonis, G., "Damage Evaluation in Laminated Advanced Composites", Composite Structures, Vol. 17, No. 2, 1991, pp. 127-139.

84. Larder, R.A., "The Stochastic Finite Element Simulation of Parallel Fiber Composites", Journal of Composite Materials, Vol. 10, 1976, pp. 21-31.

85. Cassenti, B.N., "Probabilistic Static Failure of Composite Material", AIAA Journal, Vol. 22, No. 1, 1984, pp. 103-110.

86. Fukunaga, H. and Chou, T.W., "Probabilistic Failure Strength Analysis of Graphite/Epoxy Cross-Ply Laminates", Journal of Composite Materials, Vol. 18, 1984, pp. 339-351.

87. Rosen, B.W., "Tensile Failure of Fibrous Composite", AIAA Journal, Vol. 2, No. 11, 1964, pp. 1985-1991.

88. Zweben, C., "Tensile Failure of Fiber Composite", AIAA Journal, Vol. 6, No. 12, 1968, pp. 2325-2332.

89. Harlow, D.G. and Phoenix, S.L., "The Chain of Bundles Probability Model for the

Strength of Fibrous Materials I: Analysis and Conjectures", Journal of Composite Materials, Vol. 12, 1978, pp. 195-214.

90. Harlow, D.G. and Phoenix, S.L., "The Chain of Bundles Probability Model for the Strength of Fibrous Materials II: A Numerical Study of Convergence", Journal of Composite Materials, Vol. 12, 1978, pp. 314-334.

91. Contreras, H., "The Stochastic Finite Element Method", International Journal for Computers and Structures, Vol. 12, 1980, pp.341-348.

92. Vanmarcke, E., Shinozuka, M., Nakagiri, S., Schueller, G.I., and Grigoriu, M., "Random Fields and Stochastic Finite Elements", Structural Safety, Vol. 3, 1986, pp. 143-166.

93. Benaroya, H. and Rehak, M., "Finite Element Methods in Probabilistic Structural Analysis: A Selective Review", Applied Mech. Rev., Vol. 41, No. 5, May 1988, pp.201-213.

94. Yamazaki, F., Shinozuka, M. and Dasgupta, G., "Neumann Expansion for Stochastic Finite Element Analysis", Journal of Engineering Mechanics, Vol. 114, No. 8, 1986, pp. 1335-1354.

95. Ostoja-Starzewski, M., "Micromechanics as a Basis of Stochastic Finite Elements and Differences: An Overview", Applied Mech. Rev., Vol. 46, No. 2, November 1993, pp. S136-S147.

96. Vanmarcke, E.H., "Stochastic Finite Elements and Experimental Measurements", Probabilistic Engineering Mechanics, Vol. 9, 1994, pp. 103-114.

97. Iwan, W.D. and Jensen, H., "On the Dynamic Response of Continuous Systems

Including Model Uncertainty", Journal of Applied Mechanics, Vol. 60, 1993, pp. 484-490.

98. Koyluoglu, H.U., Nielsen, S.R.K. and Cakmak, A.S., "Stochastic Dynamics of Geometrically Non-linear Structure with Random Properties Subject to Stationary Random Excitation", Journal of Sound and Vibration, Vol. 190, 1996, pp. 821-841.

99. Ramu, S.A. and Ganesan, R., "A Galerkin Finite Element Technique for Stochastic Field Problems", Computer Methods in Applied Mechanics and Engineering, Vol. 105, 1993, pp. 315-331.

100. Zhu, W.Q., Ren, Y.J. and Wu, W.Q., "Stochastic FEM Based on Local Averages of Random Vector Fields", Journal of Engineering Mechanics, Vol. 118, No. 3, 1992, pp. 496-511.

101. Jensen, H. and Iwan, W.D., "Response of Systems with Unicertain Parameters to Stochastic Excitation", Journal of Engineering Mechanics, Vol. 118, No. 5, 1992, pp. 1012-1025.

102. Liu, W.K., Belytschko, T. and Mani, A., "Applications of Probabilistic Finite Element Methods in Elastic/Plastic Dynamics", Journal of Engineering for Industry, Vol. 109, 1987, pp. 2-8.

103. Ghanem, R. and Spanos, P.D., "Polynomial Chaos in Stochastic Finite Elements", Journal of Applied Mechanics, Vol. 57, 1990, pp. 197-202.

104. Ganesan, R., Sankar, T.S. and Ramu, S.A., "Non-conservatively Loaded Stochastic Columns", Int. Journal of Solids and Structures, Vol. 30, No. 17, 1993, pp. 2407-2424.

105.Shinozuka, M., Kako, T. and Tsurui, A., "Random Vibration Analysis in Finite Element Formulation", Random Vibration-status and Recent Developments, Ed. I. Elishakoff and Lyon, R.H., Elsevier, New York, 1986.

106.Ramu, S.A. and Ganesan. R., "Free Vibration of a Stochastic Beam-column using Stochastic FEM", International Journal for Computers and Structures, Vol. 41, No. 5, 1991, pp. 987-994.

107.Ren, Y.J., Elishakoff, I. and Shinozuka, M., "Finite Element Method for Stochastic Beams Based on Variational Principles", Journal of Applied Mechanics, Vol. 64, 1997, pp. 664-669.

108.Sankar, T.S., Ramu, S.A. and Ganesan, R., "Variability of SIF and COD of Stochastic Structural Systems", International Journal for Computers and Structures, Vol. 43, No. 6, 1992, pp. 1135-1145.

109.Sankar, T.S., Ramu, S.A. and Ganesan, R., "Stochastic Finite Element Analysis for High Speed Rotors", Journal of Vibration and Acoustics, Vol. 115, 1993, pp. 59-64.

110.Liaw, D.G., and Yang H.T.Y., "Reliability of Initially Compressed Uncertain Laminated Plates in Supersonic Flow", AIAA Journal, Vol. 29, No. 6, 1991, pp. 952-945.

111.Ganesan, R. and Hoa, S.V., "Stochastic Finite Element Analysis of Composite Structure", CANCAM 95, 15th Canadian Congress of Applied Mechanics, May 95, Victoria, Canada.

112.Nakagiri, S., Takabatake, H. and Tani, S., "Uncertain Eigenvalue Analysis of Composite Laminated Plates by the Stochastic Finite Element Method", Journal of

Engineering for Industry, Vol. 109, 1987, pp. 9-12.

113.Engelstad, S.P. and Reddy, J.N., "Probabilistic Nonlinear Finite Element Analysis of Composite Structures", AIAA Journal, Vol. 31, No. 2, 1993, pp. 362-369.

114.Chang, C. and Yang, H.T.Y., "Reliability of Uncertain Flexible Laminated Skewed Plates under Random Compressions", AIAA Journal, Vol. 30, No. 2, 1992, pp. 464-472.

115.Slattery, K., "A Random-damage Finite Element for Modeling Failure in Advanced Composite Materials", In: Composite Materials: Fatigue and Fracture, Vol. 5, Ed. R..H. Martin, ASTM, Philadelphia, 1995, pp. 231-245.

116.Miki, M., Murotsu, Y. and Tanaka, T., "Optimum Fiber Orientation Angle of Multiaxially Laminated Composites Based on Reliability", AIAA Journal, Vol. 31, 1993, pp. 919-920.

117.Shao, S., Miki, M. and Murotsu, Y., "Optimum Fiber Angle of Unidirectional Composites for Load with Variations", AIAA Journal, Vol. 30, 1992, pp. 189-196.

118.Miki, M., Murotsu, Y. and Murayama, N., "Application of Lamination Parameters to Reliability-based Stiffness Design of Composites", AIAA Journal, Vol. 31, 1993, pp. 1938-1945.

119.Kogiso, N., Shao, S. and Murotsu, Y., "Effect of Correlation on Reliability-based Design of Composite Plate for Buckling", AIAA Journal, Vol. 36, No. 9, 1998, pp. 1706-1713.

120.Thomas, D.J. and Wetherhold, R.C., "Reliability Analysis of Ceramic Matrix Composite Laminates", Journal of Engineering for Gas Turbines and Power, Vol.

115, 1993, pp. 117-121.

121.Cohen, David, "Application of Reliability and Fiber Probabilistic Strength Distribution Concepts to Composite Vessel Burst Strength Design", Journal of Composite Materials, Vol. 26, 1992, pp. 1984-2014.

122.Singh, S.B., Kumar, A. and Iyengar, N.G.R., "Progressive Failure of Symmetrical Laminates Under In-plane Shear, Part-1: Positive Shear", Structural Engineering and Structural Mechanics, Vol. 6, 1998, pp. 143-159.

123.Singh, S.B., Kumar, A. and Iyengar, N.G.R., "Progressive Failure of Symmetrical Laminates Under In-plane Shear, Part-2: Negative Shear", Structural Engineering and Structural Mechanics, Vol. 6, 1998, pp. 143-159.

124.Tsai, S.W. and Wu, E.M., "A General Theory of Strength for Anisotropic Materials", Journal of Composite Materials, Vol. 5, No. 58, 1971.

125.Christensen, R.M., "Mechanics of Composite Materials", John Wiley and Sons Inc., New York, 1979.

126.Datoo, M.H., "Mechanics of Fibrous Composites", Elsevier Applied Science, London and New York, 1991.